Landslide generated impulse waves in reservoirs

Basics and computation

Versuchsanstalt für Wasserbau
Hydrologie und Glaziologie
der Eidgenössischen
Technischen Hochschule Zürich

Mitteilungen **211**

Landslide generated impulse waves in reservoirs

Basics and computation

Valentin Heller, Willi H. Hager und Hans-Erwin Minor

Zürich, 2009

Herausgeber: Prof. Dr. Robert Boes

Zitiervorschlag für VAW-Mitteilungen:

Heller, V., Hager, W.H. und Minor, H.-E. (2009).
Landslide generated impulse waves in reservoirs: *Basics and computation.*
Mitteilungen 211, Versuchsanstalt für Wasserbau, Hydrologie und Glaziologie (VAW),
R. Boes, Hrsg., ETH Zürich.

Im Eigenverlag der
Versuchsanstalt für Wasserbau,
Hydrologie und Glaziologie
ETH Zürich
CH-8092 Zürich

Tel.: +41 - 44 - 632 4091
Fax: +41 - 44 - 632 1192
e-mail: info@vaw.baug.ethz.ch

Zürich, 2009

ISSN 0374-0056

Preface

Impulse waves generated in natural lakes and reservoirs by the impact of landslides may cause damages during run-up shores or against dams. Particular attention has, in this context, to be given to dams and in particular to embankments dams which, if overtopped, may suffer serious damages or even fail completely. It is, therefore, of great importance that the size of such waves and their run-up height on the shore or dam face are known.

Over the past thirty years the VAW has carried out a number of research projects on impulse waves, and this manual presents the results of this research together with available international literature on the topic. In addition, it gives an explanation of a computation procedure that enables forecast values for all relevant parameters to be determined. This makes possible emergency planning and allows preventive action, for instance precautionary lowering of the lake or reservoir, to be taken in good time.

The objective of this manual is to make the research results available to practising engineers in appropriate form. The results of these computations may still result in estimations to certain extent so it is necessary, as so often in engineering design, to include safety factors in the computations. In many cases the possible errors are so large that a hydraulic model test or a numerical simulation has to be resorted to. Nonetheless, the order of magnitude of the characteristics of the impulse waves can be estimated.

We wish to express our thanks to the Dam Safety Section of the Swiss Federal Office of Energy SFOE, which commissioned this work, for all their cooperation, and to Dr. Andreas Huber for his critical comments. Thanks also to Mr. Ian David Clarke for the translation of the German to this English version.

This manual, as well as the spread sheets, are available in electronic form on the VAW-Website www.vaw.ethz.ch under “News & Events”, “Latest VAW Reports”. We hope that this manual finds a wide readership.

Zurich, February 2009 Valentin Heller, Willi H. Hager and Hans-Erwin Minor

Table of contents

Summary

Landslide generated impulse waves are typically caused by landslides, rockfalls, shore instabilities, snow avalanches or glacier calvings in oceans, bays, lakes or reservoirs. They are particularly relevant for the Alpine environment because of steep valley sides, possible large slide masses and impact velocities and the great number of reservoirs. In this *manual*, a state-of-the-art on the impulse wave generation and its effects on dams are presented including a computation procedure. Based on this method, engineers or natural scientists may predict the dangers originating from impulse waves efficiently and economically.

The introduction in Chapter 1 contains background information on the topic and compares the available methods dealing with landslide generated impulse waves. The method presented in this manual is based on *generally applicable equations*. Chapter 2 introduces basic principles of the water wave theory. The computation procedure is presented in Chapter 3 and shown in Figure 3-1. It is based on the findings of the two items wave generation (Appendix A) and effects of impulse waves on dams (Appendix B). The computation procedure (Figure 3-1) includes two steps: in the 1st *step* the generally applicable equations are applied according to Chapter 3, whereas in the 2nd *step* the effects not contained in the 1st step such as the effective instead of the idealized reservoir geometry are considered according to Chapter 4.

In the 1st step, the mass movement is modelled as a granular slide. To analyse the effect of impulse waves on dams the wave height, amplitude, period and length are important. These are computed with the equations of Heller (2007a) as a function of the slide parameters. Two extreme cases for estimating the wave parameters are considered: (a) laterally constricted (2D) and (b) free radial propagation of the impulse waves (3D). The wave generation in both (a) and (b) depend on the identical parameters, whereas these for the wave propagation are not identical. Once the necessary wave parameters in front of the dam are determined, the *run-up height* and the *overtopping volume* may be computed according to Müller (1995). Since the impulse wave profiles and the water particle movement may differ considerably from case to case, the *force effects* on dams are computed with two methods: for relatively small *Stokes-like waves*, including deep to intermediate-water waves of oscillatory character, the method of Sainflou (1928) is proposed, and for the *remaining wave types* involving relatively large wave heights, including intermediate to shallow-water waves of translational character, using the method of Ramsden (1996). To distinguish between these wave types the 2D criterion of Heller (2007a) is accounted for. Both methods are first applied as if the dam would be vertical since the horizontal force component is independent from the dam inclination. The additional vertical force component for inclined dams then is computed assuming static wave pressure. If an impulse wave partially overtops a dam, only a partial water pressure has to be considered resulting in a reduction method for the *remaining wave types*.

Once the results from the 1st step are available, the effects of the geometrical differences to the idealised extreme cases (a) and (b) have to be quantified in the 2nd *step* according to Chapter 4. These differences may be caused by the three-dimensional reservoir geometry differing from the idealised 2D or 3D geometries, or by the non-granular mass characteristics. The impulse wave parameters may considerably differ due to these effects. The 2nd step is also required if the spread sheets are applied, because these include only the generally applicable equations from the 1st step. Finally, Section 4.4 contains a sensitivity analysis and some reservoir safety aspects.

The Chapter 5 includes two computation examples and the application instructions for the spread sheets in Excel. In Chapter 6 the conclusions and open questions concerning landslide generated impulse waves are presented.

Although the computational results, such as the run-up height, seem to be exact, it should be kept in mind that the present method results in estimations. Safety allowances for all planned actions have to be considered. More exact predictions may emerge from a prototype-specific model test or with numerical simulations.

Zusammenfassung

Rutscherzeugte Impulswellen entstehen in Ozeanen, Meeresbuchten und in natürlichen oder künstlichen Seen typischerweise durch Erdrutsche, Felsstürze, Uferinstabilitäten, Schneelawinen oder Gletscherkalbungen. Im Alpenraum sind sie aufgrund der steilen Talflanken, dem Potential grosser Rutschvolumina mit grossen Eintauchgeschwindigkeiten und der grossen Anzahl künstlicher Stauseen relevant. In diesem Manual wird das gegenwärtige Wissen über die Impulswellengenerierung und deren Einwirkungen auf Talsperren zusammengetragen und vervollständigt. Schliesslich wird daraus ein Berechnungsverfahren entwickelt. Der Ingenieur oder Naturwissenschaftler kann somit die von Impulswellen ausgehenden Gefahren nach dem neuesten Wissensstand relativ schnell und kostengünstig abschätzen.

Die Einleitung (Kapitel 1) beinhaltet neben einigen Hintergrundinformationen einen Vergleich der verschiedenen Methoden im Umgang mit rutscherzeugten Impulswellen. Dabei basiert das in diesem Manual entwickelte Verfahren auf *allgemeingültigen Berechnungsgleichungen*. Im Kapitel 2 wird auf die theoretischen Wellengrundlagen eingegangen. Das eigentliche *Berechnungsverfahren* wird im Kapitel 3 erläutert und ist in Abbildung 3-1 dargestellt. Es basiert auf den Erkenntnissen zu den Themenkreisen Wellengenerierung (Anhang A) und Auswirkungen von Impulswellen auf Talsperren (Anhang B). Das Berechnungsverfahren (Abbildung 3-1) basiert auf zwei Schritten: Im 1. *Schritt* werden die allgemeingültigen Berechnungsgleichungen gemäss Kapitel 3 angewendet, im 2. *Schritt* werden gemäss Kapitel 4 die im 1. Schritt nicht berücksichtigten Einflüsse wie die nicht ideale Stauraumgeometrie qualitativ abgeschätzt.

Im 1. *Schritt* wird die Massenbewegung als granularer Rutsch modelliert. Hinsichtlich der Auswirkungen der Impulswellen auf Talsperren haben die Wellenhöhe, die Wellenamplitude, die Wellenperiode sowie die Wellenlänge Einfluss und werden mit den Berechnungsformeln nach Heller (2007a) in Funktion der Rutschparameter ermittelt. Zur Bestimmung dieser Wellenparameter stehen zwei Extremfälle zur Verfügung: (a) eingeengte transversale Ausbreitung (2D) bzw. (b) komplett freie radiale Ausbreitung der Impulswellen (3D). Während in beiden Fällen zur Wellengenerierung die gleichen Einflussparameter massgebend sind, sind diese bezüglich der Impulswellenabnahme verschieden. Sind die Wellenparameter vor der Talsperre bekannt, so kann die *Auflaufhöhe* bzw. das *Überschwappvolumen* nach Müller (1995) berechnet werden. Da Impulswellen hinsichtlich Profil und der inneren Wasserpartikelbewegung unterschiedlich sein können, wird ihre *Krafteinwirkung* mit zwei Methoden berechnet: Für die relativ kleinen *Stokes-ähnlichen Wellen*, welche den Tief- bis Übergangswasserwellen mit oszillatorischem Charakter zugeordnet werden, wird die Methode von Sainflou (1928) verwendet und für die *restlichen Wellentypen* mit relativ grosser Höhe, welche sich eher wie Übergangs- bis Flachwasserwellen mit translatorischem Charakter verhalten, die Methode nach Ramsden (1996). Die Unterscheidung zwischen den Wellentypen ist mit einem 2D Kriterium nach Heller (2007a) möglich. Beide Methoden werden

zuerst angewendet, als ob die Talsperre wasserseitig senkrecht wäre. Für eine geneigte Talsperre ist die horizontale Kraftkomponente unabhängig von der Talsperrenneigung, und die zusätzliche vertikale Kraftkomponente kann unter der Annahme einer statischen Wasserdruckverteilung der Welle ermittelt werden. Schwappt ein Teil der Impulswelle über, greift nicht die ganze Kraft an der Talsperre an. Deshalb kommt für die *restlichen Wellentypen* ein entsprechendes Reduktionsverfahren zur Anwendung.

Nachdem die Ergebnisse aus dem 1. Schritt vorliegen, müssen die Effekte aus den geometrischen Abweichungen zu den idealisierten Extremfällen (a) und (b) in einem 2. *Schritt* gemäss Kapitel 4 qualitativ abgeschätzt werden. Diese Abweichungen entstehen durch die dreidimensionale Stauraumgeometrie, die von der idealisierten 2D- oder 3D-Betrachtung abweicht oder wenn die Masse keine granulare Konsistenz aufweist. Die Impulswellenparameter können sich durch diese Einflüsse stark verändern. Der 2. Schritt ist ebenfalls erforderlich, wenn die elektronischen Berechnungstabellen angewendet werden, da diese nur auf den allgemeingültigen Berechnungsgleichungen des 1. Schritts basieren. Schliesslich werden in Unterkapitel 4.4 eine Sensitivitätsanalyse durchgeführt sowie einige Überlegungen zu Sicherheitszuschlägen angestellt.

Das Kapitel 5 enthält zwei Rechenbeispiele sowie eine Anleitung zur Anwendung der elektronischen Berechnungstabellen in Excel. In Kapitel 6 werden die Schlussfolgerungen gezogen sowie die noch offenen Fragen betreffend rutscherzeugter Impulswellen aufgezeigt.

Trotz der scheinbar rechnerisch genauen Ermittlung beispielsweise der Auflaufhöhe liefert das vorliegende Verfahren lediglich Abschätzungen. Bei allen geplanten Massnahmen ist daher ein Sicherheitszuschlag zu berücksichtigen. Genauere Voraussagen sind mit einer prototyp-spezifischen Modelluntersuchung oder mit numerischen Simulationen zu erzielen.

Résumé

Les ondes d'impulsions résultent du glissement de masses instables (glissement de terrain, chute de blocs, rocheux, avalanches de neige ou chute de glacier) sur un plan d'eau (océan, baies, retenues d'eau naturelles ou artificielles). Ces phénomènes sont particulièrement importants dans les vallées alpines pentues (comportant généralement beaucoup de retenues), où les masses mises en mouvement et leurs vitesses d'impacts sur les plans d'eau peuvent être considérables. Dans ce *manual*, les connaissances actuelles sur la génération et la propagation des ondes d'impulsion ainsi que leurs actions sur des barrages sont présentées et complétées pour développer un procédé de calcul, qui aide l'ingénieur dans l'estimation des dangers liés à ce phénomène.

L'introduction (Chapitre 1) contient, outre des informations de fond, une comparaison des diverses méthodes pour modéliser les ondes d'impulsion générées par des glissements. Le procédé de calcul proposé dans ce manual se base sur des *équations généralisées*. Dans le Chapitre 2, les bases théoriques des ondes hydrauliques sont introduites. Le procédé de calcul proprement dit est décrit dans le Chapitre 3 et est illustré par la Figure 3-1. Il est basé sur les connaissances acquises sur la génération d'ondes (Annexe A) et sur les effets des ondes d'impulsion sur les barrages (Annexe B). Le procédé de calcul, décrit dans la Figure 3-1, se déroule en deux étapes : Dans la 1. *étape*, les équations généralisées décrites dans le Chapitre 3 sont appliquées. Puis, dans la 2. *étape*, les effets non pris en compte dans la 1. étape (tels que la géométrie de la retenue d'eau) sont intégrés dans le Chapitre 4 à l'aide d'une estimation appropriée.

Dans la 1. *étape*, le mouvement de masse est modélisé comme un éboulement granulaire. Pour caractériser l'effet des ondes d'impulsion sur les barrages, nous déterminerons les paramètres, tels que la hauteur d'onde, l'amplitude d'onde, la période d'onde et la longueur d'onde, à l'aide des équations proposées par Heller (2007a), en fonction des paramètres de l'éboulement. En ce qui concerne la détermination de ces paramètres d'ondes, deux cas extrêmes sont proposés : (a) propagation d'ondes en canal (2D) et (b) propagation d'ondes dans l'espace sans parois latérales (3D). Tandis que dans les deux cas les mêmes paramètres influencent la propagation d'ondes, on constate des différences importantes concernant la réduction de la hauteur d'onde. Une fois les paramètres d'onde devant un barrage déterminés, la *hauteur de run-up* et *le volume de surverse* peuvent être calculés selon Müller (1995). Comme le profil de surface et la distribution des vitesses peuvent varier selon le type d'onde d'impulsion, l'effet des forces s'exerçant sur un barrage est déterminée par deux méthodes : Pour les petites ondes relatives du type de *Stokes*, (valables des eaux profondes à des eaux de profondeurs intermédiaires avec un caractère d'oscillation) le procédé de Sainflou (1928) est appliqué, tandis que le reste des ondes d'impulsion de grandes hauteurs relatives (valables des eaux de profondeurs intermédiaires à des eaux peu profondes avec un caractère de translation) ont été traitées selon la méthode de Ramsden (1996). La distinction entre les deux types d'ondes est possible grâce au critère de Heller (2007a). Les deux méthodes

sont tout d'abord appliquées au cas d'un barrage ayant un parement amont vertical. Dans le cas réel où le parement est incliné, la composante horizontale est indépendante de l'inclinaison du parement. Il est donc possible de déterminer la composante verticale de la force pour un barrage au parement incliné en admettant une répartition hydrostatique de la pression dans l'onde. Si une partie de l'onde surverse le barrage, seulement une partie de la force est à considérer. Cette force se détermine avec un procédé de réduction pour les ondes d'impulsion dans l'eau peu profonde.

Une fois les résultats de la 1. étape déterminés, les effets dus aux approximations et à l'idéalisation des cas extrêmes (a) et (b) doivent être prises en considération dans une 2. *étape*, et seront évalués qualitativement dans le Chapitre 4. Ces écarts par rapport à la réalité provient de la géométrie 3D réelle du barrage, différente des cas 2D et 3D idéalisés, ou de la nature non granulaire du glissement de terrain en masse. Ces différents effets peuvent avoir une grande influence sur les paramètres d'onde d'impulsion. Une 2. étape est également nécessaire lorsque le calcul électronique est appliqué, vu que ce procédé se base uniquement sur les équations généralisées de la 1. étape. Finalement, une analyse de sensibilité est proposée dans le Sous-chapitre 4.4 ainsi que des réflexions relatives aux marges de sécurité à adopter.

Le Chapitre 5 contient deux exemples de calcul et un procédé pour l'application des tables de calcul électronique sur Excel. Le Chapitre 6 tire les conclusions de cette étude et discute des questions ouvertes dans le domaine des ondes d'impulsion.

Il est à noter que les calculs relatifs aux ondes d'impulsion peuvent seulement être considérés comme des estimations. Des facteurs de sécurité sont à appliquer quelque soit les mesures préventives envisagées. Des informations plus précises peuvent seulement être obtenues à l'aide de prototype de modèles réduits hydrauliques ou à l'aide de simulations numériques appropriées.

Sommario

Le onde d'impulso generate da fenomeni di scivolamento si formano negli oceani, nelle baie marine e nei laghi naturali o artificiali, tipicamente in seguito a frane, smottamenti, instabilità di pendii, valanghe o distaccamenti di masse di ghiaccio. Questo tipo di onda riveste una notevole importanza nella regione alpina data la presenza di pendii ripidi, del potenziale volume delle masse in movimento con conseguenti velocità di immersione elevate e del grande numero di laghi artificiali. Il presente manuale raccoglie e completa le conoscenze odierne in materia di generazione di onde d'impulso e della loro influenza sugli sbarramenti e ne sviluppa in seguito un metodo di calcolo. Grazie ad esso l'ingegnere o il ricercatore scientifico è in grado di valutarne i pericoli in maniera relativamente veloce ed economica basandosi sulle conoscenze più attuali.

L'introduzione (Capitolo 1) contiene, oltre alle informazioni di base, un confronto dei diversi metodi in relazione alle onde d'impulso generate da fenomeni di scivolamento. Il metodo sviluppato nel presente manuale si basa su *equazioni di calcolo generalmente valide*. Nel Capitolo 2 viene approfondito il tema dei principi teorici fondamentali riguardanti le onde. Il *metodo di calcolo* vero e proprio è illustrato nel Capitolo 3 ed è rappresentato in Figura 3-1. Esso si basa sulle conoscenze nell'ambito di generazione delle onde d'impulso (Appendice A) e delle loro ripercussioni sugli sbarramenti (Appendice B). Il procedimento di calcolo (Figura 3-1) avviene in due fasi: dapprima vengono applicate le equazioni di calcolo generalmente valide secondo il Capitolo 3 e in seguito, secondo il Capitolo 4, vengono stimati qualitativamente i fattori d'influenza non considerati nella prima fase, quali ad esempio la geometria non ideale della zona di retenzione.

Nella *prima fase* la massa in movimento viene modellata come scivolamento granulare. L'altezza, l'amplitudine, il periodo e la lunghezza dell'onda d'impulso esercitano una certa influenza in relazione alle sue conseguenze sugli sbarramenti. Tali parametri vengono determinati mediante le formule di Heller (2007a) in funzione dei parametri di scivolamento. Per determinare i parametri relativi all'onda, vengono considerati due casi estremi della sua propagazione: (a) propagazione trasversale ristretta (2D) e (b) propagazione radiale completamente libera (3D). Mentre in entrambi i casi i medesimi parametri influenti sono determinanti per la generazione dell'onda, essi sono tuttavia diversi per quanto riguarda la sue diminuzione. Nel caso in cui essi siano conosciuti a monte dello sbarramento, *l'altezza traboccante* e rispettivamente il *volume di traboccamento* possono essere calcolati secondo Müller (1995). Dato che le onde d'impulso possono differire per quanto riguarda il profilo e il movimento interno delle particelle d'acqua, *l'effetto della loro forza* viene calcolato in due modi: per le *onde di tipo Stokes*, relativamente piccole, dal comportamento simile a onde in acque da profonde a intermedie con carattere oscillatorio, viene applicato il metodo di Sainflou (1928) mentre per gli *altri tipi di onde* con un'altezza relativamente grande, le quali si comportano prevalentemente come onde in profondità da intermedie a piccole con un

carattere di traslazione, viene applicato il metodo di Ramsden (1996). Il criterio bidimensionale secondo Heller (2007a) permette la differenziazione del tipo di onda. Entrambi i metodi vengono applicati inizialmente come se il paramento di monte dello sbarramento fosse perpendicolare. Per uno sbarramento inclinato la componente orizzontale della forza è indipendente dall'inclinazione dello sbarramento e la componente verticale aggiuntiva può essere determinata ammettendo una distribuzione idrostatica della pressione dell'onda. Nel caso in cui una parte dell'onda d'impulso dovesse traboccare, non tutta la forza viene esercitata sullo sbarramento, perciò si può applicare un adeguato procedimento di riduzione per gli *altri tipi di onde*.

Dopo che i risultati della prima fase sono a disposizione, nella *seconda fase*, secondo il Capitolo 4, gli effetti delle differenziazioni geometriche dai casi limiti ideali (a) e (b) sono approssimati qualitativamente. Tali differenze risultano dalla geometria tridimensionale dello sbarramento che differisce dall'analisi idealizzata bi- o tridimensionale oppure nel caso in cui la massa non presenti una consistenza granulare. A causa di questi effetti, i parametri delle onde d'impulso possono variare considerevolmente. La seconda fase è altrettanto necessaria in caso vengano impiegate tabelle elettroniche di calcolo, in quanto quest'ultime si basano unicamente sulle equazioni di calcolo generalmente valide della prima fase. Infine, nel sottocapitolo 4.4, viene eseguita un'analisi della sensibilità e vengono mostrate alcune considerazioni concernenti le sicurezze supplementari.

Il Capitolo 5 contiene due esempi di calcolo e le istruzioni per l'applicazione della tabella elettronica di calcolo in Excel. Nel Capitolo 6 sono esposte le conclusioni e vengono mostrate le questioni ancora aperte sul tema delle onde d'impulso generate da fenomeni di scivolamento.

Nonostante la valutazione aritmetica apparentemente esatta dell'altezza di traboccamento, a titolo di esempio, il presente procedimento fornisce unicamente un'approssimazione. Una sicurezza supplementare è quindi da tenere in considerazione per qualsiasi provvedimento pianificato. Previsioni più precise possono essere ricavate da uno studio specifico su prototipo oppure da simulazioni numeriche.

1 Introduction

1.1 Overview

Impulse waves typically occur in open oceans, bays, lakes and reservoirs as the result of landslides, rockfalls, shore instability, avalanches or glacier calvings. They are classed as gravity waves and can, in extreme cases, result in the overtopping of dams, with catastrophic consequences. Alpine regions face a high risk of such events in view of their steep valley flanks, their potentially large slide volumes, with high impact velocities, and their large number of reservoirs (Heller 2007a).

One extreme event was the Vaiont reservoir catastrophe which occurred in 1963. After the reservoir had been impounded for the first time behind the 261.60 m high double-curved arch dam, the left valley flank became unstable. About 300 million m^3 of earth and rock, twice the active reservoir capacity, slid into the reservoir. Displaced reservoir water spilled over the dam crest, to a depth of at least 70 m, and swept through the village of Longarone. About 2,000 people lost their lives. The dam itself withstood this extreme event with almost no damage (Schnitter 1964).

Impulse waves have also occurred in Switzerland or, as a precaution, have been analysed numerically or investigated in hydraulic models. Examples are Walensee (Huber 1975) and Urnersee (Müller and Schurter 1993). Huber (1982) summarised about fifty documented events in Switzerland over the past 600 years. On 20 June 2007, a rockfall into Lake Lucerne, near Obermatt, created an impulse wave which caused slight damage when it flowed up into the village of Weggis, on the opposite shore of the lake.

Schuster and Wieczorek (2002) presented several possible causes of mass movements. In addition to classic scenarios such as earthquake and intense rainfall, they described 46 cases of slides which followed rapid changes in the water level of reservoirs, for instance during first impounding. Only in rare cases has it been possible to arrest the mass movement; one example is Clyde reservoir in New Zealand (MacFarlane and Jenks 1996). In most cases only passive measures to minimise damage are possible and include evacuation of the population, reservoir drawdown, controlled blasting and, when designing the dam, provision of adequate freeboard. For early risk assessment of a threatening slide, empirical equations can help to determine the potential danger.

Generally applicable equations are quickly and easily used in practice. They can provide an initial estimate of the most important wave properties, such as wave height and run-up height against the dam, and this information on the effects of the impulse waves can help when taking decisions on any further preventive measures which may be needed. However, such equations provide only a first estimate, of the wave height for instance, as they largely neglect the geometry of the reservoir (Section 4.2). But impulse waves may be greatly affected by water depth variations or by the shape of the reservoir

basin. More extensive methods are available for more precise analysis, as discussed in Section 1.2.

The aim of this manual is to formulate a practical computation procedure using the generally applicable equations that are in current use. This is worthwhile because researchers' understanding of these processes has improved in recent years (e.g. Müller 1995; Ramsden 1996; Heller 2007a). Computation examples and electronic calculation spread sheets in Excel have made it easier to make use of this procedure.

The equations described in this manual are based principally on granular slide material. The parameters of the mass movement are uniformly referred to as slide, for example slide thickness, although other mass movement types such as fall or topple exist. The mass movement types and their influence on wave parameters are discussed in Section 4.3.

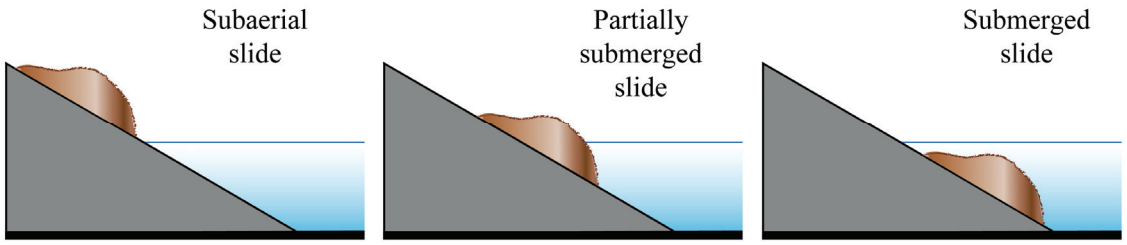

Figure 1-1 The ways in which impulse waves can be generated.

Figure 1-1 shows three ways in which impulse waves can be generated. Slides can be activated subaerial, partially submerged or wholly submerged. In this manual, only slide masses located above water level are considered, as these represent most cases encountered in Switzerland. Slides activated partially or wholly submerged are less common in Switzerland and, as most develop unnoticed, no time is available for their observation or predictive analysis.

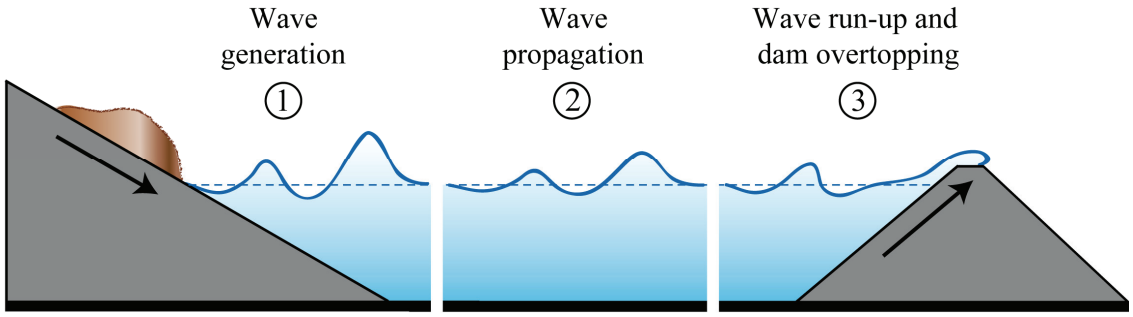

Figure 1-2 The three phases of an impulse wave above a horizontal reservoir bed: (1) slide impact with wave generation, (2) wave propagation with wave transformation and (3) impact and run-up of the impulse wave with load transfer to the dam and, in some cases, overtopping of the dam (after Heller 2007a).

Figure 1-2 shows the three phases of impulse wave development above a horizontal reservoir bed: (1) slide impact with wave generation, (2) wave propagation with wave

transformation and (3) impact and run-up of the impulse wave with load transfer to a dam and in some cases overtopping of the dam. In narrow reservoirs, phase (2) may not occur. The mechanisms of phases (1) and (2) are both covered by the same equations, which are discussed in Section 3.2 and in Appendix A. Other researchers have described phase (3) with so-called run-up equations, which are described in Section 3.3 and Appendix B.

1.2 Methods for predicting landslide generated impulse waves

In this manual, a computation procedure, based on generally applicable equations, is developed for the assessment of landslide generated impulse waves. Firstly, for a better appraisal of the advantages and disadvantages of this procedure, the available methods relating to landslide generated impulse waves are discussed. Basically the following five methods exist:

(i) Generally applicable equations developed from model tests
(ii) Prototype-specific model tests
(iii) Numerical simulations
(iv) Empirical equations derived from field data
(v) Analytical investigations

Table 1-1 Comparison of the five methods for the prediction of landslide generated impulse waves.

Criterion	Method (i)	Method (ii)	Method (iii)	Method (iv)	Method (v)
Quality of results	Estimation	Exact	Estimation - exact	Rough estimate	Rough estimate
Time requirement	Low	Very high	High - very high	Low	Low
Cost	Low	Very high	High - very high	Low	Low
User	Engineer	Engineer	Expert	Engineer	Engineer
Clarity	Medium	High	Low	Medium	Low
Effort for governing parameters	Medium	High	High	Medium	Medium

Table 1-1 compares the five methods, based on the following criteria: the quality of the results, time requirement and cost, the user of each method, the clarity of the results and the efforts needed to determine the governing parameters required for each procedure. These include the parameters describing the topography of the reservoir and the slide geometry as well as the slide characteristics. Table 1-1 shows that, in general, the more precise the results the greater the time expended and cost. Likewise, the effort needed to determine the governing parameters increases accordingly; this is because more data are needed about the geometry of the reservoir and the slide, as well as about the slide characteristics. As explained in Section 1.2, the two last methods, (iv) and (v), are still not fully developed, and this means that methods (i) to (iii) are the most suitable for use in practice. The quality of the results and the time and cost of numerical simulations depend above all on the equations applied and the simplifications made. Table 1-1 shows *where* the strengths of the generally applicable equations lie: an engineer may

make an assessment of, for example, the run-up height R on the dam face at little cost and in a short time, and only moderate effort is needed to determine the governing parameters. Particular points relating to each method, not mentioned in Table 1-1, will now be discussed individually and illustrated with examples taken from the technical literature.

(i) Generally applicable equations developed from model tests

A literature review for generally applicable equations is given in Appendices A and B. Figure 1-3 shows two generally applicable model tests in (a) a wave basin and (b) a wave channel. In addition to the points indicated in Table 1-1, the following advantage and disadvantages of this method need to be mentioned:

+ The results aid in deciding whether more precise investigations with a prototype-specific model or numerical simulations are necessary.
− Scale effects in too small models cannot be ignored and model effects (reflection, refraction, diffraction etc.) occur with geometrical variations from the prototype.
− Special cases are often not investigated, since the available equations are limited on simple geometries.

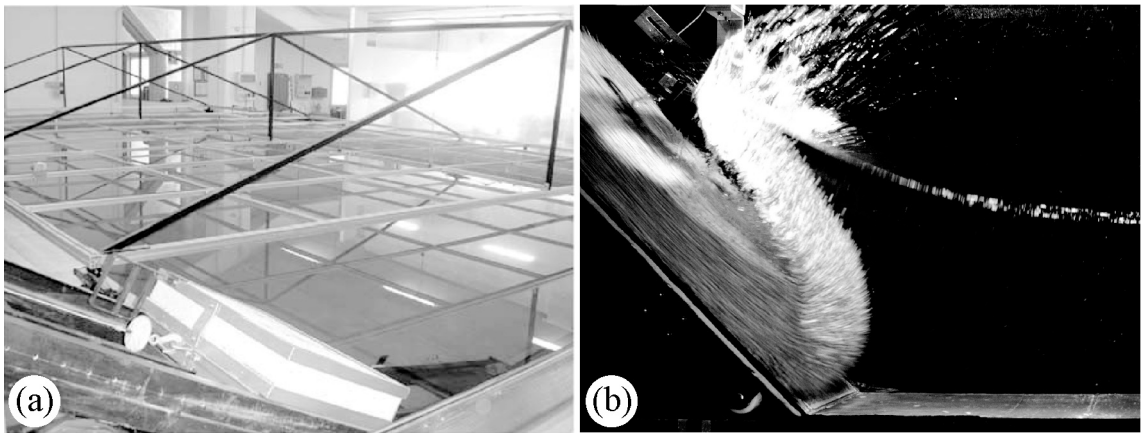

Figure 1-3 Generally applicable model tests: (a) rigid body prior to impact into a wave basin (Panizzo et al. 2005) and (b) granular slide material during impact into a wave channel (Heller et al. 2008).

This method is often the only possibility when calculations have to be done quickly, for instance when a landslide already shows signs of slow movement. In order to be able to neglect scale effects, the following rules of thumb may be followed: the still water depth in the slide impact zone should be $h \geq 0.200$ m (Heller et al. 2008) and in addition the wave period should be $T > 0.35$ s (Hughes 1993), such that the waves (as gravity waves) are dominated by gravity and not by surface tension forces (as capillary waves). For a prototype in which $h = 50$ m, the first rule leads to a mini-

mum scale of 1:250. An associated reservoir surface area of one million m^2 would correspond to a modelled area of $1{,}000{,}000/250^2 = 16\ m^2$. More precise data on scale effects related to impulse waves were defined by Heller et al. (2008). Model effects, i.e. effects arising mainly from differences between the geometry of the reservoir basin to the model may be taken into account qualitatively by employing the methods described in Section 4.2.

(ii) Prototype-specific model tests

Prototype-specific model tests were carried out for example by Müller and Schurter (1993) for planned rock blasting on Urnersee, as shown in Figure 1-4(a), as well as by the Western Canada Hydraulic Laboratories (WCHL 1970) for a potential slide above Mica reservoir as shown in Figure 1-4(b). In addition to the points shown in Table 1-1, the following disadvantages of this method should be noted:

- Scale effects cannot be neglected in too small models.
- Model effects may occur with geometric simplifications.

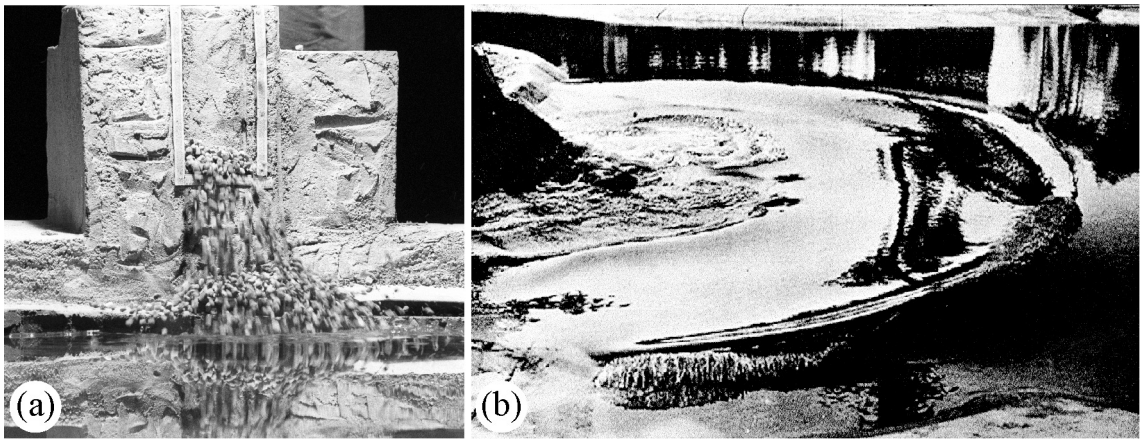

Figure 1-4 Prototype-specific model tests: (a) for planned rock blasting on Urnersee (Müller and Schurter 1993) and (b) for Mica reservoir (Western Canada Hydraulic Laboratories 1970).

To allow scale effects to be neglected, the same rules of thumb apply as for method (i): $h \geq 0.200$ m in the impact zone and $T > 0.35$ s. For a prototype with $h = 50$ m, the first of these criteria gives a minimum scale of 1:250, which means that the corresponding reservoir area of 1,000,000 m^2, according to (i), will be represented by 16 m^2 in the model. Therefore, it is often impossible to model the entire reservoir with negligible scale effects, because of limited availability of space and the corresponding cost. An alternative method is to model only the impact zone and the wave run-up zone and then attempt to estimate the wave transformation between them. Knowledge of the reservoir geometry is essential for the precise determination of the wave characteristics, especially when shallow-water or intermediate-water waves are expected. This is because waves of these types are affected by the reservoir bed

(Section 2.1). For deep-water waves, which are not affected by the reservoir bed, the reservoir geometry must be known above all in the slide impact and wave run-up zones.

(iii) Numerical simulations

Published works on numerical simulations of landslide generated impulse waves were carried out, for example, by the following researchers: Falappi and Gallati (2007) used the Smoothed Particle Hydrodynamics (SPH) method to simulate an experiment by Fritz (2002), as shown in Figure 1-5(b). Quecedo et al. (2004) used the complete Navier-Stokes equations to simulate the Lituya Bay slide of 1958. Zweifel et al. (2007) used the shallow-water equations for their simulations of model tests. Furthermore, Fäh (2005) modelled impulse waves in a snow-melt lake following a possible partial collapse of the Trift glacier, making use of shallow-water and Boussinesq equations.
In addition to the points shown in Table 1-1, the following advantage and disadvantages of this method should be noted:

+ This method will gain in significance with continuing development of computer capacity.
− Calibration and validation data are needed; for landslide generated impulse waves these are usually derived from hydraulic model tests.
− Simplifications of the Navier-Stokes equations are necessary, as well as limitation on one section of the reservoir, or the use of a coarse calculation grid, in order to keep the computation time within acceptable limits.

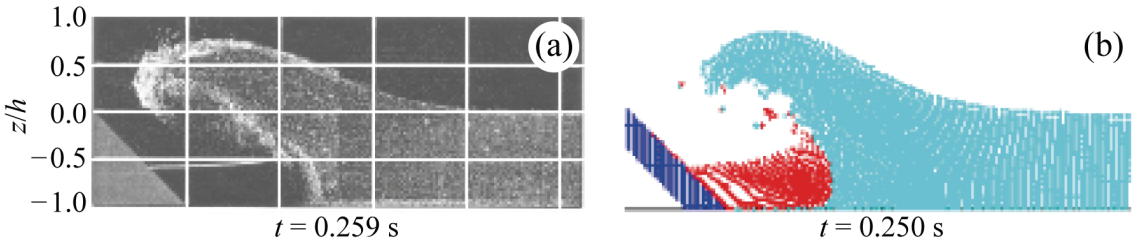

Figure 1-5 Numerical analysis using Smoothed Particle Hydrodynamics: (a) hydraulic model tests by Fritz (2002) and (b) corresponding numerical simulation by Falappi and Gallati (2007)

For the purposes of calibration and validation, most numerical models are compared with data from model tests and only then used for the given reservoir geometry. The scale or model effects of hydraulic models correspond numerically to the simplification of the basic equations adopted for the analysis. Despite good results in individual cases in comparison with data from the hydraulic models, the authors are not aware of any reliable general model for simulating landslide generated impulse

waves that may be used to analyse any given slide mass and reservoir geometry (Section 6.2).

(iv) Empirical equations derived from field data

Ataie-Ashtiani and Malek Mohammadi (2007) have derived equations from field data but no other publications on this approach are known of by the authors. In addition to the points shown in Table 1-1, the following advantage and disadvantages of this method need to be stated:

+ No scale effects.
− Based on field data which are mostly estimates rather than measurements (for instance wave heights indirectly calculated using run-up heights).
− Governing parameters are also only estimates (for example based on underwater deposits of slide material).
− The equations of Ataie-Ashtiani and Malek Mohammadi (2007) allow only the wave amplitude to be calculated; there is no known work on the determination of other wave parameters.

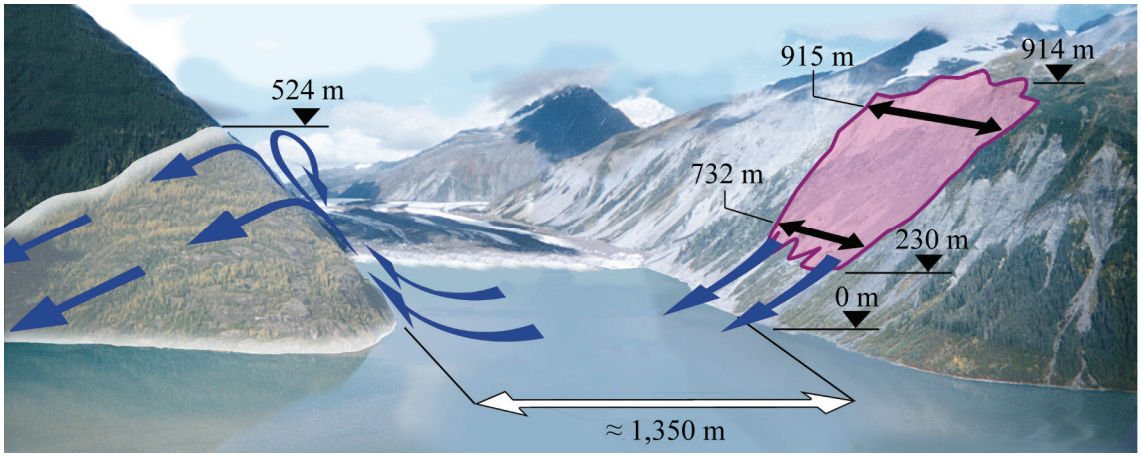

Figure 1-6 Field data: photomontage of the 1958 Lituya Bay case showing the boundaries of the slide area and the maximum wave run-up height of 524 m on the opposite shore of the bay (after Fritz 2002).

The Lituya Bay case of 1958 shown in Figure 1-6 is a rare but fortunate event for researchers because knowing the run-up height on the opposite shore yields information on an impulse wave close to the slide impact location. Few other reliable field data are known to exist. As a result, equations derived from field measurements are hardly valid for general practice.

(v) Analytical investigations

Analytical equations were derived for example by Noda (1970) and Di Risio and Sammarco (2008). A comparison of these two methods with an impulse wave generated in a hydraulic model by a solid mass (Di Risio 2005) is shown in Figure 1-7. In addition to the points shown in Table 1-1, analytical investigations have the following advantage and disadvantages:

+ No scale effects.
− The impact mechanism is too complex to be described analytically, so predictions for the far field can only be based on simplified initial conditions.
− Deduction of the results is difficult to follow.
− Simplifications are necessary, e.g. use of linear-wave theory, potential theory etc., which allows consideration of only relatively small and symmetrical waves.

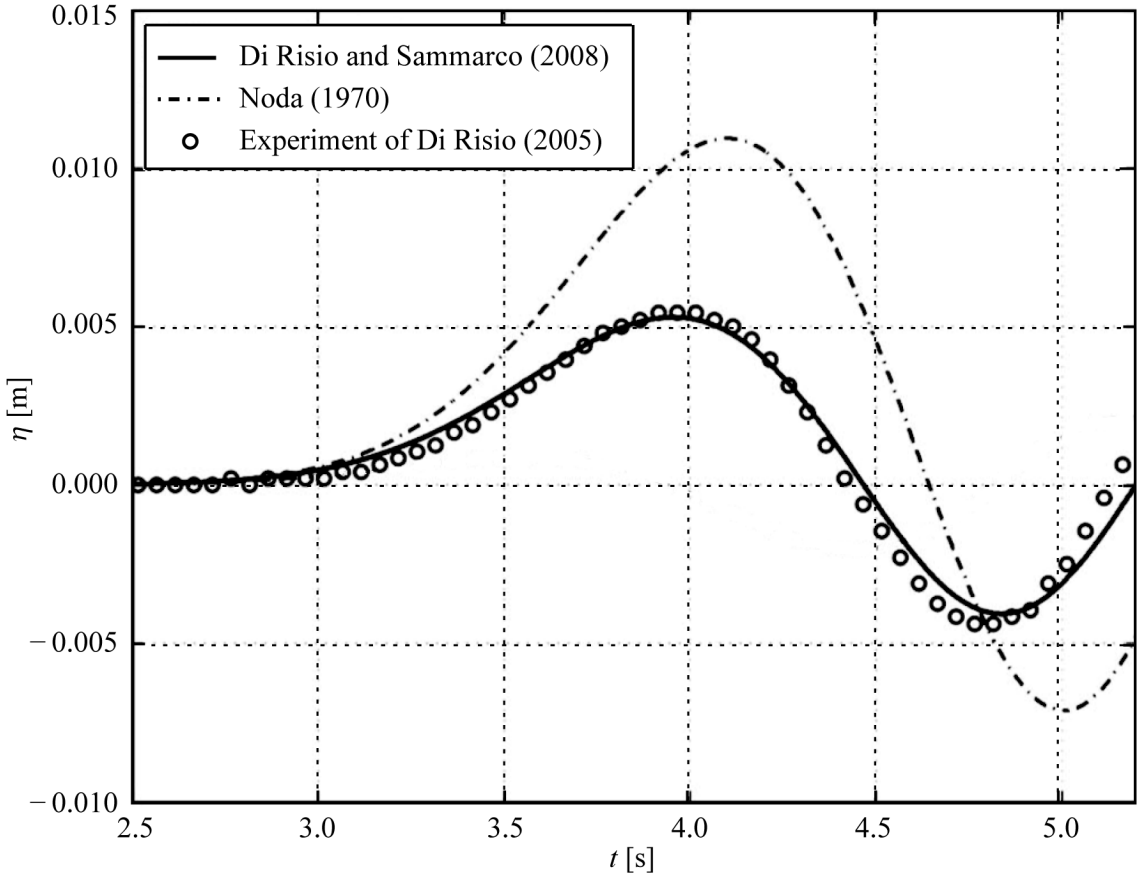

Figure 1-7 Comparison of the analytical computation of a landslide generated impulse wave profile at a distance x = 5.30 m from the impact location with an experiment (Di Risio and Sammarco 2008).

As this method may provide predictions only for very idealised slides and then only in the far field, it is not very useful for practical application.

The first three methods, (i) to (iii), are of practical relevance for the assessment of landslide generated impulse waves and their effects. Sometimes it may be better to use *hybrid modelling*, i.e. to combine model testing with numerical analysis. This may be done, for example, when the criteria for negligible scale effects in the hydraulic model allow only the investigation of the generation of the waves; the wave propagation will therefore be calculated numerically, or if a part of the reservoir is studied using a hydraulic model, the results obtained are then used to calibrate a numerical model. Naturally, the time required and the cost increase with this method.

2 Water wave theory

2.1 Introduction

This chapter explains the most important properties of water waves. Landslide generated impulse waves belong to the category of gravity waves, i.e. they are principally influenced by the gravitational force in contrast to capillary waves.

The relevant wave parameters are shown in Figure 2-1 in the (x, z) plane, on a defined *sine wave* whose profile describes a sine curve. If the sine wave is small ($H/h < 0.03$) and flat ($H/L < 0.006$) it is also referred to as a linear wave. The original water depth is defined as the still water depth h. The wave height H is measured from the trough, i.e. from the lowest point on the wave surface to the crest, the highest point. The wave amplitude is the height from the undisturbed water surface to the wave crest. For the sine wave shown in Figure 2-1, $a = H/2$. This no longer applies for impulse waves, which are generally non-linear and vary from the perfect sine wave (Figure 2-1). Furthermore the wave length L extends from wave node to node, crest to crest or trough to trough. The wave period T is the time it takes for the crests, nodes or troughs, respectively, of two successive waves, to pass a fixed point. For the sine wave, the period can be calculated as $T = L/c$, in which c is the wave celerity. The square of the celerity for a linear *sine wave* is given by

$$c^2 = \frac{gL}{2\pi}\tanh\left(\frac{2\pi h}{L}\right). \tag{2.1}$$

c [m/s]	=	Wave celerity (Figure 2-1)
g [m/s^2]	=	Gravitational acceleration; g = 9.81 m/s^2
h [m]	=	Still water depth
L [m]	=	Wave length (Figure 2-1)
π [-]	=	Circular constant; π = 3.14

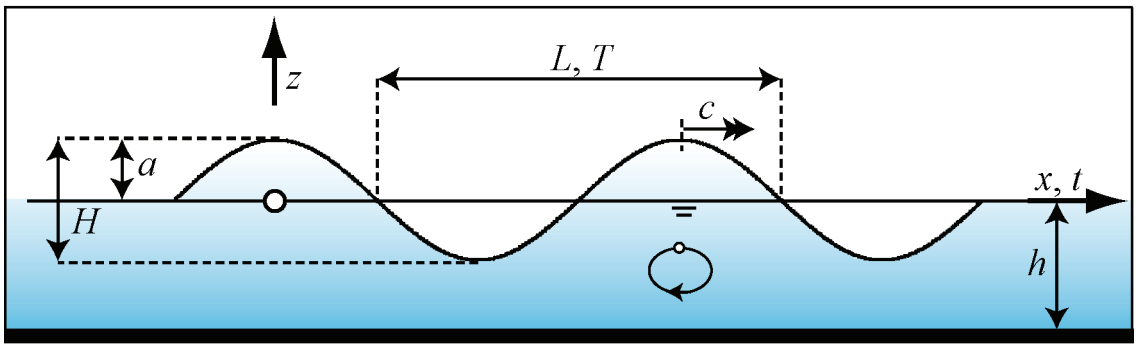

Figure 2-1 Principal wave parameters presented on an idealised sine wave (in addition, the wave is said to be linear if $H/h < 0.03$ and $H/L < 0.006$).

The following terms can be used to differentiate between various water wave types:

a) Oscillatory or translatory waves
b) Shallow, intermediate or deep-water waves
c) Periodic or non-periodic waves
d) Linear or non-linear waves

a) Oscillatory or translatory waves

In water waves, the individual particles of water do not move in the same way as the water surface or the wave celerity c. This may be seen in Figure 2-1, where the orbital motion of a water particle is shown for an *oscillatory wave*. Whilst the water surface seems to advance at the wave celerity, the water particle moves elliptically and, over the period considered, remains in the same position. Oscillatory waves do not therefore transport fluid mass, but only energy, which sets the surrounding water particles in motion. *Translatory waves* are the opposite, as the water particles move horizontally in the direction of wave propagation and there is transport of fluid mass as well as energy (Figure 2-5).

b) Shallow, intermediate or deep-water waves

The criterion for the definition of *shallow*, *intermediate* or *deep-water waves* is the ratio of wave length to still water depth L/h. Figure 2-2 shows, for an oscillatory wave, the water particle movement of waves of these three types. Figure 2-2(a) shows a *shallow-water wave*, corresponding to $L/h > 20$, in which the water particles move in elliptical orbits. With increasing water depth, these orbits become flatter and smaller, until their movement at depth is eventually parallel to the reservoir bed. The vertical movement of the particles is constrained by the bed and this for example modifies the wave height H. A tsunami, caused by tectonic plate movement, is normally a shallow-water wave. Because the ratio L/h for small, sinusoidal shallow-water waves is large, the wave celerity may be calculated using Eq. (2.1) as $c = (gh)^{1/2}$.

The opposite case is shown in Figure 2-2(c), a *deep-water wave* commensurate with $L/h < 2$. In this case the water particles move in circular orbits, which decrease with increasing water depth until no more movement can be detected on the bed. In other words, deep-water waves are not affected by the lake or sea bed. Wind waves on open water are deep-water waves. Applying Eq. (2.1) for a small sinusoidal wave a wave celerity of $c = [gL/(2\pi)]^{1/2}$ is obtained because the ratio L/h is small. Between deep and shallow-water waves is the zone of *intermediate-water waves*, for which $2 < L/h < 20$ (Figure 2-2b). Such waves are partly influenced by the lake or sea bed and their wave celerity may be calculated, for linear waves, using Eq. (2.1).

c) Periodic or non-periodic waves

Periodic waves are formed by a group of several waves as shown, for example, in Figure 2-1. A non-periodic wave occurs as a single wave (Figure 2-5).

d) Linear and non-linear waves

The term non-linearity originates from the mathematical definition of waves. Linear waves have the form of a sine curve and their relative height $H/h < 0.03$; in addition, the wave steepness must be $H/L < 0.006$ (Dean and Dalrymple 1991; Figure 2-1). Hence, in the mathematical analysis, the terms H/h and H/L are only considered linearly, with higher powers being neglected. In addition, the condition for sinusoidal waves that the wave height is $H = 2a$ no longer applies. The greater the degree of non-linearity, the more the wave profile deviates from this ideal sinusoidal profile, i.e. the ratios H/h and/or H/L increase. Normally, the greater the degree of non-linearity, the more complex and time consuming is the mathematical description of the wave profile.

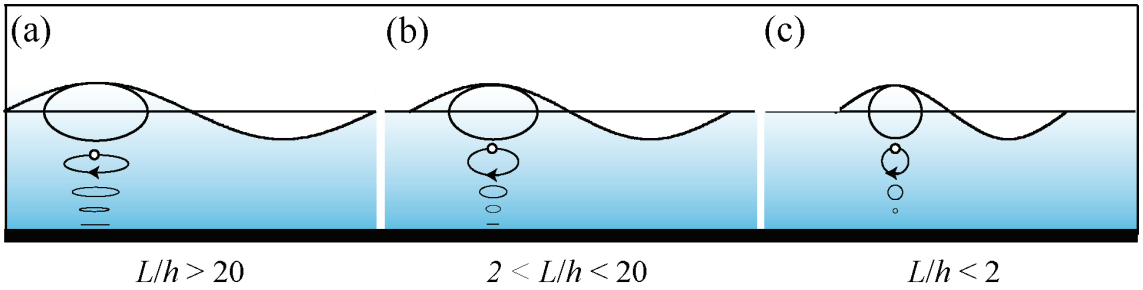

Figure 2-2 Water particle movement of an oscillatory wave in (a) shallow ($L/h > 20$), (b) intermediate ($2 < L/h < 20$) and (c) deep-water ($L/h < 2$).

Water waves naturally exhibit a combination of the properties described in a) to d). *Landslide generated impulse waves* are non-periodic waves and normally strongly non-linear; as a result they are difficult to analyse mathematically. Furthermore, fluid mass transport by such waves may vary from little to considerable and the waves are of translatory rather than oscillatory nature. Depending on the characteristics of the slide, shallow or deep-water waves may be formed, but mostly intermediate-water waves result.

2.2 Theoretical wave types

Water waves differ to a greater or lesser extent from the ideal sinusoidal profile shown in Figure 2-1, which may be described for small dimensions ($H/h < 0.03$ and $H/L < 0.006$) by the linear wave theory (Dean and Dalrymple 1991). Here a few special non-linear water waves are discussed (Section 2.1), which have been relatively well studied, both theoretically and experimentally. The four wave types presented below are

relevant, as all landslide generated impulse waves may be allocated to one of the following groups (Appendix A.3.2.1): a) Stokes wave, b) cnoidal wave, c) solitary wave and d) bore.

a) Stokes wave

Figure 2-3 shows the profile of a Stokes wave, which is a deep-water to intermediate-water wave and may therefore be applied, for example, for wind generated waves. The Stokes wave is steeper than the sinusoidal wave in Figure 2-1, and the wave trough is somewhat flatter and longer than the wave peak. The wave particles do not move in a closed orbital fashion and, in consequence, slight transport of fluid mass takes place.

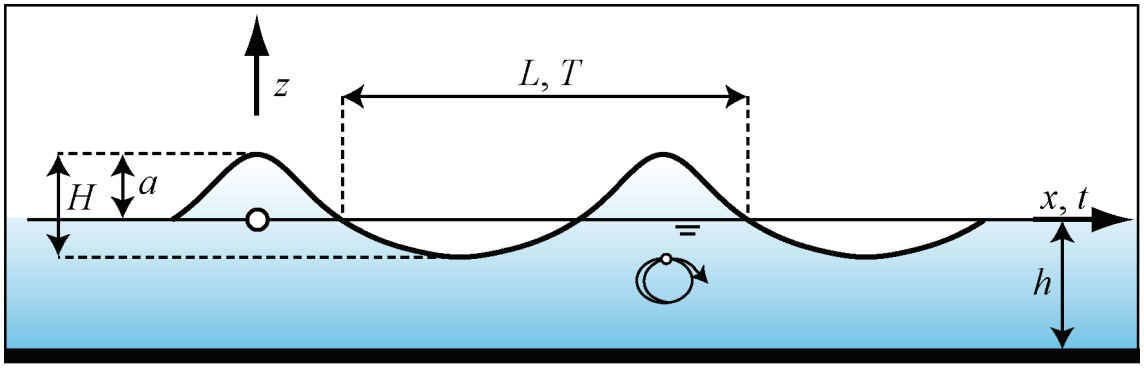

Figure 2-3 Stokes wave profile showing the most important wave parameters; slight fluid mass transport.

b) Cnoidal wave

Figure 2-4 shows a cnoidal wave, which is a periodic wave in intermediate or shallow-water. Wind generated waves in shallow-water, for example, may be described with this theory. The cnoidal wave has mainly an oscillatory character, but also exhibits open water particle orbits and hence transport of fluid mass. Using the equation for cnoidal waves, both the linear wave (sinusoidal wave) and the solitary wave are included as limiting cases.

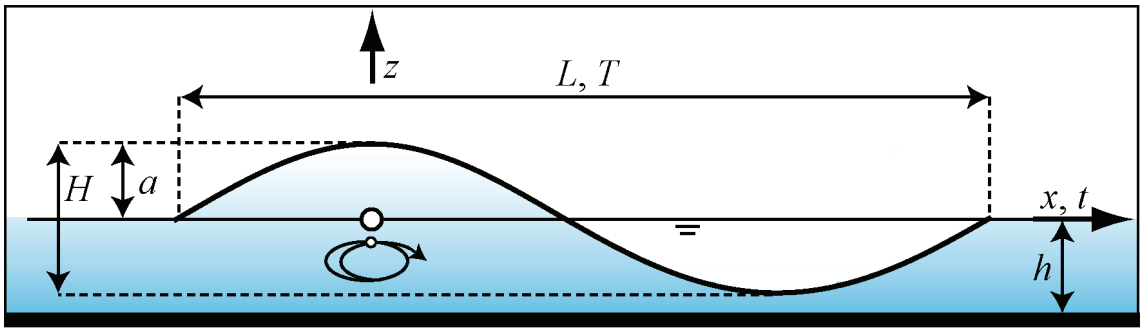

Figure 2-4 Cnoidal wave profile showing the most important wave parameters; slight fluid mass transport.

c) Solitary wave

A solitary wave is shown in Figure 2-5. Classic tsunamis, which are caused by the movement of tectonic plates, are often described with the solitary wave theory. This is the non-linear water wave which has been most researched, both by numerical simulations and laboratory experiments. It consists only of a wave peak but no trough. The wave amplitude is thus equal to the wave height $a = H$. In addition, the wave length $L = \infty$ and the wave is classed as a shallow-water wave ($L/h > 20$).

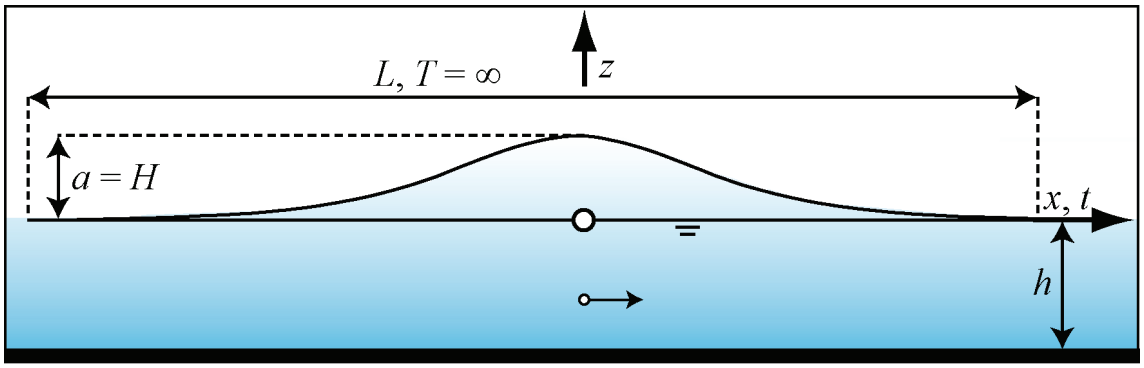

Figure 2-5 Solitary wave profile showing the most important wave parameters; major fluid mass transport.

Movement of the water particles is horizontal and as a consequence there is large fluid mass transport. In a rectangular channel on a horizontal bed, the height of this type of wave in theory does not decrease and the wave may propagate over unlimited distances without any change of shape. In reality, turbulence, created mainly on the bed of the ocean or lake, results in some reduction of wave height, but this is still less than occurs with other wave types. The solitary wave theory is developed from the cnoidal wave theory, as the wave period $T \rightarrow \infty$. The wave celerity of solitary waves is given by

$$c = [g(h + a)]^{1/2}. \tag{2.2}$$

a [m]	=	Wave amplitude (Figure 2-1)
c [m/s]	=	Wave celerity
g [m/s^2]	=	Gravitational acceleration; $g = 9.81$ m/s^2
h [m]	=	Still water depth

If the wave amplitude a of a solitary wave above a horizontal bed exceeds $0.78h$, the wave breaks and moves on as a bore. However, this process cannot realistically be described analytically.

d) Bore

Figure 2-6 shows a bore, which is created e.g. during wave breaking near the shore when air is entrained at the crest or when the top of the crest curls over. A bore is a shallow-water wave with horizontal particle movement which thus transports large fluid masses. Its profile is characterised by a steep front and a gently sloped back.

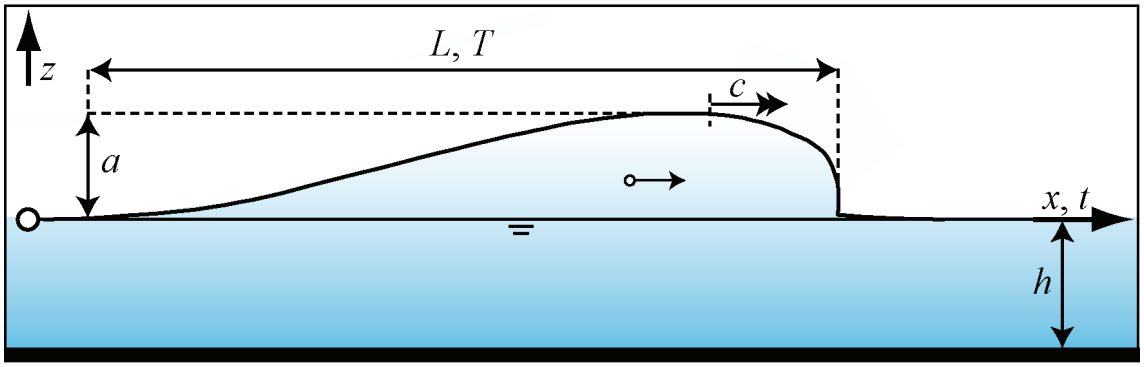

Figure 2-6 Wave profile of a bore with the most important wave parameters; large fluid mass transport.

The four wave types: Stokes, cnoidal and solitary waves, as well as bore, described above will be used in Chapter 3 and in Appendices A and B for classifying impulse waves.

3 Computation procedure and 1st step

3.1 Introduction

Chapter 3 presents the calculation procedure employed to determine the effects of landslide generated impulse waves on dams. This is valid for slide masses that are originally located above the water surface (Figure 1-1) and are based on selected studies given in the list of references in Appendices A and B. Details of the studies and the reasons justifying their inclusion in the studies are given in these Appendices. Figure 3-1 summarises the computation procedure with the corresponding literature references and the section references to this manual. Some of the original methods have been further developed or supplemented, or the corresponding equations were adjusted. The approach is in two steps (Figure 3-1).

The 1st step makes use of the generally applicable equations. With regard to the generation of the waves, a differentiation is made between studies based on a prismatic wave channel (2D) and those in a rectangular wave basin (3D), as shown in Figure 3-3. Both methods are justified in practice and cover the extreme cases of restricted transverse and completely free radial propagation of the impulse waves above a horizontal sea or reservoir bed (Figure 3-2). The 2D equations were developed by Heller (2007a), based on Zweifel (2004) and Fritz (2002), and will be converted for 3D conditions using a method implicitly contained in Huber and Hager (1997).

In contrast to those covering the generation of the waves, the generally applicable equations governing the effects of impulse waves on dams are based only on 2D models. In other words, 3D effects such as a curved dam shape are not taken into account. The run-up and overtopping of the waves are calculated using the method of Müller (1995), as shown in Figure 3-1. Impulse waves differ in terms of their profile and internal water particle movement (Appendix A.3.2.1). For this reason, the effect on a dam of forces resulting from small, Stokes-like waves will be determined by the method of Sainflou (1928) and for the remaining wave types by the method of Ramsden (1996). The Stokes-like wave type can be limited by a 2D criterion of Heller (2007a). Both methods are applied in the first place assuming that the upstream dam face is vertical ($\beta = 90°$) with full force effect but no overtopping. For the remaining wave types, overtopping is likely and a corresponding force reduction method is applied. To analyse dams with sloping upstream faces ($\beta < 90°$), it is necessary for both the Sainflou (1928) and Ramsden (1995) procedures to resolve the forces into their vertical and horizontal components. To simplify the procedures for this resolution, the total loading is assumed to be static as for the moment of the maximum run-up height, practically all kinetic energy is converted into potential wave energy (Appendix B.5).

In the 2nd step, when the results of the generally applicable equations are available, the effects of variations from the idealised reservoir geometry (prismatic, channel-form geometry, rectangular basin form; Section 4.2) must be considered, as well as those of

the mass movement type (granular slide; Section 4.3). These variations may lead to significant differences in the results obtained. Only the generally applicable equations are taken into account in the spread sheets; the 2nd step in Figure 3-1 is also needed here and must be carried out by hand after the spread sheets have been applied.

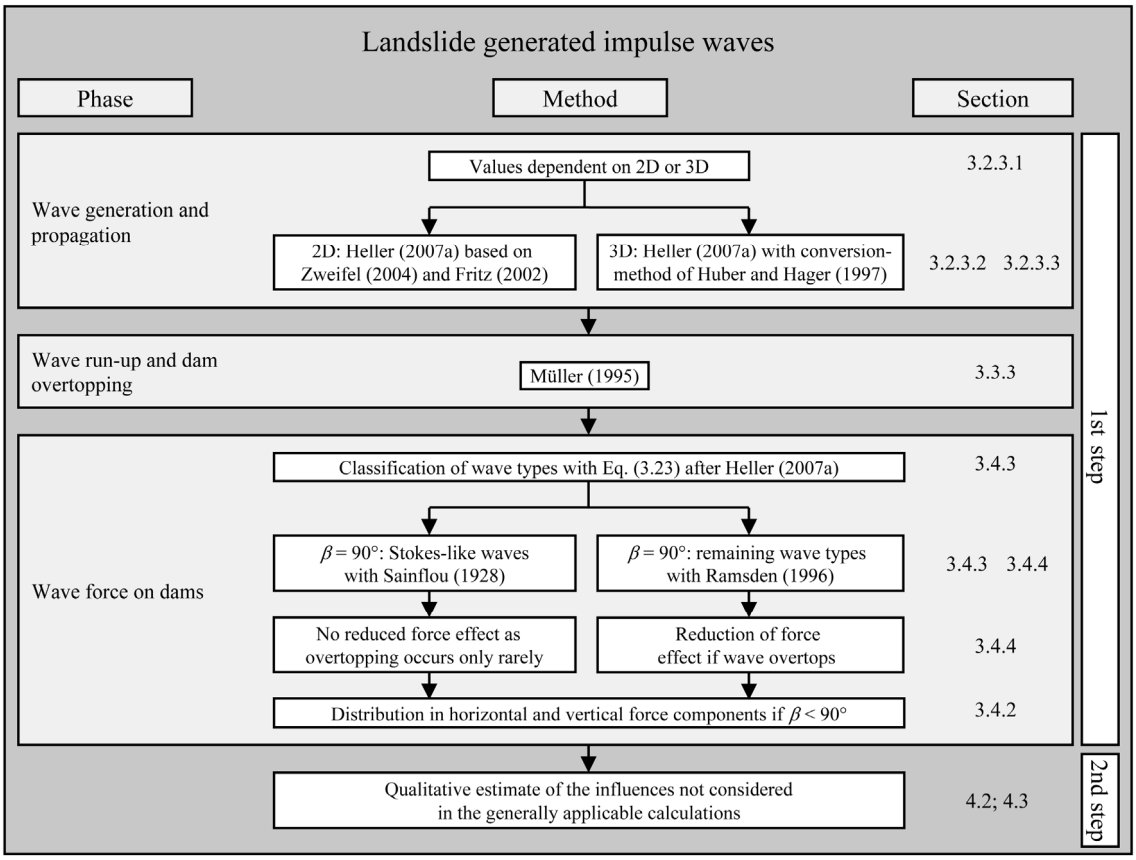

Figure 3-1 Computation procedure of landslide generated impulse waves with the phases of the impulse wave, calculation methods and references to the sections.

Chapter 3 is set out to follow the procedure shown in Figure 3-1. Section 3.2 addresses the wave generation and propagation. The individual calculation equations are presented, after an introduction and the definition and explanation of the relevant governing parameters. Distinctions are made between equations that are valid for both 2D and 3D, equations for channel-form reservoir geometry (2D) and those for basin-form geometry (3D). This differentiation covers the extreme cases of restricted transverse (2D) and completely free radial (3D) wave propagation in reservoirs (Figure 3-2). The wave parameters for general reservoir geometries are determined by either combination with or interpolation between these two extreme cases (Section 5.2). The results from Section 3.2 serve as governing parameters for the calculation of the effects of impulse waves on dams (Sections 3.3 and 3.4). Section 3.3 addresses the relevant governing parameters for the run-up and overtopping of dams. The forces acting on the dam can then be calculated in Section 3.4. After the introduction of the hydrostatic pressure in Subsection 3.4.2, methods for relatively small Stokes-like waves and for the remaining wave types are discussed in Subsections 3.4.3 and 3.4.4, respectively.

3.2 Wave generation and propagation

3.2.1 Introduction

The procedure is based on generally applicable equations. The equations for wave generation were developed by laboratory tests either (a) in a prismatic wave channel (2D) or (b) in a rectangular wave basin (3D) (Section 3.1; Appendix A). The two extreme cases (a) and (b) are shown in Figure 3-2 and can be described as follows:

- Extreme case (a): the slide mass impacts longitudinally into a long reservoir, the slide width being either the same as or greater than the width of the reservoir. The impulse waves are confined as they move along the reservoir and are not able to propagate laterally (Figure 3-2a).

- Extreme case (b): the slide mass impacts at any possible location into the reservoir, and the slide width is less than that of the reservoir. The reservoir geometry is such that the impulse wave can propagate radially and completely freely from the slide impact zone (Figure 3-2b).

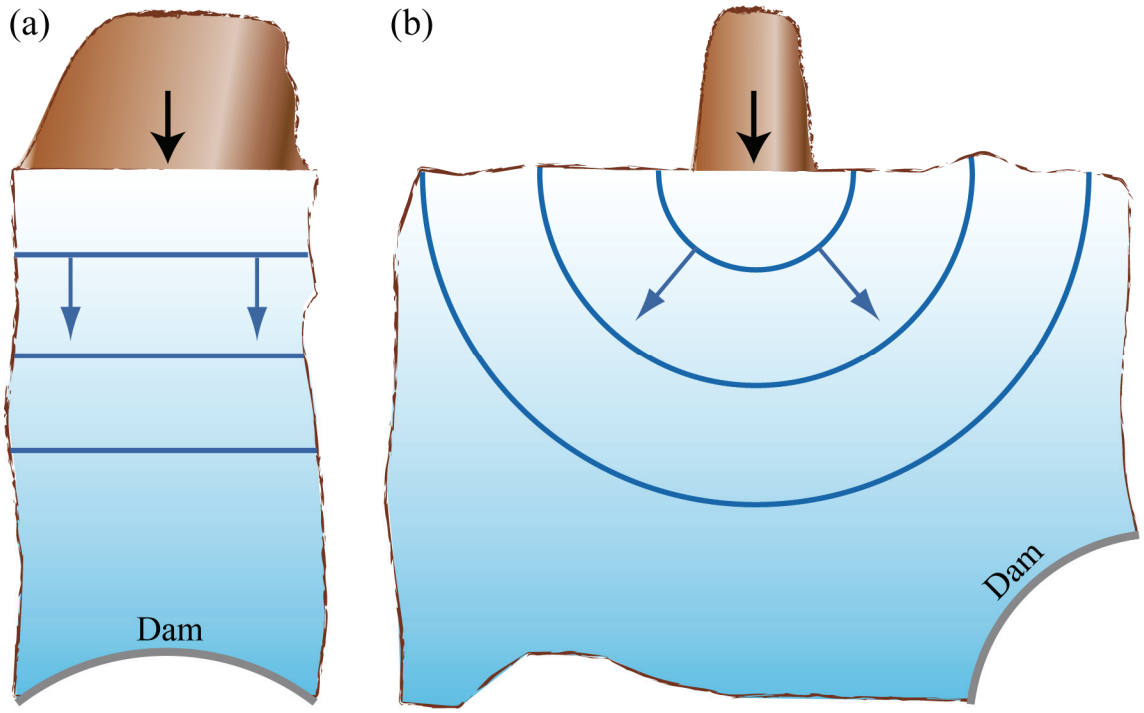

Figure 3-2 Reservoir geometries for two idealised cases which can be described directly with generally applicable equations: (a) extreme case (a) with longitudinal impacting slide and confined transverse wave propagation and (b) extreme case (b) with the slide impacting across the reservoir and completely free radial wave propagation.

The same governing parameters are relevant for the computation of the wave generation for both extreme cases (a) and (b) (Subsection 3.2.2). In fact, the parameters of the

waves vary only slightly for 2D and 3D cases in the immediate vicinity of the slide impact zone (Huber 1980). Because in extreme case (b), impulse waves (and thus their energy) propagate over a larger area, the wave height decreases more rapidly than in case (a), i.e. the attenuation terms differ for the two cases.

In order to extrapolate the results of model tests to prototypes, geometrical similarity must exist between them. Deviations of the geometry may result in model effects, for example, the relative wave heights not corresponding between model and prototype. Figure 3-2 shows geometric forms that are ideally suited to 2D and 3D model tests. In the transition zone between the wave parameters calculated for these two extreme cases, (a) and (b), the parameters are found in a general geometrical form. A prerequisite for this is that the neglected effects discussed in Sections 4.2 and 4.3 have not yet been taken into account. The more the actual form of the reservoir deviates from the two idealised geometries, the more dominant will be effects such as reflection, shoaling or constriction. In this way, the limiting values for extreme cases (a) and (b) may even be exceeded. As a result, greater insecurity in the determination of the wave parameters has to be expected in this transition zone. The neglected governing parameters are discussed in Sections 4.2 and 4.3. In this case, more precise predictions may be possible with a prototype-specific model test or a numerical simulation (Section 1.2).

3.2.2 Governing parameters

Figure 3-3 shows sketches defining the relevant parameters for the impulse wave generation in (a) channel-form (2D) as well as for (b) basin-form (3D) reservoirs. The following parameters have an effect on the calculations of the maximum wave amplitude a_M and the maximum wave height H_M in both 2D and 3D cases:

- Slide impact velocity V_s
- Bulk slide volume V_s
- Slide thickness s
- Slide width or reservoir width b
- Bulk slide density ρ_s
- Bulk slide porosity n
- Slide impact angle α
- Still water depth h

Further governing parameters such as slide length l_s and the slide front angle ϕ are discussed in Appendix A, even though these have a negligible effect on wave generation.

The origin of the coordinate system (x, z) is the intersection of the still water level and the slide slope (Figure 3-3). The governing parameters of the slide are related to the impact location and not to the original position of the slide. Of the seven slide parame-

ters given above, the first six may vary between the original position of the slide and its impact location. The bulk slide volume $\mathcal{V}_s$ and the bulk slide density ρ_s comprise the bulk slide porosity n. This is not introduced as an independent parameter in the computation procedure, nor is the slide mass $m_s = \mathcal{V}_s \cdot \rho_s$. The bulk slide volume $\mathcal{V}_s$ and the bulk slide density ρ_s, which consider the bulk slide porosity n, must be differentiated from the slide grain volume $\mathcal{V}_g$ and grain density ρ_g (Appendix A.2). The equations for conversion between grain and bulk slide properties are given in Table 3-1.

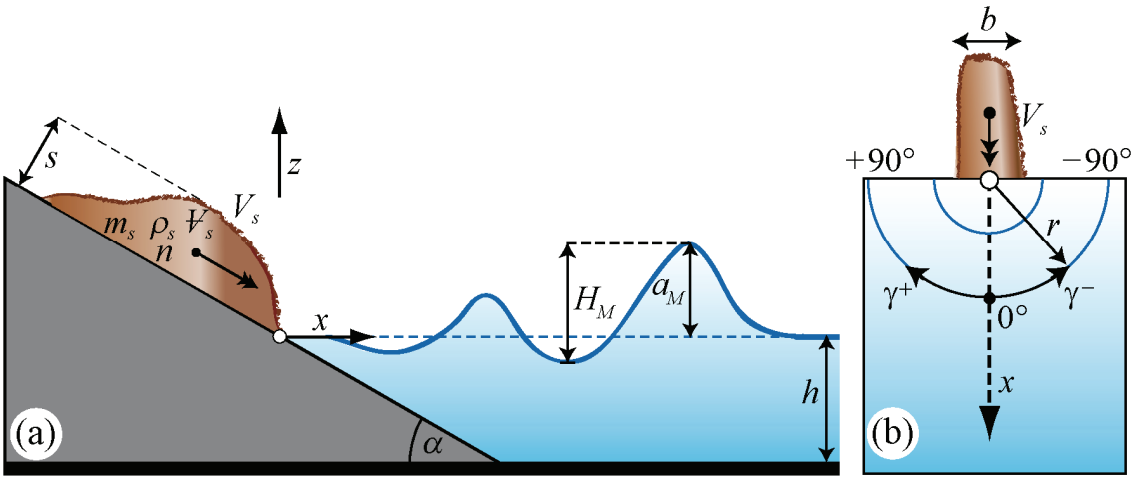

Figure 3-3 Sketches defining the governing parameters on impulse wave generation and the most important wave parameters in (a) 2D and (b) 3D.

Table 3-1 Conversion of grain to bulk slide parameters, and vice versa, with the help of the bulk slide porosity n.

	Granulate properties	Slide properties
Density	$\rho_g = \rho_s/(1-n)$	$\rho_s = (1-n)\rho_g$
Volume	$\mathcal{V}_g = (1-n)\mathcal{V}_s$	$\mathcal{V}_s = \mathcal{V}_g/(1-n)$

The slide thickness s is the maximum thickness of the slide measured perpendicularly to the slide slope at the moment of impact. The slide width b should be selected as the average width during impact. If the slide width is greater than that of the reservoir, then b should be taken to be the reservoir width. The slide impact angle α is the hill slope angle at the impact location, measured as the angle from the horizontal (Figure 3-3a). This defines the impulse transmission angle of the slide on the water body. The still water depth h is taken as the average depth in the slide impact zone, along the slide axis ($\gamma = 0°$; Figure 3-3). The slide impact velocity V_s is that of the centre of gravity of the slide mass during impact and can be expressed by the energy equation, taking into consideration the friction between the slide and the underlying slope of constant inclination (Körner 1976) as

$$V_s = \sqrt{2g\Delta z_{sc}(1 - \tan\delta \cot\alpha)} \,. \tag{3.1}$$

g [m/s^2]	=	Gravitational acceleration; g = 9.81 m/s^2
V_s [m/s]	=	Slide impact velocity (Figure 3-4)
α [°]	=	Slide impact angle (Figure 3-4)
δ [°]	=	Dynamic bed friction angle (Figure 3-4)
Δz_{sc} [m]	=	Drop height of the centre of gravity of the slide (Figure 3-4)

The parameters in Eq. (3.1) are shown in Figure 3-4(a) for a slope of constant inclination. The drop height of the centre of gravity of the slide Δz_{sc} is the vertical distance between the centre of gravity of the slide mass in its original position and at the impact location. The dynamic bed friction angle δ represents the friction at the contact between the slide mass and the underlying slope. The greater this friction the greater is the value of δ, which is normally in the range $15° \le \delta \le 35°$. A value of $\delta \approx 20°$ may be assumed, irrespective of whether the slide mass consists of rock, ice or snow (Hutter 2008). The value for the slide impact angle α is the average slope angle. Should at any point the gradient of the slope change, as shown in Figure 3-4(b), the slide velocity at point of slope change V_{sNK} may be calculated from Eq. (3.1), by introducing values for the relevant parameters Δz_{scN}, δ_N and α_N. The increase of the slide velocity to the slide impact velocity V_s can be determined from Eq. (3.2), with the value of V_{sNK} taken from Eq. (3.1), as

$$V_s = \sqrt{V_{sNK}{}^2 + 2g\Delta z_{sc}(1 - \tan\delta \cot\alpha)} \,. \tag{3.2}$$

g [m/s^2]	=	Gravitational acceleration; g = 9.81 m/s^2
V_s [m/s]	=	Slide impact velocity (Figure 3-4b)
V_{sNK} [m/s]	=	Slide velocity at point of slope change (Figure 3-4b)
α [°]	=	Slide impact angle (Figure 3-4b)
δ [°]	=	Dynamic bed friction angle (Figure 3-4b)
Δz_{sc} [m]	=	Drop height of the centre of gravity of the slide (Figure 3-4)

If a number of slope changes exist, their analysis may proceed in an analogous fashion. The slide velocity at the uppermost slope change can be computed from Eq. (3.1), by introducing the values of Δz_{scN}, δ_N and α_N, valid for the slope above the change. The slide velocity so obtained V_{sNK} is then introduced in Eq. (3.2), together with the relevant values for the next slope section. For each successive slope section the same Eq. (3.2) can be applied, introducing the values for the slope in question and the slide velocity at the end of the previous section. Equation (3.1) is therefore a particular case for

Eq. (3.2), in which V_{sNK} is equal to zero. Salm et al. (1990) address the question of the determination of the slide thickness s and slide impact velocity V_s for flow avalanches.

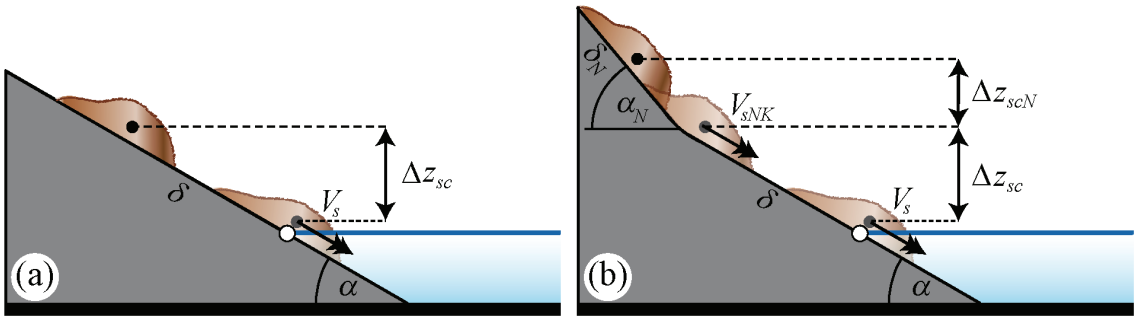

Figure 3-4 Sketches defining the parameters for determination of the slide impact velocity V_s for (a) slope of constant slide impact angle α and (b) for slopes with a slope change.

Changes of a generated impulse wave when propagating in reservoirs of horizontal, channel-form or basin-form geometry are reflected in the following parameters (Figure 3-3):

- Distance x (2D)
- Radial distance r (3D)
- Wave propagation angle γ (3D)

In a channel-form reservoir (2D; Figure 3-3a), the impulse wave changes only with regard to the distance x. In a basin-form reservoir (3D; Figure 3-3b) both the radial distance r and the wave propagation angle γ are involved.

3.2.3 Computation procedure

3.2.3.1 Values independent from 2D or 3D

The equations given below are valid for both extreme cases of idealised reservoir geometry (a) and (b) as described in Subsection 3.2.1. The celerity c of a landslide generated impulse wave can be determined using the equation for the solitary wave celerity

$$c = \left[g(h+a)\right]^{1/2}. \tag{3.3}$$

a [m]	=	Wave amplitude (Figure 3-5)
c [m/s]	=	Wave celerity
g [m/s^2]	=	Gravitational acceleration; g = 9.81 m/s^2
h [m]	=	Still water depth

The value of c can be determined locally or between two points. In the latter case, the average values of a and h, between the two points, are introduced into Eq. (3.3). An impulse wave with an amplitude of a = 20 m in water h = 100 m deep will have a celerity c of about 34 m/s or 124 km/h.

The value of a is determined indirectly from the wave height H. This can be done by applying Eqs. (3.6), (3.10) or (3.13). For a known wave height H, the wave amplitude a for subaerial landslide generated impulse waves is

$$a = (4/5)H \,. \tag{3.4}$$

a [m]	=	Wave amplitude (Figure 3-5)
H [m]	=	Wave height (Figure 3-5)

The wave trough is thus equal on average to only about 20% of the wave height H (Figure 3-3a). Equation (3.4) was developed in a prismatic wave channel, i.e. for case (a) in Figure 3-2. In this manual, Eq. (3.4) is also used for case (b), as per Figure 3-2, and also for all wave types considered, although it is poorly satisfied for Stokes-like waves (Appendix A.3.2.1). The last assumption has a small effect. Equation (3.4) leads to an over-estimation of the wave amplitude a for Stokes-like waves and hence of the wave celerity c according to Eq. (3.3). In addition, a is used in the method discussed in Subsection 3.4.4, which is, however, not applied on Stokes-like waves.

The impulse product parameter P of Heller (2007a) and Heller and Hager (2009a) has an important role in both 2D and 3D calculations and is defined as

$$\mathsf{P} = \mathsf{F} S^{1/2} M^{1/4} \left\{\cos\left[(6/7)\alpha\right]\right\}^{1/2} \qquad \text{for } 0.17 \le \mathsf{P} \le 8.13. \tag{3.5}$$

b [m]	=	Slide width (Figure 3-3b)
F [-]	=	Slide Froude number; $\mathsf{F} = V_s/(gh)^{1/2}$
g [m/s^2]	=	Gravitational acceleration; g = 9.81 m/s^2
h [m]	=	Still water depth (in the slide impact zone)
M [-]	=	Relative slide mass; $M = \rho_s \forbar{V}_s/(\rho_w b h^2)$
P [-]	=	Impulse product parameter
s [m]	=	Slide thickness (Figure 3-3a)
S [-]	=	Relative slide thickness; $S = s/h$
V_s [m/s]	=	Slide impact velocity from Eq. (3.1) or Eq. (3.2) (Figure 3-3a)
$\forbar{V}_s$ [m^3]	=	Bulk slide volume (Figure 3-3a)
α [°]	=	Slide impact angle (Figure 3-3a)
ρ_s [kg/m^3]	=	Bulk slide density (Figure 3-3a)
ρ_w [kg/m^3]	=	Water density

Apart from the water density ρ_w and the gravitational acceleration g, the value of P is determined only from governing parameters and can therefore be estimated prior to any slide event. The significance of the dimensionless values F, S, M and α, as applied in Eq. (3.5), is discussed by Heller (2007a) or Heller and Hager (2009a).

In the calculation equations given below, slide densities from compact snow to granite, slide impact angles from 30° to 90°, and distances from the coordinate origin of up to 59h are taken into account. In practice, the *limitations* given in Table 3-2 must be respected when using this procedure (Appendix A.2).

Table 3-2 Limitations for the calculation of the impulse wave generation.

Term	Range	Meaning
Slide Froude number	$0.86 \le \mathsf{F} \le 6.83$	$\mathsf{F} = V_s/(gh)^{1/2}$
Relative slide thickness	$0.09 \le S \le 1.64$	$S = s/h$
Relative slide mass	$0.11 \le M \le 10.02$	$M = \rho_s \forall_s/(\rho_w bh^2)$
Relative slide density	$0.59 \le D \le 1.72$	$D = \rho_s/\rho_w$
Relative granulate density	$0.96 \le \rho_g/\rho_w \le 2.75$	ρ_g/ρ_w
Relative slide volume	$0.05 \le V \le 5.94$	$V = \forall_s/(bh^2)$
Bulk slide porosity	$30.7\% \le n \le 43.3\%$	n
Slide impact angle	$30° \le \alpha \le 90°$	α
Relative slide width	$0.74 \le B \le 3.33$	$B = b/h$
Relative radial distance	$5 \le r/h \le 30$	r/h
Wave propagation angle	$-90° \le \gamma \le +90°$	γ
Relative streamwise distance	$2.7 \le X \le 59.2$	$X = x/h$
Impulse product parameter	$0.17 \le \mathsf{P} \le 8.13$	$\mathsf{P} = \mathsf{F}S^{1/2}M^{1/4}\{\cos[(6/7)\alpha]\}^{1/2}$

3.2.3.2 Extreme case (a) (2D)

The equations presented here are based on Heller (2007a) (Figure 3-1). They are for the calculation of impulse waves which propagate confined, longitudinally in a reservoir, following the impact of a slide mass in a longitudinal direction (Figure 3-2a; extreme case (a) in Subsection 3.2.1). With regard to the effects of impulse waves on dams, above all the wave height H and the wave amplitude a are of particular importance. In addition, the wave length L and the wave period T are taken into consideration which, according to the linear wave theory, are connected with the wave celerity c as $L = Tc$ (Section 2.1). The maximum wave height H_M in the slide impact zone is often formed by a wall of water rather than by a coherent wave as such (Figure A-11; Figure A-15 in Appendix A). For this reason, a difference will be made between the maximum wave height H_M in the slide impact zone and the wave height H in the wave propagation zone. The former may be determined from Figure A-6(a) in Appendix A as

$$H_M = (5/9)\mathsf{P}^{4/5} h \,. \tag{3.6}$$

h [m]	=	Still water depth (in the slide impact zone)
H_M [m]	=	Maximum wave height (Figure 3-3a)
P [-]	=	Impulse product parameter from Eq. (3.5)

The distance of the maximum wave height from the slide impact location x_M is given according to Figure A-6(b) in Appendix A by

$$x_M = (11/2)\mathsf{P}^{1/2} h \,. \tag{3.7}$$

h [m]	=	Still water depth (in the slide impact zone)
P [-]	=	Impulse product parameter from Eq. (3.5)
x_M [m]	=	Streamwise distance of the maximum wave amplitude from the impact location (Figure 3-3a)

The wave period T_M of the maximum wave height H_M can be calculated, as per Appendix A.3.2.1, as

$$T_M = 9\mathsf{P}^{1/2} (h/g)^{1/2} \,. \tag{3.8}$$

g [m/s^2]	=	Gravitational acceleration; g = 9.81 m/s^2
h [m]	=	Still water depth (in the slide impact zone)
H_M [m]	=	Maximum wave height (Figure 3-3a)
P [-]	=	Impulse product parameter from Eq. (3.5)
T_M [s]	=	Wave period from H_M

With T_M from Eq. (3.8), and with the linear relationship $L = Tc$, the wave length L_M of H_M can be determined as

$$L_M = T_M c \,. \tag{3.9}$$

c [m/s]	=	Solitary wave celerity from Eq. (3.3)
H_M [m]	=	Maximum wave height (Figure 3-3a)
L_M [m]	=	Wave length of H_M
T_M [s]	=	Wave period of H_M

For the evaluation of wave run-up, the wave height at the dam or reservoir shore is required, and not only the maximum wave height H_M in the slide impact zone. Furthermore, the streamwise coordinate x must be considered (Figure 3-3a). If the wave height H sought is located farther from the slide impact location than where the maximum

wave height H_M occurs ($x/h = X > X_M = x_M/h$), then the wave height H as shown in Figure A-7 of Appendix A, can be determined as

$$H(x) = (3/4)\left(\Pi X^{-1/3}\right)^{4/5} h \qquad \text{for } X > X_M. \tag{3.10}$$

h [m]	=	Still water depth (in the slide impact zone)
H [m]	=	Wave height (Figure 3-5)
Π [-]	=	Impulse product parameter from Eq. (3.5)
x [m]	=	Streamwise coordinate in the longitudinal channel direction (Figure 3-3a)
x_M [m]	=	Streamwise distance of the maximum wave amplitude from the impact location
X [-]	=	Relative streamwise distance; $X = x/h$
X_M [-]	=	Relative streamwise distance of the maximum wave amplitude from the impact location; $X_M = x_M/h$

Equation (3.10) is only to be used when $X > X_M$. The wave period $T(x)$ is determined in Appendix A.3.2.1 as

$$T(x) = 9\Pi^{1/4} X^{5/16} (h/g)^{1/2} \qquad \text{for } X > X_M. \tag{3.11}$$

g [m/s^2]	=	Gravitational acceleration; g = 9.81 m/s^2
h [m]	=	Still water depth (in the slide impact zone)
Π [-]	=	Impulse product parameter from Eq. (3.5)
T [s]	=	Wave period (Figure 3-5)
x [m]	=	Streamwise coordinate in the longitudinal channel direction (Figure 3-3a)
x_M [m]	=	Streamwise distance of the maximum wave amplitude from the impact location
X [-]	=	Relative streamwise distance; $X = x/h$
X_M [-]	=	Relative streamwise distance of the maximum wave amplitude from the impact location; $X_M = x_M/h$

The wave length $L(x)$ can, again in accordance with the linear wave theory, be determined from

$$L(x) = T(x)c(x). \tag{3.12}$$

c [m/s]	=	Solitary wave celerity from Eq. (3.3)
L [m]	=	Wave length (Figure 3-5)
T [s]	=	Wave period from Eq. (3.11) (Figure 3-5)
x [m]	=	Streamwise coordinate in longitudinal channel direction (Figure 3-3a)

3.2.3.3 Extreme case (b) (3D)

The equations for the 3D case are based on Heller (2007a) as well as the conversion method of Huber and Hager (1997) (Figure 3-1). They can be used to analyse impulse waves propagating radially and completely freely in a reservoir (Figure 3-2b; extreme case (b) in Section 3.2). The difference in the size of impulse waves between 2D and 3D models in the slide impact zone is small (Huber 1980). Estimation of the maximum values of wave height H_M in the slide impact zone, and the corresponding period T_M and wave length L_M, respectively, may therefore also be determined from Eqs. (3.6), (3.8) and (3.9). The wave height $H(r, \gamma)$ at any given location in the reservoir for $r/h > X_M$, can be determined according to Appendix A.3.2.2 as

$$H(r,\ \gamma) = (3/2)\mathsf{P}^{4/5} \cos^2\left(\frac{2\gamma}{3}\right)(r/h)^{-2/3} h \quad \text{for } r/h > X_M. \tag{3.13}$$

h [m]	=	Still water depth (in the slide impact zone at $\gamma = 0°$)
H [m]	=	Wave height (Figure 3-5)
P [-]	=	Impulse product parameter from Eq. (3.5)
r [m]	=	Radial distance from the impact location in the wave basin (Figure 3-3b)
x_M [m]	=	Streamwise distance of the maximum wave amplitude from the impact location
X_M [-]	=	Relative streamwise distance of the maximum wave amplitude from the impact location; $X_M = x_M/h$
γ [°]	=	Wave propagation angle (Figure 3-3b)

The wave period $T(r, \gamma)$ corresponding to the wave height $H(r, \gamma)$ from Eq. (3.13) can be determined according to Appendix A.3.2.1 as

$$T\,(r,\ \gamma) = 15\left(\frac{H}{h}\right)^{1/4} (h/g)^{1/2} \qquad \text{for } r/h > X_M. \tag{3.14}$$

g [m/s^2]	=	Gravitational acceleration; $g = 9.81$ m/s^2
h [m]	=	Still water depth (at a given position)
H [m]	=	Wave height from Eq. (3.13) (Figure 3-5)
r [m]	=	Radial distance from the impact location in the wave basin (Figure 3-3b)
T [s]	=	Wave period (Figure 3-5)
x_M [m]	=	Streamwise distance of the maximum wave amplitude from the impact location
X_M [-]	=	Relative streamwise distance of the maximum wave amplitude from the impact location; $X_M = x_M/h$
γ [°]	=	Wave propagation angle (Figure 3-3b)

Finally, the wave length $L(r, \gamma)$, again according to the linear wave theory, is given by

$$L(r, \gamma) = T(r, \gamma) c(r, \gamma). \tag{3.15}$$

c [m/s]	=	Solitary wave celerity from Eq. (3.3)
L [m]	=	Wave length (Figure 3-5)
r [m]	=	Radial distance from the impact location in the wave basin (Figure 3-3b)
T [s]	=	Wave period from Eq. (3.14) (Figure 3-5)
γ [°]	=	Wave propagation angle (Figure 3-3b)

3.3 Wave run-up and dam overtopping

3.3.1 Introduction

In contrast to wave generation, the equations for wave run-up and dam overtopping are based only on 2D investigations. 3D effects such as curvature of the dam or asymmetrical wave impact angles cannot be taken into account generally. They must be estimated in the 2nd step in Section 4.2, using the generally applicable equations, *after* the initial calculation has been completed. In this regard, for the 2D run-up formula, it is irrelevant whether the wave parameters have been determined using the equations given in Subsections 3.2.3.2 or 3.2.3.3.

3.3.2 Governing parameters

Figure 3-5 shows a sketch defining the effects of impulse waves on dams, together with the relevant parameters. The following parameters have an influence in this procedure on the run-up height R, the overtopping volume V per unit length dam crest or the force effects:

- Wave height H (2D)
- Wave amplitude a (2D)
- Wave length L (2D)
- Wave period T (2D)
- Still water depth h (2D)
- Run-up angle equal to dam face slope β (2D)
- Freeboard f (2D)
- Crest width b_K (2D)

The first four parameters H, a, L and T characterise the approaching impulse wave. They refer to the cross-section in front of the dam, where they are still not influenced by

the dam (Figure 3-5). These values are determined in Subsection 3.2.3. The still water depth h should be taken as that immediately upstream of the dam. The run-up angle β is measured from the horizontal (Figure 3-5). For the overtopping volume V per unit length dam crest, as shown in Figure 3-5, the freeboard f and the crest width b_K are of relevance. These parameters are discussed in more detail in Appendix B, together with the rationale for neglecting the roughness of the dam slope.

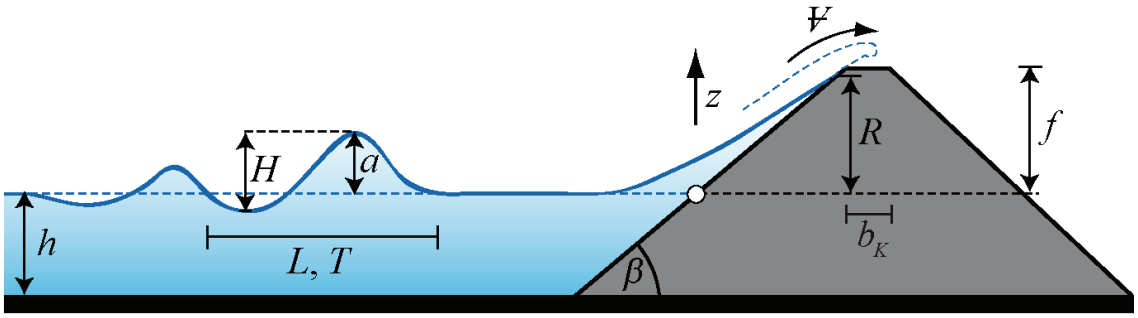

Figure 3-5 Sketch defining the parameters for the wave run-up and dam overtopping.

3.3.3 Wave run-up and overtopping

The following equations are taken from Müller (1995) (Figure 3-1). The run-up height R can be determined, according to Appendix B.3.2, by

$$R = 1.25\left(\frac{H}{h}\right)^{5/4}\left(\frac{H}{L}\right)^{-3/20}\left(\frac{90°}{\beta}\right)^{1/5} h\,. \tag{3.16}$$

h [m]	=	Still water depth (in front of the dam)
H [m]	=	Wave height (in front of the dam) (Figure 3-5)
L [m]	=	Wave length (in front of the dam) (Figure 3-5)
R [m]	=	Run-up height (Figure 3-5)
β [°]	=	Run-up angle equal to dam face slope (Figure 3-5)

Limitations on the use of Eq. (3.16), according to Appendix B.3.2, are shown in Table 3-3.

Table 3-3 Limitations for the calculation of the wave run-up.

Term	Range	Term	Range
Relative wave height	$0.011 \le H/h \le 0.521$	Relative angle	$1.0 \le 90°/\beta \le 4.9$
Wave steepness	$0.001 \le H/L \le 0.013$		

In order to determine the overtopping volume per unit length dam crest $\not{V}$ an intermediate step is required. Firstly, the overtopping volume $\not{V}_0$ per unit length dam crest for $f = 0$ is calculated with

$$\not{V}_0 = 1.45\kappa\left(\frac{H}{h}\right)^{4/3}\left(\frac{T}{\sqrt{h/g}}\right)^{4/9} h^2. \qquad (3.17)$$

f [m]	=	Freeboard (Figure 3-5)
g [m/s^2]	=	Gravitational acceleration; g = 9.81 m/s^2
h [m]	=	Still water depth (in front of the dam)
H [m]	=	Wave height (in front of the dam) (Figure 3-5)
T [s]	=	Wave period (in front of the dam) (Figure 3-5)
$\not{V}_0$ [m^3/m]	=	Overtopping volume per unit length dam crest for $f = 0$
κ [-]	=	Overfall coefficient for overtopping; $\kappa = \kappa_q \kappa_b \kappa_w^{3/2}$
κ_b [-]	=	Overfall coefficient for the crest width
κ_q [-]	=	Overfall coefficient for the steady case
κ_w [-]	=	Overfall coefficient for the increased flow energy compared with the steady case

The overfall coefficient $\kappa = \kappa_q \kappa_b \kappa_w^{3/2}$ in Eq. (3.17) was defined in a similar way as in the formula of Poleni (e.g. Hager 1995). In this, κ_q is the overfall coefficient for the steady case, κ_b takes account of the influence of the crest width of the dam and κ_w takes account of the greater wave energy, compared with the steady case and hence the higher flow velocity over the dam. The three values are

(a) $\kappa_q = 0.41$ ($\beta = 90°$), $\kappa_q = 0.47$ ($\beta = 45°$) and $\kappa_q = 0.51$ ($\beta = 18.4°$), whereby intermediate values may be interpolated,

(b) κ_b is determined from Figure 3-6(a) as a function of the relative maximum overtopping depth $a_{Max,T}/b_K$ and

(c) $\kappa_w = 1.3$ for the whole range $18.4° \le \beta \le 90°$.

The maximum overtopping depth over the dam $a_{Max,T}$ is shown in Figure 3-6(b). This is somewhat greater than the wave amplitude a in front of the dam and was, therefore, taken by Müller (1995) to be approximately equal to the wave height H in front of the dam (Figure 3-5).

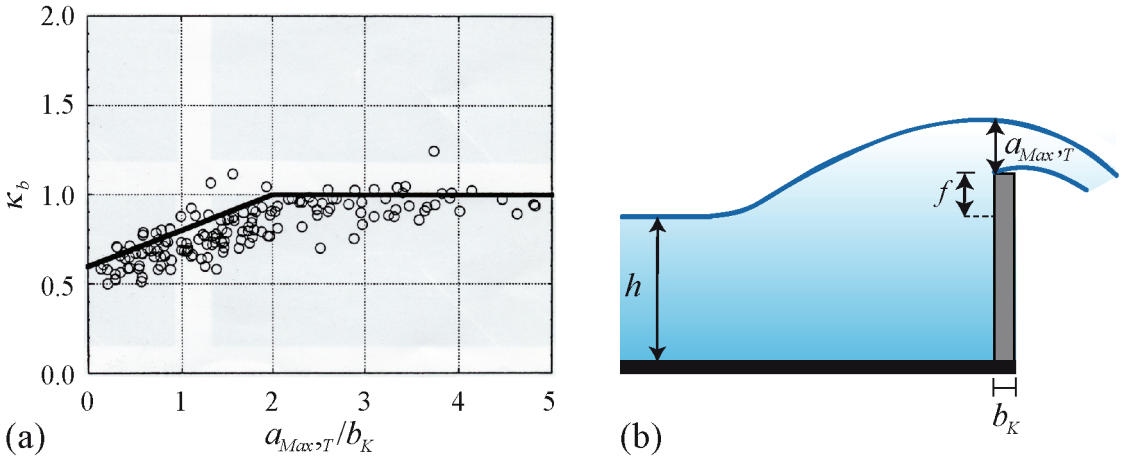

Figure 3-6 (a) Overfall coefficient κ_b for the crest width b_K as a function of the maximum overtopping depth over a dam $a_{Max,T}/b_K$ (Müller 1995) and (b) corresponding definition sketch.

In the prototype, the freeboard is normally $f > 0$, and the overtopping volume $\forall_0$ per unit length dam crest for $f = 0$, when calculated from Eq. (3.17), will be correspondingly reduced. The equation to determine the overtopping volume per unit length dam crest is obtained for $f > 0$, according to Figure B-3(a) in Appendix B, as

$$\forall = \left(1 - \frac{f}{R}\right)^{11/5} \forall_0. \tag{3.18}$$

f [m]	=	Freeboard (Figure 3-5)
R [m]	=	Run-up height (Figure 3-5)
$\forall$ [m^3/m]	=	Overtopping volume per unit length dam crest (Figure 3-5)
$\forall_0$ [m^3/m]	=	Overtopping volume per unit length dam crest for $f = 0$

According to Appendix B.3.2, the limitations given in Table 3-4 apply to the use of Eqs. (3.17) and (3.18).

Table 3-4 Limitations for the calculation of overtopping.

Term	Range	Term	Range
Relative wave height	$0.019 \le H/h \le 0.488$	Relative wave celerity	$0.83 \le c^2/(gh) \le 1.40$
Non-linearity	$0.59 \le a/H \le 0.95$	Relative wave length	$6.0 \le L/h \le 24.0$
Wave steepness	$0.001 \le H/L \le 0.023$	Relative angle	$1.0 \le 90°/\beta \le 4.9$
Relative period	$9.0 \le T(g/h)^{1/2} \le 21.0$		

In addition to $\forall$, the discharge per unit length dam crest is also important. According to Müller (1995) only the average discharge q_{0m} per unit length dam crest for $f = 0$ may be estimated. For this, Müller (1995) determined that the duration of overtopping t_0 for $f = 0$, as a function of the wave period with maximum variation of −12% (Figure B-4a in Appendix B) is calculated from

$$t_0 = 4\left(T\sqrt{g/h}\right)^{4/9}(h/g)^{1/2}. \tag{3.19}$$

g [m/s^2]	=	Gravitational acceleration; g = 9.81 m/s^2
h [m]	=	Still water depth (in front of the dam)
t_0 [s]	=	Duration of overtopping for f = 0
T [s]	=	Wave period (in front of the dam) (Figure 3-5)

The average discharge q_{0m} per unit length dam crest for f = 0 is determined from

$$q_{0m} = \not{V}_0/t_0. \tag{3.20}$$

q_{0m} [m^2/s]	=	Average discharge per unit length dam crest for f = 0
t_0 [s]	=	Duration of overtopping for f = 0
$\not{V}_0$ [m^3/m]	=	Overtopping volume per unit length dam crest for f = 0

The maximum discharge q_{0M} per unit length dam crest for f = 0 is $q_{0M} \approx 2 \cdot q_{0m}$ (Appendix B.3.2; Figure B-4). The limitations for the calculation of the duration of overtopping for f = 0 are given in Table 3-5.

Table 3-5 Limitations for the calculation of the duration of overtopping t_0.

Term	Range	Term	Range
Relative period	$14 \le T(g/h)^{1/2} \le 22$	Relative duration of overtopping	$10.5 \le t_0(g/h)^{1/2} \le 13.5$

No empirical equation is available on the discharge for f > 0. As $\not{V} < \not{V}_0$, the values of q_{0m} and q_{0M} are higher for f = 0 and constitute upper limiting values for the unknown values with f > 0. To determine the freeboard f for which the impulse wave no longer overtops, an iterative procedure is required, as described for example 1 in Section 5.1.

3.4 Wave force on dams

3.4.1 Introduction

This section covers the impulse wave force acting on dams. The prediction of such force is limited by great uncertainty; even when the forces of identical waves are measured in model tests, there can be considerable scatter of the results. Walkden (1999) generated 330 identical waves but found that their maximum force on bank protection varied by up to +100% and −50% from the mean value. The variation may be smaller for forces acting on a flat surface, e.g. the face of a dam. The calculations which follow are based on an estimation of the run-up height R and therefore the calculation of R with Eq. (3.16) is not necessary. However, they do require the wave height H, the wave amplitude a and the wave length L given in Subsection 3.2.3.

Subsection 3.4.2 considers the effects resulting from the still water pressure. Impulse waves can have different profiles and hence properties (Appendix A.3.2.1). In order to make a reliable estimate of the force acting on a dam, it is necessary to consider different wave types. To this end, a rough differentiation will be made between two basically different types of wave, namely: (i) The effects of Stokes-like waves, which behave as deep to intermediate-water waves, with principally oscillatory character, are calculated in Subsection 3.4.3; (ii) The effects of the remaining wave types, which behave as intermediate to shallow-water waves, with mainly translatory character, are determined using the method given in Subsection 3.4.4. When considering the force on dams, it must be borne in mind that this is the maximum wave force which often acts in the prototype for only a few seconds (Figure B-8b in Appendix B).

3.4.2 Hydrostatic pressure

Figure 3-7(a) shows a reservoir with a still water depth h impounded by a vertical gravity dam. The resulting hydrostatic pressure distribution is shown in Figure 3-7(b). The maximum water pressure $\rho_w g h$ acts on the foundation and the horizontal force component $K_{RW,h}$ acts $h/3$ above the foundation level (e.g. Schröder and Saenger 2002).

The horizontal force component $K_{RW,h}$ per unit length dam crest resulting only from the hydrostatic pressure, can be calculated as

$$K_{RW,h} = \rho_w g h^2 / 2 . \tag{3.21}$$

g [m/s^2]	=	Gravitational acceleration; g = 9.81 m/s^2
h [m]	=	Still water depth (in front of the dam)
$K_{RW,h}$ [N/m]	=	Horizontal force component per unit length dam crest resulting only from hydrostatic pressure
ρ_w [kg/m^3]	=	Water density

The horizontal force component in Eq. (3.21) has to be added to the wave force determined by the following method for Stokes-like waves (Subsection 3.4.3). On the other hand, the still water pressure is already taken into account for the method of the remaining wave types (Subsection 3.4.4).

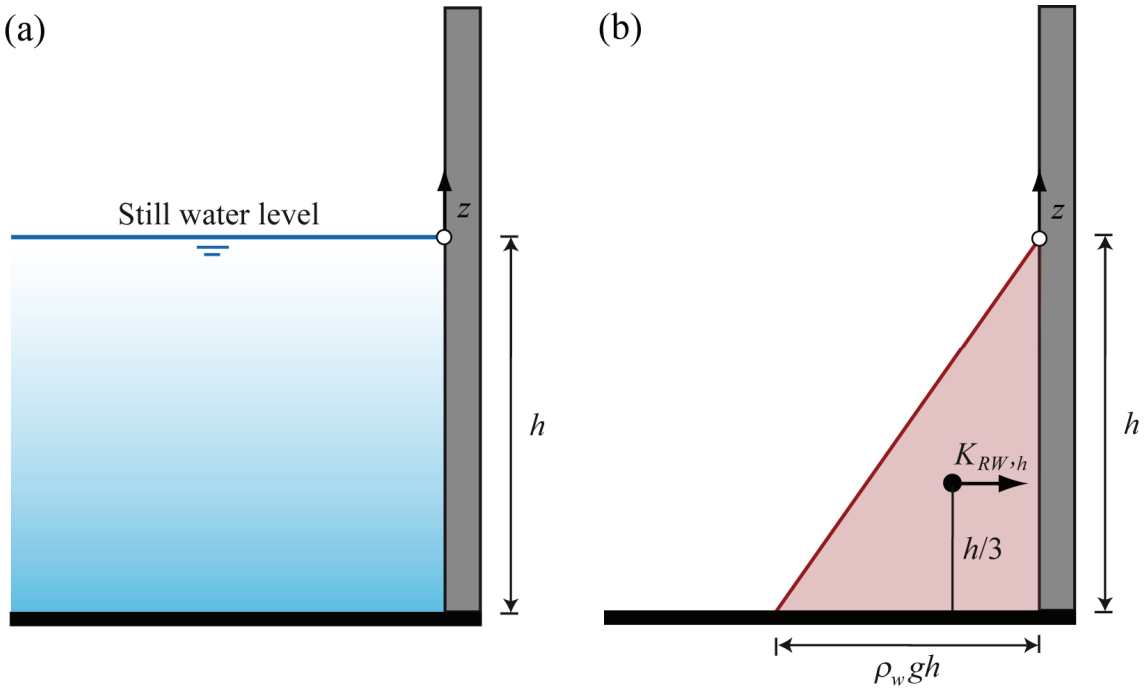

Figure 3-7 Effect of impounded volume on a vertical dam: (a) still water surface for still water depth h and (b) hydrostatic pressure distribution with horizontal force component $K_{RW,h}$ per unit length dam crest and elevation $h/3$ of the resultant of $K_{RW,h}$.

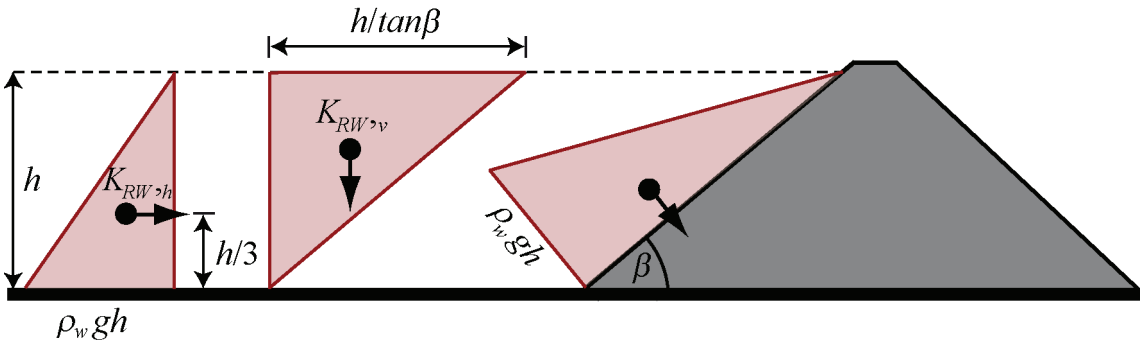

Figure 3-8 Pressure distribution for a still water depth h impounded by the inclined dam face: on the left the horizontal force component, in the centre the vertical force component and on the right the total force (after Schröder and Saenger 2002).

If the dam face is inclined at angle β, the water load results in a vertical force component, in addition to the horizontal force component (Figure 3-8). This vertical force component is of importance e.g. for the determination of the safety of a gravity dam against sliding. The horizontal still water pressure is not affected by the dam face slope β and can be calculated for $\beta < 90°$ using Eq. (3.21). The vertical force component $K_{RW,v}$ per unit length dam crest is given, according to Figure 3-8, by

$$K_{RW,v} = \rho_w g h^2 / (2 \tan\beta) = K_{RW,h} / \tan\beta . \quad (3.22)$$

g [m/s^2]	=	Gravitational acceleration; g = 9.81 m/s^2
h [m]	=	Still water depth (in front of the dam)
$K_{RW,h}$ [N/m]	=	Horizontal force component per unit length dam crest resulting only from hydrostatic pressure
$K_{RW,v}$ [N/m]	=	Vertical force component per unit length dam crest resulting only from hydrostatic pressure
β [°]	=	Dam face slope (Figure 3-5)
ρ_w [kg/m^3]	=	Water density

3.4.3 Stokes-like waves

Stokes-like waves from the wave channel of Heller (2007a) are shown in Figure 3-9. They are created when a relatively small slide mass impacts relatively slowly into a relatively large body of water. Several relatively small waves of similar size are formed. This is the case most often to be expected in the reservoirs of the Alpine regions. The wave type can be determined with the wave type product $S^{1/3} M \cos[(6/7)\alpha]$. Specifically, Stokes-like waves occur if, according to Heller (2007a) or Heller and Hager (2009b) and as shown in Figure A-8 in Appendix A, the following criterion is satisfied

$$S^{1/3} M \cos\left[(6/7)\alpha\right] < (4/5)\mathsf{F}^{-7/5} . \quad (3.23)$$

b [m]	=	Slide width (Figure 3-3b)
F [-]	=	Slide Froude number; $\mathsf{F} = V_s/(gh)^{1/2}$
g [m/s^2]	=	Gravitational acceleration; g = 9.81 m/s^2
h [m]	=	Still water depth (in the slide impact zone)
M [-]	=	Relative slide mass; $M = \rho_s \forall_s / (\rho_w b h^2)$
s [m]	=	Slide thickness (Figure 3-3a)
S [-]	=	Relative slide thickness; $S = s/h$
V_s [m/s]	=	Slide impact velocity (Figure 3-3a)
$\forall_s$ [m^3]	=	Bulk slide volume (Figure 3-3a)
α [°]	=	Slide impact angle (Figure 3-3a)
ρ_s [kg/m^3]	=	Slide density (Figure 3-3a)
ρ_w [kg/m^3]	=	Water density

The force effect of Stokes-like waves may be calculated using Sainflou's (1928) standing wave theory. Due to the total reflection at a vertical dam face, the approaching and reflected waves are practically identical and form a standing wave, on which the

wave nodes always remain in the same position whilst the area between the nodes moves up and down. This leads to run-up movement at the dam.

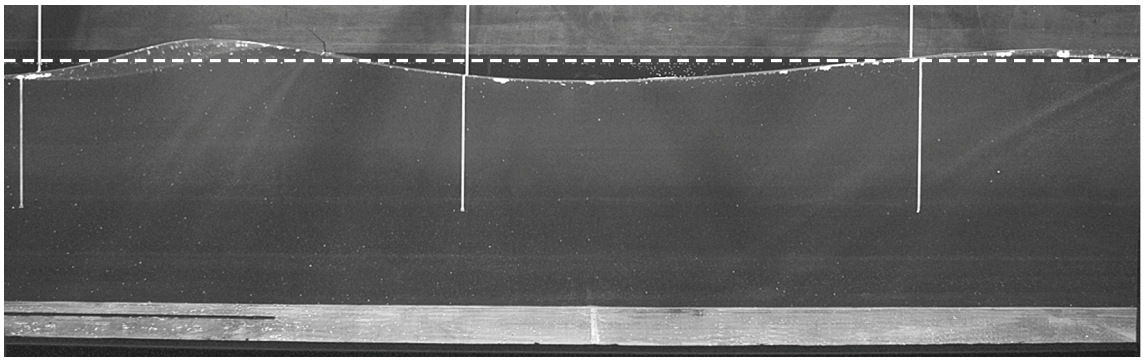

Figure 3-9 Stokes-like waves in a 2D wave channel with (--) initial still water level (Heller 2007a).

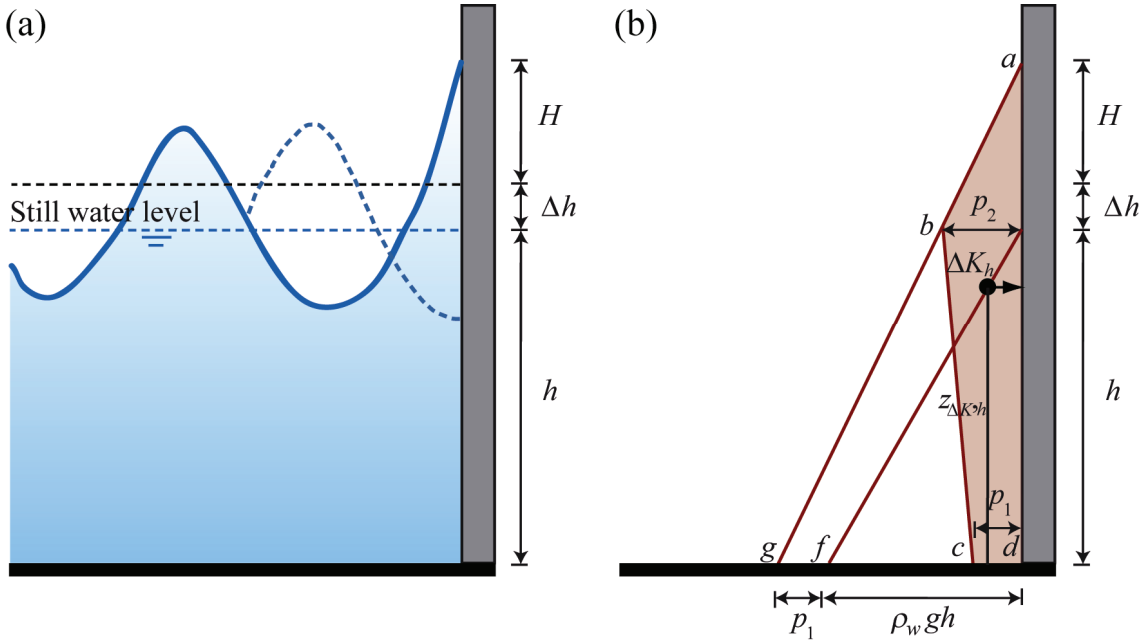

Figure 3-10 Run-up of a standing wave on a vertical dam: (a) definition sketch and (b) corresponding pressure distribution as per Eqs. (3.24) to (3.26) (after Minikin 1950).

Figure 3-10(a) shows the definition sketch of the run-up of a standing wave. The most important assumptions of the theory of Sainflou (1928) are:

- The mean water level of a standing wave, when running-up, is at a height Δh above the still water level, which can be calculated from Eq. (3.25).
- At a height of $H + \Delta h$ above the still water level, where H is the wave height, the water pressure is zero.
- The maximum pressure p_2 due solely to wave action, occurs at the still water level (Figure 3-10b).

Figure 3-10(b) shows the pressure distribution in a standing wave running-up the vertical dam face. That part of the distribution resulting solely from the wave is shown by the area "abcd", and the total pressure distribution, with still water pressure from Figure 3-10, is determined from the triangle "agd". Calculation of the effect resulting *only* from the wave run-up is done in several stages.

a) Calculation of the additional pressure p_1 on the dam foundation

$$p_1 = \frac{\rho_w g H}{\cosh(2\pi h / L)}. \tag{3.24}$$

g [m/s^2]	=	Gravitational acceleration; g = 9.81 m/s^2
h [m]	=	Still water depth (in front of the dam)
H [m]	=	Wave height (in front of the dam) (Figure 3-5)
L [m]	=	Wave length (in front of the dam) (Figure 3-5)
p_1 [N/m^2]	=	Pressure on dam foundation (Figure 3-10b)
π [-]	=	Circular constant; π = 3.14
ρ_w [kg/m^3]	=	Water density

b) Calculation of the average water level rise Δh

$$\Delta h = \frac{\pi H^2}{L} \coth\left(\frac{2\pi h}{L}\right). \tag{3.25}$$

h [m]	=	Still water depth (in front of the dam)
H [m]	=	Wave height (in front of the dam) (Figure 3-5)
L [m]	=	Wave length (in front of the dam) (Figure 3-5)
Δh [m]	=	Average water level rise (Figure 3-10)
π [-]	=	Circular constant; π = 3.14

c) Calculation of the pressure p_2 at the still water level

$$p_2 = \frac{(\rho_w g h + p_1)(\Delta h + H)}{H + \Delta h + h}. \tag{3.26}$$

g [m/s^2]	=	Gravitational acceleration; g = 9.81 m/s^2
h [m]	=	Still water depth (in front of the dam)
H [m]	=	Wave height (in front of the dam) (Figure 3-5)
p_1 [N/m^2]	=	Pressure on dam foundation (Eq. 3.24; Figure 3-10b)
p_2 [N/m^2]	=	Pressure at still water level (Figure 3-10b)
Δh [m]	=	Average water level rise (Figure 3-10)
ρ_w [kg/m^3]	=	Water density

d) Calculation of the additional horizontal force component ΔK_h per unit length dam crest resulting from impulse wave

$$\Delta K_h = \frac{p_2(\Delta h + H)}{2} + \frac{(p_1 + p_2)h}{2}. \tag{3.27}$$

h [m]	=	Still water depth (in front of the dam)
H [m]	=	Wave height (in front of the dam) (Figure 3-5)
p_1 [N/m^2]	=	Pressure on dam foundation (Eq. 3.24; Figure 3-10b)
p_2 [N/m^2]	=	Pressure at still water level (Eq. 3.26; Figure 3-10b)
Δh [m]	=	Average water level rise (Figure 3-10)
ΔK_h [N/m]	=	Additional horizontal force component per unit length dam crest resulting from impulse wave

The hyperbolic cosine function $\cosh(y) = (e^y + e^{-y})/2$ and the hyperbolic cotangent function $\coth(y) = (e^y + e^{-y})/(e^y - e^{-y})$ are applied, taking y as any rational number. The graphical solution of $\cosh(2\pi h/L)$ is shown in Figure 3-11(a) and that of $\coth(2\pi h/L)$ in Figure 3-11(b). Both functions tend asymptotically to unity.

The elevation $z_{\Delta K,h}$ of the resultant of ΔK_h is shown in Figure 3-10(b) and is equal to

$$z_{\Delta K,h} = \frac{p_1 \frac{h^2}{6} + p_2 \frac{h^2}{3} + \frac{p_2}{2}(\Delta h + H)\left[h + \frac{\Delta h + H}{3}\right]}{p_1 \frac{h}{2} + p_2 \frac{h}{2} + \frac{p_2}{2}(\Delta h + H)}. \tag{3.28}$$

h [m]	=	Still water depth (in front of the dam)
H [m]	=	Wave height (in front of the dam) (Figure 3-5)
p_1 [N/m^2]	=	Pressure on dam foundation (Eq. 3.24; Figure 3-10b)
p_2 [N/m^2]	=	Pressure at still water level (Eq. 3.26; Figure 3-10b)
$z_{\Delta K,h}$ [m]	=	Elevation of the resultant of ΔK_h
Δh [m]	=	Average water level rise (Figure 3-10)
ΔK_h [N/m]	=	Additional horizontal force component per unit length dam crest resulting from impulse wave

In addition to the horizontal force component ΔK_h from Eq. (3.27), the hydrostatic still water pressure has to be taken into account from Eq. (3.21).

If Stokes-like waves overtop a dam, their full force is not imposed on the structure. However, as the probability of overtopping by such waves is only slight, and the force reduction would be relatively limited compared with the total loading, a corresponding force reduction procedure has been dispensed with.

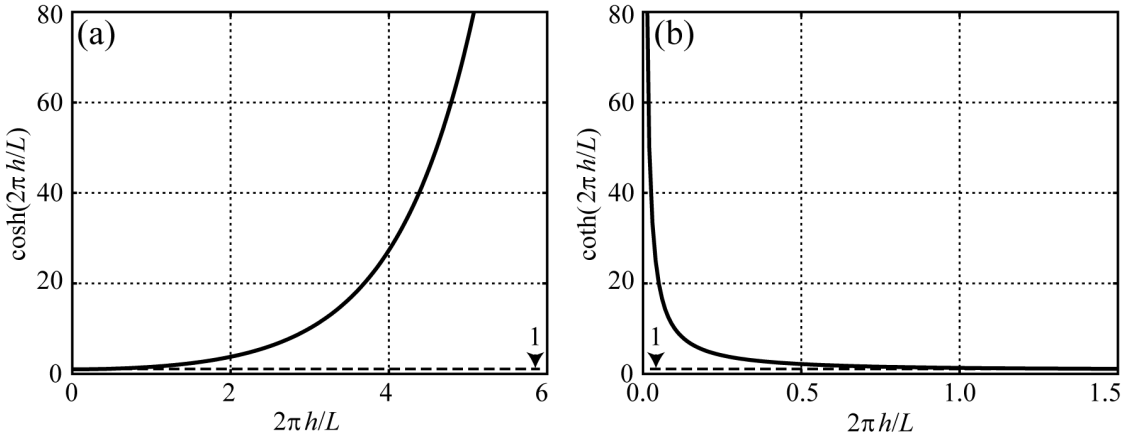

Figure 3-11 Representation of the (a) hyperbolic cosine and (b) hyperbolic cotangent functions; both functions tend to unity for decreasing ordinate values.

The static horizontal force component remains unaffected by the dam face slope β. However, an additional vertical force component exists if the dam face is inclined ($\beta < 90°$), as shown in Figure 3-8. This is equal to the force calculated in Eq. (3.27), divided by $\tan\beta$ (Subsection 3.4.2). To simplify, the total force effect is thereby considered to approximate static conditions (Appendix B.5).

3.4.4 Remaining wave types

Waves larger and stronger than Stokes-like waves are formed when the slide mass and the slide volume meet the criteria given in Eq. (3.29). Solitary or cnoidal-like waves then formed are as shown in Figure 3-12. As distinct from Stokes-like waves, these consist of an initial dominant wave, sometimes followed by smaller waves. In Heller (2007a) the first wave of the remaining wave types was always the biggest and thus the relevant wave. The profile of the solitary wave is just a wave peak with no trough. The solitary-like wave in Figure 3-12(b) has a profile which is very close to this ideal. Also for the cnoidal-like wave in Figure 3-12(a) the depth of the trough is only about 25% of the crest height. Heller (2007a) generally found that the criterion $H = (5/4)a$ from Eq. (3.4) applies for landslide generated impulse waves, hence the depth of the wave trough represents on average 25% of the wave amplitude. The effects of cnoidal-like waves on dams will therefore be considered in the following sections using the method of Ramsden (1996), which is intended for solitary waves.

The wave type product $S^{1/3}M\cos[(6/7)\alpha]$ serves to determine the wave type (Appendix A.3.2.1). The corresponding criterion which rules out Stokes-like waves, whilst defining the remaining wave types, is given as

$$S^{1/3} M \cos[(6/7)\alpha] \geq (4/5)\mathsf{F}^{-7/5} . \qquad (3.29)$$

b [m]	=	Slide width (Figure 3-3b)
F [-]	=	Slide Froude number; $\mathsf{F} = V_s/(gh)^{1/2}$
g [m/s^2]	=	Gravitational acceleration; $g = 9.81$ m/s^2
h [m]	=	Still water depth (in the slide impact zone)
M [-]	=	Relative slide mass; $M = \rho_s \forbidden_s/(\rho_w b h^2)$
s [m]	=	Slide thickness (Figure 3-3a)
S [-]	=	Relative slide thickness; $S = s/h$
V_s [m/s]	=	Slide impact velocity (Figure 3-3a)
$\forbidden_s$ [m^3]	=	Bulk slide volume (Figure 3-3a)
α [°]	=	Slide impact angle (Figure 3-3a)
ρ_s [kg/m^3]	=	Slide density (Figure 3-3a)
ρ_w [kg/m^3]	=	Water density

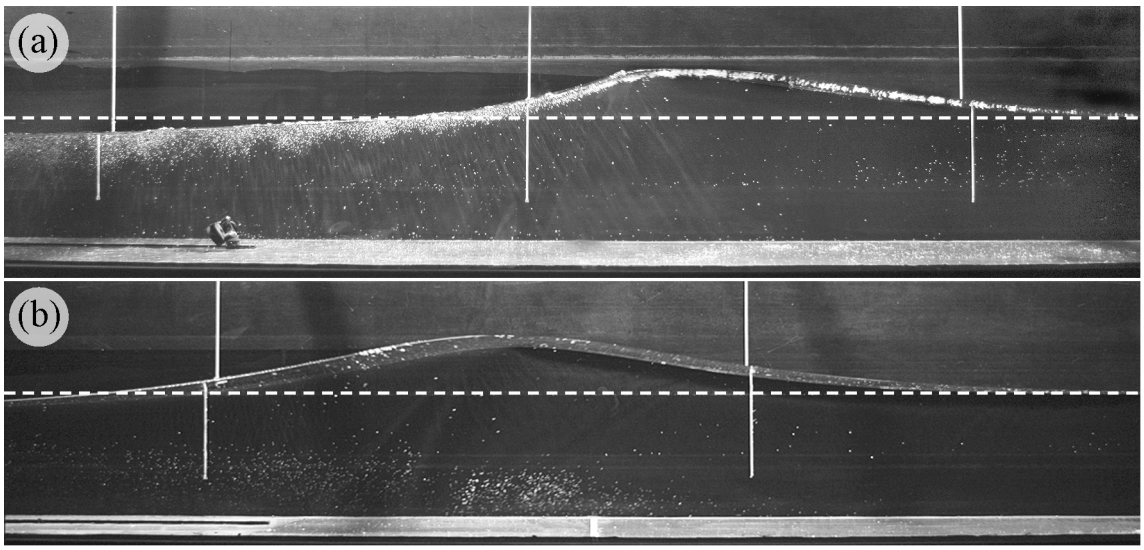

Figure 3-12 Wave types in a 2D wave channel showing (--) the original still water level: (a) cnoidal-like wave and (b) solitary-like wave (Heller 2007a).

In extreme cases, bore-like waves can also develop (Figure A-15 in Appendix A). If they are created in the slide impact zone, they transform over a short distance into cnoidal or solitary-like waves. They are therefore also analysed by the following method.

As shown in Figure 3-13(a), the pressure distribution of a solitary-like wave is approximated to a triangular form (Appendix B.4.2). For the assessment of the force effect, the run-up height R is considered to be independent from the values calculated in Eq. (3.16), and is assumed to be equal to $2a$. Equation (3.30) for the determination of the total horizontal force component $K_{tot,h}$ per unit length dam crest resulting from an impulse wave and hydrostatic pressure is based on the measured values of Ramsden (1996), as shown in Figure B-7 in Appendix B.4.2. The component $K_{tot,h}$ is indi-

cated as a function of the relative wave amplitude a/h. The measured points in Figure B-7(a) may be approximated by

$$K_{tot,h} = \left[1 - 1.5(a/h)\right]^{1/6} K_{hs,h} \qquad \text{for } 0 \le a/h \le 0.6. \qquad (3.30)$$

a [m]	=	Wave amplitude (in front of the dam) (Figure 3-5)
h [m]	=	Still water depth (in front of the dam)
$K_{hs,h}$ [N/m]	=	Horizontal component of hydrostatic force per unit length dam crest resulting from a still water level displaced upwards by $2a$, according to Ramsden (1996)
$K_{tot,h}$ [N/m]	=	Total horizontal force component per unit length dam crest resulting from an impulse wave and hydrostatic pressure

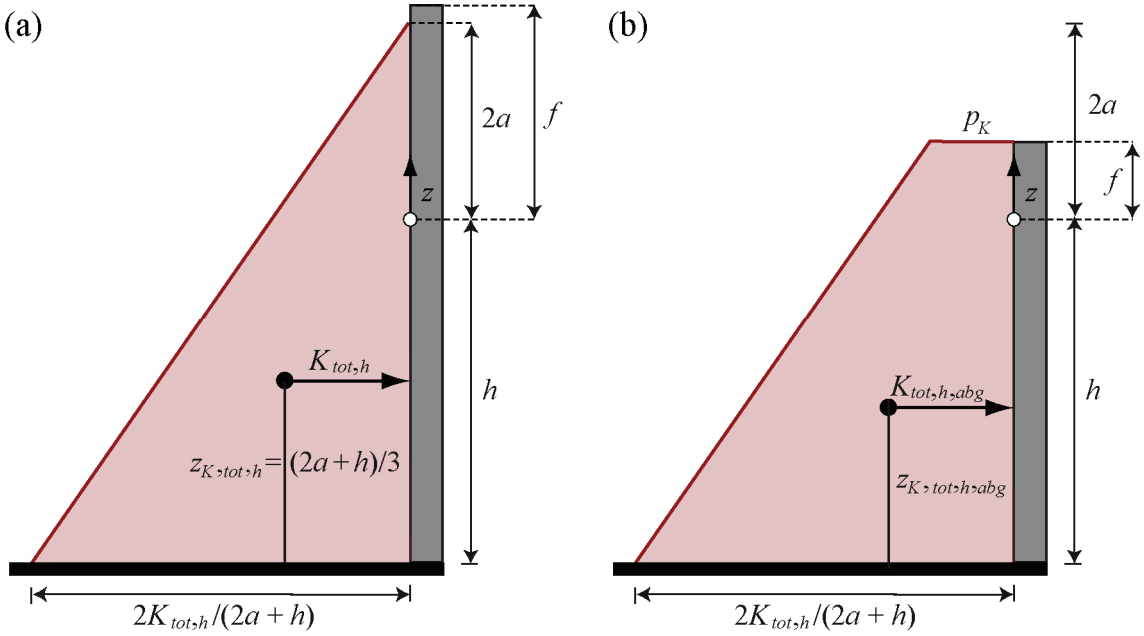

Figure 3-13 Pressure distribution on the vertical dam face as a result of a solitary-like wave with a maximum value of $2K_{tot,h}/(2a + h)$ for the cases of (a) $f \ge 2a$ and (b) reduced pressure effects if $f < 2a$.

The wave amplitude a can be determined from the wave height H as $a = (4/5)H$ (Eq. 3.4). In Figure B-7(a) of Appendix B, and in Eq. (3.30), the horizontal component of hydrostatic force $K_{hs,h}$ resulting from a still water level displaced upwards by $2a$, is applied. Ramsden (1996) made use of this parameter $K_{hs,h}$ for the calibration of his measurement points, and this is given by

$$K_{hs,h} = (1/2)\rho_w g(2a+h)^2 . \tag{3.31}$$

a [m]	=	Wave amplitude (in front of the dam) (Figure 3-5)
g [m/s^2]	=	Gravitational acceleration; g = 9.81 m/s^2
h [m]	=	Still water depth (in front of the dam)
$K_{hs,h}$ [N/m]	=	Horizontal component of hydrostatic force per unit length dam crest resulting from a still water level displaced upwards by 2a, according to Ramsden (1996)
ρ_w [kg/m^3]	=	Water density

The elevation $z_{K,tot,h}$ of the resultant of $K_{tot,h}$ is located $(2a + h)/3$ above the dam foundation (Figure 3-13a).

Should the wave overtop the dam crest, i.e. if the freeboard is less than twice the wave amplitude $f < 2a$, the force effect is reduced as shown in Figure 3-13(b). The pressure at dam crest p_K is determined in proportion

$$p_K = \frac{2K_{tot,h}}{(2a+h)^2}(2a-f) \qquad \text{for } f < 2a. \tag{3.32}$$

a [m]	=	Wave amplitude (in front of the dam) (Figure 3-5)
f [m]	=	Freeboard (Figure 3-5)
h [m]	=	Still water depth (in front of the dam)
$K_{tot,h}$ [N/m]	=	Total horizontal force component per unit length dam crest resulting from an impulse wave and hydrostatic pressure (Eq. 3.30)
p_K [N/m^2]	=	Pressure at dam crest (Figure 3-13b)

With the help of Eq. (3.32) the reduced total horizontal force component per unit length dam crest $K_{tot,h,abg}$ resulting from an impulse wave and hydrostatic pressure for $f < 2a$ may be generally formulated as

$$K_{tot,h,abg} = \frac{(h+f)}{2}\left[p_K + \frac{2K_{tot,h}}{2a+h} \right] \qquad \text{for } f < 2a. \tag{3.33}$$

a [m]	=	Wave amplitude (in front of the dam) (Figure 3-5)
f [m]	=	Freeboard (Figure 3-5)
h [m]	=	Still water depth (in front of the dam)
$K_{tot,h}$ [N/m]	=	Total horizontal force component per unit length dam crest resulting from an impulse wave and hydrostatic pressure (Eq. 3.30)
$K_{tot,h,abg}$ [N/m]	=	Reduced total horizontal force component per unit length dam crest resulting from an impulse wave and hydrostatic pressure (Eq. 3.30)
p_K [N/m^2]	=	Pressure at dam crest (Figure 3-13b)

The elevation $z_{K,tot,h,abg}$ of the resultant of the reduced total horizontal force component $K_{tot,h,abg}$ is shown in Figure 3-13(b) and may be expressed as

$$z_{K,tot,h,abg} = \frac{[2K_{tot,h}/(2a+h) - p_K]\frac{(h+f)^2}{6} + p_K\frac{(h+f)^2}{2}}{[2K_{tot,h}/(2a+h) - p_K]\frac{h+f}{2} + p_K(h+f)}. \qquad (3.34)$$

a [m]	=	Wave amplitude (in front of the dam) (Figure 3-5)
f [m]	=	Freeboard (Figure 3-5)
h [m]	=	Still water depth (in front of the dam)
$K_{tot,h}$ [N/m]	=	Total horizontal force component per unit length dam crest resulting from an impulse wave and hydrostatic pressure (Eq. 3.30)
$K_{tot,h,agb}$ [N/m]	=	Reduced total horizontal force component per unit length dam crest resulting from an impulse wave and hydrostatic pressure (Eq. 3.30)
p_K [N/m^2]	=	Pressure at dam crest (Figure 3-13b)
$z_{K,tot,h,abg}$ [m]	=	Elevation of the resultant of $K_{tot,h,abg}$

The effect of the hydrostatic pressure in accordance with Eq. (3.21) is already taken into account in the computation procedure in Subsection 3.4.4. The horizontal force effect remains independent of the dam face slope β. On the other hand, for $\beta < 90°$ an additional vertical force component exists (Figure 3-8). This is equal to the force determined in Eq. (3.30) or Eq. (3.33) respectively, divided by $\tan\beta$ (Subsection 3.4.2). To simplify, the total force effect is thereby considered to approximate to static conditions (Appendix B.5).

3.5 Final comments

The computation procedure presented in accordance with Figure 3-1 are based on generally applicable equations which were established from model tests in a prismatic wave channel or in a rectangular wave basin. Deviations from these ideal forms may lead to model laboratory effects (Subsection 3.2.1). It is absolutely essential to estimate the effects which are neglected in the generally applicable equations, such as reservoir geometry and the mass movement type. In the computation procedure shown in Figure 3-1, this is explained in the 2nd step. These effects are described in Chapter 4. They also have to be considered when the spread sheets are applied (Section 5.3).

4 2nd step, sensitivity analysis and safety allowance

4.1 Introduction

Sections 4.2 and 4.3 cover the 2nd step of the computation procedure shown in Figure 3-1 for the analysis of landslide generated impulse waves. The influences explained here may lead to significant changes in the wave parameters and thus the run-up heights, as compared with these determined in the 1st step. This 2nd step also has to include the effects of exceeding the limitations for the calculation of impulse waves, in accordance with Tables 3-2, 3-3, 3-4 and 3-5. Large deviations from the values calculated in the 1st step, as a result of breaching the limitations in question, are generally not to be expected, but they do increase their level of uncertainty.

In addition to the impulse transmission there will be a displacement mechanism if the slide volume is large in relation to the reservoir capacity. The resulting increase of the reservoir level is not allowed for in the procedure shown in Figure 3-1, but an approximation of it can be made by dividing the slide volume by the surface area of the reservoir (Subsections 5.1.3 and 5.2.3).

The equations in Chapter 3 are based on a 2D prismatic channel, or a rectangular, 3D wave basin, in each case with a horizontal bed. The influence which a reservoir shape varying from one or the other of these ideal forms has on the wave parameters is discussed in Section 4.2. The equations in Chapter 3 are based on movement of a granular slide, but mass movement can also comprise of a solid body. The various *mass movement types* are discussed in Section 4.3. Then the difference between the maximum wave amplitude generated by a solid body, compared with that created by granular slide, is addressed. In Section 4.4, a *sensitivity analysis* of the run-up height R, as a function of the governing parameters, is described. Finally, some comments are made on the accuracy of the results and on *safety allowances*.

4.2 Effects of the reservoir shape

This Section considers these effects of reservoir geometry that deviate from the two extreme cases of (a) confined transversal and (b) completely free, radial propagation of the generated waves, according to Figure 3-2. They are presented here in order that their influence on wave height, and thus on the run-up height, can be qualitatively assessed in the 2nd step, in accordance with Figure 3-1. The shape of the reservoir has a significant effect on the propagation of impulse waves (Camfield 1980). As the still water depth h decreases, a deep-water wave ($L/h < 2$) at first changes to an intermediate-water wave ($2 < L/h < 20$) before becoming a shallow-water wave ($L/h > 20$), i.e. then influenced by the bed. The contact with the bed results normally in an increase of the wave height, as the friction losses of the bed may be neglected when compared with shoaling. A shallow-water wave will be influenced not only by shoaling but also by refraction. Irrespec-

tive of whether it is classed as a shallow, intermediate or deep-water wave, any wave will be subject to diffraction, constriction and reflection (Coastal Engineering Manual USCE 2006). These effects may be described as follows:

a) Refraction (Figure 4-1a): a shallow-water wave changes direction such that it moves mostly frontally onto the shore.

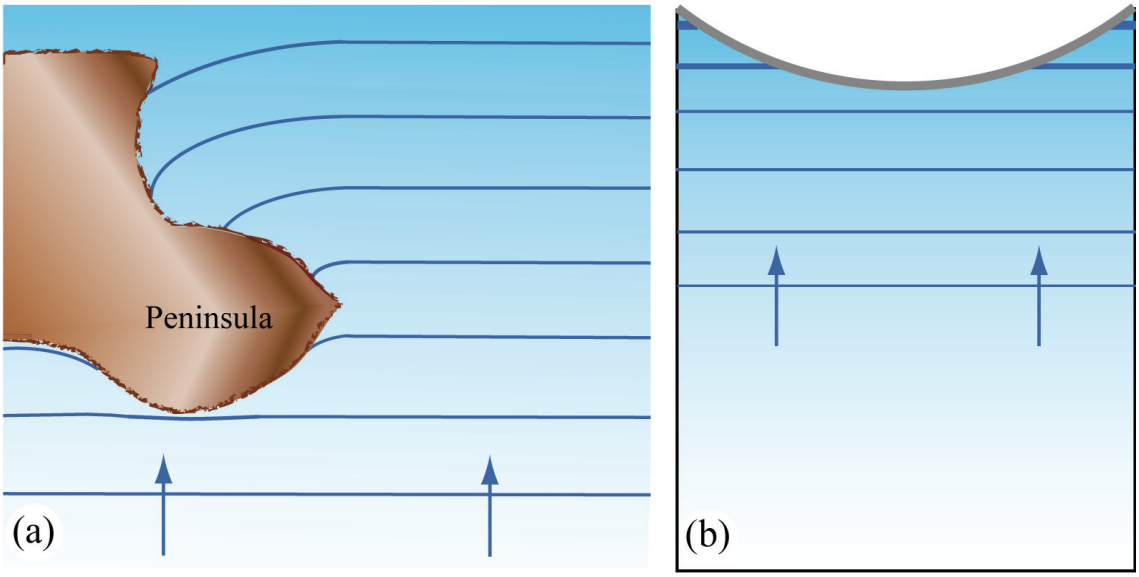

Figure 4-1 (a) Principles of refraction near a shore and diffraction around a peninsula and (b) wave height increase resulting from constrictions near the flanks of an arch dam.

b) Shoaling (Figure 4-2b): the height of a shallow-water wave increases whilst, at the same time, the wave length decreases. The increase in wave height due to shoaling may be determined according to Dean and Dalrymple (1991) as

$$\frac{H_2}{H_1} = \left(\frac{h_1}{h_2}\right)^{1/4} \left(\frac{b_1}{b_2}\right)^{1/2} . \tag{4.1}$$

b_1 [m]	=	Reservoir width at cross-section 1 of Figure 4-2(b)
b_2 [m]	=	Reservoir width at cross-section 2 of Figure 4-2(b)
h_1 [m]	=	Still water depth at cross-section 1 of Figure 4-2(b)
h_2 [m]	=	Still water depth at cross-section 2 of Figure 4-2(b)
H_1 [m]	=	Wave height at cross-section 1 of Figure 4-2(b)
H_2 [m]	=	Wave height at cross-section 2 of Figure 4-2(b)

Equation (4.1) is based on the assumption of a constant energy flux between cross-sections 1 and 2, as shown in Figure 4-2(b). If the widths between cross-sections 1 and 2 are constant, $b_1 = b_2$, then Eq. (4.1) can be reduced to $H_2/H_1 = (h_1/h_2)^{1/4}$, known as Green's law.

c) Diffraction (Figure 4-1a): a wave passes around an obstacle and gives up some of its energy laterally into the area of the wave shadow.

d) Constriction (Figure 4-1b): a wave in a constricted area of a reservoir will increase in height, due to the concentration of wave energy. This can occur, for instance, against the flank of a dam. For shallow-water waves, the estimation is again possible using Eq. (4.1) and for deep-water waves Eq. (4.1) can be simplified to $H_2/H_1 = (b_1/b_2)^{1/2}$ because $h_2 \approx h_1$. The effects of constrictions at dam flanks will be quantified below in Section 4.2.

e) Reflection (Figure 4-2a): on reaching the shore, a wave is reflected and moves with reduced height back. The height of the reflected wave depends on how much of the wave energy is dissipated during run-up. The energy dissipation during run-up against dams with vertical faces, where wave overtopping cannot take place, is almost nothing resulting in total reflection. The height and amplitude of the reflected wave are practically the same as for the arriving wave $a \approx a_R$ (Figure 4-2a). When a reflected wave meets an approaching wave, nonlinear superposition occurs at the meeting point, providing neither of the waves has broken. The individual waves move amongst each other and their profiles, after the waves have crossed, are practically uninfluenced by their encounter (Figure 4-3).

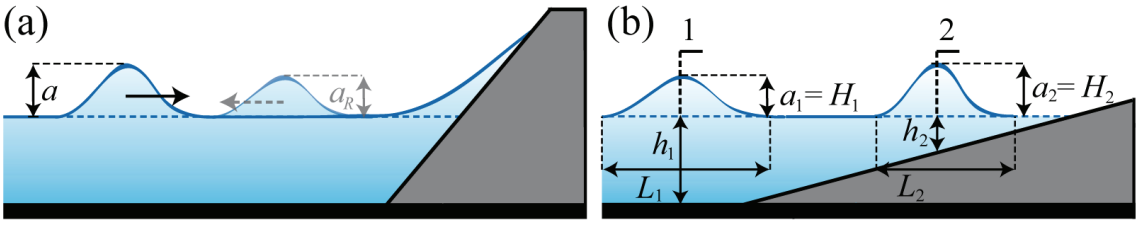

Figure 4-2 Principle sketches from (a) reflection of a solitary wave by the face of a dam with $a > a_R$ and (b) shoaling of a solitary wave close to the shore with $a_1 < a_2$ and $L_1 > L_2$.

Müller (1995) measured the run-up height on dam faces taking account of a lateral reservoir flank. The angle between the dam and the valley slope acts as a constriction (Figure 4-4a). Even if a deep-water wave approaches the shore it will, as the still water depth decreases, transform into a shallow-water wave and be influenced by the bed due to shoaling. Figure 4-4(b) shows, for a lateral shore inclination of 3:4, the relation of the run-up height to the run-up height at the dam centre R/R_m, as a function of the relative width of reservoir flank l/l_F. The wave run-up heights in the vicinity of the inclined shore are about 20-30% greater than at the centre of the dam. For purposes of comparison, the run-up height according to Green's law according to Eq. (4.1) is also shown; however, the height at the dam flank is too large. Müller (1995) gives two possible explanations: (i) the wave in the model does not approach the lateral reservoir flank directly, and (ii) the friction losses at the bed reduce the run-up height in the model compared with its theoretical value as deduced from Green's law.

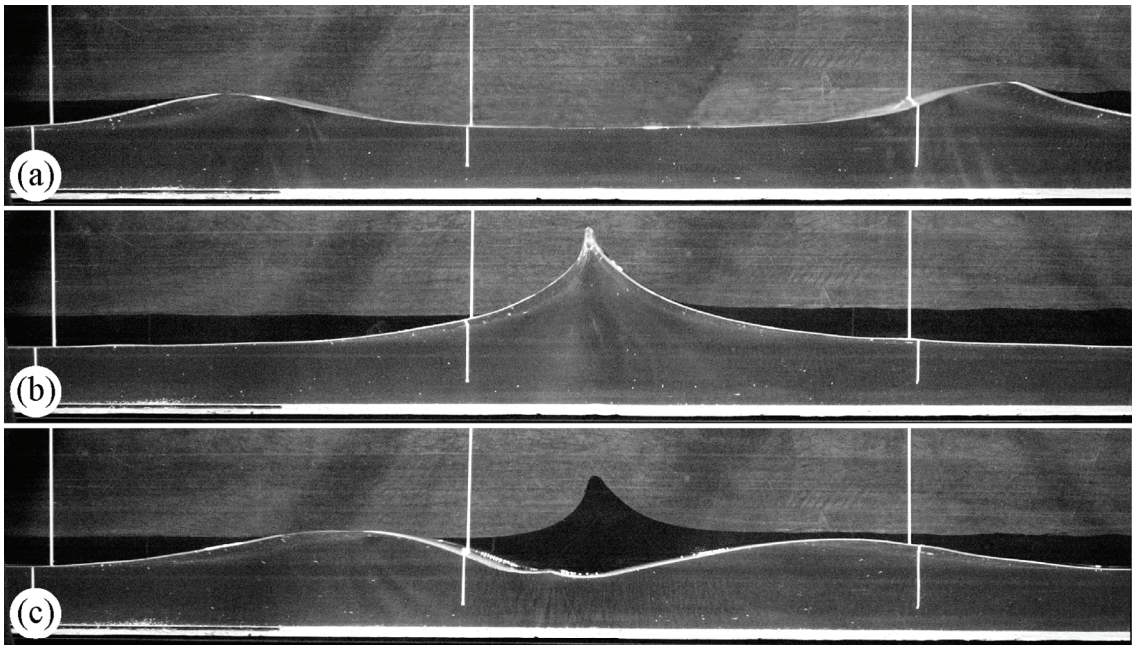

Figure 4-3 Collision of two waves in the VAW channel: (a) two similar solitary waves approach each other, (b) they meet and form a non-linear water oscillation and (c) after they have crossed their profiles have changed only insignificantly as a result of the collision (Heller 2007a).

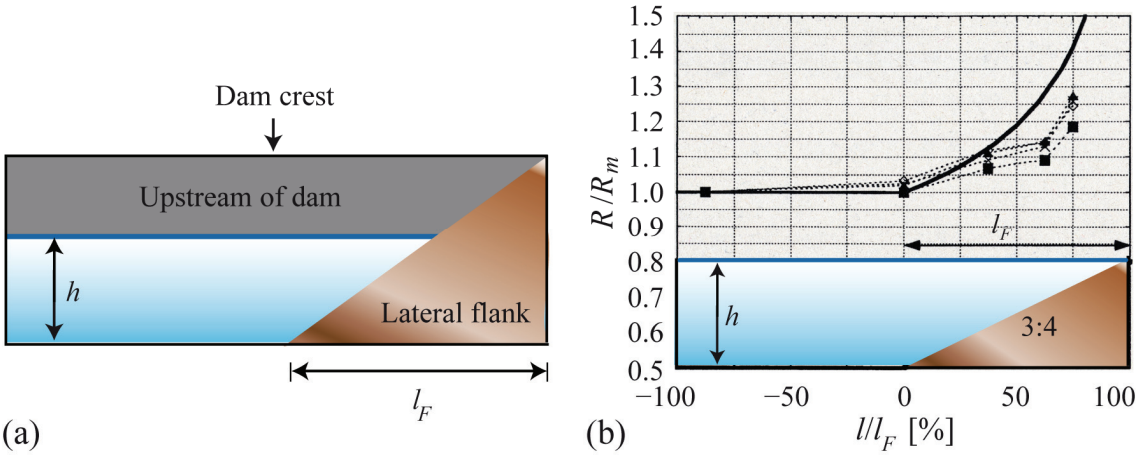

Figure 4-4 Run-up height as consequence of an inclined lateral reservoir flank and constriction: (a) definition sketch showing the lateral flank of the reservoir and (b) relationship of the run-up height to the run-up height at the dam centre R/R_m as a function of the relative width of the reservoir flank l/l_F [%] as well as the values calculated from Green's law (—) according to Eq. (4.1) (after Müller 1995).

The effects of *ice cover* on impulse waves were investigated by Müller (1995). Ice up to 0.5 m thick has only a negligible effect on wave attenuation, irrespective of whether the cover is broken or compact. A prerequisite for this is that the slide mass pierces and passes through the ice layer. If a snow avalanche does not succeed in penetrating the ice layer two dangers may nevertheless arise on the shore; the additional weight may cause the ice cover to tip into an inclined position and thus create a small impulse wave, or water which is displaced under the ice cover may, for instance, flow up from under the ice on the shore.

4.3 Mass movement types

The equations in Chapter 3 assume the slide consists of granular material. In natural conditions, however, there exists a whole range of mass movement types. If the mass moves as a solid body, the wave height H, as compared with that for granular material, is about the same for high impact velocities, but considerably greater if the impact velocity is low. When a granular slide impacts at low velocity, water can enter the pore volume, whereas a solid body of porosity $n \approx 0$ displaces all the water. Furthermore, the shape of a granular slide may change during impact (Zweifel 2004).

Classification helps to judge whether a mass moves as a granular slide rather than as a solid body. The following Section discusses the mass movement types and their processes, as described by Cruden and Varnes (1996), for rock, debris or earth. This information also helps the understanding of the processes for snow and ice avalanches as well as for glacier calving. An alternative classification was, for example, developed by Nemcok et al. (1972).

A mass movement may be roughly defined by two nouns; the material in question followed by the movement type, for example landslide or rockfall. Cruden and Varnes (1996) identified five mass movement types (Figure 4-5):

- *Sliding* (Figure 4-5a): the slide mass can move rotating (Figure 4-5a) along a curved concave slide plane or by translation on a plane. Slides can move as solid body or granular; in the latter case the bulk slide volume V_s increases correspondingly as far as the impact zone (Subsection 3.2.2).

- *Flowing* (Figure 4-5b): the mass behaves as a viscous liquid.

- *Falling* (Figure 4-5c): a fall may be considered to be mostly free-fall, if the hill slope angle $\alpha > 76°$; if this angle is smaller the mass falls onto the slope where it may break.

- *Toppling* (Figure 4-5d): the mass moves around a rotation point or axis located below its centre of gravity.

- *Spreading* (Figure 4-5e): the mass volume spreads and breaks into finer material. This movement type occurs when the slope angle is small $0.3° \leq \alpha \leq 5°$ and is most often triggered by an earthquake. This form of movement is rarely significant, in particular in Alpine regions, for the generation of impulse waves.

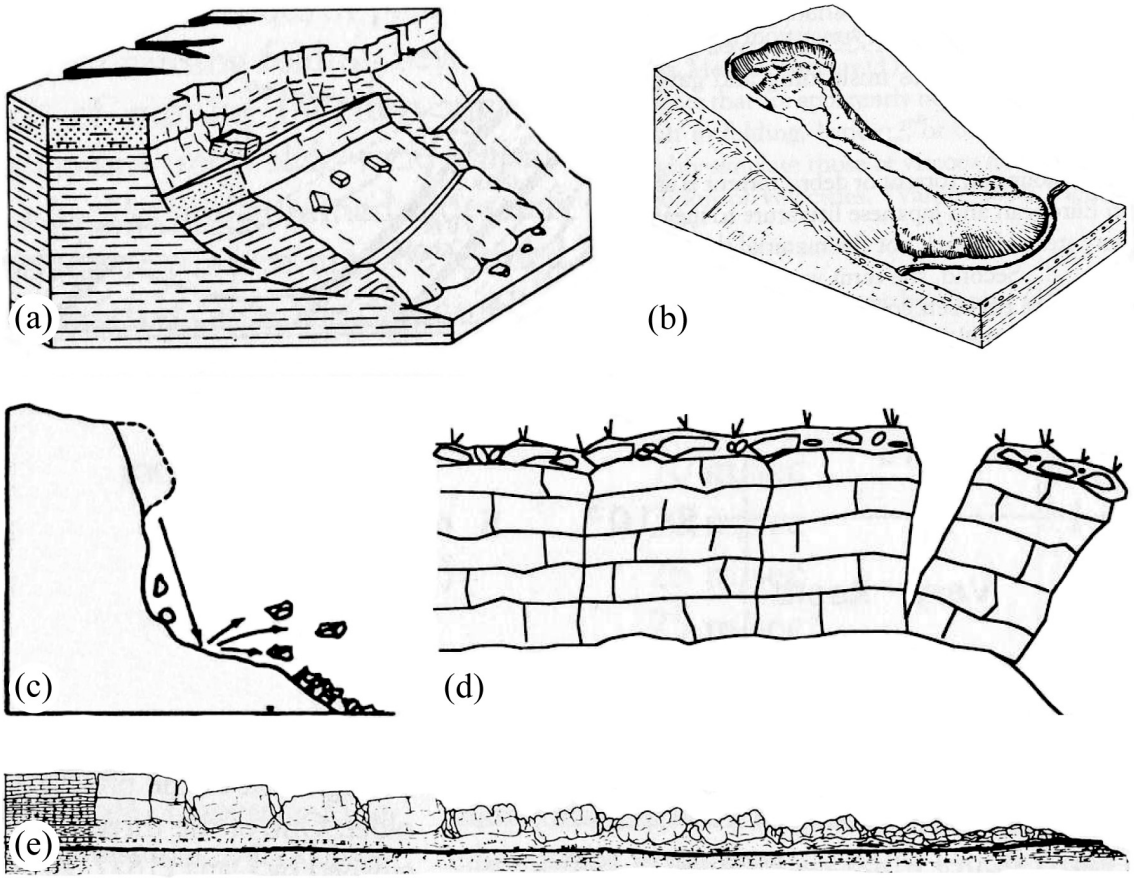

Figure 4-5 Mass movement types: (a) sliding (b) flowing (c) falling (d) toppling and (e) spreading (Cruden and Varnes 1996).

Zweifel (2004) studied the difference between impulse waves resulting from granular slides and from solid bodies. He carried out 11 tests with a solid body of constant density ρ_s = 1,340 kg/m^3 for a range of still water depths 0.150 m $\leq h \leq$ 0.600 m. Most of the equations in Subsection 3.2.3 are based on tests conducted in the same hydraulic model, but with granular slides, as distinct from the 11 tests of Zweifel (2004). His dimensionless parameters are $0.5 \leq \mathsf{F} \leq 2.8$, $0.3 \leq S \leq 1.4$, $0.3 \leq M \leq 4.1$ and $\alpha = 45°$. The maximum wave amplitudes a_{Mb} as result of solid bodies were compared by Zweifel (2004) with corresponding values from empirical equations for the maximum wave amplitudes a_M (Figure 3-3) resulting from a granular slide. This comparison is shown in Figure 4-6. The relative percentage difference of the maximum wave amplitude $(a_{Mb}/h - a_M/h)/(a_{Mb}/h)$ is plotted on the ordinate against the slide Froude number F on the abscissa. To determine a_M, the maximum wave height H_M from Eq. (3.6) can be multiplied by the factor (4/5) (Subsection 3.2.3.1). The differences between the maximum wave amplitudes generated by a solid body and granular slide were described with a coefficient of determination R^2 = 0.97 and a deviation of less than ±10% in Figure 4-6 as

$$\frac{a_{Mb}/h - a_M/h}{a_{Mb}/h} = 1 - 0.26\mathsf{F} \qquad \text{for } 0.5 \le \mathsf{F} \le 3.0. \qquad (4.2)$$

a_M [m]	=	Maximum wave amplitude (due to granular slide)
a_{Mb} [m]	=	Maximum wave amplitude as result of a solid body
F [-]	=	Slide Froude number; $\mathsf{F} = V_s/(gh)^{1/2}$
g [m/s^2]	=	Gravitational acceleration; g = 9.81 m/s^2
h [m]	=	Still water depth (in the slide impact zone)
V_s [m/s]	=	Slide impact velocity

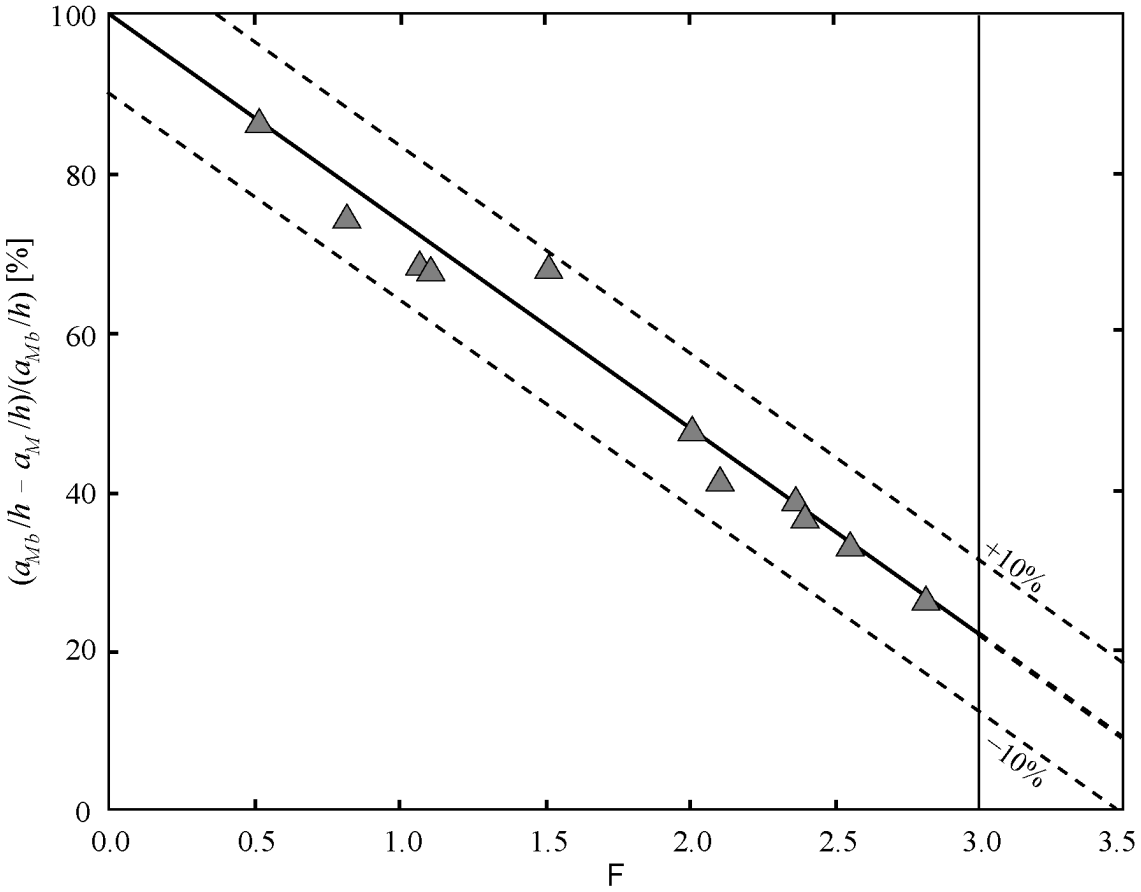

Figure 4-6 Comparison between the maximum wave amplitude generated by a solid body and a granular slide (after Zweifel 2004).

Whereas Zweifel (2004) determined that, for small Froude numbers, the maximum wave amplitude a_{Mb} is up to seven times greater for solid bodies than for granular slides, the difference for $\mathsf{F} > 3.0$ is small. This is because, for high Froude numbers and slide impact velocities V_s, the water is not able to enter the pore volume of the slide. Zweifel's (2004) comparison refers only to the maximum wave amplitude a_M in a very limited range. More comprehensive experiments on this effect have not been conducted.

4.4 Sensitivity analysis and safety allowance

This Section discusses the sensitivity of the run-up height R to variations of the governing parameters and defines those parameters to which R reacts particularly sensitively. As comprehensive calculation equations are available only for the 1st step, the sensitivity analysis relates only to them (Figure 3-1).

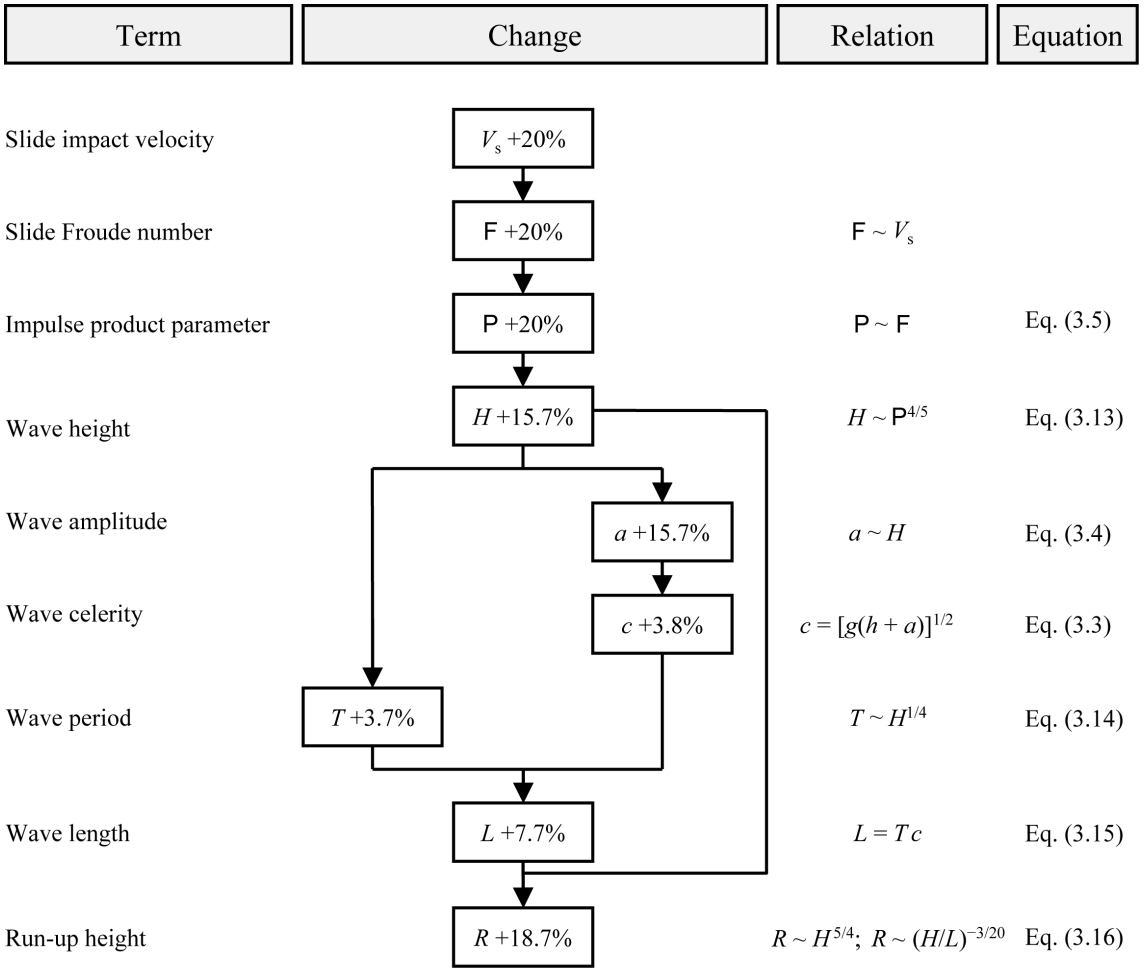

Figure 4-7 Calculation sequence to determine the effect on the run-up height R of a change of the slide impact velocity V_s by +20%.

Figure 4-7 shows the calculation sequence to determine the effect on the run-up height R of a change of the slide impact velocity V_s by +20%. In this procedure, V_s was each time made equal to 1.2 rather than 1.0, in order to determine the relative change. The value V_s occurs linearly in F and P. Equation (3.13) shows that the wave height H is proportional to $P^{4/5}$, and the relative change decreases to $(1.2/1.0)^{4/5} = 1.157$ or +15.7%. The percentage change may be determined in steps for all those variables which are influenced directly or indirectly by V_s. Finally, the change of R may be determined. An increase of V_s by +20% raises R by +18.7% (Figure 4-7). As the value of R is sensitive to V_s, the precise determination of the latter variable is important.

Analogous to Figure 4-7, the sensitivity of the run-up height R to a change by ±20% may be determined for each of the individual governing parameters. These are illustrated in Figure 4-8 for the 3D case (Eqs. 3.13, 3.14, 3.15 and 3.16). The individual parameters are presented in percentages as a bar chart, giving the variations and the extent of the effect on R. The following variables are included as governing parameters for wave generation and propagation: slide impact velocity V_s, still water depth h in the slide impact zone, slide thickness s, bulk slide volume $\forall_s$, bulk slide density ρ_s, slide width b, slide impact angle α and the wave propagation angle γ (Subsection 3.2.2). The governing parameters considered for wave run-up and dam overtopping are the still water depth h in front of the dam and the run-up angle β (Subsection 3.3.2). The following parameters were intentionally not considered as they may be determined precisely: distance x, radial distance r, freeboard f and the crest width b_K of the dam. The bulk slide porosity n was neglected as it is only indirectly included in the equations through ρ_s. The basis $\alpha = \gamma = 45°$ was selected to determine the relative deviation of the angles.

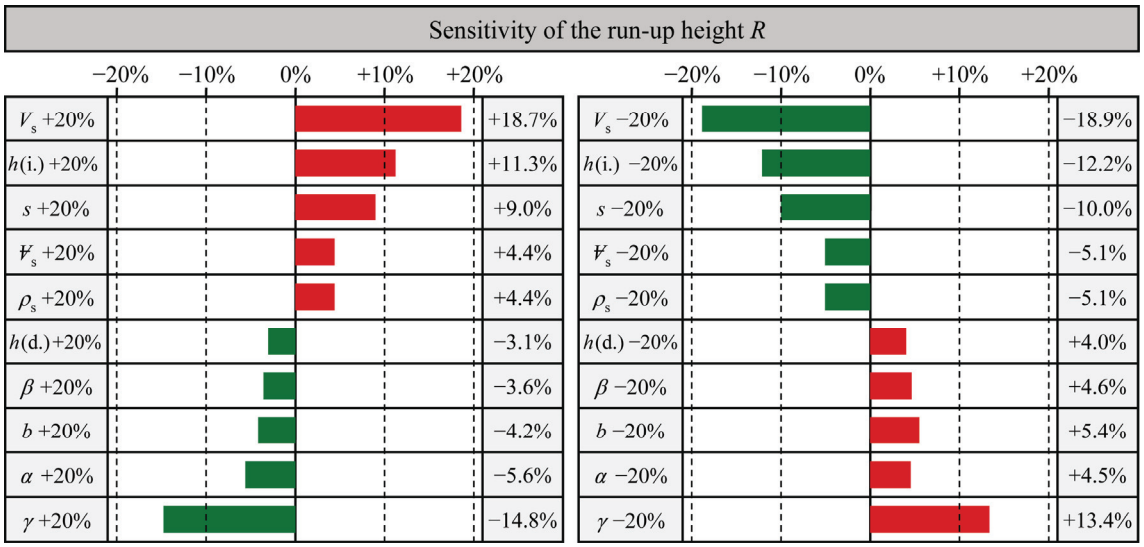

Figure 4-8 Sensitivity of the run-up height R according to Eq. (3.16) as a consequence of a variation of +20% (left) and −20% (right) of the governing parameters for the 3D case, with an increasing effect in red and a decreasing effect in green on R; Abbreviations: i. = impact zone and d. = dam.

The run-up height is particularly sensitive to the slide impact velocity V_s because any variation of V_s acts on R in a proportion of almost 1:1 (Figure 4-8). The wave propagation angle γ is not known exactly if the slide slope is inclined laterally and the principal impulse direction of the slide cannot be given unequivocally. The value R also reacts sensitively to γ. Finally, a relatively precise determination of the still water depth h in the slide impact zone and of the slide thickness s are important. The effects on R of $\forall_s$, ρ_s, h (in front of the dam), β, b and α are of secondary importance. From Figure 4-8 it can also be seen whether an increase or a decrease of a governing parameter acts negatively (red) or positively (green) on the value of R. To be on the safe side, the se-

lected values of V_s and h in the slide impact zone, as well as of s, should be rather greater than estimated, and the corresponding value of γ rather smaller.

Figure 4-8 shows only the sensitivity of R to variations in each of the governing parameters by ±20%. Combinations of changes in the governing parameters were not considered, neither was the sensitivity of further variables such as the additional horizontal force component ΔK_h or the overtopping volume V per unit length dam crest. These more complex cases may be analysed with the spread sheets (Section 5.3).

Basically, any dam overtopping by impulse waves should be prevented by precautionary water level lowering of the reservoir. Some safety considerations are given in this section. Further points are possible, depending on the prototype, and must be considered from case to case. The following factors affect the selection of *safety reserves*, for instance with regard to the run-up height R:

(i) Scatter of the measurement points in the empirical calculation equations
(ii) Probability of occurrence of mass movement
(iii) Extent of the deviations from the idealisation of the 1st step
(iv) Dam type (concrete dam, embankment dam with or without protective face)
(v) Damage potential in the valley downstream of the dam

(i) Scatter of the measurement points in the empirical calculation equations

The right-hand side of Eq. (3.16) for the determination of the run-up height R consists of a product. Analogous to the error calculation (e.g. Demidovich and Maron 1987) the maximum relative scatter for a product is equal *at most* to the sum of the individual values of the relative scatter of the parameters involved. Expressed mathematically, relevant for the product $u = x'_1 \cdot x'_2 \cdot \ldots \cdot x'_n$ is

$$\left|\frac{\Delta u}{u}\right| \le \left|\frac{\Delta x'_1}{x'_1}\right| + \left|\frac{\Delta x'_2}{x'_2}\right| + \ldots + \left|\frac{\Delta x'_n}{x'_n}\right|. \tag{4.3}$$

Equation (3.16) for the determination of R can be converted, with the help of $L = Tc$ (e.g. Eq. 3.15) to

$$R = 1.25 h^{-1/4} \left(\frac{90°}{\beta}\right)^{1/5} H^{11/10} T^{3/20} c^{3/20}. \tag{4.4}$$

From this, it follows that

$$\mathrm{d}R = 1.25 h^{-1/4} \left(\frac{90°}{\beta}\right)^{1/5} \left[\frac{11}{10} H^{1/10} \mathrm{d}H + \frac{3}{20} T^{-17/20} \mathrm{d}T + \frac{3}{20} c^{-17/20} \mathrm{d}c\right]. \tag{4.5}$$

The governing parameters h and β are not subjected to the scatter discussed here and were treated in Eq. (4.5) as constants. If Eq. (4.4) is divided by Eq. (4.5), the absolute value is formed and the maximum calculated value is considered, it follows in analogy to Eq. (4.3)

$$\left|\frac{\Delta R}{R}\right| = \frac{11}{10}\left|\frac{\Delta H}{H}\right| + \frac{3}{20}\left|\frac{\Delta T}{T}\right| + \frac{3}{20}\left|\frac{\Delta c}{c}\right|. \tag{4.6}$$

Most data points for H lie between ±40% (Figure A-7 in Appendix A), those of T between ±100% (Figure A-17b in Appendix A) and those of the wave celerity c between ±10% (Heller 2007a). The Eq. (4.6) results in (11/10)·40% + (3/20)·100% + (3/20)·10% ≈ 60%, whereby it may be predicted that R has a *maximum* scatter of about ±60%.

The maximum scatter for the calculation equations for other relevant values may be determined in a similar way to that used for R. For example, for the additional horizontal force component ΔK_h per unit length dam crest resulting from impulse wave, as calculated by Ramsden (1996), the scatter is ±50% and for ΔK_h, as calculated by Sainflou (1928), it is ±60%.

(ii) Probability of occurrence of mass movement

If a mass has started to creep, the risk of a slide occurring is greater than when only a potential slide mass exists. The higher the risk of occurrence of a slide, the more safety allowances are recommended.

(iii) Extent of the deviations from the idealisation of the 1st step

In the 1st step according to Figure 3-1 calculation equations are available. In the 2nd step, the effects of deviations from the idealisation in the 1st step can be determined only qualitatively or with estimation equations. The greater the deviation from the idealised concept (e.g. rectangular reservoir form, granular slide), the more safety allowances is needed.

(iv) Dam type (concrete dam, embankment dam with or without protective face)

Embankment dams with unprotected faces may be eroded by overtopping caused by impulse waves and, in the extreme case, this may lead to dam failure (Singh 1996). Gravity and arch dams are more resistant in this respect. The Vaiont arch dam withstood overtopping by an impulse wave and suffered no damage except at the left hand end of the dam crest (Schnitter 1964).

(v) Damage potential in the valley downstream of the dam

The greater the population of the downstream valley that would be affected by the effects of overtopping caused by an impulse wave or the greater the importance of the infrastructure of the valley, the more the safety allowances that have to be decided on. To determine the areas which would be affected, a numerical dam break calculation may be carried out.

Points (ii) to (v) must be assessed case by case. Selection of the safety allowances depends much on the characteristics of the prototype. A publication by the International Commission On Large Dams ICOLD (2002) addresses risk management with regard to potential slides into reservoirs.

5 Computational examples

5.1 Example 1

5.1.1 Problem description and governing parameters

Figure 5-1 shows the reservoir geometry assumed for example 1. A rockfall at location A threatens to impact into a reservoir, which is covered by a 0.25 m thick layer of ice. The maximum run-up height at point B on the opposite shore has to be determined. In addition, it has to be estimated whether the arch dam will be overtopped by the impulse wave and if so by how much the reservoir would have to be drawn down in order to prevent this overtopping. The freeboard is f =7 m. The sections A-B and A-C, corresponding to the broken lines in Figure 5-1, are shown in Figure 5-3.

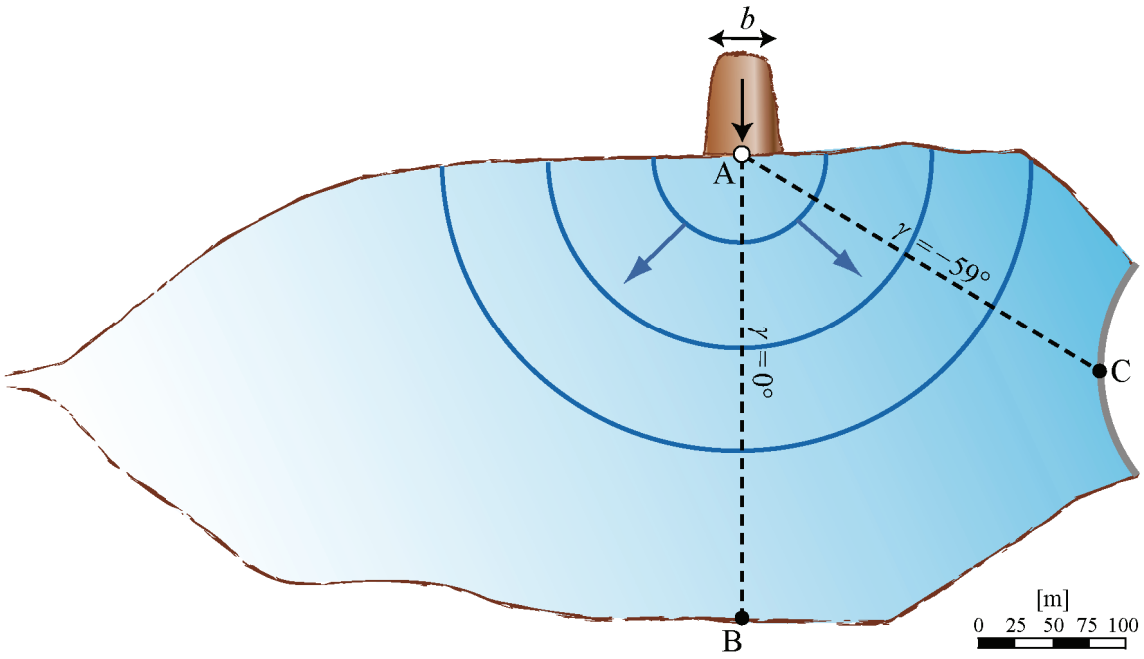

Figure 5-1 Reservoir geometry for example 1 with a rockfall impacting at point A; the reservoir is impounded by an arch dam.

The slide impact velocity V_s can be calculated using the detail from Figure 5-3(a) as shown in Figure 5-2. The parameters required to do this are given in Table 5-1. As there is a slope change, it is necessary to use both Eq. (3.1) and Eq. (3.2) for the calculation of V_s. The slide velocity at the point of slope change V_{sNK} is given by

$$V_{sNK} = \sqrt{2g\Delta z_{scN}(1-\tan\delta_N \cot\alpha_N)} \qquad \text{after Eq. (3.1)}$$

$$V_{sNK} = \sqrt{2 \cdot 9.81 \cdot 40(1-\tan 20° \cot 70°)} = 26.1 \text{ m/s.}$$

From this the slide impact velocity V_s can be calculated as

$$V_s = \sqrt{V_{sNK}{}^2 + 2g\Delta z_{sc}(1 - \tan\delta \cot\alpha)} \qquad \text{Eq. (3.2)}$$

$$V_s = \sqrt{26.1^2 + 2 \cdot 9.81 \cdot 60(1 - \tan 20° \cot 40°)} = 36.7 \text{ m/s}.$$

The calculated value of V_s, the governing parameters for wave generation, and those for the determination of the effects on the arch dam and on the opposite shore of the reservoir, are summarised in Table 5-2. The value b denotes the mean slide width and s is the maximum slide thickness in the impact zone. The values of bulk slide density ρ_s and bulk slide volume V_s also refer to the impact zone. The slide axis ($\gamma = 0°$) is governing for the selection of the still water depth h (Figure 3-3b).

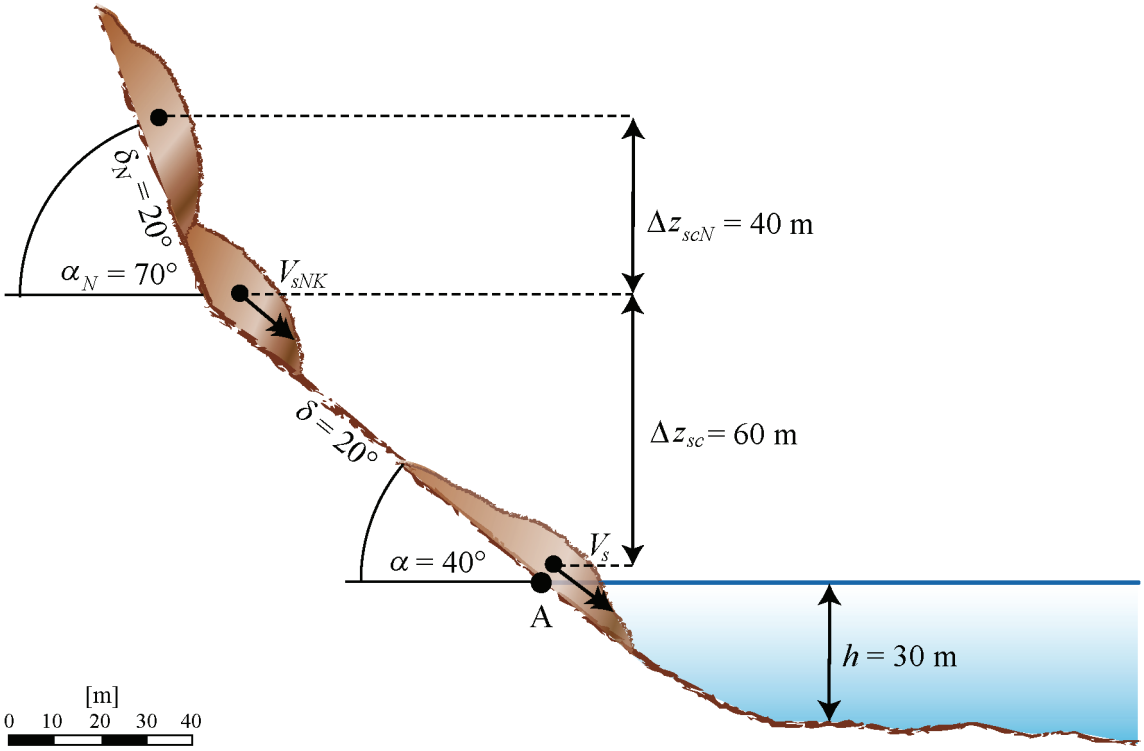

Figure 5-2 Parameters for the calculation of the slide impact velocity V_s.

Table 5-1 Governing parameters for the slide impact velocity V_s according to Figure 5-2.

First slope section				Second slope section			
Term	Symbol	Unit	Value	Term	Symbol	Unit	Value
Drop height of centre	Δz_{scN}	[m]	40	Drop height of centre	Δz_{sc}	[m]	60
Dynamic bed friction angle	δ_N	[°]	20	Dynamic bed friction angle	δ	[°]	20
Hill slope angle	α_N	[°]	70	Hill slope angle	α	[°]	40

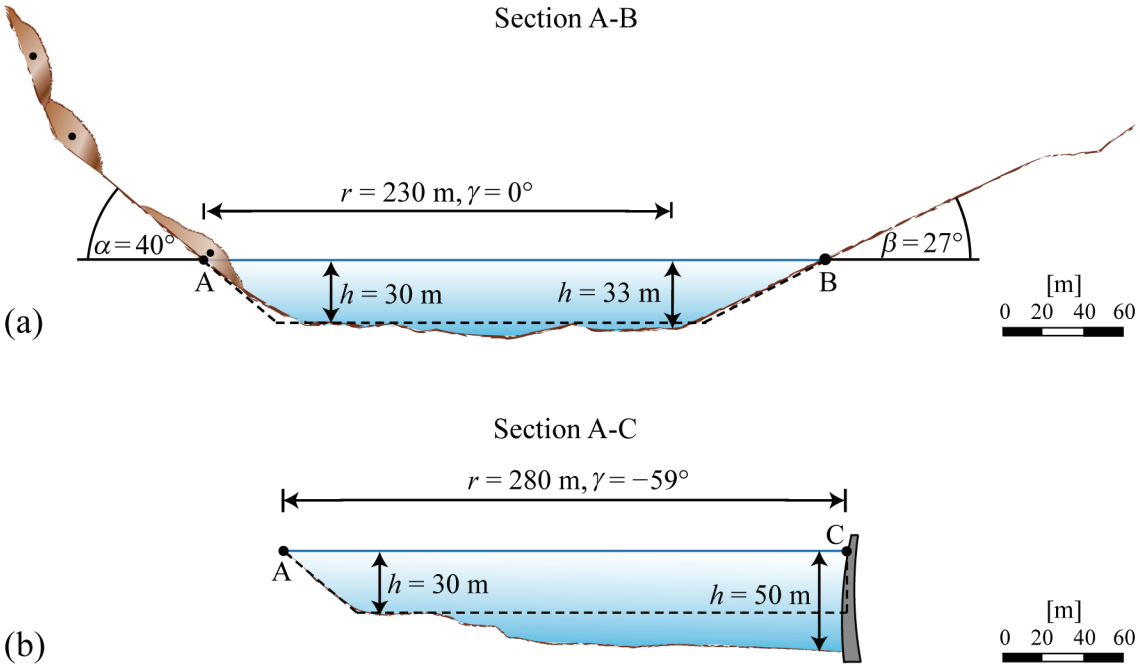

Figure 5-3 Sections for example 1 after Figure 5-1: (a) section A-B with rockslide and still water depth $h = 30$ m on the slide axis, and (b) section A-C; the broken lines indicate the idealised geometry for the 1st step.

Table 5-2 Governing parameters for impulse wave generation and the effects on the opposite shore, as well as on the arch dam.

Term	Symbol	Unit	Value	Term	Symbol	Unit	Value
Still water depth (impact zone)	h	[m]	30	Bulk slide density	ρ_s	[kg/m^3]	1,700
Slide thickness	s	[m]	12	Bulk slide porosity	n	[%]	35
Slide width	b	[m]	45	Slide impact angle	α	[°]	40
Slide impact velocity	V_s	[m/s]	37	Crest width	b_K	[m]	5
Bulk slide volume	$\forall_s$	[m^3]	22,000	Freeboard	f	[m]	7
Section A-B				Section A-C			
Radial distance	r	[m]	230	Radial distance	r	[m]	280
Wave propagation angle	γ	[°]	0	Wave propagation angle	γ	[°]	−59
Still water depth (run-up zone)	h	[m]	33	Still water depth (at dam)	h	[m]	50
Run-up angle	β	[°]	27	Run-up angle	β	[°]	90

5.1.2 1st step

In this section, the 1st step is carried out, in accordance with Figure 3-1. The impulse wave propagates radially and completely freely. Hence, the wave parameters can be calculated using the 3D equations for the reservoir of rectangular form (Subsection 3.2.1). The calculation proceeds in several partial steps:

a) Dimensionless parameters and limitations control on the calculation of the wave generation and propagation

For optimum prediction with this computation procedure the dimensionless parameters of the prototype must be within the range of limitations for use of the calculation equa-

tions. The relevant dimensionless parameters and limitations (Subsection 3.2.3.1) are given in Table 5-3.

Table 5-3 Dimensionless parameters and limitations control for the calculation of the wave generation and propagation.

Term	Dimensionless parameter	Range	Satisfied?
Slide Froude number	$\mathsf{F} = 37/(9.81 \cdot 30)^{1/2} = 2.16$	$0.86 \le \mathsf{F} \le 6.83$	Yes
Relative slide thickness	$S = 12/30 = 0.40$	$0.09 \le S \le 1.64$	Yes
Relative slide density	$D = 1{,}700/1{,}000 = 1.70$	$0.59 \le D \le 1.72$	Yes
Relative slide volume	$V = 22{,}000/(45 \cdot 30^2) = 0.54$	$0.05 \le V \le 5.94$	Yes
Relative slide mass	$M = 1{,}700 \cdot 22{,}000/(1{,}000 \cdot 45 \cdot 30^2) = 0.92$	$0.11 \le M \le 10.02$	Yes
Bulk slide porosity	$n = 35\%$	$30.7\% \le n \le 43.3\%$	Yes
Relative slide width	$B = 45/30 = 1.50$	$0.74 \le B \le 3.33$	Yes
Slide impact angle	$\alpha = 40°$	$30° \le \alpha \le 90°$	Yes
Impulse product parameter (Eq. 3.5)	$\mathsf{P} = 2.16 \cdot 0.40^{1/2} \cdot 0.92^{1/4} \cdot \{\cos[(6/7)40°]\}^{1/2} = 1.22$	$0.17 \le \mathsf{P} \le 8.13$	Yes
Relative radial distance section A-B	$r/h = 230/30 = 7.7$	$5 \le r/h \le 30$	Yes
Relative radial distance section A-C	$r/h = 280/30 = 9.3$	$5 \le r/h \le 30$	Yes
Wave propagation angle A-B	$\gamma = 0°$	$-90° \le \gamma \le +90°$	Yes
Wave propagation angle A-C	$\gamma = -59°$	$-90° \le \gamma \le +90°$	Yes

In the wave generation phase all limitations are satisfied.

b) Calculation of wave generation and propagation

Wave generation will be analysed using the 3D method, as described in Subsection 3.2.3.3, for which important variables are the wave height H, wave amplitude a, wave period T and the wave length L. The maximum wave parameter values in the slide impact zone are determined, independently of the 2D or 3D geometry, by applying Eqs. (3.6), (3.8) and (3.9). If, however, for the distance to the point for which the wave parameters are sought $x > x_M$ (2D) or $r > x_M$ (3D), the calculation equations differ for the 2D and 3D cases (Subsections 3.2.3.2 and 3.2.3.3). The streamwise distance x_M of the maximum wave height H_M can be determined with Eq. (3.7) as

$$x_M = (11/2)\mathsf{P}^{1/2} h \qquad \text{Eq. (3.7)}$$

$$x_M = (11/2)1.22^{1/2}30 = 182.2 \text{ m.}$$

As the two radial distances r to the reservoir bed in front of point B and to point C on the dam exceed 182.2 m (Table 5-2), the wave parameters have to be determined using Eqs. (3.13), (3.14) and (3.15) and *not* Eqs. (3.6), (3.8) and (3.9).

Section A-B

$$H(r, \gamma) = (3/2)\mathsf{P}^{4/5} \cos^2\left(\frac{2\gamma}{3}\right)(r/h)^{-2/3} h \qquad \text{Eq. (3.13)}$$

$$H = (3/2)1.22^{4/5} \cos^2\left(\frac{2 \cdot 0°}{3}\right)(230/30)^{-2/3} 30 = 13.6 \text{ m}$$

$a = (4/5)H$ Eq. (3.4)

a = (4/5)13.5 = 10.9 m

$$T(r,\ \gamma) = 15\left(\frac{H}{h}\right)^{1/4}(h/g)^{1/2}$$ Eq. (3.14)

$$T = 15\left(\frac{13.6}{33}\right)^{1/4}(33/9.81)^{1/2} = 22.0 \text{ s}$$

$L(r,\ \gamma) = T(r,\ \gamma)c(r,\ \gamma)$ Eq. (3.15)

L = 22.0[9.81(33 + 10.9)]$^{1/2}$ = 457.0 m

Section A-C

$$H(r,\ \gamma) = (3/2)\mathsf{P}^{4/5}\cos^2\left(\frac{2\gamma}{3}\right)(r/h)^{-2/3}h$$ Eq. (3.13)

$$H = (3/2)1.22^{4/5}\cos^2\left(\frac{2(-59°)}{3}\right)(280/30)^{-2/3}30 = 7.1 \text{ m}$$

$a = (4/5)H$ Eq. (3.4)

a = (4/5)7.1 = 5.7 m

$$T(r,\ \gamma) = 15\left(\frac{H}{h}\right)^{1/4}(h/g)^{1/2}$$ Eq. (3.14)

$$T = 15\left(\frac{7.1}{50}\right)^{1/4}(50/9.81)^{1/2} = 20.8 \text{ s}$$

$L(r,\ \gamma) = T(r,\ \gamma)c(r,\ \gamma)$ Eq. (3.15)

L = 20.8[9.81(50 + 5.7)]$^{1/2}$ = 486.2 m

The greater wave height is to be expected on the opposite shore, on the slide axis γ= 0°. Laterally to the slide axis γ= 0°, the wave height decreases (Figure A-4 in Appendix A). At point B, the wave height is with H = 13.6 m noticeably greater than at point C, where H = 7.1 m, even though the radial distances r are not significantly different.

To determine the *wave celerity c* between the points A and B and between A and C (Figure 5-1), the maximum wave amplitude a_M in the impact zone has to be known. This can be determined from the maximum wave height H_M using the relationship $a_M = (4/5)H_M$, and is thus

$a_M = (4/5)H_M = (4/5)(5/9)\mathsf{P}^{4/5}h$ Eqs. (3.6) and (3.4)

a_M = (4/5)(5/9)1.22$^{4/5}$30 = 15.6 m.

With a mean still water depth of (30 + 33)/2 = 31.5 m (Figure 5-3a) and a mean wave amplitude of (15.6 + 10.9)/2 = 13.3 m between point A and the base of the slope, in front of point B, it follows that

$c = [g(h + a)]^{1/2}$ Eq. (3.3)

c = [9.81(31.5 + 13.3)]$^{1/2}$ = 21.0 m/s.

The impulse wave covers the distance $r = 230$ m in roughly $r/c = 230/21.0 = 11$ s. The remaining quarter of the total distance, i.e. from the base of the slope to point B, will be covered in $(1/3)\cdot 11 \approx 4$ s. The total time for the wave to travel from A to B is, therefore, 15 s.

The wave celerity between A and C may be calculated in the same way. The mean still water depth is equal to $(30 + 50)/2 = 40$ m (Figure 5-3b) and the mean amplitude is $(15.6 + 5.7)/2 = 10.7$ m, therefore

$$c = \left[g(h + a)\right]^{1/2} \qquad \text{Eq. (3.3)}$$

$$c = [9.81(40 + 10.7)]^{1/2} = 22.3 \text{ m/s}.$$

The impulse wave takes about $r/c = 280/22.3 = 13$ s to travel the 280 m from point A to the arch dam (point C).

c) Wave run-up including limitations control

With help of the wave parameters calculated in b), the dimensionless parameters for the arch dam as well as the run-up height R may be calculated. Equation (3.16) is valid only for the run-up calculation on dams. As on the opposite shore the run-up angle $\beta = 27°$ satisfies the limitation $1.0 \leq 90°/\beta \leq 4.9$ for Eq. (3.16), this equation may anyway be used to estimate the run-up height. As distinct from the case when waves run-up dams, the neglected governing parameters in Eq. (3.16), i.e. the permeability and roughness of the shore, are relevant, as they attenuate the run-up height R. The value obtained with Eq. (3.16) for point B thus tends to over-estimate the run-up height R. In Tables 5-4 and 5-5 compliance with the limiting parameters is verified and then the run-up height R is computed.

Section A-B

Table 5-4 Dimensionless parameters and limitations control for the calculation of wave run-up at point B.

Term	Dimensionless parameter	Range	Satisfied?
Relative wave height	$H/h = 13.6/33 = 0.412$	$0.011 \leq H/h \leq 0.521$	Yes
Wave steepness	$H/L = 13.6/457.0 = 0.030$	$0.001 \leq H/L \leq 0.013$	No
Relative angle	$90°/\beta = 90°/27° = 3.3$	$1.0 \leq 90°/\beta \leq 4.9$	Yes

$$R = 1.25\left(\frac{H}{h}\right)^{5/4}\left(\frac{H}{L}\right)^{-3/20}\left(\frac{90°}{\beta}\right)^{1/5} h \qquad \text{Eq. (3.16)}$$

$$R = 1.25\left(\frac{13.6}{33}\right)^{5/4}\left(\frac{13.6}{457.0}\right)^{-3/20}\left(\frac{90°}{27°}\right)^{1/5} 33 = 29.4 \text{ m}$$

Section A-C

Table 5-5 Dimensionless parameters and limitations control for the calculation of wave run-up at point C.

Term	Dimensionless parameter	Range	Satisfied?
Relative wave height	$H/h = 7.1/50 = 0.142$	$0.011 \le H/h \le 0.521$	Yes
Wave steepness	$H/L = 7.1/486.2 = 0.015$	$0.001 \le H/L \le 0.013$	No
Relative angle	$90°/\beta = 90°/90° = 1.0$	$1.0 \le 90°/\beta \le 4.9$	Yes

$$R = 1.25\left(\frac{H}{h}\right)^{5/4}\left(\frac{H}{L}\right)^{-3/20}\left(\frac{90°}{\beta}\right)^{1/5} h \qquad \text{Eq. (3.16)}$$

$$R = 1.25\left(\frac{7.1}{50}\right)^{5/4}\left(\frac{7.1}{486.2}\right)^{-3/20}\left(\frac{90°}{90°}\right)^{1/5} 50 = 10.3 \text{ m}$$

As only the wave steepness H/L breaches the limitations for sections A-B and A-C, this may have a small effect on the results. The impulse waves will, according to the preceding calculations, overtop a dam with a freeboard of $f = 7$ m at point C, since $R > f$.

d) Wave overtopping

As the freeboard of $f = 7$ m is smaller than the run-up height of $R = 10.3$ m at point C, a part of the impulse wave will overtop the dam. New limitations govern the determination of the overtopping volume (Subsection 3.3.3):

Point C

Table 5-6 Dimensionless parameters and limitations control for the calculation of wave overtopping at point C.

Term	Dimensionless parameter	Range	Satisfied?
Relative wave height	$H/h = 7.1/50 = 0.142$	$0.019 \le H/h \le 0.488$	Yes
Non-linearity	$a/H = 5.7/7.1 = 0.80$	$0.59 \le a/H \le 0.95$	Yes
Wave steepness	$H/L = 7.1/486.2 = 0.015$	$0.020 \le H/L \le 0.023$	No
Relative period	$T(g/h)^{1/2} = 20.8(9.81/50)^{1/2} = 9.2$	$9.0 \le T(g/h)^{1/2} \le 21.0$	Yes
Relative wave celerity	$c^2/(gh) = [9.81(50 + 5.7)]/(9.81 \cdot 50) = 1.11$	$0.83 \le c^2/(gh) \le 1.40$	Yes
Relative wave length	$L/h = 486.2/50 = 9.7$	$6.0 \le L/h \le 24.0$	Yes
Relative angle	$90°/\beta = 90°/90° = 1.0$	$1.0 \le 90°/\beta \le 4.9$	No

In order to determine the overtopping volumes $\forall$ the corresponding volume $\forall_0$ for $f = 0$ has first to be calculated as

$$\forall_0 = 1.45\kappa\left(\frac{H}{h}\right)^{4/3}\left(\frac{T}{\sqrt{h/g}}\right)^{4/9} h^2 \qquad \text{Eq. (3.17)}$$

$$\forall_0 = 1.45 \cdot 0.41 \cdot 0.88 \cdot 1.3^{3/2}\left(\frac{7.1}{50}\right)^{4/3}\left(\frac{20.8}{\sqrt{50/9.81}}\right)^{4/9} 50^2 = 385.3 \text{ m}^3/\text{m},$$

in which $\kappa_q = 0.41$, as $\beta = 90°$, $\kappa_b = 0.88$, from Figure 3-6(a) with $a_{Max,T}/b_K = 7.1/5 = 1.42$ ($a_{Max,T} \approx H$ after Subsection 3.3.3) and $\kappa_w = 1.3$. The overtopping volume $\forall_0$ for $f > 0$ is thus equal to

$$\forall = \left(1 - \frac{f}{R}\right)^{11/5} \forall_0 \qquad \text{Eq. (3.18)}$$

$$\forall = \left(1 - \frac{7}{10.3}\right)^{11/5} 385.3 = 31.5 \text{ m}^3/\text{m}.$$

The duration of overtopping t_0 for the overtopping volume $\forall_0 = 385.3$ m^3/m for $f = 0$ can be determined as

$$t_0 = 4\left(T\sqrt{g/h}\right)^{4/9}(h/g)^{1/2} \qquad \text{Eq. (3.19)}$$

$$t_0 = 4\left(20.8\sqrt{9.81/50}\right)^{4/9}(50/9.81)^{1/2} = 24.2 \text{ s}.$$

The average discharge per unit length dam crest for $f = 0$ is thus

$$q_{0m} = \forall_0/t_0 \qquad \text{Eq. (3.20)}$$

$$q_{0m} = 385.3/24.2 = 15.9 \text{ m}^2/\text{s}.$$

The maximum discharge per unit length dam crest for $f = 0$ is according to Subsection 3.3.3 $q_{0M} \approx 2 \cdot q_{0m} = 2 \cdot 15.9 = 31.8$ m^2/s, but this occurs for only a few seconds (Figure B-4b in Appendix B). From Table 3-5 it may be seen that the first limitation criterion $14 < T(g/h)^{1/2} < 22$ is not satisfied as $20.8(9.81/50)^{1/2} = 9$. However, the second criterion $10.5 < t_0(g/h)^{1/2} < 13.5$ equal to $24.2(9.81/50)^{1/2} = 10.7$ is satisfied. The fact that one of the criteria is not met reduces the dependability of the calculation. The values $q_{0m} = 15.9$ m^2/s and $q_{0M} = 31.8$ m^2/s are upper limits of the unknowns for $f = 7$.

e) Force effect on the arch dam during overtopping

Firstly, the wave type is determined with the wave type product $S^{1/3}M\cos[(6/7)\alpha]$:

$$S^{1/3} M \cos\left[(6/7)\alpha\right] \geq (4/5)\mathsf{F}^{-7/5} \qquad \text{Eq. (3.29)}$$

$0.40^{1/3}0.92 \cdot \cos[(6/7)40°] = 0.56$

$(4/5)2.16^{-7/5} = 0.27$

$0.56 \geq 0.27$

Hence, the force effect will be calculated using the method for the remaining wave types, as detailed in Subsection 3.4.4. The total horizontal force component at point C with $a/h = 0.11$ is

$$K_{tot,h} = \left[1 - 1.5(a/h)\right]^{1/6} K_{hs,h} \qquad \text{Eq. (3.30)}$$

$K_{tot,h} = [1 - 1.5(5.7/50)]^{1/6}(1/2)1{,}000 \cdot 9.81(2 \cdot 5.7 + 50)^2 = 17.9 \cdot 10^6$ N/m.

As some of the impulse wave will overtop the arch dam, the structure does not receive the full horizontal force component, as shown in Figure 3-13(b). Firstly the pressure at dam crest p_K is determined as

$$p_K = \frac{2K_{tot,h}}{(2a+h)^2}(2a-f) \qquad \text{Eq. (3.32)}$$

$$p_K = \frac{2 \cdot 17.9 \cdot 10^6}{(2 \cdot 5.7 + 50)^2}(2 \cdot 5.7 - 7) = 41{,}783 \text{ N/m}^2.$$

The reduced total horizontal force component $K_{tot,h,abg}$ per unit length dam crest resulting from an impulse wave and hydrostatic pressure is

$$K_{tot,h,abg} = \frac{(h+f)}{2}\left[p_K + \frac{2K_{tot,h}}{2a+h} \right] \qquad \text{Eq. (3.33)}$$

$$K_{tot,h,abg} = \frac{(50+7)}{2}\left[41{,}783 + \frac{2 \cdot 17.9 \cdot 10^6}{2 \cdot 5.7 + 50} \right] = 17.8 \cdot 10^6 \text{ N/m}.$$

The elevation $z_{K,tot,h,abg}$ of the resultant of $K_{tot,h,abg}$ is

$$z_{K,tot,h,abg} = \frac{[2K_{tot,h}/(2a+h) - p_K]\frac{(h+f)^2}{6} + p_K \frac{(h+f)^2}{2}}{[2K_{tot,h}/(2a+h) - p_K]\frac{h+f}{2} + p_K (h+f)} \qquad \text{Eq. (3.34)}$$

$$z_{K,tot,h,abg} = \frac{\left[2 \cdot 17.9 \cdot 10^6/(2 \cdot 5.7 + 50) - 41{,}783\right]\frac{(50+7)^2}{6} + 41{,}783\frac{(50+7)^2}{2}}{\left[2 \cdot 17.9 \cdot 10^6/(2 \cdot 5.7 + 50) - 41{,}783\right]\frac{50+7}{2} + 41{,}783(50+7)}$$

$$= 20.3 \text{ m}.$$

If $K_{tot,h,abg}$ is reduced by the horizontal force component $K_{RW,h}$ resulting from hydrostatic pressure then the additional horizontal force component resulting only from the impulse wave is obtained as

$$\Delta K_h = K_{tot,h,abg} - K_{RW,h} = K_{tot,h,abg} - \rho_w g h^2/2 \qquad \text{Eq. (3.33)} - \text{Eq. (3.21)}$$

$$\Delta K_h = 17.8 \cdot 10^6 - (1/2)1{,}000 \cdot 9.81 \cdot 50^2 = 5.5 \cdot 10^6 \text{ N/m}.$$

The additional horizontal force component ΔK_h resulting only from the impulse wave is relative to the hydrostatic effect $5.5 \cdot 10^6/[(1/2)1{,}000 \cdot 9.81 \cdot 50^2] = 45\%$. This additional impulse wave force component acts on the arch dam for only a short time, typically for a few seconds (Figure B-8b in Appendix B). The total horizontal force component $K_{tot,h}$ is only marginally reduced by the overtopping depth over the dam crest, which is $2a - f = 4.4$ m. Furthermore, no vertical force component is created as the upstream dam face is vertical (Subsection 3.4.2).

f) Required freeboard to prevent overtopping

The required freeboard f sufficient to ensure that the arch dam is not overtopped by the impulse wave, can now be determined. The run-up height at point C is equal to R = 10.3 m, whereas the freeboard is 7 m. Whether emergency drawdown of the reservoir by the difference $R - f$ = 3.3 m will be adequate to prevent overtopping, is difficult to judge before a new calculation is made. This is because, when the reservoir level is lowered, certain governing parameters such as the slide impact velocity V_s may change in an unfavourable sense. In this example, lowering the reservoir level by 5 m is assumed, giving a new freeboard of f = 12 m, and all calculations for section A-C have then to be repeated.

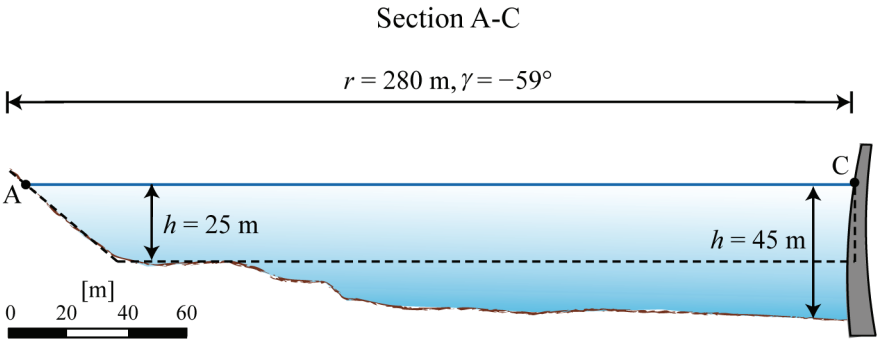

Figure 5-4 Section A-C after 5 m emergency drawdown of the reservoir and still water depth h = 25 m on the slide axis; the broken line indicates the idealised geometry for the 1st step.

The new slide impact velocity is

$$V_s = \sqrt{V_{sNK}{}^2 + 2g\Delta z_{sc}(1 - \tan\delta\cot\alpha)} \qquad \text{Eq. (3.2)}$$

$$V_s = \sqrt{26.1^2 + 2 \cdot 9.81 \cdot 65(1 - \tan 20° \cot 40°)} = 37.5 \text{ m/s.}$$

New dimensionless parameters (step a):
F = 2.39, S = 0.48, D = 1.70, V = 0.78, M = 1.33, n = 35%, B = 1.50, α = 40°, P = 1.62, r/h = 11.2 and γ = −59°. The limitations of the parameters in the impact zone are therefore still satisfied.

New wave parameters (step b):

$$H(r, \gamma) = (3/2)\mathrm{P}^{4/5} \cos^2\left(\frac{2\gamma}{3}\right)(r/h)^{-2/3} h \qquad \text{Eq. (3.13)}$$

$$H = (3/2)1.62^{4/5} \cos^2\left(\frac{2(-59°)}{3}\right)(280/25)^{-2/3} 25 = 6.6 \text{ m}$$

$$a = (4/5)H \qquad \text{Eq. (3.4)}$$

$$a = (4/5)6.6 = 5.3 \text{ m}$$

$$T(r,\ \gamma) = 15\left(\frac{H}{h}\right)^{1/4}(h/g)^{1/2} \qquad \text{Eq. (3.14)}$$

$$T = 15\left(\frac{6.6}{45}\right)^{1/4}(45/9.81)^{1/2} = 19.9 \text{ s}$$

$$L(r,\ \gamma) = T(r,\ \gamma)c(r,\ \gamma) \qquad \text{Eq. (3.15)}$$

$$L = 19.9[9.81(45 + 5.3)]^{1/2} = 442.1 \text{ m}$$

New wave run-up height (step c):

$$R = 1.25\left(\frac{H}{h}\right)^{5/4}\left(\frac{H}{L}\right)^{-3/20}\left(\frac{90°}{\beta}\right)^{1/5} h \qquad \text{Eq. (3.16)}$$

$$R = 1.25\left(\frac{6.6}{45}\right)^{5/4}\left(\frac{6.6}{442.1}\right)^{-3/20}\left(\frac{90°}{90°}\right)^{1/5} 45 = 9.6 \text{ m}$$

Table 5-7 Dimensionless parameters and limitations control for the calculation of wave run-up at point C, following drawdown by 5 m.

Term	Dimensionless parameter	Range	Satisfied?
Relative wave height	H/h = 6.6/45 = 0.147	$0.011 \le H/h \le 0.521$	Yes
Wave steepness	H/L = 6.6/442.1 = 0.015	$0.001 \le H/L \le 0.013$	No
Relative angle	$90°/\beta$ = 90°/90° = 1.0	$1.0 \le 90°/\beta \le 4.9$	Yes

Wave overtopping (step d):
For R = 9.6 m < f = 12 m, overtopping by an impulse wave after the 1st step is improbable. The assessment of the 2nd step is given in Subsection 5.1.3.

New force effect (step e):
The wave type has not changed as

$$S^{1/3} M \cos[(6/7)\alpha] \ge (4/5)\mathrm{F}^{-7/5} \qquad \text{Eq. (3.29)}$$

$0.48^{1/3}1.33\cdot\cos[(6/7)40°] = 0.86$
$(4/5)2.39^{-7/5} = 0.24$
$0.86 \ge 0.24$

The horizontal force components $K_{tot,h}$ and ΔK_h are

$$K_{tot,h} = [1 - 1.5(a/h)]^{1/6} K_{hs,h} \qquad \text{Eq. (3.30)}$$

$K_{tot,h} = [1 - 1.5(5.3/45)]^{1/6}(1/2)1{,}000\cdot 9.81(2\cdot 5.3 + 45)^2 = 14.7\cdot 10^6$ N/m,

$$\Delta K_h = K_{tot,h} - K_{RW,h} = K_{tot,h} - \rho_w g h^2/2 \qquad \text{Eq. (3.30)} - \text{Eq. (3.21)}$$

$\Delta K_h = 14.7\cdot 10^6 - (1/2)1{,}000\cdot 9.81\cdot 45^2 = 4.8\cdot 10^6$ N/m.

The elevation $z_{K,tot,h}$ of the resultant of $K_{tot,h}$ is located at $(2a + h)/3 = (2 \cdot 5.3 + 45)/3 = 18.5$ m (Subsection 3.4.4). The additional horizontal force component ΔK_h resulting from impulse wave is $4.8 \cdot 10^6/[(1/2)1{,}000 \cdot 9.81 \cdot 45^2] = 48\%$ relative to the hydrostatic effect.

The equations used in this section are based on laboratory test results some of which have a high degree of scatter (Section 4.4). When drawing down the reservoir, therefore, a safety allowance should be allowed for. Decisive is now the 2nd step, described in Subsection 5.1.3.

5.1.3 2nd step

Basically the characteristics of an impulse wave can be relatively well predicted from the reservoir geometry shown in Figure 5-1 with the help of generally applicable equations, as the reservoir geometry allows freely, radial wave propagation in 3D according to extreme case (b) (Subsection 3.2.1).

In the following section, the parameters *after* reservoir drawdown are applied. The deviations discussed below relate to the wave height H, the wave amplitude a or directly to the run-up height R. As the wave height H is related almost linearly as $H^{11/10}$ in Eq. (3.16) for the calculation of the run-up height, and in this manual the linear relationship $a = (4/5)H$ is applied, the changes for H and a will be carried over without modification to the run-up height R. Compared with the 1st step as shown in Figure 3-1, the following phenomena could lead to deviations:

- Exceeding of the limitations
- Solid body movement instead of granular slide
- Ice cover
- Volumetric displacement due to rockfall
- Reflection
- Shoaling
- Constriction

The *limitations* relating to the wave steepness H/L for points B and C, as well as those for the calculation of the overtopping discharge, are not satisfied. As the effect of this is not known, the uncertainty of the results will increase.

How big will be an impulse wave if the slide impacts into the reservoir as a solid body? This will result in a higher impulse wave, compared with the modelled granular slide in the 1st step. The increase in height may be estimated from Figure 4-6. The Froude number for an impacting solid body after drawdown is $\mathsf{F} = 2.39$. If Figure 4-6 is applied not only for the maximum amplitude a_M but also for any given amplitude a in the reservoir, it follows with the amplitude $a = 5.3$ m in front of the arch dam that

$$\frac{a_{Mb}/h - a_M/h}{a_{Mb}/h} = 1 - 0.26\mathsf{F} \qquad \text{Eq. (4.2)}$$

$$\frac{a_{Mb}/25 - 5.3/25}{a_{Mb}/25} = 1 - 0.26 \cdot 2.39 = 0.38.$$

Solved for the amplitude a_{Mb} as result of a solid body, it follows that a_{Mb} = 8.5 m and hence 8.5/5.3 = 1.60. This corresponds to an increase of about 60% compared with the calculation in the 1st step.

The *ice cover* of 0.25 m thickness will be pierced by the slide. As the ice sheet is lifted by the wave crest it will break up under its own weight, so that resulting damping of the impulse wave will only be insignificant (Section 4.2).

The reservoir surface area is about $2 \cdot 10^5$ m^2 (Figure 5-1). The reservoir water level will rise as a result of the *volumetric displacement* by the bulk slide mass of V_s = 22,000 m^3 by only about 22,000/200,000 = 0.11 m, if the bulk slide porosity n is neglected.

Wave reflections also have no effect in Figure 5-1, as $a_R \leq a$ (Figure 4-2a), which is also valid for the wave height. In addition, the wave will be reflected vertically at point B (angle of incidence equals angle of reflection) and is not directed against the dam.

The relative wave length L/h shows whether the impulse wave propagates as deep, intermediate or shallow-water wave. At point C, L/h = 442.1/45 = 9.8 and, therefore, the impulse wave behaves accordingly as an intermediate-water wave ($2 \leq L/h \leq 20$; Section 2.1), and is partly influenced by the reservoir bed. An increase of the water depth leads to a decrease of the height of intermediate-water waves. This effect may be estimated for section A-C in Figure 5-3(b) by assuming a constant energy flux for shallow and intermediate-water waves (Section 4.2). The value of H = 6.6 m was determined in partial step c), providing h = 25 m remains constant as far as the arch dam. These values are marked with index 1. If the still water depth h is greater, some of the wave energy will be needed for the additional water depth, and the wave height will be reduced. Index 2 denotes the condition when h = 25 m (indicated by a broken line in Figure 5-4b) changes to h = 45 m. As the widths $b_1 = b_2$ remain identical, the new wave height H_2 at point C is given by

$$\frac{H_2}{H_1} = \left(\frac{h_1}{h_2}\right)^{1/4} \qquad \text{for } b_1 = b_2 \qquad \text{after Eq. (4.1)}$$

$$H_2 = H_1\left(\frac{h_1}{h_2}\right)^{1/4} = 6.6\left(\frac{25}{45}\right)^{1/4} = 5.7 \text{ m}.$$

Due to the increase of the still water depth from 25 m to 45 m, the wave height close to the shore decreases from 6.6 m to 5.7 m, or by 15%. Close to the shore by point B (Figure 5-3a) the opposite occurs as the impulse wave height increases as a consequence

of the shallower still water (Figure 4-2b). This effect is already accounted for in the run-up formula, as the shallower still water corresponds to the lengthening of the shore with an identical run-up angle of $\beta = 27°$.

Constriction of the dam abutments leads to an increase of the wave height and hence also of the run-up height. If, furthermore, the lateral flank near the abutments is inclined this leads to an additional increase of the run-up height. The narrowing and inclination of the flank, as shown in Figure 4-4, have an effect of about 30%.

In summary an increase of the still water depth h towards the arch dam results in a decrease of H and thus of R; on the other hand, however, constriction and the lateral flank inclination in the dam abutments, as well as the slide behaving as a solid body, may lead to a significant increase. The constriction (≈ +30%) and the influence of the solid body (≈ +60%) are dominant compared with the effect of the decrease of the still water depth (≈ −15%). In total, these effects lead to an additional run-up height of (30% + 60% − 15%)R = 0.75·9.6 = 7.3 m. Together with the run-up height R = 9.6 m as calculated in the 1st step, a total of 9.6 m + 7.3 m = 16.9 m is obtained. Even when the freeboard f = 12 m is deduced, the impulse wave would still overtop the dam crest by 4.9 m. Hence, to prevent any overtopping, the reservoir drawdown of 5 m has to be increased by a further 4.9 m. The calculation has, therefore, to be repeated for the greater estimated drawdown value of about 10 m and the corresponding parameters.

5.1.4 Conclusions

The reservoir shape shown in Figure 5-1 is ideal for the computation procedure shown in Figure 3-1. The run-up height at the arch dam, as determined in the 1st step, is R = 10.3 m, and exceeds the freeboard of f = 7 m (Table 5-2). An impulse wave will therefore overtop the dam crest. Following reservoir drawdown of 5 m (Figure 5-4) to give a freeboard of f = 12 m, the calculated run-up height according to the 1st step is R = 9.6 m.

The use of the 2nd step, as per Figure 3.1, leads to a run-up height R which is 75% greater than that calculated in the 1st step. The reason for this is above all the fact that, as distinct from the 1st step, the slide behaves as a solid body, but also the greater run-up height in the dam abutments. In order to prevent dam overtopping, the reservoir level must be lowered a further 5 m, to give a total freeboard of f = 17 m. Whether overtopping will be avoided with the new value of f = 17 m has to be proven with a new calculation as well as the choice of suitable safety allowance (Section 4.4).

The additional horizontal force component on the dam resulting from impulse wave is of the order of 50% of the force component due to hydrostatic pressure. However, this additional force only acts for a few seconds (Figure B-8b in Appendix B).

5.2 Example 2

5.2.1 Problem description and governing parameters

Figure 5-5 shows the reservoir geometry for example 2. An icefall threatens to impact into an artificial reservoir at point A. The effects on the embankment dam of the impulse wave generated by the ice mass and the extent to which the reservoir should be drawn down to avoid dam overtopping have to be determined. On impact with the reservoir the icefall will consist of granular material. The freeboard is $f = 10$ m. The reservoir sections, which are shown in Figure 5-5 as broken lines, are presented in Figure 5-7.

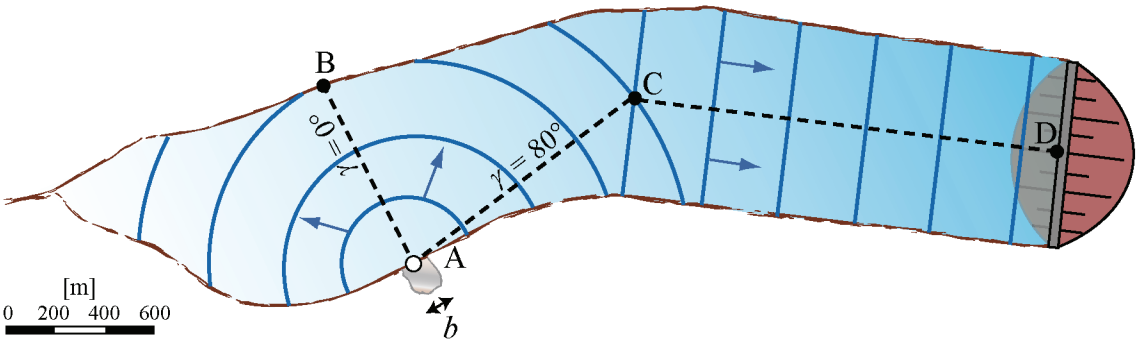

Figure 5-5 Reservoir geometry for example 2 with impacting icefall at point A; the reservoir is impounded by an embankment dam.

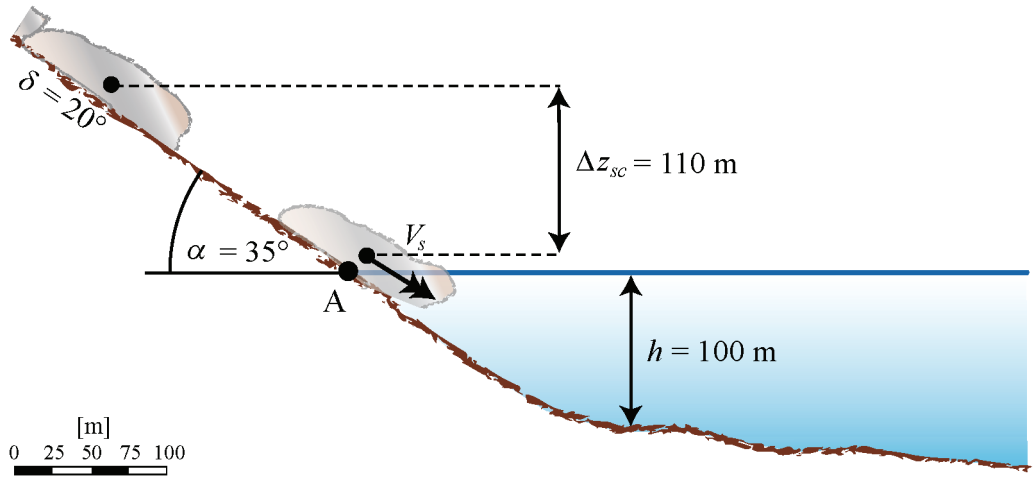

Figure 5-6 Parameters for the calculation of the slide impact velocity V_s.

For the reservoir geometry shown in Figure 5-5 the dam is not visible from the impact zone of the icefall. In the zone of the reservoir farthest from the dam the impulse waves may, however, propagate almost freely and radially (case b in Figure 3-2). Therefore, the wave parameters for point C will be determined using the 3D equations (Subsection 3.2.3.3). Between points C and D the reservoir geometry resembles that of a

laboratory wave channel (case a in Figure 3-2). Therefore, between these two latter points, the analysis accounts for 2D wave damping, on the assumption that the waves will move parallel to the bank. This assumption is on the safe side (Subsection 5.2.3).

Using Eq. (3.1), the slide impact velocity V_s can be calculated for a drop height of the centre of gravity of the slide of $\Delta z_{sc} = 110$ m, a dynamic bed friction angle of $\delta = 20°$ and a hill slope angle of $\alpha = 35°$, as

$$V_s = \sqrt{2g\Delta z_{sc}(1 - \tan\delta \cot\alpha)} \qquad \text{Eq. (3.1)}$$

$$V_s = \sqrt{2 \cdot 9.81 \cdot 110(1 - \tan 20° \cot 35°)} = 32.2 \text{ m/s}.$$

The slide impact velocity V_s as well as all the other governing parameters such as those for wave generation and for the determination of the effects on the embankment dam and on the reservoir shore, are given in Table 5-8. The parameter b indicates the mean slide width and s the mean slide thickness, both in the impact zone. The bulk slide density ρ_s and the bulk slide volume V_s are also relative to the impact zone (Subsection 3.2.2). The governing still water depth h lies on the slide axis ($\gamma = 0°$; Figure 3-3b).

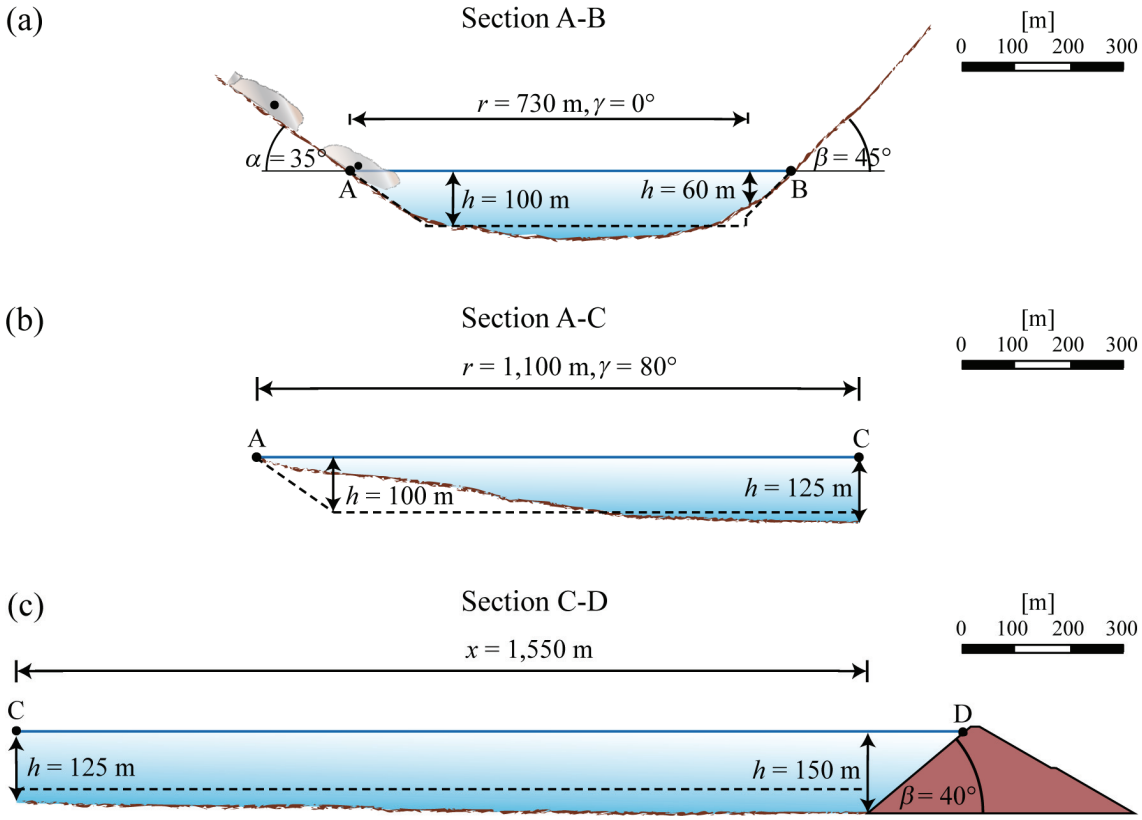

Figure 5-7 Sections for example 2, according to Figure 5-5: (a) section A-B with icefall and still water depth h = 100 m on the slide axis, (b) section A-C and (c) section C-D; the broken lines indicate the idealised geometries for the 1st step.

Table 5-8 Governing parameters for impulse wave generation, the effects on the opposite reservoir shore and on the embankment dam.

Term	Symbol	Unit	Value	Term	Symbol	Unit	Value
Still water depth (impact zone)	h	[m]	100	Bulk slide density	ρ_s	[kg/m^3]	500
Slide thickness	s	[m]	40	Bulk slide porosity	n	[%]	45
Slide width	b	[m]	120	Slide impact angle	α	[°]	35
Slide impact velocity	V_s	[m/s]	32	Crest width	b_K	[m]	12
Bulk slide volume	$\forall_s$	[m^3]	600,000	Freeboard	f	[m]	10
Section A-B				Section A-C			
Radial distance	r	[m]	730	Still water depth (impact zone)	h	[m]	100
Wave propagation angle	γ	[°]	0	Radial distance	r	[m]	1,100
Still water depth (run-up zone)	h	[m]	60	Wave propagation angle	γ	[°]	80
Run-up angle	β	[°]	45	Section C-D			
				Streamwise distance	x	[m]	1,550
				Still water depth (at dam)	h	[m]	150
				Run-up angle	β	[°]	40

5.2.2 1st step

The 1st step will now be carried out according to Figure 3-1. Firstly, the wave parameters for point C are calculated using the 3D equations given in Subsection 3.2.3.3. Then their variation between C and D is determined with the 2D damping terms, as given in Subsection 3.2.3.2. This calculation proceeds in the following partial steps:

a) Dimensionless parameters and limitations control on the calculation of the wave generation and propagation

The dimensionless parameters relevant for wave generation are given in Table 5-9.

Table 5-9 Dimensionless parameters and limitations control for the calculation of wave generation and propagation.

Term	Dimensionless parameter	Range	Satisfied?
Slide Froude number	$\mathsf{F} = 32/(9.81 \cdot 100)^{1/2} = 1.02$	$0.86 \le \mathsf{F} \le 6.83$	Yes
Relative slide thickness	$S = 40/100 = 0.40$	$0.09 \le S \le 1.64$	Yes
Relative slide density	$D = 500/1{,}000 = 0.50$	$0.59 \le D \le 1.72$	No
Relative slide volume	$V = 600{,}000/(120 \cdot 100^2) = 0.50$	$0.05 \le V \le 5.94$	Yes
Relative slide mass	$M = 500 \cdot 600{,}000/(1{,}000 \cdot 120 \cdot 100^2) = 0.25$	$0.11 \le M \le 10.02$	Yes
Bulk slide porosity	$n = 45\%$	$30.7\% \le n \le 43.3\%$	No
Relative slide width	$B = 120/100 = 1.20$	$0.74 \le B \le 3.33$	Yes
Slide impact angle	$\alpha = 35°$	$30° \le \alpha \le 90°$	Yes
Impulse product parameter (Eq. 3.5)	$\mathsf{P} = 1.02 \cdot 0.40^{1/2} \cdot 0.25^{1/4} \cdot \{\cos[(6/7)35°]\}^{1/2} = 0.42$	$0.17 \le \mathsf{P} \le 8.13$	Yes
Relative radial distance section A-B	$r/h = 730/100 = 7.3$	$5 \le r/h \le 30$	Yes
Relative radial distance section A-C	$r/h = 1{,}100/100 = 11.0$	$5 \le r/h \le 30$	Yes
Relative distance section C-D	$x/h = (1{,}100 + 1{,}550)/100 = 26.5$	$5 \le r/h \le 30$	Yes
Wave propagation angle A-B	$\gamma = 0°$	$-90° \le \gamma \le +90°$	Yes
Wave propagation angle A-C	$\gamma = 80°$	$-90° \le \gamma \le +90°$	Yes

Therefore, all limitations for wave generation are satisfied, with the exception of the bulk slide porosity $n = 45\%$ and the relative slide density $D = 0.50$. This will be discussed in Subsection 5.2.3, where the 2nd step is described. To verify the limitations on the relative distance x/h between points C and D, the distances A-C and C-D were added in Table 5-9.

b) Calculation of wave generation and propagation

Of interest for this calculation are the wave height H, wave amplitude a, wave period T and the wave length L. These parameters will be determined in front of point B and at point C using the 3D method, as per Subsection 3.2.3.3. Firstly, however, it has to be determined whether the wave parameters have to be calculated using the equations for the maxima or with these which also contain the damping terms. The streamwise distance x_M of the maximum wave height H_M is

$$x_M = (11/2)\mathrm{P}^{1/2}h \qquad \text{Eq. (3.7)}$$

$x_M = (11/2)0.42^{1/2}100 = 356.4$ m.

The radial distances r to points B and C are greater than $x_M = 356.4$ m, hence the wave parameter has to be computed with the Eqs. (3.13), (3.14) and (3.15), and *not* with Eqs. (3.6), (3.8) and (3.9).

Section A-B

$$H(r,\gamma) = (3/2)\mathrm{P}^{4/5}\cos^2\left(\frac{2\gamma}{3}\right)(r/h)^{-2/3}h \qquad \text{Eq. (3.13)}$$

$$H = (3/2)0.42^{4/5}\cos^2\left(\frac{2\cdot 0°}{3}\right)(730/100)^{-2/3}100 = 19.9 \text{ m}$$

$$a = (4/5)H \qquad \text{Eq. (3.4)}$$

$a = (4/5)19.9 = 15.9$ m

$$T(r,\gamma) = 15\left(\frac{H}{h}\right)^{1/4}(h/g)^{1/2} \qquad \text{Eq. (3.14)}$$

$$T = 15\left(\frac{19.9}{60}\right)^{1/4}(60/9.81)^{1/2} = 28.2 \text{ s}$$

$$L(r,\gamma) = T(r,\gamma)c(r,\gamma) \qquad \text{Eq. (3.15)}$$

$L = 28.2[9.81(60 + 15.9)]^{1/2} = 769.5$ m

Section A-C

$$H(r,\gamma) = (3/2)\mathrm{P}^{4/5}\cos^2\left(\frac{2\gamma}{3}\right)(r/h)^{-2/3}h \qquad \text{Eq. (3.13)}$$

$$H = (3/2)0.42^{4/5}\cos^2\left(\frac{2\cdot 80°}{3}\right)(1{,}100/100)^{-2/3}100 = 5.4 \text{ m}$$

$a = (4/5)H$ Eq. (3.4)

$a = (4/5)5.4 = 4.3$ m

$T(r,\ \gamma) = 15\left(\frac{H}{h}\right)^{1/4}(h/g)^{1/2}$ Eq. (3.14)

$T = 15\left(\frac{5.4}{125}\right)^{1/4}(125/9.81)^{1/2} = 24.4$ s

$L(r,\ \gamma) = T(r,\ \gamma)c(r,\ \gamma)$ Eq. (3.15)

$L = 24.4[9.81(125 + 4.3)]^{1/2} = 869.0$ m

Next the damping of the wave height $H = 5.4$ m and the increase of the wave period $T = 24.4$ s from point C to the embankment dam base in front of point D will be determined using the 2D damping terms. According to Eq. (3.10), an impulse wave is attenuated in the wave channel (Figure 3-2a) in proportion to $(x/h)^{-4/15}$, and the wave period increases, according to Eq. (3.11), in proportion to $(x/h)^{5/16}$. The wave parameters at the dam foot are given by:

Section C-D

$H(x) \sim X^{-4/15}$ after Eq. (3.10)

$H = 5.4(1{,}550/100)^{-4/15} = 2.6$ m

$a = (4/5)H$ Eq. (3.4)

$a = (4/5)2.6 = 2.1$ m

$T(x) \sim X^{5/16}$ after Eq. (3.11)

$T = 24.4(1{,}550/100)^{5/16} = 57.5$ s

$L(x) = T(x)c(x)$ Eq. (3.12)

$L = 57.5[9.81(150 + 2.1)]^{1/2} = 2{,}221.1$ m

The wave parameters $H = 2.6$ m, $a = 2.1$ m, $T = 57.5$ s and $L = 2{,}221.1$ m are therefore governing for the determination of the run-up height R on the slope of an embankment dam.

How long does it take the first impulse wave to reach the opposite shore of the reservoir or the embankment dam? For the estimation of the wave celerity c, the maximum wave amplitude a_M in the impact zone is required. This is determined from the maximum wave height as $a_M = (4/5)H_M$ and hence

$a_M = (4/5)H_M = (4/5)(5/9)\Psi^{4/5}h$ after Eqs. (3.6) and (3.4)

$a_M = (4/5)(5/9)0.42^{4/5}100 = 22.2$ m.

For section A-B (Figure 5-7a) the mean still water depth $(100 + 60)/2 = 80.0$ m and the mean wave amplitude $(22.2 + 15.9)/2 = 19.1$ m are governing. The mean wave celerity is hence

$$c = [g(h+a)]^{1/2} \qquad \text{Eq. (3.3)}$$

$c = [9.81(80 + 19.1)]^{1/2} = 31.2$ m/s.

The impulse wave covers the distance $r = 730$ m in $r/c = 730/31.2 = 23$ s and a few seconds later reaches point B on the opposite shore of the reservoir.

The impulse wave takes somewhat longer to reach the embankment dam. For a mean still water depth of $(100 + 125)/2 = 112.5$ m and mean wave amplitude of $(22.2 + 4.3)/2 = 13.3$ m between points A and C, it follows

$$c = [g(h+a)]^{1/2} \qquad \text{Eq. (3.3)}$$

$c = [9.81(112.5 + 13.3)]^{1/2} = 35.1$ m/s.

The impulse wave will propagate the radial distance of $r = 1{,}100$ m (Table 5-8) to the point C in about $r/c = 1{,}100/35.1 = 31$ s. For the distance C-D, a mean still water depth of $(125 + 150)/2 = 137.5$ m and a mean wave amplitude of $(4.3 + 2.1)/2 = 3.2$ m are the relevant parameters, for which

$$c = [g(h+a)]^{1/2} \qquad \text{Eq. (3.3)}$$

$c = [9.81(137.5 + 3.2)]^{1/2} = 37.2$ m/s.

The impulse wave propagates the distance of $x = 1{,}550$ m in $x/c = 1{,}550/37.2 = 42$ s, hence the total time required to move from the impact zone A to the embankment dam equals $31 + 42 = 73$ s.

c) Wave run-up including limitations control

With the aid of the wave parameters determined in b), the dimensionless parameters in front of the embankment dam as well as, subsequently, the run-up height R can be calculated. Equation (3.16) is valid only for run-up on the dam. As for the run-up angle $\beta = 45°$ on the opposite shore the limitation $1.0 \le 90°/\beta \le 4.9$ for Eq. (3.16) is satisfied, it may anyway be used to estimate the run-up height. However, as distinct from run-up on the dam, those governing parameters neglected in Eq. (3.16), namely the permeability and the roughness of the shore, become relevant, as they reduce the run-up height R. The values calculated with Eq. (3.16) for point B hence tend rather to over-estimate the run-up height R. Verification of limitations is shown in Table 5-10 and Table 5-11. Subsequently, the run-up height R is calculated.

Point B

Table 5-10 Dimensionless parameters and limitations control for the calculation of wave run-up at point B on the opposite shore.

Term	Dimensionless parameter	Range	Satisfied?
Relative wave height	$H/h = 19.9/60 = 0.33$	$0.011 \le H/h \le 0.521$	Yes
Wave steepness	$H/L = 19.9/769.0 = 0.026$	$0.001 \le H/L \le 0.013$	No
Relative angle	$90°/\beta = 90°/45° = 2.00$	$1.0 \le 90°/\beta \le 4.9$	Yes

$$R = 1.25\left(\frac{H}{h}\right)^{5/4}\left(\frac{H}{L}\right)^{-3/20}\left(\frac{90°}{\beta}\right)^{1/5} h \qquad \text{Eq. (3.16)}$$

$$R = 1.25\left(\frac{19.9}{60}\right)^{5/4}\left(\frac{19.9}{769.0}\right)^{-3/20}\left(\frac{90°}{45°}\right)^{1/5} 60 = 37.5 \text{ m}$$

Point D

Table 5-11 Dimensionless parameters and limitations control for the calculation of wave run-up on the dam at point D.

Term	Dimensionless parameter	Range	Satisfied?
Relative wave height	$H/h = 2.6/150 = 0.02$	$0.011 \le H/h \le 0.521$	Yes
Wave steepness	$H/L = 2.6/2{,}221.1 = 0.001$	$0.001 \le H/L \le 0.013$	Yes
Relative angle	$90°/\beta = 90°/40° = 2.25$	$1.0 \le 90°/\beta \le 4.9$	Yes

$$R = 1.25\left(\frac{H}{h}\right)^{5/4}\left(\frac{H}{L}\right)^{-3/20}\left(\frac{90°}{\beta}\right)^{1/5} h \qquad \text{Eq. (3.16)}$$

$$R = 1.25\left(\frac{2.6}{150}\right)^{5/4}\left(\frac{2.6}{2{,}221.1}\right)^{-3/20}\left(\frac{90°}{40°}\right)^{1/5} 150 = 3.8 \text{ m}$$

d) Wave overtopping

As the dam freeboard $f = 10$ m at point D is greater than the wave run-up height $R = 3.8$ m the situation analysed in the 1st step does not result in overtopping. Evaluation of the 2nd step has still to be considered (Subsection 5.2.3).

e) Force effect on the embankment dam

Firstly the wave type is determined by calculating the wave type product $S^{1/3}M\cos[(6/7)\alpha]$:

$$S^{1/3}M\cos[(6/7)\alpha] < (4/5)\mathsf{F}^{-7/5} \qquad \text{Eq. (3.23)}$$

$0.40^{1/3}0.25\cdot\cos[(6/7)35°] = 0.17$

$(4/5)1.02^{-7/5} = 0.78$

$0.17 < 0.78$

The force effect may then be calculated using the method for Stokes-like waves, as described in Subsection 3.4.3. The corresponding pressure distribution is shown in Figure 3-10(b). The pressure p_1 on dam foundation, the average water level rise Δh, the pressure p_2 at still water level, as well as the additional horizontal force component ΔK_h per unit length dam crest resulting from impulse wave may be calculated, according to Sainflou (1928), as

$$p_1 = \frac{\rho_w g H}{\cosh(2\pi h / L)} \qquad \text{Eq. (3.24)}$$

$$p_1 = \frac{1{,}000 \cdot 9.81 \cdot 2.6}{\cosh(2 \cdot 3.14 \cdot 150 / 2{,}221.1)} = 23{,}372 \text{ N/m}^2,$$

$$\Delta h = \frac{\pi H^2}{L} \coth\left(\frac{2\pi h}{L}\right) \qquad \text{Eq. (3.25)}$$

$$\Delta h = \frac{3.14 \cdot 2.6^2}{2{,}221.1} \coth\left(\frac{2 \cdot 3.14 \cdot 150}{2{,}221.1}\right) = 0.02 \text{ m},$$

$$p_2 = \frac{(\rho_w g h + p_1)(\Delta h + H)}{H + \Delta h + h} \qquad \text{Eq. (3.26)}$$

$$p_2 = \frac{(1{,}000 \cdot 9.81 \cdot 150 + 23{,}372)(0.02 + 2.6)}{2.6 + 0.02 + 150} = 25{,}662 \text{ N/m}^2 \text{ and}$$

$$\Delta K_h = \frac{p_2(\Delta h + H)}{2} + \frac{(p_1 + p_2)h}{2} \qquad \text{Eq. (3.27)}$$

$$\Delta K_h = \frac{25{,}662(0.02 + 2.6)}{2} + \frac{(23{,}372 + 25{,}662)150}{2} = 3.7 \cdot 10^6 \text{ N/m}.$$

The elevation $z_{\Delta K,h}$ of the resultant of ΔK_h is

$$z_{\Delta K,h} = \frac{p_1 \frac{h^2}{6} + p_2 \frac{h^2}{3} + \frac{p_2}{2}(\Delta h + H)\left[h + \frac{\Delta h + H}{3}\right]}{p_1 \frac{h}{2} + p_2 \frac{h}{2} + \frac{p_2}{2}(\Delta h + H)} \qquad \text{Eq. (3.28)}$$

$$z_{\Delta K,h} = \frac{23{,}372 \frac{150^2}{6} + 25{,}662 \frac{150^2}{3} + \frac{25{,}662}{2}(0.0 + 2.6)\left[150 + \frac{0.0 + 2.6}{3}\right]}{23{,}372 \frac{150}{2} + 25{,}662 \frac{150}{2} + \frac{25{,}662}{2}(0.0 + 2.6)} = 102.8 \text{ m}.$$

The horizontal force component ΔK_h results only from the impulse wave. In addition, the horizontal force component resulting from hydrostatic pressure acts on the dam with

$$K_{RW,h} = \rho_w g h^2 / 2 \qquad \text{Eq. (3.21)}$$

$$K_{RW,h} = 1{,}000 \cdot 9.81 \cdot 150^2 / 2 = 110.4 \cdot 10^6 \text{ N/m}.$$

The additional horizontal force component due to the impulse wave, relative to the horizontal force component due to hydrostatic pressure, is equal to $(3.7 \cdot 10^6 / 110.4 \cdot 10^6)100 = 3.4\%$. The total horizontal force component $K_{tot,h}$ per unit length dam crest resulting from impulse wave and hydrostatic pressure is therefore

$$K_{tot,h} = 3.7 \cdot 10^6 + 110.4 \cdot 10^6 = 114.1 \cdot 10^6 \text{ N/m}.$$

The upstream dam face is inclined at an angle of $\beta = 40°$. The forces so far computed describe the horizontal force components when $\beta = 90°$, but they do not change if $\beta < 90°$. However, an additional total vertical force component $K_{tot,v}$ also acts on the inclined dam face (Subsection 3.4.2). This component can be determined for the effects of the impulse wave including hydrostatic pressure as

$$K_{tot,v} = K_{tot,h} / \tan\beta \qquad \text{after Eq. (3.22)}$$

$K_{tot,v} = 114.1 \cdot 10^6 / \tan 40° = 136.0 \cdot 10^6$ N/m.

5.2.3 2nd step

The deviations determined in this subsection, which referred to the wave height H or the wave amplitude a, will be applied unchanged to the run-up height R (Subsection 5.1.3). The following phenomena may lead to variations as compared with the 1st step as shown in Figure 3-1:

- Exceeding of the limitations
- Volumetric displacement due to icefall
- Shoaling
- Reflection
- Constriction of the radial wave propagation and in the dam abutments

The following *limitations* are not satisfied: bulk slide porosity $n = 45\%$ ($30.7\% \le n \le 43.3\%$), bulk slide density $\rho_s = 500$ kg/m^3 (590 kg/m$^3 \le \rho_s \le 1{,}720$ kg/m^3) and wave steepness at point B for $H/L = 0.026$ ($0.001 \le H/L \le 0.013$). These will increase the uncertainty of the results.

The water level increase, as a result of the *volumetric displacement* by the icefall, for the reservoir surface area of $2.5 \cdot 10^6$ m^2 (Figure 5-5) and for a bulk slide volume of $V_s = 600{,}000$ m^3, is $600{,}000/2.5 \cdot 10^6 = 0.24$ m. Considering a value of bulk slide porosity of $n = 45\%$ and the bulk slide density $\rho_g = 900$ kg/m^3 (i.e. < 1,000 kg/m^3) the reservoir surface rise would be even less. For this reason, volumetric displacement may be neglected.

A further effect is s*hoaling* (Section 4.2). Using the ratio of wave length to still water depth, the waves can be grouped as shallow ($L/h \ge 20$), intermediate ($2 < L/h < 20$) and deep-water waves ($L/h \le 2$). Approaching the dam intermediate-water waves are formed as $L/h = 2{,}221.1/150 = 14.8$. These will be partly influenced by the reservoir bed. The still water depth of $h = 100$ m used in the 1st step is constant up to the embankment dam, as shown by the broken lines in Figure 5-7(b) and (c). As some of the wave energy is used to bring into motion the 50 m water column below the broken line in Figure 5-7(c), the wave height H at point D will be correspondingly smaller than that calculated in Subsection 5.2.2. This effect may be calculated according to Green's law

using Eq. (4.1). In doing this, values with the index 1 are denominated as idealised geometry with $h = 100$ m = constant, whilst the index 2 denotes the condition with change from $h = 100$ m to $h = 150$ m (Figure 5-7). As the widths $b_1 = b_2$ are for both cases identical, the new wave height H_2 at point D may be determined as

$$\frac{H_2}{H_1} = \left(\frac{h_1}{h_2}\right)^{1/4} \qquad \text{for } b_1 = b_2 \qquad \text{after Eq. (4.1)}$$

$$H_2 = H_1\left(\frac{h_1}{h_2}\right)^{1/4} = 2.6\left(\frac{100}{150}\right)^{1/4} = 2.3 \text{ m}.$$

This corresponds to a reduction from 2.6 m to 2.3 m, or about 10% compared with the 1st step.

Next, possible *reflections* are discussed. If a wave encounters an obstruction the angle of incidence is equal to the angle of reflection (Figure 5-8). The reflection of the largest waves on the slide axis is not relevant for the dam, as they remain in the far end of the reservoir. The governing reflection is shown in Figure 5-8. From the calculation in the 1st step (Subsection 5.2.2) the wave movement from point C was assumed vertical to the shore line, in order to minimise the distance and remain on the safe side, therefore. In reality, the impulse waves follow a polygonal zig-zag course. The distance will thus be about 2,200 m, i.e. longer than the straight-line distance of $x = 1{,}550$ m between C and D (Table 5-8). In addition, at every reflection, the waves decrease in height (Section 4.2). From $H = 5.4$ m at point C, the wave height decreases to less than 2.6 m at point D.

A final effect is *constriction*. The free, radial wave propagation on section A-C is to a large extent fulfilled. Only by the last portion is it somewhat restricted (Figure 5-5). This effect is classed as slight. At the dam abutments, the constriction may lead to an increase of the run-up height by about 20-30%, compared with the values calculated in the 1st step for the centre of the embankment dam (Section 4.2).

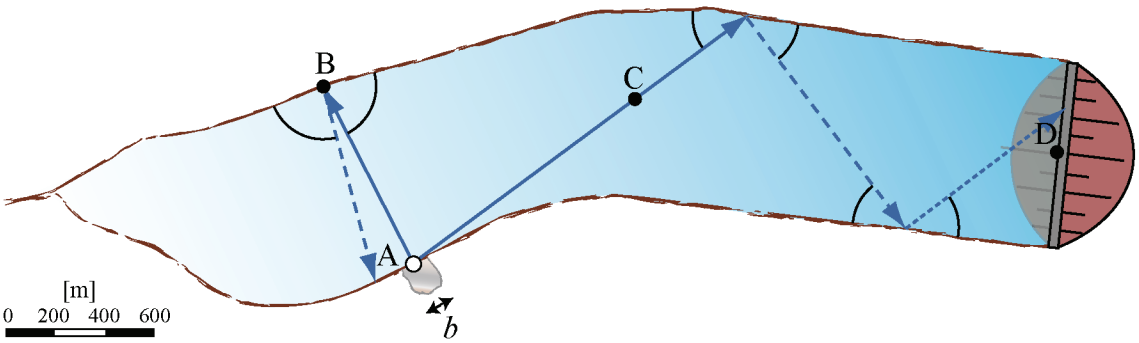

Figure 5-8 Wave reflection at point B has no consequences for the embankment dam. The wave departing towards point C reaches the embankment dam. Angles of incidence and reflection at the run-up points are in each case the same.

In summary, the phenomena of shoaling leads to a slight decrease (≈ −10%), the longer distance and the two reflections to a clear reduction of the wave height and the constriction to an increase (≈ +20-30%) of the wave and run-up heights. These increases and decreases in the 2nd step are more or less balanced. The freeboard of f = 10 m is sufficient to ensure that, with a run-up height R = 3.8 m, any overtopping is prevented.

5.2.4 Conclusions

In order to assess the effects of an impulse wave in a reservoir of the geometry shown in Figure 5-5, a calculation for the proximity of the impact zone, as far as point B on the opposite shore as well as to point C, is made by the 3D method. Between Points C and D the reservoir geometry resembles the geometry of a wave channel (Figure 5-5). Changes of the wave parameters between C and D will thus be determined with the 2D damping terms. According to the 1st step, this method gives a run-up height of R = 3.8 m on the embankment dam. Use of the 2nd step, shown in Figure 3.1, may change this result slightly, as the deviations from the idealised conditions of the 1st step effect the run-up height R in both positive and negative senses. The available freeboard of f = 10 m is sufficient to prevent overtopping. The additional horizontal force component due to impulse wave acting on the dam is only about 3% of the force component resulting from hydrostatic pressure.

5.3 Application of spread sheets

5.3.1 Introduction

The files with the spread sheets can be down-loaded from the VAW-Website www.vaw.ethz.ch under “News & Events”, “Latest VAW Reports”. In this section, the application of these spread sheets in Excel is explained. With these sheets, the effects of impulse waves on both dams and shores can be evaluated. The spread sheet facilitates the 1st step of the computation procedure (Figure 3-1) but the 2nd step must be carried out afterwards, *without* electronic help, as described in Chapter 4.

The spread sheet file includes unsigned *macros*, i.e. programs which contain a predefined sequence of instructions, actions or key combinations. By clicking on a given button, the corresponding macro is instructed to carry out the desired calculation. In Excel, when a file is opened with a macro, one is asked whether the macro in question should be activated, provided the *medium* security level has been chosen. The spread sheets function only when the macros have been activated. The security level can be adjusted in the menu listing under “Tools”, “Macro”, “Security…”. The security question refers only to the macros. Any possible macro viruses will as a result be neither identified nor deleted. The original file, which cannot be manipulated by third-parties, should therefore always be used.

5.3.2 Structure of the sheets

The file with the spread sheets contains three sheets. A sheet can be selected by clicking on the sheet name in the lower, left-hand corner of the screen. The most important functions of the three sheets are now explained. The names of the sheets are:

a) Input and output
b) Computation
c) Limitations

a) Input and output

First the project name, the computational point, the operator's name and the date are specified. In the space "Governing parameters", the parameters in the orange cells are entered. More details can be found on the governing parameters under the referred subsections. On the right are control buttons as well as definition sketches (Figure 3-2 and Figure 3-3). After completion of the calculations, the main results will be shown in the green cells. The number of limitations which have not been satisfied is also shown. A print-out of this sheet contains all important information and results of a calculation (Figure 5-9).

b) Computation

At the top, the computation procedure is shown (Figure 3-1). It has three buttons, with which the calculations are carried out and the results are given. The labels must be activated in order, from top to bottom, as certain calculations require results from those preceding them.

c) Limitations

This sheet contains all limitations on the use of the spread sheets as explained in Chapter 3. The dimensionless parameters are shown in the green cells and it is also shown whether each limitation is "Satisfied" or "Not satisfied". The more of the limitations are not satisfied, the greater will be the uncertainty of the calculated results (Section 4.1).

5.3.3 Application

The three sheets described in Subsection 5.3.2 should be used in order, from Input and output, to Computation, to Limitations and then back to Input and output. The required sheet can be selected by clicking on to the corresponding sheet name on the lower left of the screen. Input cells and buttons for calculations are highlighted in orange, the result

cells in light green. There is no access to any other cells. The calculation takes place in the following seven steps. The name of each corresponding sheet is thereby given in brackets.

(i) Input of project name, computational point, operator and date (upper part of Input and output).

(ii) Input of all governing parameters. For wave generation all governing parameters must be introduced, for wave propagation only the 3D (r, γ) or the 2D (x) parameters. In the Wave run-up and overtopping section parameters must always be given for the still water depth h and the run-up angle β. Values for the freeboard f and crest width b_K are needed only when the effects of the impulse wave on a dam have to be determined. If these effects have to be determined for the shore of the reservoir, these two cells have to be left empty. Empty orange cells must be shown with a hyphen (middle Input and output).

(iii) The button "Input control" has to be activated and the instructions or any error messages have to be followed. Firstly, it must be indicated whether the wave effects have to be determined for a dam (input "1") or for the shore (input "2"). This selection determines whether the values for freeboard f and crest width b_K are necessary. Error messages must not be ignored, otherwise the calculation will be erroneous. Only if no error message is received, after clicking on "Input control", the inputs are correct (right Input and output).

(iv) Change to the Computation sheet and activate the three buttons on the computation procedures, from top to bottom. Then it has to be indicated whether 2D (input "2") or 3D (input "3") calculations are to be made. The results will appear below. Cells which may not contain any data are indicated by "No value". The calculation of the wave parameters H, a, T and L is done for two distinct cases, as described in Chapter 3: for $X \leq X_M$ or $r/h \leq X_M$, the calculation is done with the equations for the maximum values (Eqs. 3.6, 3.4, 3.8, 3.9), whereas for $X > X_M$ or $r/h > X_M$ the equations with damping terms are applied (Eqs. 3.10, 3.4, 3.11, 3.12 for 2D and Eqs. 3.13, 3.4, 3.14, 3.15 for 3D cases, respectively). That is the reason, for example, why both symbols for wave height H and H_M are indicated in the identical cell (Computation).

(v) Change to the sheet Limitations and determine the dimensionless parameters with the button "Computation". The values of the dimensionless parameters will appear, together with "Satisfied" or "Not satisfied". "No value" appears if a limitation is not relevant, for example for x/h in a 3D calculation. The number of limitations not met is shown at the bottom (Limitations).

(vi) Change to the Input and output sheet and activate the button “Prepare to Print”. The most important results and the number of Limitations not satisfied are carried over into the print area (Figure 5-9). If more than one sheet is required for the area to be printed the Menu list “File”, “Page setup…”, “Margins” should be used to adjust the page margins. Here also some cells contain “No value”. At the beginning of each line giving values relating to forces it is indicated whether they were determined with the method for Stokes-like waves (Stokes), or that for the remaining wave types (Remaining). The printing procedure itself is initiated in the usual way with “File” and “Print…” (right Input and output).

(vii) To calculate the wave parameters for a new point on the same prototype (governing parameters do not change) the button “Delete all governing parameters except slide parameters” has to be activated. For calculations with other values of the governing variables or with a different reservoir still water depth (governing parameters change) use the button “Delete all governing parameters”. The button “Delete all” deletes all input data. For a new calculation, start again by (i) (Input and output).

Afterwards, an assessment of the effects from the 2nd step, as shown in Figure 3-1, has to be carried out but *without* electronic help (Subsection 5.3.3).

5.3.4 Example 1

In this example the effects of the impulse waves from example 1 for point C (Figure 5-1), according to Section 5.1, are determined using the spread sheets. The relevant print-out page is presented in Figure 5-9. The procedure consists of the seven steps explained in Subsection 5.3.3:

(i) The input data for the project are as shown in Figure 5-9.

(ii) The governing parameters are taken from Table 5-2 and the calculation is 3D. Hence, the cells for the streamwise distance x [m] contains no value, i.e. only a hyphen (Figure 5-9).

(iii) After activating the button “Input control”, indicate whether the effects of the impulse wave should be determined for a dam (input “1”) or on the shore (input “2”). For input “1” the data will be checked with regard to the calculation for a dam. No error messages appear, therefore the input is correct.

(iv) On the sheet Computation the three buttons “Computation” will be activated from top to bottom and in order. The results are shown in the lower part of

the sheet. As the calculation will be made in 3D and impulse waves will be computed with the method for the remaining wave types, the 2D cells and those for Stokes-like waves give “No value”.

(v) With the sheet Limitations, using the button “Computation” the dimensionless parameters are calculated and it can be checked if they satisfy the limitations. In this example, 2 of the limitations are not satisfied.

(vi) By clicking the button “Prepare to print” on the Input and output sheet, the most important results are given, together with the number of limitations not satisfied. Only the area shown in Figure 5-9 will be printed. Apart from small rounding-up variations, the results agree with those from example 1 (Section 5.1).

(vii) With the button “Delete all”, all values in the spread sheets are removed.

The assessment of the 2nd step, in accordance with Figure 3-1, has now to be carried out *without* electronic help (Subsection 5.1.3).

Landslide generated impulse waves in reservoirs - Basics and computation Spread sheets			
Project name	Example 1	Operator	John Doe
Computational point	Point C	Date	31.01.2009

Governing parameters			
Wave generation (Subsection 3.2.2)			
Slide impact velocity V_s [m/s]	37	Bulk slide density ρ_s [kg/m^3]	1,700
Bulk slide volume $\mathcal{V}_s$ [m^3]	22,000	Bulk slide porosity n [%]	35
Slide thickness s [m]	12	Slide impact angle α [°]	40
Slide or reservoir width b [m]	45	Still water depth h [m]	30
Wave propagation (3D or 2D) (Subsection 3.2.2)			
Wave basin (3D)		Wave channel (2D)	
Radial distance r [m]	280	Streamwise distance x [m]	-
Wave propagation angle γ [°]	-59		
Wave run-up and overtopping (Subsection 3.3.2)			
Still water depth h [m]	50	Freeboard f [m]	7
Run-up angle β [°]	90	Crest width b_K [m]	5

Main results	
Wave heigth H (H_M) [m]	7.1
Wave amplitude a (a_M) [m]	5.7
Wave period T (T_M) [s]	20.8
Wave length L (L_M) [m]	485.8
Run-up height R [m]	10.3
Overtopping volume $\mathcal{V}_0$ per unit length dam crest for f = 0 [m^3/m]	386.0
Duration of overtopping t_0 for f = 0 [s]	24.2
Average discharge q_{0m} per unit length dam crest for f = 0 [m^2/s]	15.9
Maximum discharge q_{0M} per unit length dam crest for f = 0 [m^2/s]	31.9
Overtopping volume per unit length dam crest $\mathcal{V}$ [m^3/m]	31.1
Hor. force comp. p.u.l. dam crest resulting only from hydrostatic pressure $K_{RW,h}$ [N/m]	12,262,500
Ver. force comp. p.u.l. dam crest resulting only from hydrostatic pressure $K_{RW,v}$ [N/m]	0
Wave type (Stokes-like wave 3.4.3 or remaining wave types 3.4.4)	Remaining
Remaining: total horizontal force component per unit length dam crest resulting from an impulse wave and hydrostatic pressure $K_{tot,h}$ [N/m]	17,900,676
Remaining: reduced total horizontal force component per unit length dam crest resulting from an impulse wave and hydrostatic pressure $K_{tot,h,abg}$ [N/m]	17,810,351
Remaining: elevation $z_{K,tot,h,abg}$ of the resultant of $K_{tot,h,abg}$ [m]	20.3
S/r: additional hor. force comp. p.u.l. dam crest resulting from impulse wave ΔK_h [N/m]	5,547,851
Stokes: elevation $z_{\Delta K,h}$ of the resultant of ΔK_h [m]	No value
S/r: ad. vertical force component p.u.l. dam crest resulting from impulse wave ΔK_v [N/m]	0

Limitations	
Number of not satisfied limitations out of 23 (2D) or 24 (3D), respectively	2

Figure 5-9 Print area of the spread sheets with project data, governing parameters, the main results as well as the number of limitations not satisfied; abbreviations: ad. = additional, comp. = component, hor./Hor. = Horizontal, p.u.l. = per unit length, S/r = Stokes/remaining, Vert. = Vertical.

5.3.5 Troubleshooting

Table 5-12 shows possible errors which may arise with the use of spread sheets with their possible cause and ways to correct them.

Table 5-12 Possible errors arising from the use of spread sheets with their causes and means to correct them.

Error	Cause	Correction
Nothing happens when clicking a button	Macros are disabled	Close file and open it again enabling macros (perhaps toggle security level under menu "Tools", "Macro", "Security..." to medium)
Computation is not working	Macros are disabled	Close file and open it again enabling macros (perhaps toggle security level under menu "Tools", "Macro", "Security..." to medium)
	Wrong/incomplete input	Enable button "Input control" on Input and output sheet and follow instructions
Print area requires more than one page	Margins are too large	Adjust margins under menu "File", "Page setup...", "Margins"
Cell displays #VALUE!	Wrong/incomplete input	Enable button "Input control" on Input and output sheet and follow instructions
Visual Basic Editor is launched	Wrong/incomplete input	Close file and open it again

6 Conclusions

6.1 Summary

This manual describes the present state of research on subaerial landslide generated impulse waves (Figure 1-1). The most important conclusions may be summarised as follows:

- Landslide generated impulse waves occur typically in oceans, bays, lakes or reservoirs as a result of landslides, rock falls, shore instability, avalanches or glacier calvings. Various distinct theoretical wave types are considered when describing the impulse wave spectrum (Section 2.2).

- A *complete procedure* (Figure 3-1) has been developed for the assessment of the effects on dams of landslide generated impulse waves; this takes into consideration parameters such as run-up height, overtopping volume and force effect, and is based on the use of generally applicable, semi-empirical equations.

- The analysis of the wave generation, as well as wave propagation and the overtopping of dams, considers all important governing parameters over a wide range. However, the procedure is limited to slide volumes that are significantly smaller than the volume of the reservoir or lake. For the cases described, the rise of the water surface level resulting from *volumetric displacement* by the slide is negligible compared with the wave height created by the slide impact.

- The procedure is based on the technical literature which is summarised in the Appendices A and B.

- The *user* of the procedure can estimate, for example, the run-up height on the dam face, both at little cost and in a short time (Section 1.2).

- In the *1st step* of the procedure, generally applicable equations are used under idealised conditions; principally by considering granular slide material as well as a channel-shaped (Figure 3-2a) or a rectangular-shaped (Figure 3-2b) reservoir, with a horizontal bed.

- In the *2nd step* of the procedure, the effects of deviations from the idealised conditions assumed in the 1st step are discussed. These relate above all to the reservoir shape and associated effects such as wave reflection, constriction or shoaling (Section 4.2), as well as the mass movement as a solid body rather than as a granular slide (Section 4.3).

- The procedure was successfully applied on two notional examples, as described in Chapter 5. A spread sheet facilitates the 1st step, but the 2nd step must be carried out *without* electronic aids.

- The procedure is based on laboratory test results, many of which exhibit significant scatter and may only be used approximately for complex reservoir geometries. The results have, therefore, to be considered only as *estimates*. Safety allowances must be provided; these depend on the damage potential and the dam type, but cannot be generally formulated (Section 4.4). More precise results, also for cases where the geometry is complex, may be obtained from a prototype-specific model test (Section 1.2).

- Potential exists for further research on landslide generated impulse waves, and the most important points in this respect are discussed in Section 6.2.

6.2 Research gaps

It is not possible today to analyse in a dependable manner, using generally applicable equations, each particular case of impulse wave generation. The reliability of predictions needs, therefore, still be improved and work on the questions given below would contribute to this. There is also a need for more research into the use of numerical simulations. The preparation of this manual revealed research gaps in the following fields:

- The methods of the future for the analysis of landslide generated impulse waves are numerical simulations. The aim should be to develop a generally applicable program into which it is only necessary to introduce data on the reservoir and slide geometries. This will enable the effects of landslide generated waves on dams to be determined with relatively high precision and only moderate effort (Section 1.2). Numerical methods already yield good results for individual experiments (Figure 1-5). Some experiments covering slide and wave profiles, as well as velocity vector fields in the slide impact zone, have been documented by Heller (2007a). In a subsequent step, such data could be used to develop this generally applicable program.

- The computation procedure presented in Figure 3.1 is based on a granular slide, although a natural slide may behave as a solid body (Cruden and Varnes 1996). Numerous investigations have been conducted on impulse waves generated by a solid body. A procedure to transform impulse waves resulting from granular slides to waves resulting from solid bodies would be useful. To date, however, only the findings of Zweifel (2004) are available and these have a limited range of use.

- The two extreme cases (a) a wave channel with confined longitudinally wave propagation and (b) a wave basin with free, radiating wave propagation, have already been studied several times (Figure 3-2). The wave parameters for more general reservoir geometries can only be estimated with the help of the parameters derived from analysing these two extreme geometric cases. Easier prediction of impulse waves for more general reservoir geometries would be possible by the investigation of the influence of the reservoir side angle γ. In addition to the values already studied ($\gamma = 0$ and $\gamma = \pm 90°$), it would be interesting to analyse e.g. values of $\gamma = \pm 15°$, $\gamma = \pm 30°$ (Figure 6-1), $\gamma = \pm 45°$, $\gamma = \pm 60°$ and $\gamma = \pm 75°$.

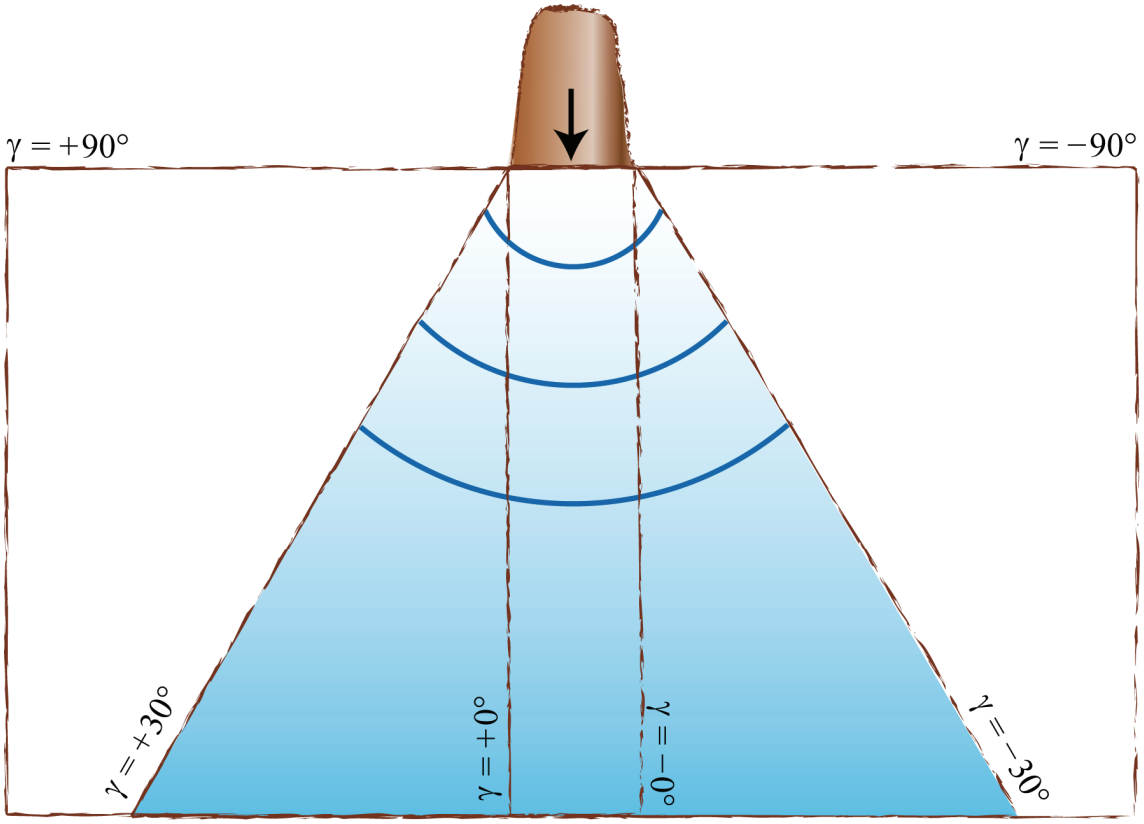

Figure 6-1 Reservoir geometry with side angles $\gamma = \pm 30°$ in addition to those already investigated, namely wave basin with $\gamma = \pm 90°$ and wave channel with $\gamma = \pm 0°$.

- Several points in the computation procedure are based on theoretical assumptions which have not been tested experimentally. Examples are the transformation of the wave height from that in the wave channel to that in the wave basin (Appendix A.3.2.2), or Eq. (3.14), which was defined for 2D and converted for 3D, but still has to be verified.

- Irrespective of reservoir geometry, the force effect was calculated based on the wave type classification procedure according to Heller (2007a). This is based on the results obtained from tests in a wave channel. In a wave basin, basically similar wave types were observed, for example by Huber (1980) or Panizzo et al. (2005), even though some of these had different designations. The 2D wave type defined by Heller (2007a) was used, because a clear classification for the 3D type is not available. A final wave type allocation in 3D or the relationship between the allocation in 2D (Figure A-8 in Appendix A) and 3D would be useful.

References

Ataie-Ashtiani, B., Malek Mohammadi, S. (2007). Near field amplitude of subaerial landslide generated waves in dam reservoirs. *Dam Engineering* 17(4):197-222.

Camfield, F.E. (1980). Tsunami Engineering. *Special Report* SR-6, U.S. Army Corps of Engineering, Coastal Engineering Research Center, Virginia.

Cooker, M.J., Weidman, P.D., Bale, D.S. (1997). Reflection of a high-amplitude solitary wave at a vertical wall. *Journal of Fluid Mechanics* 342:141-158.

Cruden, D.M., Varnes, D.J. (1996). Landslide types and processes. *Landslides*, Special Report 247:36-75. Turner, I., Schuster, A. eds. Transportation Research Board, Washington DC.

Dean, R.G., Dalrymple, R.A. (1991). *Water wave mechanics for engineers and scientists*. Advanced series on ocean engineering 2. World Scientific, Singapore.

Demidovich, B.P., Maron, I.A. (1987). *Computational mathematics*. Mir, Moscow.

Di Risio, M. (2005). Landslide generated impulse waves: generation, propagation and interaction with plane slopes. *PhD Thesis*, Third University of Rome, Rome.

Di Risio, M., Sammarco, P. (2008). Analytical modeling of landslide-generated impulse waves. *Journal of Waterway, Port, Coastal, and Ocean Engineering* 134(1):53-60.

DVWK (1997). Freibordbemessung an Stauanlagen. *Merkblätter zur Wasserwirtschaft* 246:1-21.

Falappi, S., Gallati, M. (2007). SPH simulation of water waves generated by granular landslides. Proc. 32nd *Congress of IAHR* Venice 933:1-10. IAHR, Madrid.

Fäh, R. (2005). Numerik an der VAW: Entwicklungen und Beispiel des Triftgletschers. *VAW-Mitteilung* 190:187-200. Minor, H.-E., ed. ETH Zurich, Zurich.

Fenton, J.D., Rienecker, M.M. (1982). A Fourier method for solving nonlinear water-wave problems: application to solitary-wave interactions. *Journal of Fluid Mechanics* 118:411-443.

Fritz, H.M. (2002). Initial phase of landslide generated impulse waves. *Dissertation* 14871. ETH Zurich, Zurich.

Fuminori, K. Shigeki, I., Masaya, F. (2003). Wave force on coastal dike due to tsunami. Proc. 50th Japanese Conf. *Coastal Engineering*, JSCE.

Gedik, N., Irtem, E., Kabdasli, S. (2005). Laboratory investigation on tsunami run-up. *Ocean Engineering* 32:513-528.

Hager, W.H. (1995). *Abwasserhydraulik*. Springer, Berlin.

Hall, J.V., Watts, G.M. (1953). Laboratory investigation of the vertical rise of solitary wave on impermeable slopes. *Technical Memo* 33, U.S. Army Corps of Engineers, Beach Erosion Board.

Heller, V. (2007a). Landslide generated impulse waves: prediction of near field characteristics. *Dissertation* 17531, ETH Zurich, Zurich.

Heller, V. (2007b). Massstabseffekte im hydraulischen Modell. *Wasser Energie Luft* 99(2):153-159.

Heller, V. (2008). Landslide generated impulse waves - Experimental results. Proc. 31st *Coastal Engineering Conference*, Hamburg. ASCE, New York (in press).

Heller, V., Hager, W.H. (2009a). Impulse product parameter in landslide generated impulse waves. *Journal of Waterway, Port, Coastal, and Ocean Engineering* (provisionally accepted).

Heller, V., Hager, W.H. (2009b). Wave types of landslide generated impulse waves. *Coastal Engineering* (submitted).

Heller, V., Hager, W.H., Minor, H.-E. (2008). Scale effects in subaerial landslide generated impulse waves. *Experiments in Fluids* 44(5):691-703.

Huber, A. (1975). Schwallwellen in einem See als Folge eines Felssturzes. Modellversuche zur Voraussage der Auswirkungen des Absturzes einer Gesteinsmasse in den Walensee. Proc. *Interpraevent* 1975:241-254.

Huber, A. (1980). Schwallwellen in Seen als Folge von Felsstürzen. *VAW-Mitteilung* 180, Vischer, D., ed. ETH Zurich, Zurich.

Huber, A. (1982). Felsbewegungen und Uferabbrüche an Schweizer Seen, ihre Ursachen und Auswirkungen. *Eclogae geologicae Helvetiae* 75(3):563-578.

Huber, A. (1987). Auswirkungen von Massenstürzen und Lawinenniedergängen auf Stauhaltungen. *Wasser Energie Luft* 79(11/12):309-313.

Huber, A. (2008). Oral statement, Zurich.

Huber, A., Hager, W.H. (1997). Forecasting impulse waves in reservoirs. Proc. 19th *Congrès des Grands Barrages*, Florence C.31:993-1,005. ICOLD, Paris.

Hughes, S.A. (1993). *Physical models and laboratory techniques in coastal engineering*. Advanced Series on Ocean Engineering 7. World Scientific, London.

Hunt, A. (1959). Design of seawalls and breakwaters. *Journal of the Waterways and Harbor Division* ASCE 85(WW3):123-152.

Hutter, K. (2008). Oral statement, Zurich.

ICOLD (2002). *Reservoir landslides: investigation and management - Guidelines and case histories*. Bulletin 124, ICOLD, Paris.

Ikeno, M., Mori, N., Tanaka, H. (2001). Experimental study on tsunami force and impulsive force by a drifter under breaking bore like tsunamis. Proc. 48th Japanese Conf. *Coastal Engineering*, JSCE.

Kamphuis, J.W., Bowering, R.J. (1972). Impulse waves generated by landslides. Proc. 12th *Coastal Engineering Conference*, Washington DC, 1:575-588. ASCE, New York.

Körner, H.J. (1976). Reichweite und Geschwindigkeit von Bergstürzen und Fliessschneelawinen. *Rock Mechanics* 8(4):225-256.

MacFarlane, D.F., Jenks, D.G. (1996). Stabilisation and performance of No. 5 Creek Slide, Clyde Power Project, New Zealand. Proc. 7th Intl. Symp. *Landslides* Trondheim 3:1,739-1,746. Senneset, K. ed. Balkema, Rotterdam.

Maxworthy, T. (1976). Experiments on the collision between two solitary waves. *Journal of Fluid Mechanics* 76:177-185.

Miche, R. (1951). Le pouvoir refléchissant des ouvrages maritimes. *Annales des Ponts et Chaussées* 121(May/June):285-319.

Miller, R.L. (1968). Experimental determination of run-up of undular and fully developed bores. *Journal of Geophysical Research* 73(14):4,497-4,510.

Minikin, R.R. (1950). *Winds, waves and maritime structures*. Charles Griffin & Company Limited, London.

Morris, H.M., Wiggert, J.M. (1972). *Applied hydraulics in engineering*. The Ronald Press Company, New York.

Müller, D. (1995). Auflaufen und Überschwappen von Impulswellen an Talsperren. *VAW-Mitteilung* 137, Vischer, D., ed. ETH Zurich, Zurich.

Müller, D., Schurter, M. (1993). Impulse waves generated by an artificially induced rockfall in a swiss lake. Proc. 25th *IAHR Congress* Tokyo. IAHR, Madrid.

Müller, D., Vischer, D. (1996). Bemessungsansätze für das Auflaufen und Überschwappen von Impulswellen an Talsperren. *Wasserwirtschaft* 86(11):560-564.

Nemcok, A., Pasek, J., Rybar, J. (1972). Classification of landslides and other mass movements. *Rock Mechanics* 4:71-78.

Noda, E. (1970). Water waves generated by landslides. *Journal of Waterways, Harbors and Coastal Engineering Division* ASCE 96(WW4):835-855.

Novak, P., Maffat, A.I.B., Nalluri, C., Narayanan, R. (2001). *Hydraulic structures*. Spon Press, London.

Panizzo, A., De Girolamo, P., Petaccia, A. (2005). Forecasting impulse waves generated by subaerial landslides. *Journal of Geophysical Research* 110 C12025:1-23.

Peregrine, D.H. (2003). Water-wave impact on walls. *Annual Review of Fluid Mechanics* 35:23-43.

Quecedo, M., Pastor, M., Herreros, M.I. (2004). Numerical modelling of impulse wave generated by fast landslides. *International Journal for Numerical Methods in Engineering* 59:1,633-1,656.

Ramsden, J.D. (1996). Forces on a vertical wall due to long waves, bores, and dry-bed surges. *Journal of Waterway, Port, Coastal, and Ocean Engineering* 122(3):134-141.

Sainflou, G. (1928). Essai sur les digues maritimes verticales. *Annales des Ponts et Chaussées* 128.

Salm, B., Burkard, A., Gubler, H.U. (1990). Berechnung von Fliesslawinen - Eine Anleitung für Praktiker mit Beispielen. *Mitteilung des Eidgenössischen Instituts für Schnee und Lawinenforschung* 47, SLF, Davos.

Schnitter, G. (1964). Die Katastrophe von Vaiont in Oberitalien. *Wasser- und Energiewirtschaft* 56(2/3):61-69.

Schröder, W., Saenger, N. (2002). Wasserbau und Wasserwirtschaft. *Bautabellen für Ingenieure mit Berechnungshinweisen und Beispielen* 13.0-13.146. Schneider, K.-J., ed. Werner, Düsseldorf.

Schuster, R.L., Wieczorek, G.F. (2002). Landslide triggers and types. Proc. 1st European Conf. *Landslides*, Prague, 59-78. Rybář, J., Stemberk, J., Wagner, P. eds. Balkema, Tokyo.

Shen, M.C., Meyer, R.E. (1963). Climb of a bore on a beach. *Journal of Fluid Mechanics* 16:113-125.

Singh, V.P. (1996). *Dam breach modeling technology*. Kluwer Academic Publisher, London.

Synolakis, C.E. (1987). The runup of solitary waves. *Journal of Fluid Mechanics* 185:523-545.

Synolakis, C.E. (1991). Tsunami runup on steep slopes: How good linear theory really is. *Natural Hazards* (4):221-234.

Tanimoto, K., Tsuruya, K., Nakano, S. (1984). Tsunami force of Nihonkai-Chubu Earthquake in 1983 and cause of revetment damage. Proc. 31th Japanese Conf. *Coastal Engineering*, JSCE.

Teng, M.H., Feng, K., Liao, T.I. (2000). Experimental study on long wave run-up on plane beaches. Proc. 10th *Intl. Offshore and Polar Engineering Conference* (3):660-664. Seattle, USA.

Thomas, R.S., Hall, B. (1992). *Seawall design*. Butterworth-Heinemann, Oxford.

USCE (1977). *Shore protection manual* I. U.S. Government Printing Office, Washington D.C.

USCE (2006). *Coastal Engineering Manual*. Online: http://chl.erdc.usace.army.mil/chl.aspx?p=s&a=Publications;8.

Walkden, M.J.A. (1999). Model wave impulse loads on caisson breakwaters: aeration, scale and structural response. *PhD Thesis*, University of Plymouth, UK.

Walkden, M.J.A., Bruce, T.B. (2000). Scatter in wave impulse load maxima: a review. Proc. Intl. Conf. *Coastal Structures*, Santander, Spain (1):439-444. Balkema, Rotterdam.

WCHL (1970). Hydraulic model studies - wave action generated by slides into Mica Reservoir - British Columbia. *Report*. Western Canada Hydraulic Laboratories, Vancouver.

Wiegel, R.L. (1964). *Oceanographical engineering*. Prentice-Hall, London.

Zweifel, A. (2004). Impulswellen: Effekte der Rutschdichte und der Wassertiefe. *Dissertation* 15596, ETH Zurich, Zurich.

Zweifel, A., Zuccalà, D., Gatti, D. (2007). Comparison between computed and experimentally generated impulse waves. *Journal of Hydraulic Engineering* 133(2):208-216.

Notation

a	[m]	=	wave amplitude
a_M	[m]	=	maximum wave amplitude
$a_{Max,T}$	[m]	=	maximum overtopping depth over a dam
a_{Mb}	[m]	=	maximum wave amplitude as result of a solid body
a_R	[m]	=	wave amplitude of a reflected wave
a_1	[m]	=	wave amplitude at cross-section 1 of Figure 4-2(b)
a_2	[m]	=	wave amplitude at cross-section 2 of Figure 4-2(b)
A	[-]	=	relative wave amplitude; $A = a/h$
A_M	[-]	=	relative maximum wave amplitude; $A_M = a_M/h$
b	[m]	=	slide or reservoir width in the prototype; channel width in the model
b_K	[m]	=	crest width
b_1	[m]	=	reservoir width at cross-section 1 of Figure 4-2(b)
b_2	[m]	=	reservoir width at cross-section 2 of Figure 4-2(b)
B	[-]	=	relative slide width; $B = b/h$
$BM_{hs,h}$	[Nm/m]	=	bending moment per unit length dam crest about the foundation resulting from the horizontal force of the hydrostatic pressure and a still water level displaced upwards by $2a$, according to Ramsden (1996)
$BM_{tot,h}$	[Nm/m]	=	bending moment per unit length dam crest about the foundation resulting from the horizontal force of an impulse wave and hydrostatic pressure, according to Ramsden (1996)
c	[m/s]	=	wave celerity
d	[-]	=	differential
d_b	[m]	=	block diameter
d_g	[m]	=	grain diameter
D	[-]	=	relative slide density; $D = \rho_s/\rho_w$
e	[-]	=	logarithmic constant; $e = 2.72$
f	[m]	=	freeboard
F	[-]	=	slide Froude number; $\mathsf{F} = V_s/(gh)^{1/2}$
g	[m/s^2]	=	gravitational acceleration; $g = 9.81$ m/s^2
G	[-]	=	combination of the governing parameters according to Huber and Hager (1997); $G = 0.88(\sin\alpha)(\rho_g/\rho_w)^{1/4}[\forall_g/(bh^2)]^{1/2}$
h	[m]	=	still water depth

h_1	[m]	=	still water depth at cross-section 1 of Figure 4-2(b)
h_2	[m]	=	still water depth at cross-section 2 of Figure 4-2(b)
H	[m]	=	wave height
H_{st}	[m]	=	stable wave height according to Kamphuis and Bowering (1972)
H_M	[m]	=	maximum wave height
H_1	[m]	=	wave height at cross-section 1 of Figure 4-2(b)
H_2	[m]	=	wave height at cross-section 2 of Figure 4-2(b)
I	[-]	=	Iribarren number; $I = \tan\beta/(H/L)^{1/2}$
k_D	[-]	=	reduction factor to allow for permeability
k_R	[-]	=	reduction factor to allow for roughness
$K_{hs,h}$	[N/m]	=	horizontal component of hydrostatic force per unit length dam crest resulting from a still water level displaced upwards by 2a, according to Ramsden (1996)
$K_{tot,h}$	[N/m]	=	total horizontal force component per unit length dam crest resulting from an impulse wave and hydrostatic pressure
$K_{tot,v}$	[N/m]	=	total vertical force component per unit length dam crest resulting from an impulse wave and hydrostatic pressure
$K_{tot,h,abg}$	[N/m]	=	reduced total horizontal force component per unit length dam crest resulting from an impulse wave and hydrostatic pressure
$K_{tot,v,abg}$	[N/m]	=	reduced total vertical force component per unit length dam crest resulting from an impulse wave and hydrostatic pressure
$K_{RW,h}$	[N/m]	=	horizontal force component per unit length dam crest resulting only from hydrostatic pressure
$K_{RW,v}$	[N/m]	=	vertical force component per unit length dam crest resulting only from hydrostatic pressure
l	[m]	=	coordinate along dam crest
l_s	[m]	=	slide length
l_F	[m]	=	width of reservoir flank
l_K	[m]	=	crest length
L	[m]	=	wave length
L_M	[m]	=	wave length of H_M
L_1	[m]	=	wave length at cross-section 1 of Figure 4-2(b)
L_2	[m]	=	wave length at cross-section 2 of Figure 4-2(b)
m_g	[kg]	=	slide grain mass identical to slide mass; $m_g = m_s$
m_s	[kg]	=	slide mass identical to slide grain mass; $m_s = m_g$
M	[-]	=	relative slide mass; $M = D \cdot V = m_s/(\rho_w b h^2) = \rho_s \forall_s/(\rho_w b h^2)$

n	[%]	=	bulk slide porosity
p	[N/m^2]	=	pressure on dam
p_d	[N/m^2]	=	dynamic pressure according to Minikin (1950)
p_s	[N/m^2]	=	static pressure according to Minikin (1950)
p_K	[N/m^2]	=	pressure at dam crest
p_1	[N/m^2]	=	pressure on dam foundation according to Sainflou (1928)
p_2	[N/m^2]	=	pressure at still water level according to Sainflou (1928)
P	[-]	=	impulse product parameter; $\mathsf{P} = \mathsf{F}S^{1/2}M^{1/4}\{\cos[(6/7)\alpha]\}^{1/2}$
q_{0m}	[m^2/s]	=	average discharge per unit length dam crest for $f = 0$
q_{0M}	[m^2/s]	=	maximum discharge per unit length dam crest for $f = 0$
r	[m]	=	radial distance from the impact location in the wave basin
R	[m]	=	run-up height
R^2	[-]	=	coefficient of determination
R_m	[m]	=	run-up height at the dam centre
$R_{\gamma \neq 0°}$	[m]	=	run-up height for oblique flow against a dam
s	[m]	=	slide thickness
s_1	[m]	=	slide thickness in Figure A-5(a) of Appendix A
s_2	[m]	=	slide thickness in Figure A-5(b) of Appendix A
S	[-]	=	relative slide thickness; $S = s/h$
t	[s]	=	time from slide impact; time
t_s	[s]	=	time of underwater slide motion
t_0	[s]	=	duration of overtopping for $f = 0$
T	[s]	=	wave period
T_M	[s]	=	wave period of H_M
u	[divers]	=	product for determining the scatter of a product
V	[-]	=	relative slide volume; $V = \forbidden{V}_s/(bh^2)$
V_s	[m/s]	=	slide impact velocity
V_{sNK}	[m/s]	=	slide velocity at point of slope change (Figure 3-4b)
V_{s1}	[m/s]	=	slide impact velocity in Figure A-5(a) in Appendix A
V_{s2}	[m/s]	=	slide impact velocity in Figure A-5(b) in Appendix A
$\forbidden{V}$	[m^3/m]	=	overtopping volume per unit length dam crest
$\forbidden{V}_g$	[m^3]	=	slide grain volume
$\forbidden{V}_s$	[m^3]	=	bulk slide volume
$\forbidden{V}_0$	[m^3/m]	=	overtopping volume per unit length dam crest for $f = 0$
x	[m]	=	streamwise coordinate in longitudinal channel direction and distance in 2D
x’	[divers]	=	parameter for determining scatter

x_M	[m]	=	streamwise distance of the maximum wave amplitude from the impact location
X	[-]	=	relative streamwise distance; $X = x/h$
X_M	[-]	=	relative streamwise distance of a_M (or H_M) from the impact location; $X_M = x_M/h$
y	[-]	=	rational number in the hyperbolic function
Y	[-]	=	relative wave height; $Y = H/h$
Y_M	[-]	=	relative maximum wave height; $Y_M = H_M/h$
z	[m]	=	vertical coordinate
$z_{K,tot,h}$	[m]	=	elevation of the resultant of $K_{tot,h}$
$z_{K,tot,h,abg}$	[m]	=	elevation of the resultant of $K_{tot,h,abg}$
$z_{\Delta K,h}$	[m]	=	elevation of the resultant of ΔK_h

Greek symbols

α	[°]	=	slide impact angle equal to hill slope angle
α_N	[°]	=	hill slope angle for a hill slope section (Figure 3.4b)
β	[°]	=	run-up angle equal to dam face slope
γ	[°]	=	wave propagation angle; reservoir side angle
δ	[°]	=	dynamic bed friction angle
δ_N	[°]	=	dynamic bed friction angle for a hill slope section (Figure 3.4b)
Δh	[m]	=	average water level rise according to Sainflou (1928)
ΔK_h	[N/m]	=	additional horizontal force component per unit length dam crest resulting from impulse wave
ΔK_v	[N/m]	=	additional vertical force component per unit length dam crest resulting from impulse wave
Δu	[-]	=	scatter of u
Δx'	[-]	=	scatter of x'
Δz_{sc}	[m]	=	drop height of the centre of gravity of the slide
Δz_{scN}	[m]	=	drop height of the centre of gravity of the slide between any two slide positions
η	[m]	=	water surface displacement
κ	[-]	=	overfall coefficient for overtopping; $\kappa = \kappa_q \kappa_b \kappa_w^{3/2}$
κ_b	[-]	=	overfall coefficient for the crest width
κ_q	[-]	=	overfall coefficient for the steady case

κ_w	[-]	=	overfall coefficient for the increased flow energy compared with the steady case
π	[-]	=	circular constant; $\pi = 3.14$
ρ_g	[kg/m^3]	=	grain density
ρ_s	[kg/m^3]	=	bulk slide density
ρ_w	[kg/m^3]	=	water density
φ	[-]	=	parameter of Ikeno et al. (2001) for the conversion of the pressure distribution of an intermediate sine wave to the distribution of a bore
ϕ	[°]	=	slide front angle

Subscripts

abg	=	reduced (German abgemindert)
b	=	dam crest width; block
c	=	centre of gravity; centroid
d	=	dynamic
D	=	permeability (German Durchlässigkeit)
F	=	flank
g	=	grain
h	=	horizontal
hs	=	hydrostatic
K	=	crest (German Krone)
m	=	middle; averaged
M	=	maximum
Max	=	maximum (on dam crest)
n	=	whole number
NK	=	slope change (German Neigungsknick)
R	=	reflection; roughness
RW	=	still water (German Ruhewasser)
s	=	static; slide
st	=	stable
tot	=	total
T	=	dam (German Talsperre)
v	=	vertical
w	=	water

0	=	for $f = 0$
1	=	cross-section 1 in Figure 4-2(b)
2	=	cross-section 2 in Figure 4-2(b)

Abbreviations

ad.	=	additional
blw	=	bore-like waves
comp.	=	component
cosh(y)	=	hyperbolic cosine; cosh(y) = $(e^{y} + e^{-y})/2$
coth(y)	=	hyperbolic cotangent; coth(y) = $(e^{y} + e^{-y})/(e^{y} - e^{-y})$
cslw	=	cnoidal and solitary-like waves
d.	=	dam
hor./Hor.	=	horizontal/Horizontal
H. & H. (1997)	=	Huber and Hager (1997)
i.	=	impact zone
K. & B. (1972)	=	Kamphuis and Bowering (1972)
p.u.l.	=	per unit length
P. et al. (2005)	=	Panizzo et al. (2005)
Slw	=	Stokes-like waves
SPH	=	Smoothed Particle Hydrodynamics
S/r	=	Stokes/remaining
unk.	=	unknown
VAW	=	Laboratory of Hydraulics, Hydrology and Glaciology (German Versuchsanstalt für Wasserbau, Hydrologie und Glaziologie)
Ver.	=	Vertical
2D	=	two-dimensional (in a wave channel or in a lake having the form of a wave channel)
3D	=	three-dimensional (in a wave basin or in a lake having the form of a wave basin)

Glossary

The following definitions apply to terms used in this manual.

Bore	A theoretical, non-linear wave type, characterised by a dominant peak with a steep front and gradually-falling back slope (Figure 2-6; Figure A-15b in Appendix A). Certain impulse waves or broken waves near the shore approximate to this type of wave (Figure A-8 in Appendix A).
Breaking	Unstable condition of a wave when air is entrained into the crest or the crest collapses forwards. This happens with deep-water waves when the wave steepness H/L, with shallow-water waves when the relative wave height H/h or with intermediate-water waves when both these parameters exceed a given limiting value.
Capillary water wave	A surface wave principally influenced by capillary forces; it has a wave length $L < 1.7$ cm.
Clapotis	Also known as standing wave: this results from the superimposition of two wave groups which approach each other with the same wave celerity and the waves are of identical height and length. The wave nodes always remain in the same position.
Cnoidal wave	A theoretical, non-linear wave type; it includes both linear as well as solitary waves as limiting cases (Figure 2-4). Certain impulse waves approximate to this wave type (Figure A-8 in Appendix A).
Dam break wave	This is the gravity wave which results from the failure of a dam. In model tests such a wave may be simulated by the sudden removal of an impounding wall.
Deep-water wave	A wave which does not mobilise the water column down to the full depth to the bed and is therefore not influenced by this. After the linear wave theory a wave is classified as a deep-water wave if $L/h < 2$. The opposite is a shallow-water wave.

Diffraction	A wave moving towards and past an obstacle gives up some of its energy laterally into the area of the wave shadow (Figure 4-1a).
Far field	Typically, this is several wave lengths from the slide impact zone beyond where the generated impulse wave undergoes no further significant change of shape (except due to friction and frequency dispersion). A constant relationship has established itself between kinetic and potential wave energy. The opposite is the near field.
Freeboard	The distance, measured vertically, between the current still water level of a reservoir and the crest level of the dam.
Froude similitude	The relationship of inertia to gravity forces (Froude number) in the model corresponds to that in the prototype. However, the relation of inertia to surface tension force (Weber number), to friction force (Reynolds number) and to compressibility force (Cauchy number) cannot be satisfied at the same time. This leads to scale effects when the model scale is not 1:1, but these are often negligible.
Generally applicable equation	A generally applicable equation is one that can be applied for any slide or reservoir parameters, provided that the dimensionless limitations are satisfied. Such an equation is developed from the evaluation of the results of tests carried out on the basis of systematic and independent variation of all important governing parameters.
Geometric similarity	The similar shape of prototype and model, which differ only in their size; this is a basic requirement for the extrapolation of model test results to the prototype.
Granulate properties	Properties related to the granular material of the slide mass; they are indicated with the subscript g ($\forall_g$, ρ_g).
Gravity water wave	A water wave that is influenced principally by gravity force.
Impulse product parameter	The parameter $P = FS^{1/2}M^{1/4}\{\cos[(6/7)\alpha]\}^{1/2}$, which contains only governing parameters, with which Heller (2007a) and Heller and Hager (2009a) describe the prediction of most wave parameters such as the maximum

	amplitude, height and period, the wave volume as well as the wave amplitude and height decay. The parameter refers to the streamwise slide momentum flux component.
Impulse waves	Individual or groups of waves generated by mass movements into water bodies.
Intermediate-water wave	A wave whose movement is slightly affected by the bed. According to the linear wave theory its relative length is between that of a deep and shallow-water wave ($20 \leq L/h \leq 2$).
Iribarren number	The number $I = \tan\beta/(H/L)^{1/2}$ is used to classify the breaking type of a wave, on the basis of the wave height and length as well as the run-up angle.
Kinetic wave energy	Energy stored in the water particle movement.
Linear wave	Theoretical wave type in the form of a sine curve for which, in addition, $H/h < 0.03$ and $H/L < 0.006$ (Figure 2-1).
Mass movement	A pronounced mass location change at the ground surface; The mass may consist of material such as rock, earth, ice or snow propagating e.g. as slide or fall (Section 4.3).
Model effects	Deviations of results between a hydraulic model and the corresponding prototype due to non-identical geometry.
Navier-Stokes equations	Differential equations describing the three velocity components, the density and the pressure at any point in a fluid (water). Analytic solutions only exist for simplified cases but, with the required effort, the equations can be completely solved by numerical means (Direct Numerical Simulation).
Near field	Typically extending up to several wave lengths from the slide impact zone, this zone is where large changes in the form of the generated impulse wave take place. The potential wave energy is normally greater than the kinetic energy. A constant relationship of potential to kinetic wave energy has not established itself. The opposite is far field.

Non-periodic wave	An individual wave.
Oscillatory wave	The water particles follow elliptical paths and, over time, stay in the same position. There is transport of energy but not of fluid mass.
Periodic wave	A wave in a group of waves.
Plunging breaker	Form of wave breaking when the crest collapses forward and, for a short time, with the wave front forms an "air tube", as is often seen on photographs of surfing (Figure B-10a of Appendix B).
Potential theory	Mathematically idealised description of a fluid as frictionless and irrotational. The streamlines in the fluid are so aligned that they possess a potential field. Many phenomena in hydraulics are analysed using the potential theory, for example water waves, ground water flow or pipeline flow.
Potential wave energy	Energy expended in the displacement of water from its mean position.
Reflection	After striking the shore, a wave moves back with the same (total reflection) or reduced wave height.
Refraction	A wave experiences a change of direction in shallow-water due to the shoaling effect and finally moves mostly frontally towards the shore.
Run-up height	The vertical distance between the still water level and the highest point reached by the wave during run-up.
Scale effect	Deviation of the relative results in hydraulic model testing from those in the prototype as a result of those force ratios (Weber number, Reynolds number, Cauchy number) which cannot be correctly represented in the model.
Shallow-water wave	A wave which mobilises the entire water depth, down to the bed and therefore is influenced by the bed due to the phenomenon of shoaling. According to linear wave theory, $L/h > 20$ for such waves. The opposite type is the deep-water wave.
Shoaling	Wave transformation in the vicinity of the shore due to the decrease of the still water depth.

Sine wave	See linear wave.
Slide properties	Properties which relate to the slide mass including the porosity; they are indicated by the subscript *s* (V_s, ρ_s).
Solitary wave	Theoretical, non-linear wave type consisting only of a wave crest but no wave trough (Figure 2-5). This wave type is used as approximation for certain impulse waves (Figure A-8 in Appendix A).
Standing wave	See Clapotis.
Stokes wave	Theoretical, non-linear wave type which is somewhat steeper than a sine wave but has a rather flatter and longer trough (Figure 2-3). This wave type approximates to certain impulse waves (Figure A-8 in Appendix A).
Total reflection	A wave is reflected by a vertical shore and moves back without any loss of height.
Translatory wave	The water particles move in the direction of movement of the wave and both energy and fluid mass are transported.
Tsunami	From the Japanese "Tsu" for harbour and "Nami" for wave. Caused by a sudden movement of a large volume of water, as a result of earthquakes (seismic sea waves) but also subaerial or underwater slides, meteorite impacts, volcanic explosions, releases of natural gas etc.
Wave breaking	See breaking.
Wave crest	The highest point of a wave.
Wave peak	That part of a wave above the original still water level.
Wave trough	That part of the wave which is below the original still water level.
Wave type product	The product $S^{1/3}M\cos[(6/7)\alpha]$, composed only of governing parameters, which Heller (2007a) and Heller and Hager (2009b) use to distinguish the four observed wave types from each other.
2D tests	Two-dimensional: tests carried out in a prismatic wave channel, with the wave parameters measured only in the

	centre of the channel. The impulse waves propagate longitudinally and may therefore be considered 2D.
3D tests	Three-dimensional: tests carried out in a rectangular wave basin in which the wave parameter measurements can be conducted over the whole water surface area. The impulse waves propagate freely, radiating from the slide impact location, and may therefore be considered 3D.

A Literature review on wave generation

A.1 Introduction

This appendix presents generally applicable equations for the determination of landslide generated impulse wave generation. Their advantages and disadvantages are discussed and the selection of the methods in Figure 3-1 and in Section 3.2 is justified. Heller (2007a; 2008) presents literature studies on the subject of the generation of landslide generated impulse waves in physical models covering some 30 and 20 publications, respectively. In this report only those publications most relevant for practical use are discussed. This is work which provides generally applicable results, i.e. several parameters such as slide impact velocity or bulk slide volume were varied. Only generally applicable approaches can be used for any given prototype. Studies based on only one prototype are not therefore given priority. For practical applications, the estimation of the wave height in front of the shore or dam is of interest, as this is the most important parameter in the wave run-up height equation (Section 3.3). A few studies present only one equation for the *maximum* wave height in the impact zone, but not its transformation with the distance. These studies are also not considered in this appendix. Applying these limitations reduces the number of publications considered from the 20 to 30 reviewed by Heller (2007a; 2008) to four which are examined herein.

All generally applicable investigations are based on a wave channel or basin with a horizontal bed. Effects such as refraction (Section 4.2), resulting from variable water depths, are not considered. The most important differences between the hydraulic model studies are the way in which the slide is modelled (as solid body or as granular slide) as well as whether the wave is created in a channel or in a basin (2D or 3D). These differences are discussed in Appendix A.2. In order that the results can be transformed from a specific hydraulic model to the prototype, their geometrical forms must be similar. Effects such as energy concentration at a constriction or diffraction (Section 4.2) are, therefore, also not considered by generally applicable equations, which are based on simplified geometries.

In Appendix A.2, the relevant parameters and the parameter ranges of the individual investigations are defined and the most important differences between the hydraulic models are discussed. A literature review in Appendix A.3 covers investigations with solid bodies (Appendix A.3.1) and granulate slides (Appendix A.3.2). The investigations are further classified into those conducted in wave channels (2D) and those in wave basins (3D). Conclusions are given in Appendix A.4, together with the justification for the selection of the methods for the computation procedure covered by Figure 3-1 and Section 3.2.

A.2 Parameter definitions

Figure A-1(a) and (b) shows definition sketches of the relevant parameters for impulse wave generation in a wave channel (2D) and in a wave basin (3D). As distinct from Subsection 3.2.2, those governing parameters found to have a negligible effect in the test results are also discussed here. The following parameters have an effect on the maximum wave amplitude a_M and the maximum wave height H_M both in 2D and 3D:

- Slide impact velocity V_s
- Bulk slide volume $\forall_s$ or slide grain volume $\forall_g$
- Slide thickness s
- Slide width or channel width b
- Bulk slide density ρ_s or grain density ρ_g
- Bulk slide porosity n
- Slide impact angle α
- Still water depth h

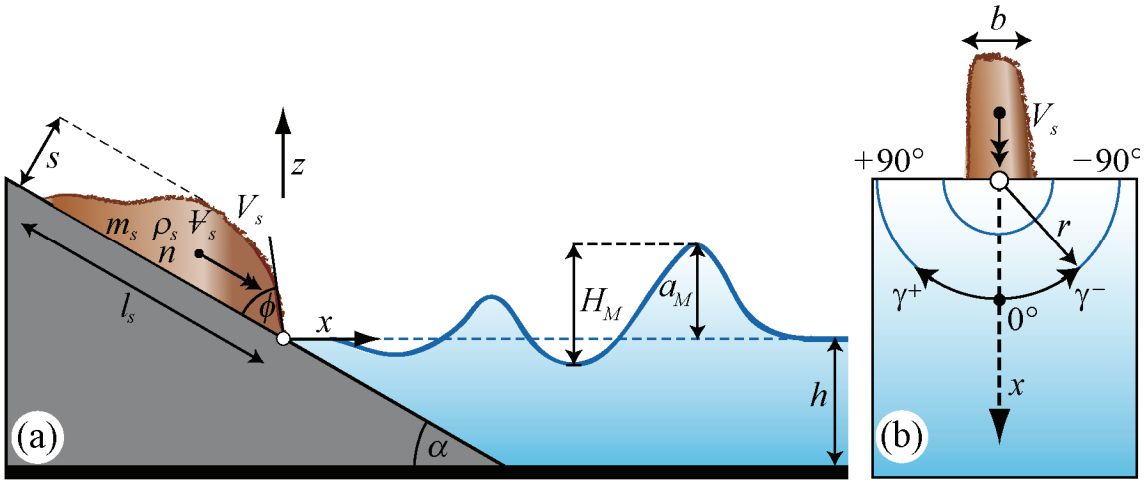

Figure A-1 Sketches defining the governing parameters on impulse wave generation and the most important wave parameters in (a) 2D and (b) 3D.

Few researchers have investigated the effects of the slide front angle ϕ and the slide length l_s, however, these governing parameters were always found to have a negligible effect. Heller (2007a) also found that the effect of the grain size distribution could be neglected. Panizzo et al. (2005) used the time of underwater slide motion t_s as a further governing parameter for the maximum wave height H_M. As the value of t_s, prior to an incident, is difficult to estimate, Panizzo et al. (2005) deduced it as a function of the remaining governing parameters.

An impulse wave changes as it propagates in a horizontal wave channel or wave basin, as a function of the following parameters:

- Streamwise distance x (2D)
- Radial distance r (3D)
- Wave propagation angle γ (3D)

Figure A-2 shows schematically the classification of the investigations to generate generally applicable impulse waves for solid bodies and granular slides for both 2D and 3D models. The tests illustrated are discussed in Appendix A.3. Zweifel (2004) also satisfies most of the criteria given in Appendix A.1 for inclusion in this literature review. However, only the amplitude decrease was evaluated, yet not the wave height decrease which is relevant for the calculation of the run-up height. The work of Heller (2007a) (Appendix A.3.2.1) includes the data of Fritz (2002) as well as that of Zweifel (2004). Therefore, to be concise, only the definitive equations of Heller (2007a) are discussed.

In Figure A-2 two basic criteria must be taken into consideration when using the equations:

a) Was the test carried out with a solid body or with granulate?
b) Was the test conducted in a wave channel (2D) or in a wave basin (3D)?

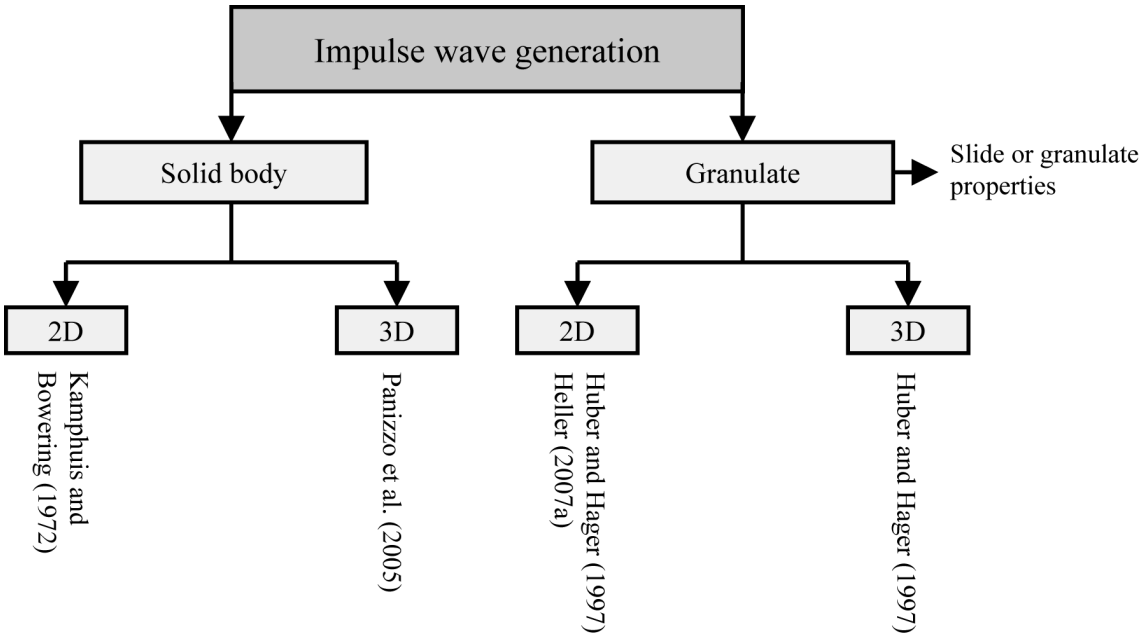

Figure A-2 Classification of the tests for the generation of generally applicable impulse waves and the corresponding research studies as discussed in Appendix A.3.

a) Figure A-3(a) shows the modelling of the slide with granulate and Figure A-3(b) as a solid body, respectively. Generally, solid bodies and granulate slides are defined by the same parameters; for solid bodies, however, the number of test parameters is reduced by the assumption of constant porosity $n = 0$ and neglecting the granulometry. A solid body with the same governing parameters tends to generate larger waves than a granular slide. For the former, the water can only

be displaced forward or over the solid body whereas with a granular slide some of the water enters its voids. Zweifel (2004) compared granular and solid slides (Section 4.3). He showed that for identical governing parameters the waves created by a solid body were up to seven times larger applying a slide Froude number of F = 0.51 (Figure 4-6). The comparison was based on 11 tests for a relatively small parameter range. Further publications on this topic are not known. It is therefore only to a limited extent possible to convert data for waves created by solid bodies to those resulting from granular slides.

When considering granular slides it must also be differentiated between the granulate properties and slide properties (Figure A-2). The granulate has, for example, a density of ρ_g, whereas the slide density is designated as ρ_s. As distinct from the granulate parameters, the slide parameters also include the bulk slide porosity n. The same is the case for the slide grain volume $\not{V}_g$ and the bulk slide volume $\not{V}_s$. The slide mass and the granular mass are on the other hand identical ($m_s = m_g$). For block models, furthermore, $\rho_g = \rho_s$ and $\not{V}_g = \not{V}_s$, as the porosity n is equal to zero. In Table 3-1, the conversion equations from slide to granulate parameters, and vice versa, are indicated, taking account of $\not{V}_s = m_s/\rho_s$ and $\not{V}_g = m_g/\rho_g$.

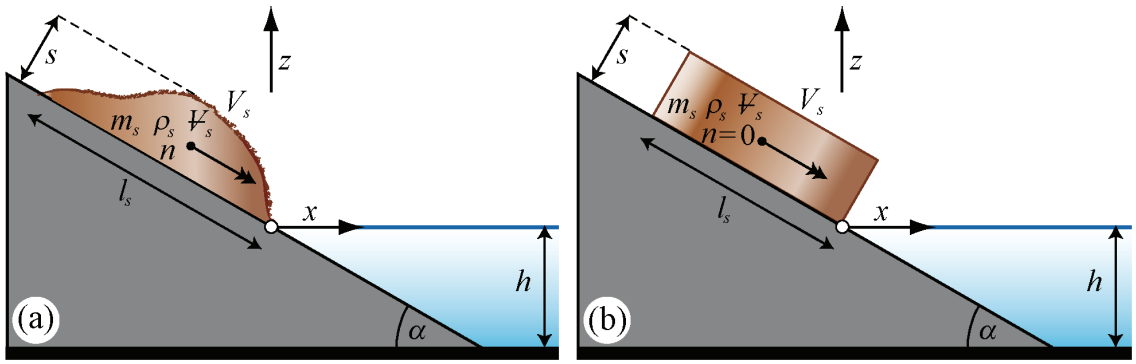

Figure A-3 Most important governing slide parameters modelled in a wave channel with either (a) granulate or (b) a solid body.

b) Generation of impulse waves in a wave basin depends on the same governing parameters as in a wave channel. In addition there is little difference in the maximum wave heights H_M in the slide impact zone (Huber 1980). However, impulse waves in a rectangular wave basin lose height, as a function of the radial distance r and the wave propagation angle γ, much more quickly than in a prismatic wave channel. The reason for this is the distribution of the wave energy over a larger area in the wave basin. Equations based on 2D can only be applied on certain reservoir geometries. An example is Lituya Bay in Alaska where, in 1958, the wave propagation was restricted on one side by a glacier. The calculation of this with the 2D model of Heller (2007a) agrees well with the field observations. Conversion of the wave height generated in 2D to 3D was implicitly

carried out by Huber and Hager (1997) and is now applied on the 2D data of Heller (2007a) (Appendix A.3.2.2).

Table A-1 Range of dimensionless parameters in the studies of Kamphuis and Bowering (1972) (K. & B. (1972)), Huber and Hager (1997) (H. & H. (1997)), Panizzo et al. (2005) (P. et al. (2005)) and Heller (2007a); unk. = unknown specifies parameter ranges which are not tested or mentioned.

Study	Model type	Dimensionless parameters				
		$F = V_s/(gh)^{1/2}$ [-]	$S = s/h$ [-]	$M = m_s/(\rho_w bh^2)$ [-]	$D = \rho_s/\rho_w$ [-]	ρ_g/ρ_w [-]
K. & B. (1972)	Solid body in 2D	0.9 - 3.1	0.25 - 0.88	unk.	2.7	2.7
H. & H. (1997)	Granulate in 2D	0.5 - 3.69	unk.	unk.	unk.	0.9 - 2.7
H. & H. (1997)	Granulate in 3D	1.06 - 1.84	unk.	unk.	unk.	0.9 - 2.7
P. et al. (2005)	Solid body in 3D	1.00 - 2.22	0.11 - 0.45	unk.	2.2	2.2
Heller (2007a)	Granulate in 2D	0.86 - 6.83	0.09 - 1.64	0.11 - 10.02	0.59 - 1.72	0.96 - 2.75
Study	Model type	Dimensionless parameters				
		$V = \forall_s/(bh^2)$ [-]	$\forall_g/(bh^2)$ [-]	n [%]	α [°]	$B = b/h$ [-]
K. & B. (1972)	Solid body in 2D	unk.	unk.	0	20 - 90	2.17 - 4.35
H. & H. (1997)	Granulate in 2D	unk.	0.03 - 2.57	unk.	28 - 60	1.39 - 4.17
H. & H. (1997)	Granulate in 3D	unk.	0.09 - 2.57	unk.	30 - 60	1.39 - 4.17
P. et al. (2005)	Solid body in 3D	unk.	unk.	0	16 - 36	0.38 - 1.50
Heller (2007a)	Granulate in 2D	0.05 - 5.94	unk.	30.7 - 43.3	30 - 90	0.74 - 3.33
Study	Model type	Dimensionless parameters					
		$t_s(g/h)^{1/2}$ [-]	$(l_s/h)(s/h)$ [-]	$(s/h)(b/h)$ [-]	$X = x/h$ [-]	r/h [-]	γ [°]
K. & B. (1972)	Solid body in 2D	unk.	0.05 - 1.0	unk.	10 - 74.3	-	-
H. & H. (1997)	Granulate in 2D	unk.	unk.	unk.	5 - 100	-	-
H. & H. (1997)	Granulate in 3D	unk.	unk.	unk.	-	5 - 30	−90 - +90
P. et al. (2005)	Solid body in 3D	0.39 - 5.11	unk.	0.04 - 0.68	-	1.3 - 15.1	−90 - +90
Heller (2007a)	Granulate in 2D	unk.	unk.	unk.	2.7 - 59.2	-	-

In order to be able to compare the governing parameters with a prototype, they must be expressed in dimensionless form. The relative wave parameters in the model are identical with those of a prototype, providing that each of these dimensionless parameters is identical. In the four investigations presented in Appendix A.3, not always the same governing parameters are varied and analysed, and this leads to different dimensionless parameters. Table A-1 gives an overview of the investigated ranges of dimensionless parameters of Kamphuis and Bowering (1972) (K. & B. (1972)), Huber and Hager (1997) (H. & H. (1997)), Panizzo et al. (2005) (P. et al. (2005)) and Heller (2007a). The parameter ranges that were not studied or mentioned are indicated as unk., i.e. unknown. Huber and Hager (1997) considered for the relative grain density ρ_g/ρ_w, comprised of the grain density ρ_g and the water density ρ_w, compared with Huber (1980) who investigated only $\rho_g/\rho_w = 2.7$, additional snow and glacier investigations from prototype-specific model tests with relative grain densities of up $\rho_g/\rho_w = 0.92$ (Huber 2008). The relative slide width $B = b/h$ resulted in 2D models only from change of the still water depth h, as the slide width b was always constant and identical with the channel width. Dimensionless parameters are abbreviated with a new symbol whenever

they appear in the work of Heller (2007a). The dimensionless parameters and their ranges, as shown in Table A-1, will be discussed in Appendix A.3.

A.3 Literature review

A.3.1 Solid body models

A.3.1.1 Wave channel (2D)

Impulse waves generated by solid bodies are generally somewhat higher than waves resulting from granular slides (Section 4.3). The wave height decay in 2D is larger than that for the 3D model (Appendix A.2). Kamphuis and Bowering (1972) conducted experiments in a channel 45 m long and 1 m wide, with still water depths in the range $h = 0.23$ m and 0.46 m. The slide was modelled as a solid body having a constant density $\rho_g = 2{,}700$ kg/m^3 and a porosity $n = 0$. The still water depth, the slide impact angle α, the slide dimensions s and l_s, the slide impact velocity V_s and the slide front angle ϕ were also varied. The slide front angle ϕ had a negligible effect on the impulse wave generation, as was later confirmed by Heller (2007a).

The dimensionless parameters used by Kamphuis and Bowering (1972) were the slide Froude number $\mathsf{F} = V_s/(gh)^{1/2}$, the relative slide thickness $S = s/h$, the grain or bulk slide density $D = \rho_s/\rho_w$, the slide impact angle α, the relative width $B = b/h$, the two-dimensional slide volume per unit width $(l_s/h)(s/h)$ and the relative streamwise distance $X = x/h$ (Table A-1). The ranges studied, which are also given in Table A-1, were $0.9 \le \mathsf{F} \le 3.1$, $0.25 \le S \le 0.88$, $20° \le \alpha \le 90°$, $2.17 \le B \le 4.35$, $0.05 \le (l_s/h)(s/h) \le 1.0$, $10 \le X \le 74.3$, and $D = 2.7$ = constant. The data from Kamphuis and Bowering (1972) showed a great number of dependences of the wave characteristics on the test parameters. Hence, tests were excluded and only in certain ranges of parameters were generally applicable equations derived. These authors found that, from a given relative distance, the wave heights mostly decreased only slightly. This stable wave height H_{st} was always reached if $X < 80$ and, for the parameter limitations $0.05 < (l_s/h)(s/h) < 1.0$, $S \ge 0.5$, $(\alpha + \phi) \ge 90°$ and $\alpha \approx 30°$, could be calculated as

$$\frac{H_{st}}{h} = \mathsf{F}^{0.7}\left(0.31 + 0.2\log\left(\frac{l_s}{h}\frac{s}{h}\right)\right). \tag{A.1}$$

This stable wave height H_{st} was further used to determine the wave height decay in the parameter ranges $0.1 < (l_s/h)(s/h) < 1.0$ and $10 \le X \le 48$ as

$$\frac{H(x)}{h} = \frac{H_{st}}{h} + 0.35\exp(-0.08X). \tag{A.2}$$

The wave height decay has an exponential character, therefore. The effect of the slide impact angle α is negligible.

Kamphuis and Bowering (1972) also determined that the impulse wave celerity c may be described with the solitary wave celerity (Section 2.2), which is given by

$$c = \left[g(h+a)\right]^{1/2}. \tag{A.3}$$

Whilst Eq. (A.3) was later verified for landslide generated impulse waves, for example by Huber (1980) or Heller (2007a), the concept with a stable wave height H_{st} is not confirmed. The advantage and disadvantages of the investigation of Kamphuis and Bowering (1972) are:

+ Most relevant governing parameters were varied.
− The wave decay is large in comparison with other tests.
− The slide was modelled as a solid body (n = 0).
− The work is based on an outdated measurement system (wire gauges).
− The tests were conducted in a wave channel (2D).
− Only one grain density of ρ_g = 2,700 kg/m^3 was tested.
− Equation (A.2) covers only some of the conducted tests.
− A diagram with the measurement points for Eq. (A.2), for optical control, is only available for a few of the tests.
− The number of tests is relatively small (probably < 50).

A.3.1.2 Wave basin (3D)

The heights of impulse waves generated by a solid body tend to be overestimated compared with those due to granular slide material (Section 4.3; Appendix A.2). In a wave basin the radial distance r replaces the streamwise distance x in the wave channel. The wave propagation angle γ is an additional parameter as distinct from 2D. Panizzo et al. (2005) modelled the slide with a solid body of constant density ρ_g = 2,200 kg/m^3 which generated impulse waves in a wave basin. Hence, the block slides into a corner on a ramp in the 6 m × 12 m wave basin. By combining several tests it was possible on grounds of symmetry to simulate a wave basin with a surface area four times as large, in which the solid body impacted in the middle of one side of the basin. In total, 288 tests were conducted. Panizzo et al. (2005) used the following dimensionless parameters: the slide Froude number $\mathsf{F} = V_s/(gh)^{1/2}$, the relative slide thickness $S = s/h$, the relative grain or slide density $D = \rho_s/\rho_w$, the slide impact angle α, the relative width $B = b/h$, the relative time of underwater slide motion $t_s(g/h)^{1/2}$, the parameter $(s/h)(b/h)$, the relative radial distance r/h and the wave propagation angle γ (Table A-1). The relative slide length l_s/h, which was also investigated, had no effect in any of the equations presented.

Table A-1 shows further the ranges studied by Panizzo et al. (2005) as $1.00 \le \mathsf{F} \le 2.22$, $0.11 \le S \le 0.45$, $D = 2.2 = \text{constant}$, $16° \le \alpha \le 36°$, $0.38 \le B \le 1.50$, $0.39 \le t_s(g/h)^{1/2} \le 5.11$, $0.04 \le (s/h)(b/h) \le 0.68$, $1.3 \le r/h \le 15.1$ and $-90° \le \gamma \le +90°$. Of special interest in the investigation of Panizzo et al. (2005) is the use of the time of underwater slide motion t_s. It lasts from the moment of impact to when the slide comes to rest. It is difficult to predict prior to an event and it was, therefore, developed empirically as a function of the other known dimensionless governing parameters as

$$t_s\sqrt{(g/h)} = 0.43\left((s/h)(b/h)\right)^{-0.27}\mathsf{F}^{-0.66}\left(\sin\alpha\right)^{-1.32}. \tag{A.4}$$

The relative wave height $Y(r/h,\ \gamma) = H(r,\ \gamma)/h$ is given, with a coefficient of determination $R^2 = 0.79$, as

$$\frac{H(r,\ \gamma)}{h} = 0.07\left(\frac{t_s\sqrt{(g/h)}}{(s/h)(b/h)}\right)^{-0.45}\left(\sin\alpha\right)^{-0.88}\exp\left(0.6\cos\gamma\right)(r/h)^{-0.44}. \tag{A.5}$$

An impulse wave in a wave basin of constant depth h will only change as a result of the decay term $\exp(0.6\cos\gamma)(r/h)^{-0.44}$. This term is presented in Figure A-4(a) as a function of the relative wave height $H(r,\ \gamma)/h$ and the wave propagation angle γ. The individual lines represent constant relative radial distances r/h. The wave height is greatest in the slide impulse direction ($\gamma = 0°$; Figure A-1b) but decreases with increasing or decreasing wave propagation angle γ. It reaches a minimum at $\gamma = \pm 90°$.

The relative wave period $T(r,\ \gamma)(g/h)^{1/2}$ of the wave height $H(r,\ \gamma)$ was determined, with a coefficient of determination $R^2 = 0.64$, as

$$T(r,\ \gamma)\sqrt{g/h} = 2.50\left(t_s\sqrt{(g/h)}\right)^{-0.22}\left(\sin\alpha\right)^{-0.25}\left(r/h\right)^{0.17}. \tag{A.6}$$

The influence of the wave propagation angle γ on $T(r,\ \gamma)(g/h)^{1/2}$ was negligible and was not considered in Eq. (A.6). According to Eq. (A.6) the wave period increases only slightly as a function of the relative distance r/h. The advantages and disadvantages of the tests conducted by Panizzo et al. (2005) are:

+ An equation for both $H(r,\ \gamma)$ and $T(r,\ \gamma)$ is available.
+ The results are valid for 3D which, compared with a 2D-limitation, more often represents a prototype.
+ The number of tests, 288, is large.
+ The effects of the governing parameters appear to be physically comprehensible.
− The slide was modelled with a solid body ($n = 0$).

- The relative wave height H/h depends on the relative time of underwater slide motion $t_s(g/h)^{1/2}$, which is unknown and therefore has to be determined empirically from Eq. (A.4) as a function of the remaining governing parameters.
- Only one bulk slide density (ρ_s = 2,200 kg/m^3) was investigated.
- The slide impact angle range of $16° \leq \alpha \leq 36°$ is too small for an Alpine environment.

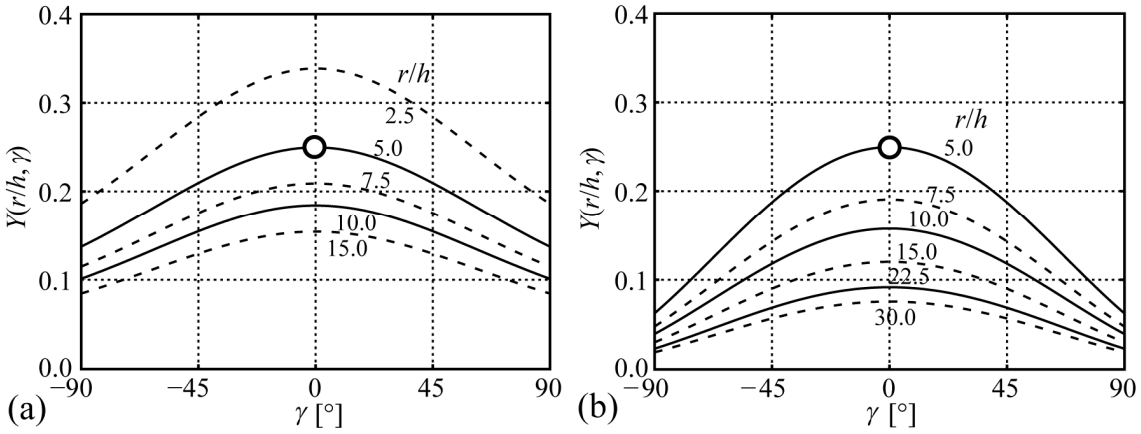

Figure A-4 Comparison of the effects of the decay terms (a) Panizzo et al. (2005) with $\exp(0.6\cos\gamma)(r/h)^{-0.44}$ and (b) Huber and Hager (1997) with $\cos^2(2\gamma/3)(r/h)^{-2/3}$. Point (○) with $Y(r/h = 5, \gamma = 0°) = 0.25$ (Heller 2007a) is taken as comparison point.

A.3.2 Granular slide models

A.3.2.1 Wave channel (2D)

The equations for wave height developed by Huber and Hager (1997) were based on the data set of Huber (1980). The 2D results are available for about 1,000 tests conducted in a wave channel 30.4 m long and 0.50 m wide. The 3D equations of Huber and Hager (1997) are discussed in Appendix A.3.2.2. Huber (1980) used a constant grain density of ρ_g = 2,700 kg/m^3. However, Huber and Hager (1997) included further tests with snow avalanches and glacier calving from prototype specific model tests, with relative densities of up to ρ_g/ρ_w = 0.92 (Huber 2008). The granular slide consisted of grains with various sizes but these were always in the same composition. The slide mass was varied in the range 5 kg $\leq m_s \leq$ 50 kg and the range of still water depths considered was 0.12 m $\leq h \leq$ 0.36 m. Huber and Hager (1997) worked with the granulate properties $\forall_g$ and ρ_g (Appendix A.2). The slide Froude number $\mathsf{F} = V_s/(gh)^{1/2}$, the relative grain density ρ_g/ρ_w, the relative slide grain volume $\forall_g/(bh^2)$, the slide impact angle α, the relative width $B = b/h$ and the relative streamwise distance $X = x/h$ served as dimensionless governing parameters. The ranges for which the dimensionless parameters were determined were $0.5 \leq \mathsf{F} \leq 3.69$, $0.9 \leq \rho_g/\rho_w \leq 2.7$, $0.03 \leq \forall_g/(bh^2) \leq 2.57$, $28° \leq \alpha \leq 60°$,

$1.39 \le B \le 4.17$ and $5 \le X \le 100$ (Table A-1). The relative wave height $H(x)/h$ is calculated as

$$\frac{H(x)}{h} = 0.88(\sin\alpha)\left(\frac{\rho_g}{\rho_w}\right)^{1/4} [\Psi_g/(bh^2)]^{1/2} X^{-1/4}. \qquad \text{(A.7)}$$

The slide impact velocity does not appear in Eq. (A.7) and has only a negligible effect on the relative wave decay. The advantages and disadvantages of the Eq. (A.7) of Huber and Hager (1997) are discussed in Appendix A.3.2.2, together with the 3D results.

The work of Heller (2007a) is a continuation of that of Fritz (2002) and Zweifel (2004), and completes the project on impulse wave generation at VAW. These two authors developed equations to determine the maximum wave amplitude a_M, and in addition Zweifel (2004) developed one for the wave amplitude decay $a(x)$. However, not all governing parameters for wave generation were considered. In addition, Heller (2007a) deduced a relationship for the wave height decay $H(x)$. As he also took into account, in addition to his own tests, those of Fritz (2002) and Zweifel (2004), only the final equations of Heller (2007a) are discussed hereafter. They are based on a total of 434 tests.

Heller's (2007a) work was carried out in the 11.0 m long and 0.50 m wide test facility designed by Fritz (2002). The granulate slide is accelerated to the required impact velocity V_s by means of a pneumatic landslide generator. As distinct from other tests based on granulate, such as for example those reported by Huber and Hager (1997), the governing parameters could be varied independently from one another. Figure A-5 shows the dependence of the slide thickness s on the slide impact velocity V_s, for the tests of Huber (1980), who stored the granulate slide in the starting position behind a vertical wall. On removing this wall upwards, the slide started to move under the effect of gravity. As the starting position in Figure A-5(a) is nearer to the impact location than in Figure A-5(b), the slide impact velocity will be lower, namely $V_{s1} < V_{s2}$. Hence, in Figure A-5(b), the slide thickness decreases more, due to the longer distance to the impact zone, because $s_1 > s_2$. The higher the slide impact velocity V_s, the smaller is the slide thickness s. These two important governing parameters s and V_s cannot therefore be varied independently. If, for instance, the maximum wave height H_M changes this is not to be definitely attributed to the change of *one* governing parameter. The interpretation of the results is, therefore, more difficult. The pneumatic landslide generator described by Heller (2007a) makes possible, in addition to the independent parameter variation, also a high degree of test reproducibility; this is shown by the relatively small scatter of the test results seen in Figure A-6 and Figure A-7.

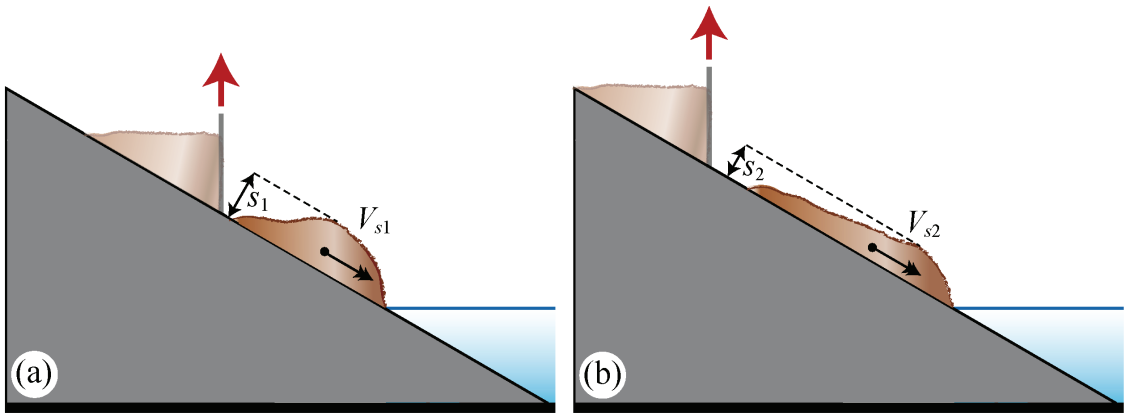

Figure A-5 Dependence of slide thickness s and slide impact velocity V_s, for the tests of Huber and Hager (1997): $V_{s1} < V_{s2}$ but $s_1 > s_2$.

In the equations of Heller (2007a) the following dimensionless governing parameters were varied (Table A-1): the slide Froude number $\mathsf{F} = V_s/(gh)^{1/2}$, the relative slide thickness $S = s/h$, the relative slide mass $M = m_s/(\rho_w bh^2)$, the relative grain $D = \rho_g/\rho_w$ and slide $D = \rho_s/\rho_w$ densities, respectively, the relative slide volume $V = \forall_s/(bh^2)$, the bulk slide porosity n, the slide impact angle α, the relative width $B = b/h$ and the relative streamwise distance $X = x/h$. The ranges studied were $0.86 \le \mathsf{F} \le 6.83$, $0.09 \le S \le 1.64$, $0.11 \le M \le 10.02$, $0.59 \le D \le 1.72$, $0.96 \le \rho_g/\rho_w \le 2.75$, $0.05 \le V \le 5.94$, $30.7\% \le n \le 43.3\%$, $30° \le \alpha \le 90°$, $0.74 \le B \le 3.33$ and $2.7 \le X \le 59.2$ (Table A-1).

The slide parameters V_s, $\forall_s$, s and ρ_s refer to the slide impact zone, not to the initial position of the slide. In addition, the effect of the granulometry was investigated by using various grain diameters between 0.002 m and 0.008 m. However, their effect on the wave characteristics, for instance on the wave height, was found to be negligible. The slide mass $m_s = \forall_s \cdot \rho_s$ and the bulk slide porosity n were not systematically investigated, but were determined subsequently, with the help of the remaining governing parameters.

In the slide impact zone, above all the relative maximum wave height $Y_M = H_M/h$, its relative streamwise distance $X_M = x_M/h$ and wave period T_M are relevant. Figure A-6(a) shows the relative maximum wave height $Y_M = H_M/h$ as a function of the impulse product parameter $\mathsf{P} = \mathsf{F}S^{1/2}M^{1/4}\{\cos[(6/7)\alpha]\}^{1/2}$. This parameter consists of slide or water parameters, which can be estimated prior to an event. In Figure A-6(a), all tests conducted by Fritz (2002), Zweifel (2004) and Heller (2007a) are taken into account. The data points (×) were measured at small still water depth of $h = 0.150$ m. As they could be affected by scale effects, corresponding to distortion of the measured values in the model, as compared with the respective values in the prototype (Heller 2007b), they are specially marked. Were the scale effects to be corrected, these points would move upwards by about 15% at most, relative to the ordinate. The character of all data points and hence of Eq. (A.8) would thus only change insignificantly. The work of Huber and Hager (1997) also included many tests conducted in the range of non-negligible scale effects. However, these were not studied in detail. The data points in

Figure A-6(a) for the relative maximum wave height $Y_M = H_M/h$ may be expressed, with a coefficient of determination $R^2 = 0.85$, as

$$Y_M = (5/9)\mathsf{P}^{4/5}. \tag{A.8}$$

The relative streamwise distance $X_M = x_M/h$ of the relative maximum wave amplitude $A_M = a_M/h$ is shown on Figure A-6(b), also as a function of the impulse product parameter P. As the location at which the relative maximum wave amplitude A_M was measured coincides in more than 90% of the cases with the location of relative maximum wave height Y_M, the following Eq. (A.9) may also be used to determine the distance Y_M. The coordinate system is double logarithmic. It is not possible to estimate whether a test point (×), with non-negligible scale effects, is too near or too far from the coordinate origin. The relative streamwise distance X_M may, with a coefficient of determination of $R^2 = 0.13$, be defined as

$$X_M = (11/2)\mathsf{P}^{1/2}. \tag{A.9}$$

The parameter X_M can, therefore, only be predicted with relatively low accuracy in the range $2.67 \le X_M \le 17.13$.

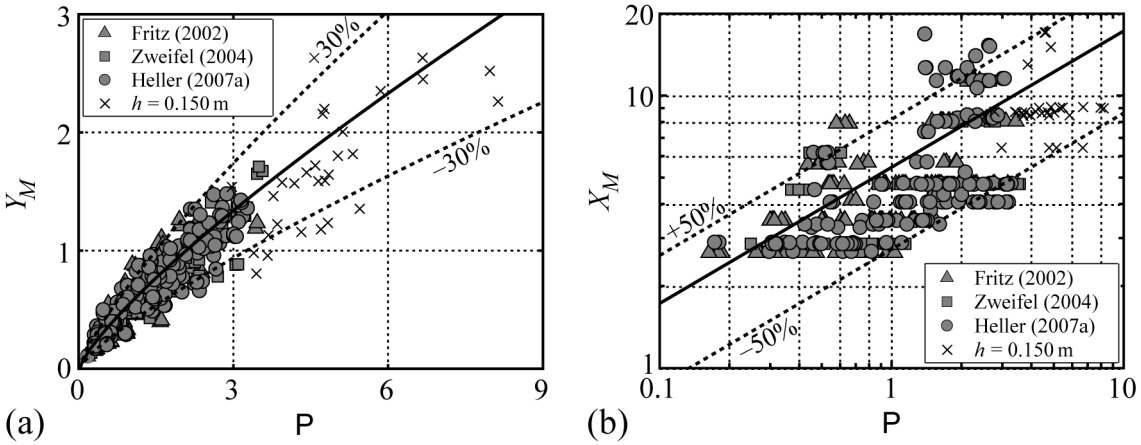

Figure A-6 (a) Relative wave height Y_M as a function of the impulse product parameter P with (−) Eq. (A.8) and (--) ±30% deviation ($R^2 = 0.85$); the data (×) are as a result of scale effects relative to the ordinate at most 15% too low and (b) double logarithmic diagram for the relative streamwise distance X_M of the relative maximum wave height Y_M as a function of the impulse product parameter P, with (−) Eq. (A.9) and (--) ±50% deviation ($R^2 = 0.13$); The influence of scale effects on (×) cannot be estimated (after Heller 2007a).

The relative wave period $T_M(g/h)^{1/2}$ corresponding to the maximum wave height H_M can, with a coefficient of determination of $R^2 = 0.39$, be calculated as

$$T_M (g/h)^{1/2} = 9\mathsf{P}^{1/2}. \tag{A.10}$$

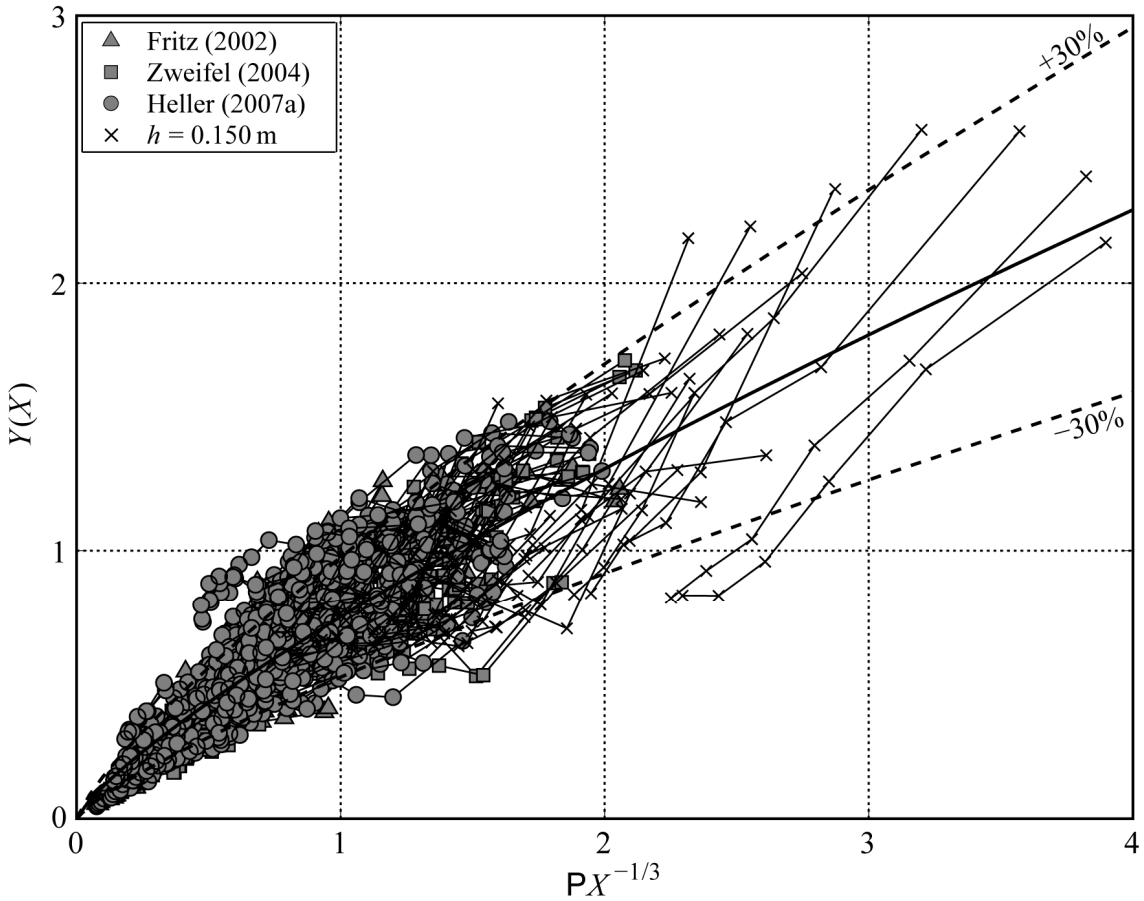

Figure A-7 Wave height decay $Y(X)$ as a function of the parameter $\mathrm{P}X^{-1/3}$ with (−) Eq. (A.11) and (--) ±30% deviation (R^2 = 0.84); for each test the six measured values of wave height are connected with a line; due to scale effects the data points (×) are rather low, relative to the ordinate and the wave decay is too large (after Heller 2007a).

In the *wave propagation zone*, above all the relative wave height decay $Y(X)$ is of importance. The corresponding diagram is shown in Figure A-7. It shows the unknown relative wave height $Y(X) = H(x)/h$ as a function of the parameter $\mathrm{P}X^{-1/3}$. The measurement points of each test are connected with a line. As the relative streamwise distance X has a negative exponent, $X = \infty$ is located at the origin in Figure A-7, where the wave height must be equal to zero. The waves at the data points (×) are subject to scale effects and are too quickly damped as compared with tests with negligible scale effects. Their influence on the subsequent Eq. (A.11) is again small. Equation (A.11) considers above all the overall decay character, but to a lesser extent the maximum relative wave height Y_M. The worst-case scenario for the greatest wave height occurring in the impact zone should, therefore, be estimated using Eq. (A.8). The decay of relative wave height $Y(X) = H(x)/h$, based on Figure A-7, is expressed with $R^2 = 0.84$ as

$$Y(X) = (3/4)\left(\mathrm{P}X^{-1/3}\right)^{4/5}. \qquad \text{(A.11)}$$

After Heller (2007a) or Heller and Hager (2009a), the relative wave amplitude $A(X) = a(x)/h$ may be determined from the relative wave height $Y(X) = H(x)/h$ as $A(X) = (4/5)Y(X)$. This result was found on average for both the comparison of the maximum wave heights with the maximum wave amplitudes as well as for the wave height and amplitude decays, respectively. The water volume of the impulse wave thus moves mainly above the original water level and the wave trough is only one fifth of the wave height (Figure A-1). Therefore, similarity to the profile of the theoretical solitary wave exists. A perfect solitary wave has no trough as the wave consists only of a crest (Section 2.2).

The classification of impulse waves into different *wave types* is important for the determination of the run-up characteristics when the wave reaches a dam. A Stokes-like wave results in a different force effect on the dam than a solitary wave (Section 2.2). In addition, the properties of these theoretical waves are relatively well known. In hydraulic model tests on wave run-up it was usually attempted to generate exactly these waves, so that the model results could be compared with theoretical data. Hence, a tsunami is usually modelled as a solitary wave. Possible wave classifications were already presented in earlier research studies such as that of Huber (1980) or Panizzo et al. (2005). Similar wave types to those described by Heller (2007a) were observed. New in the study of Heller (2007a) is the clear differentiation of the wave types.

Impulse waves may be classified as Stokes, cnoidal, solitary and bore-like waves, as discussed in Section 2.2. Figure A-8 differentiates these four wave types. The slide Froude number F is plotted on the abscissa against the *wave type product* $S^{1/3}M\cos[(6/7)\alpha]$ on the ordinate. Figure A-8 indicates the three zones in which, with a few exceptions, only the following wave types occur:

$$S^{1/3}M\cos\left[(6/7)\alpha\right] < (4/5)\mathsf{F}^{-7/5} \qquad \text{Stokes-like waves,} \qquad \text{(A.12)}$$

$$(4/5)\mathsf{F}^{-7/5} \le S^{1/3}M\cos\left[(6/7)\alpha\right] \le 1.1\mathsf{F}^{-5/2} \qquad \text{cnoidal or solitary-like waves and} \qquad \text{(A.13)}$$

$$S^{1/3}M\cos\left[(6/7)\alpha\right] > 1.1\mathsf{F}^{-5/2} \qquad \text{bore-like waves.} \qquad \text{(A.14)}$$

The cnoidal and solitary-like waves appear in the same area of Figure A-8; this is due to the similarity of these two wave types. The equation of the profile of the solitary wave is a limiting case of the cnoidal wave equation, if a wave period $T \to \infty$ is considered (Section 2.2).

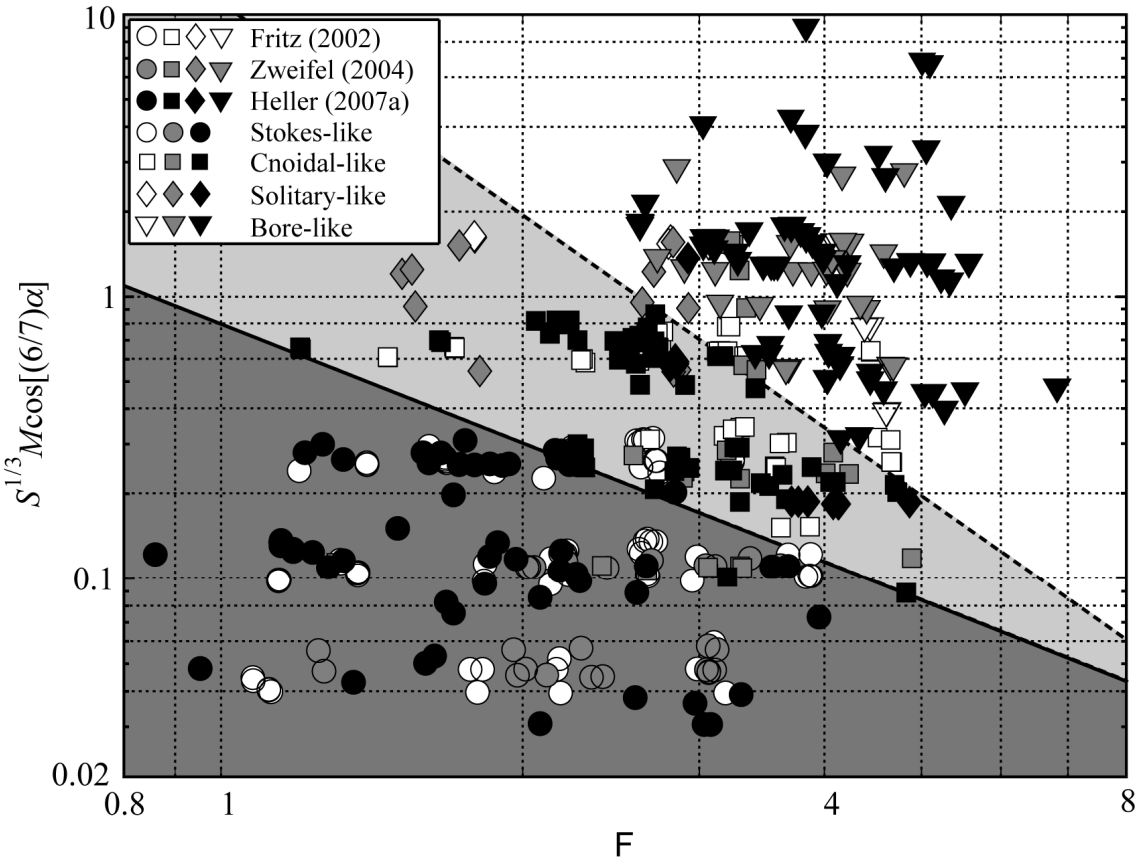

Figure A-8 Classification of wave types with the axes $S^{1/3}M\cos[(6/7)\alpha]$ and F with (–) Eq. (A.12) and „=“ instead of „<“ and (--) Eq. (A.14) with „=“ instead of „>“; in the dark grey area almost only Stokes-like waves occur, in the light grey area almost only cnoidal and solitary-like waves and in the white area practically only bore-like waves (after Heller 2007a).

The following photographs show the four wave types observed by Heller (2007a) both in the impact zone during wave generation and in the wave propagation zone. Figure A-9 shows Stokes-like waves, Figure A-11 a cnoidal-like wave, Figure A-13 a solitary-like wave and Figure A-15 a bore-like wave. In addition, two profiles for each wave are shown in Figure A-10, Figure A-12, Figure A-14 and Figure A-16, respectively. The relative wave profiles η/h are shown for each as a function of relative time $t(g/h)^{1/2}$, as measured with fixed wave gauges at various relative streamwise distances X. The value t indicates the time after slide impact and the zero value on the ordinate corresponds to the undisturbed water surface. The grey areas in Figures A-10 and A-16 are each distorted by wave reflection close to the channel end.

The Stokes waves were presented in Section 2.2. Stokes-like waves occur if Eq. (A.12) is satisfied. The dimensionless parameters the relative slide thickness S and relative slide mass M are small and the slide impact angle α tends to be large. As shown in Figure A-9, several small and symmetrical water waves occur. This wave type is in the range of the deep to intermediate-water waves (Section 2.1).

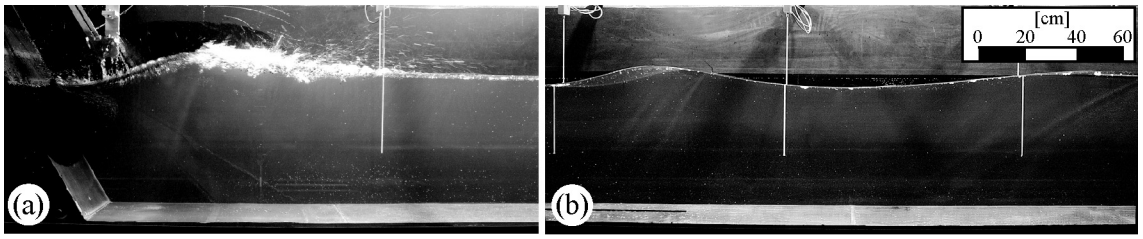

Figure A-9 Stokes-like impulse waves with $h = 0.600$ m, $\rho_s = 608$ kg/m^3, $\alpha = 60°$, $\mathsf{F} = 1.36$, $S = 0.23$ and $M = 0.11$ in (a) slide impact zone and (b) wave propagation zone with $X = 6.1$ - 10.7 (Heller 2007a).

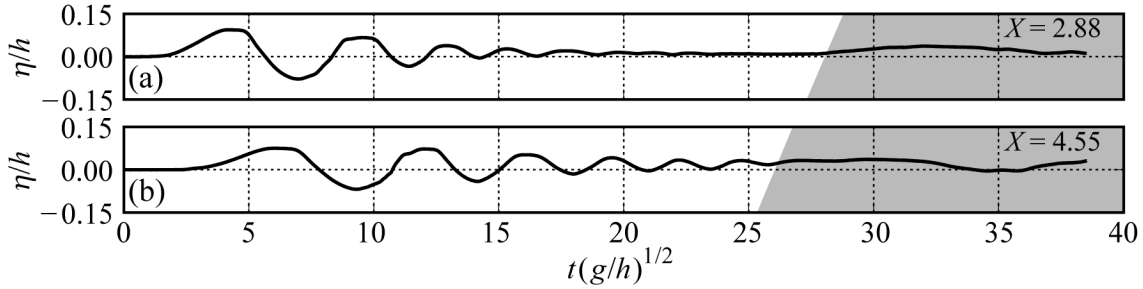

Figure A-10 Relative wave profiles η/h of a Stokes-like impulse wave as a function of relative time $t(g/h)^{1/2}$ with $h = 0.600$ m, $\rho_s = 608$ kg/m^3, $\alpha = 45°$, $\mathsf{F} = 1.18$, $S = 0.17$ and $M = 0.29$: (a) measured at $X = 2.88$ and (b) at $X = 4.55$ (Heller 2007a).

Cnoidal and solitary waves, which are generated if Eq. (A.13) is satisfied, are discussed in Section 2.2. The dimensionless parameters such as the relative slide thickness S, relative slide mass M and slide impact angle α are medium-sized. As shown in Figures A-11 and A-13, the wave height is larger than of the Stokes-like waves. In addition, the wave trough amplitude is significantly smaller than the positive wave amplitude and for the solitary waves in Figure A-13 the trough amplitude is nearly equal to zero. The two wave types are in the range of the intermediate to shallow-water waves (Section 2.1).

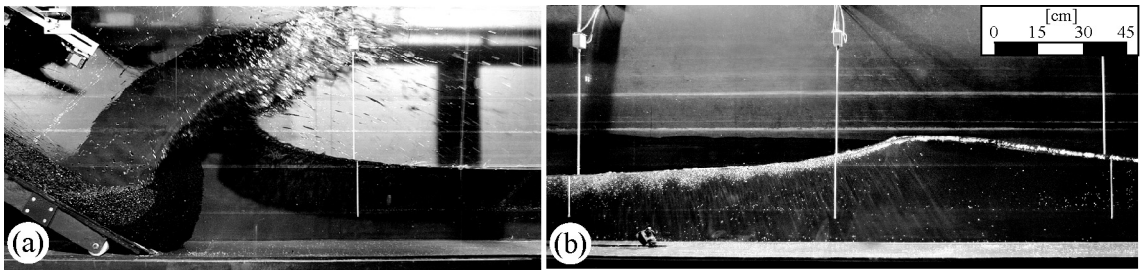

Figure A-11 Cnoidal-like impulse waves with $h = 0.300$ m, $\rho_s = 610$ kg/m^3, $\alpha = 30°$, $\mathsf{F} = 2.27$, $S = 0.40$ and $M = 0.45$ in (a) slide impact zone and (b) wave propagation zone with $X = 10.3$ - 17.6 (Heller 2007a).

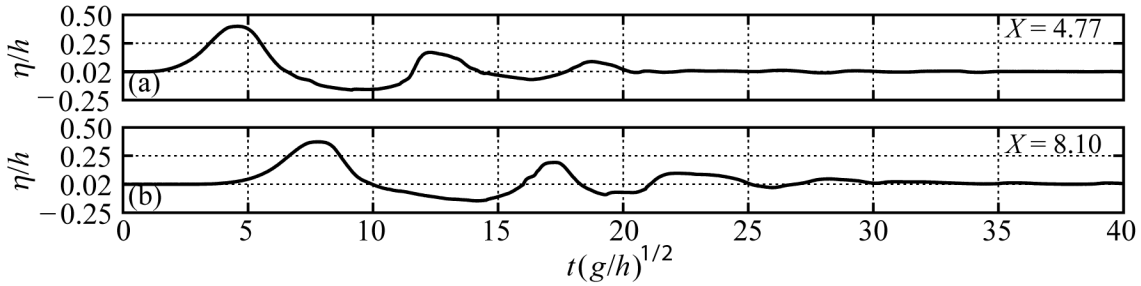

Figure A-12 Relative wave profiles η/h of a cnoidal-like impulse wave as a function of relative time $t(g/h)^{1/2}$ with $h = 0.300$ m, $\rho_s = 610$ kg/m^3, $\alpha = 45°$, $\mathsf{F} = 2.70$, $S = 0.34$ and $M = 1.11$: (a) measured at $X = 4.77$ and (b) at $X = 8.10$ (Heller 2007a).

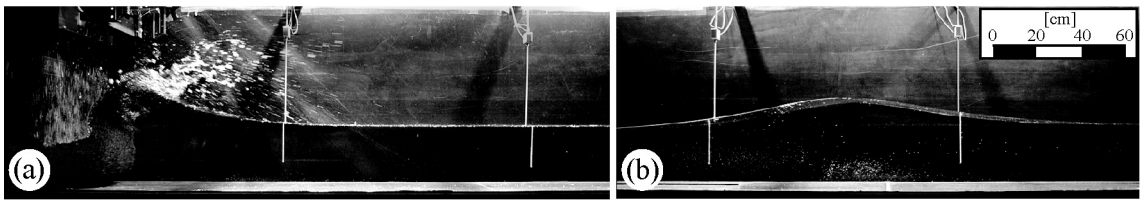

Figure A-13 Solitary-like impulse wave with $h = 0.300$ m, $\rho_s = 609$ kg/m^3, $\alpha = 90°$, $\mathsf{F} = 3.77$, $S = 0.81$ and $M = 0.90$ in (a) slide impact zone and (b) wave propagation zone for $X = 15.3$ - 24.3 (Heller 2007a).

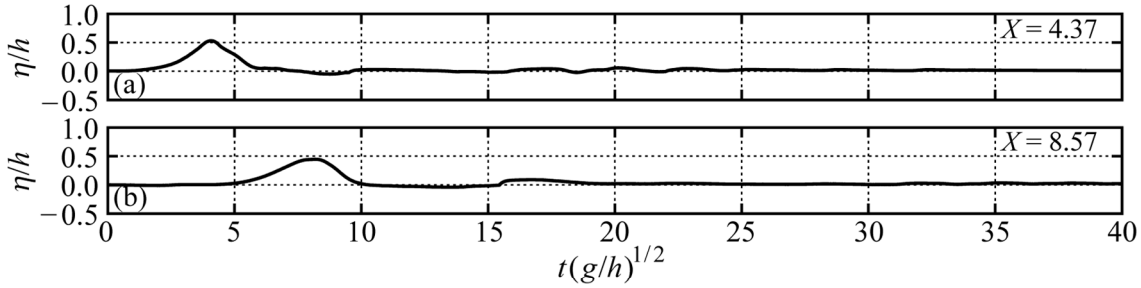

Figure A-14 Relative wave profiles η/h of a solitary-like impulse wave as a function of relative time $t(g/h)^{1/2}$ for the test in Figure A-13: (a) measured at $X = 4.37$ and (b) at $X = 8.57$ (Heller 2007a).

The bore was also discussed in Section 2.2. Bore-like waves are formed if Eq. (A.14) is satisfied. The dimensionless parameters: relative slide thickness S, relative slide mass M and slide Froude number F are all relatively large and the slide impact angle α tends to be small. Figure A-15(b) shows this wave type which consists of a sort of water roller which entrains and transports a large air volume. As seen from Figure A-16, the wave profile consists practically only of a wave crest. This wave type is grouped in the intermediate to shallow-water wave range (Section 2.1).

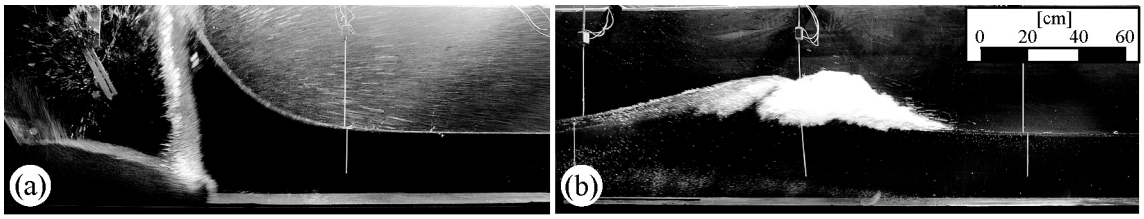

Figure A-15 Bore-like impulse wave with $h = 0.300$ m, $\rho_s = 1{,}664$ kg/m^3, $\alpha = 60°$, $\mathsf{F} = 4.22$, $S = 0.61$ and $M = 2.47$ in (a) slide impact zone and (b) wave propagation zone for $X = 14.9$ - 24.3 (Heller 2007a).

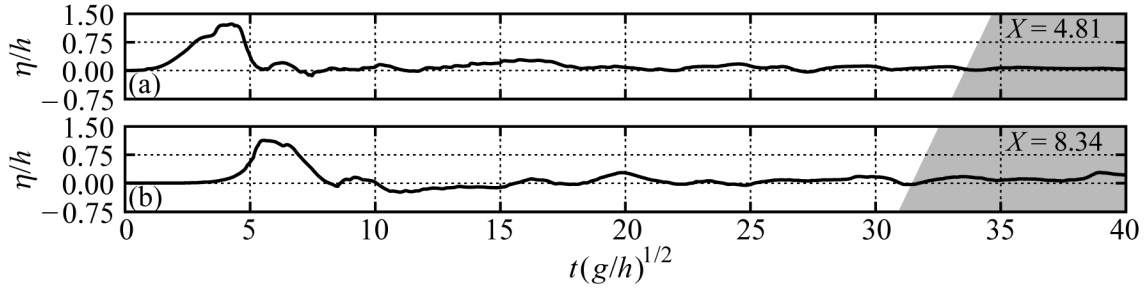

Figure A-16 Relative wave profiles η/h of a bore-like impulse wave as a function of relative time $t(g/h)^{1/2}$ for the test in Figure A-15: (a) measured at $X = 4.81$ and (b) at $X = 8.34$ (Heller 2007a).

The wave type may change during a test as the relative streamwise distance X increases. Hence, a bore loses ever more air and tends to change into a cnoidal or solitary-like wave. Up to now, a reliable wave type classification in 3D does not exist.

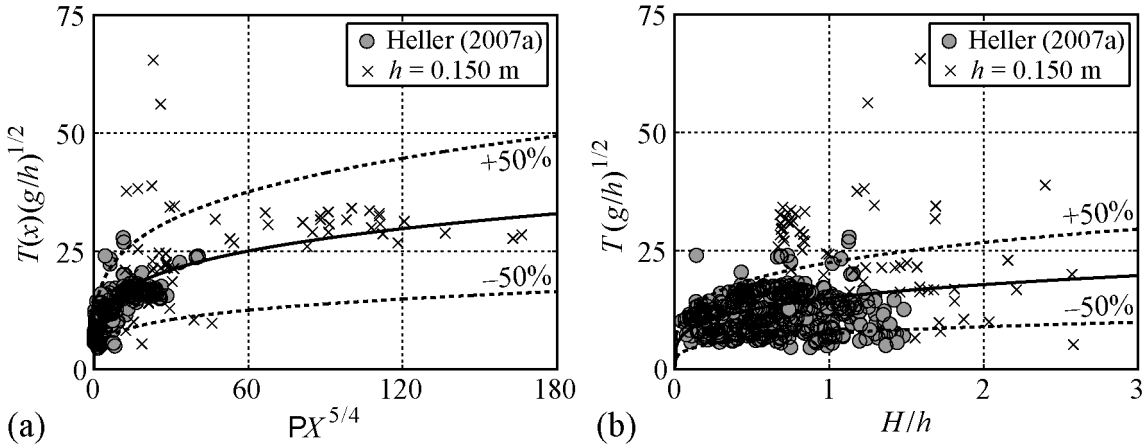

Figure A-17 (a) Decay of the relative wave period $T(x)(g/h)^{1/2}$ as a function of $\mathsf{P}X^{5/4}$ with (−) Eq. (A-15) and (--) ±50% deviation ($R^2 = 0.64$) and (b) relative wave period $T(g/h)^{1/2}$ as a function of the relative wave height H/h with (−) Eq. (A-16) and (--) ±50% deviation ($R^2 = 0.10$).

For determining the effect of impulse waves on dams, Heller (2007a) does not give a relationship for the wave period decay $T(x)$. However, the wave period T is required for example in Eq. (3.17) and T is herein analysed and shown in Figure A-17(a) from the test data of Heller (2007a). Figure A-17(a) shows the relative wave period $T(x)(g/h)^{1/2}$ as a function of $\mathsf{P}X^{5/4}$. The data (×) were measured in the range $h < 0.200$ m

of non-negligible scale effects. The data points in Figure A-17(a) can, with a coefficient of determination $R^2 = 0.64$, be described as

$$T(x)(g/h)^{1/2} = 9\left(\mathsf{P}X^{5/4}\right)^{1/4}. \tag{A.15}$$

Heller and Hager (2009a) confirmed Eq. (A.15) with a larger data set than shown in Figure A-17(a).

In Appendix A.3.2.2, Eq. (A.11) for determining wave heights $H(x)$ in a wave channel is transformed to wave basins $H(r, \gamma)$. In order that in the wave basin the wave period $T(r, \gamma)$ can be determined, based on the known values $H(r, \gamma)$, Figure A-17(b) shows the relative wave period $T(g/h)^{1/2}$ as a function of the relative wave height H/h for the data of Heller (2007a). These are described with $R^2 = 0.10$ as

$$T(g/h)^{1/2} = 15\left(\frac{H}{h}\right)^{1/4}. \tag{A.16}$$

Also shown in Figure A-17(b) are the data points (×) for tests with $h < 0.200$ m, with non-negligible scale effects. The rather large scatter in Figure A-17 does not have a great influence on the effect of the impulse waves on dams, as the influence of the wave period T in Eq. (3.17) is substantially less than that of the more exactly predicted wave height H according to Figure A-6(a). The investigation of Heller (2007a) has the following advantages and disadvantages:

+ It covers a large range of governing parameters, e.g. rock or ice masses, or slide impact angles in the range $30° \le \alpha \le 90°$ (Table A-1).
+ The number of tests, 434, is large.
+ It is based on data from three mutually-consistent dissertations.
+ There is relatively little scatter of data.
+ The equations are easy to use because the impulse product parameter P accounts for several wave parameters.
+ It contains the most practice-relevant wave parameters and a wave type classification.
+ It includes a systematic and independent governing parameter variation.
+ The governing parameters seem to act in a physically meaningful manner.
+ Granular material was used for the tests and this, compared with a solid body, corresponds more often to typical prototype conditions.
+ Diagrams are available with which the accuracy of the calculation equations may be followed visually.
− The tests were conducted in a wave channel (2D) but Eq. (A-11), as described in Appendix A.3.2.2, is converted to 3D.

− The wave period T_M is introduced by Heller (2007a) only for the maximum wave height H_M, but its decrease or increase with the relative streamwise distance X is now belatedly determined in Figure A-17(a).

A.3.2.2 Wave basin (3D)

In addition to the work using the wave channel, Huber (1980) carried out about 150 tests in a 10.0 m × 6.0 m wave basin, and these were re-analysed by Huber and Hager (1997). The governing parameters were selected in a similar way to that already used for the 2D investigation (Appendix A.3.2.1). In addition, in 3D the radial distance r replaces the streamwise distance x, with the wave propagation angle γ as a further governing parameter (Figure A-1b). The ranges of the dimensionless parameters are $1.06 \le F \le 1.84$, $0.9 \le \rho_g/\rho_w \le 2.7$, $0.09 \le \forall_g/(bh^2) \le 2.57$, $30° \le \alpha \le 60°$, $1.39 \le B \le 4.17$, $5 \le r/h \le 30$ and $-90° \le \gamma \le +90°$ (Table A-1). The relative wave height $H(r, \gamma)/h$ is determined, with a scatter of about ±30%, from

$$\frac{H(r,\ \gamma)}{h} = 2 \cdot 0.88 (\sin\alpha) \cos^2\left(\frac{2\gamma}{3}\right)\left(\frac{\rho_g}{\rho_w}\right)^{1/4} [\forall_g/(bh^2)]^{1/2} (r/h)^{-2/3}. \qquad \text{(A.17)}$$

Equation (A.17) for 3D and Eq. (A.7) for 2D are similar. The only difference is the change of the decay term from $X^{-1/4}$ in Eq. (A.7) to $\cos^2(2\gamma/3)(r/h)^{-2/3}$ in Eq. (A.17), as well as a constant factor of 2 in Eq. (A.17). This allows the results from the wave channel to be transformed to the wave basin. Figure A-4(b) shows the effects of the decay parameter $\cos^2(2\gamma/3)(r/h)^{-2/3}$ on the relative wave height decay $H(r, \gamma)/h$, in proportion to the wave propagation angle γ. The lines indicate constant relative radial distances r/h. The influence of the decay parameter $\cos^2(2\gamma/3)(r/h)^{-2/3}$ of Huber and Hager (1997) in Figure A-4(b) is compared directly with the decay parameter $\exp(0.6\cos\gamma)(r/h)^{-0.44}$ of Panizzo et al. (2005) in Figure A-4(a). As basis of comparison the reference point (○) is selected at $Y(r/h = 5,\ \gamma = 0°) = 0.25$. Both decay terms agree well from a qualitative point of view. In Figure A-4(b), the wave height decreases more rapidly, both with the relative radial distance r/h as well as with the wave propagation angle γ, than in Figure A-4(a).

The advantages and the disadvantages of the investigation of Huber and Hager (1997) and of Huber (1980) are:

+ Both 2D and 3D tests are included, allowing for direct comparisons.
+ The numbers of tests, 150 (3D) and 1,000 (2D), is large.
+ Granular material was used for the tests, corresponding more often to the conditions in the prototype as compared with a solid body.
+ The grain densities in the range 920 kg/m^3 ≤ ρ_g ≤ 2,700 kg/m^3 cover snow avalanches, glacier calving as well as rock masses.

- The effects of the governing parameters are sometimes physically difficult to follow so the parameter limitations should be strictly considered.
- The governing parameters could not be investigated independently from one another (s depends on V_s, and V_s on α).
- Diagrams for the visual control of Eqs. (A.7) and (A.17) are not available.
- A substantial proportion of the tests are in the range in which scale effects cannot be neglected.

The wave height decrease according to Eq. (A.11) of Heller (2007a) for the wave channel (2D) is converted here for use in a wave basin (3D), using the procedure developed by Huber and Hager (1997). They considered both 2D and 3D tests (Appendices A.3.2.1 and A.3.2.2). Huber and Hager (1997) deduced the wave height decay with Eq. (A.7) for the wave channel and with Eq. (A.17) for the wave basin, for an identical combination of governing parameters $G = 0.88(\sin\alpha)(\rho_g/\rho_w)^{1/4}[V_g/(bh^2)]^{1/2}$, as

$$\frac{H(x)}{h} = GX^{-1/4} \qquad \text{for 2D} \qquad \text{(A.18)}$$

and as

$$\frac{H(r,\ \gamma)}{h} = 2G\cos^2\left(\frac{2\gamma}{3}\right)(r/h)^{-2/3} \qquad \text{for 3D.} \qquad \text{(A.19)}$$

The parameter G consists only of non-variable governing parameters for the wave propagation and Eqs. (A.18) and (A.19) differ only in the pre-factor 2 and the decay terms. These are, according to Figure A-1(a), the relative streamwise distance $X = x/h$ for 2D in Eq. (A.18) and, according to Figure A-1(b), the relative radial distance r/h and the wave propagation angle γ for 3D in Eq. (A.19).

The composition of Eq. (A.19) may be explained with Figure A-18, showing the wave height decay in the wave basin of Huber and Hager (1997) and the parameter definition sketch according to Figure A-1(b). The relative wave height on the ordinate $H(r/h,\ \gamma)/H(r/h = 5,\ \gamma = 0°)$ consists of the wave height $H(r/h,\ \gamma)$ and a wave height reference $H(r/h = 5,\ \gamma = 0°)$ on the radial relative distance $r/h = 5$ and the wave propagation angle $\gamma = 0°$. On the abscissa of Figure A-18 the radial relative distance r/h is plotted. For different wave propagation angles of $-90° \le \gamma \le +90°$ after Figure A-18 different functions are observed of the form

$$\frac{H(r/h,\ \gamma)}{H(r/h = 5, \gamma = 0°)} = 3\cos^2\left(\frac{2\gamma}{3}\right)(r/h)^{-2/3}. \qquad \text{(A.20)}$$

Equation (A.20) contains the applied decay terms for the impulse waves, as shown in Eq. (A.19), although with a constant factor of 3 rather than 2. Equations (A.18) and

(A.19), for the following reason, were coupled by Huber and Hager (1997) near to the impact zone.

"*Near to the impact zone, the heights of the 2- and 3-dimensional waves deviate little from each other*" (Huber 1980).

If Eqs. (A.18) and (A.19) are applied near to the impact zone at $X = r/h = 5$ and $\gamma = 0°$, they both result in an identical wave height, namely Eq. (A.18) in $GX^{-1/4} = G5^{-1/4} \approx (2/3)G$ and Eq. (A.19) in $2G\cos^2(2\gamma/3)(r/h)^{-2/3} = 2G\cos^2(2\cdot 0/3)5^{-2/3} \approx (2/3)G$. Equation (A.18) may therefore be converted into Eq. (A.19) provided that the 2D damping term $X^{-1/4}$ is replaced by the 3D damping term $\cos^2(2\gamma/3)(r/h)^{-2/3}$ and the additional pre-factor of 2.

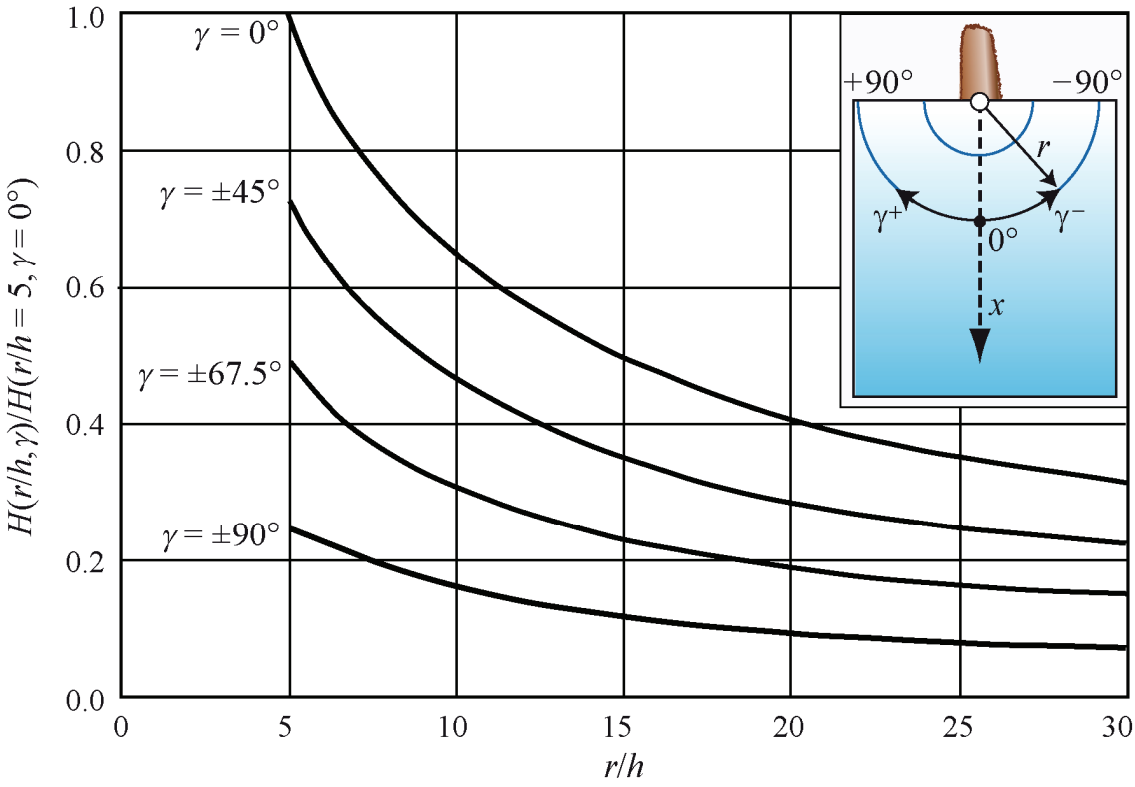

Figure A-18 Wave height decay in a wave basin with parameter definition sketch after Figure A-1(b): relative wave height $H(r/h, \gamma)/H(r/h = 5, \gamma = 0°)$ as a function of the relative radial distance r/h for various wave propagation angles γ (after Huber and Hager 1997).

Equation (A.11) of Heller (2007a) contains an almost identical 2D damping term $X^{-4/15}$, like Eq. (A.18) of Huber and Hager (1997) with $X^{-1/4}$, which at the position $X = 5$ again yields $X^{-4/15} \approx 2/3$. Equation (A.11) may therefore similarly be converted to 3D, as reported by Huber and Hager (1997), in that the 2D decay term $X^{-4/15}$ is replaced by the 3D decay term $\cos^2(2\gamma/3)(r/h)^{-2/3}$ and the additional factor 2. Hence, the wave height decay for wave basins is obtained, based on Eq. (A.11) of Heller (2007a), as

$$Y(r/h,\ \gamma) = (3/2)\mathrm{P}^{4/5}\cos^2\left(\frac{2\gamma}{3}\right)(r/h)^{-2/3}. \qquad (A.21)$$

Besides the limitations of the governing parameters according to Heller (2007a) in Table A-1, the limitations of 3D decay parameters of Huber and Hager (1997) given as $5 < r/h < 30$ and $-90° \leq \gamma \leq +90°$ are relevant for the application of Eq. (A.21).

The advantage and disadvantage of Eq. (A.21) are:

+ It is based on data of Heller (2007a) and has most of the advantages of this work, for instance the extensive variation of the governing parameters (Appendix A.3.2.1).
− It is theoretically deduced, analogously to the method of Huber and Hager (1997), but experimental proof is lacking to date.

A.4 Summary and literature used in the computation procedure

The description of the wave celerity c of landslide generated impulse waves with Eq. (A.3) has been confirmed by several studies. The investigation of Kamphuis and Bowering (1972), however, is by now rather unsuitable as a modern computation method as a solid body in a wave channel was investigated using outdated measurement methods.

The investigation of Panizzo et al. (2005) in 3D, with a solid body, do not correspond to conditions in the Alpine environment, above all because of the small slide impact angles of $\alpha \leq 36°$ and the constant slide density based on rock and not on ice.

The investigation of Huber and Hager (1997) was based both on granular slides and a wave basin (3D). A disadvantage is that the governing parameters were not varied independently, resulting in physically difficult to follow effects of the governing parameters in Eq. (A.17). Hence, for example, the slide impact velocity V_s has no influence on the wave height H. The parameter limitations of Huber and Hager (1997) must therefore be strictly adhered to.

The investigation of Heller (2007a) was based on granular slides. Practically all governing parameters were systematically varied in a large spectrum, independent from each other (Table A-1). The tests of Heller (2007a) may therefore be considered the most generally applicable 2D tests presently available. A further advantage is the wave type classification shown in Figure A-8. A definite disadvantage is that the tests were carried out in a wave channel (2D), which is seldom representative of prototype conditions, and not in a wave basin (3D). The transformation of the wave height from 2D in Eq. (A.11) to 3D in Eq. (A.21) was therefore made using the procedure of Huber and Hager (1997). For the reasons mentioned, in the computation procedure in Figure 3-1 and in Section 3.2, the investigation of Heller (2007a) was therefore applied.

B Literature review on effects of impulse waves on dams

B.1 Introduction

This Appendix B reviews the relevant literature on the effects of impulse waves on dams and explains which methods and why they are selected in the computation procedure shown in Figure 3-1 and in Sections 3.3 and 3.4. When considering wave run-up a basic differentiation between *periodic* and *non-periodic* waves must be made (Section 2.1). Wind waves are periodic; their run-up will be influenced by the run-down of the preceding wave. Impulse waves are mostly non-periodic and, with respect to run-up, they can best be compared with that of a classic tsunami, resulting from a tectonic plate movement (Müller 1995). The first wave is usually the largest and therefore the governing wave, whose run-up is not affected by the run-down of a previous wave. An exception are small Stokes-like waves (Section 2.2; Appendix A.3.2.1) as these are periodic and consist of several waves of the same size in which the first is not necessarily the largest.

As already for the impulse wave generation, this literature review is restricted to generally applicable equations, i.e. studies conducted specifically for a prototype are not discussed. Dam break wave studies, where the wave flows against a vertical wall, are not relevant with regard to the force effect as they approach the dam over either a dry or only slightly wetted reservoir bed. Impulse waves discussed herein already encounter an impounded volume of water behind the dam.

In Appendix B.2 the governing parameters for run-up, overtopping and the force effect are introduced, and an overview is given of the herein presented studies. Depending on their type, the run-up behaviour of waves differs. Therefore, the literature review on wave run-up and overtopping (Appendix B.3) as well as on wave force effect (Appendix B.4) is presented for three categories: Stokes-like waves, cnoidal and solitary-like waves as well as bore-like waves. These wave types were introduced in Section 2.2 and Appendix A.3.2.1. With respect to the force effect, a fourth case has to be considered, namely waves that break as plunging breaker directly on a dam (Figure B-10a). In Appendix B.5 conclusions are given on the technical literature considered together with a justification of why the methods were selected for the computation procedure given in Figure 3-1 and in Sections 3.3 and 3.4, respectively.

B.2 Parameter definitions

Figure B-1 shows the definition sketch for wave run-up and overtopping with the relevant parameters. As distinct from Subsection 3.3.2, those governing parameters whose effects, although investigated, could not be integrated in generally applicable 2D equations are discussed. The following parameters affect the run-up height R and the overtopping volume V per unit length dam crest:

- Wave height H (2D and 3D)
- Wave amplitude a (2D and 3D)
- Wave length L (2D and 3D)
- Wave period T (2D and 3D)
- Still water depth h (2D and 3D)
- Run-up angle or dam face slope β (2D and 3D)
- Freeboard f (2D and 3D)
- Crest width b_K (2D and 3D)
- Dam surface characteristics: roughness, permeability (2D and 3D)
- Wave breaking type (2D and 3D)
- Reservoir geometry (3D)
- Incidence wave angle (3D)

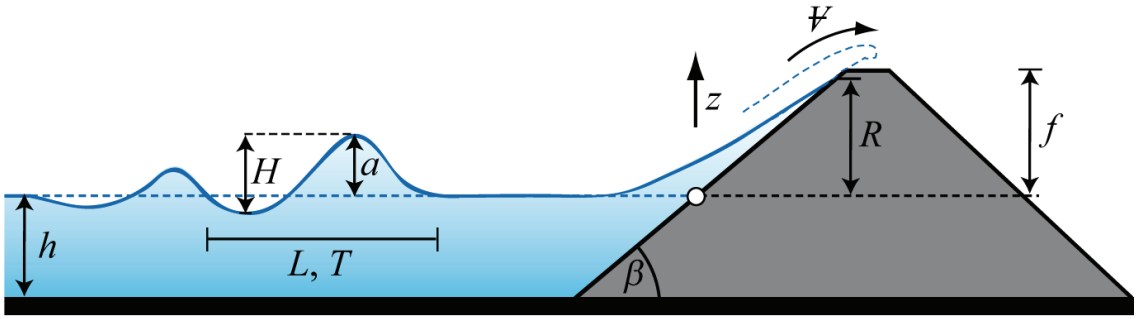

Figure B-1 Definition sketch for wave run-up and overtopping.

Whilst the first ten governing parameters are relevant both for the wave channel (2D) and for the wave basin (3D), the last two are only considered in the wave basin. The first four parameters H, a, L and T are characteristics of the approaching impulse wave. The wave breaking type essentially describes whether a wave reaches the dam intact or as a bore. The influences of the dam surface characteristics, the reservoir geometry and of the incidence wave angle, although discussed in Appendix B, have not been generally assessed and are *not* therefore integrated in the corresponding generally applicable equations. According to the German Association for Water Management and Land Improvement [Deutscher Verband für Wasserwirtschaft und Kulturbau DVWK] (1997), the run-up angle β for embankment dams is usually in the range 1:5 ($\beta = 11.3°$) to 1:1.6 ($\beta = 32.0°$), whereas it is up to $\beta = 90°$ for gravity dams. The wave parameters H, a, L and T refer to the cross-section in front of the dam (Figure B-1), where the wave is still unaffected by shoaling (Section 4.2). In addition, for the overtopping volume V per unit length dam crest, in Figure B-1, the freeboard f and the crest width b_K are of significance.

If a slide mass succeeds in breaking through an ice layer on a lake or reservoir, the impulse waves are only slightly damped by the broken ice pieces (Huber 1987). Neglecting an ice layer in the computation of an impulse wave is, according to Müller (1995), possible up to a thickness of 0.50 m. Dam curvature is often mentioned in the

technical literature as a further governing parameter, but no research quantifying its effect is available.

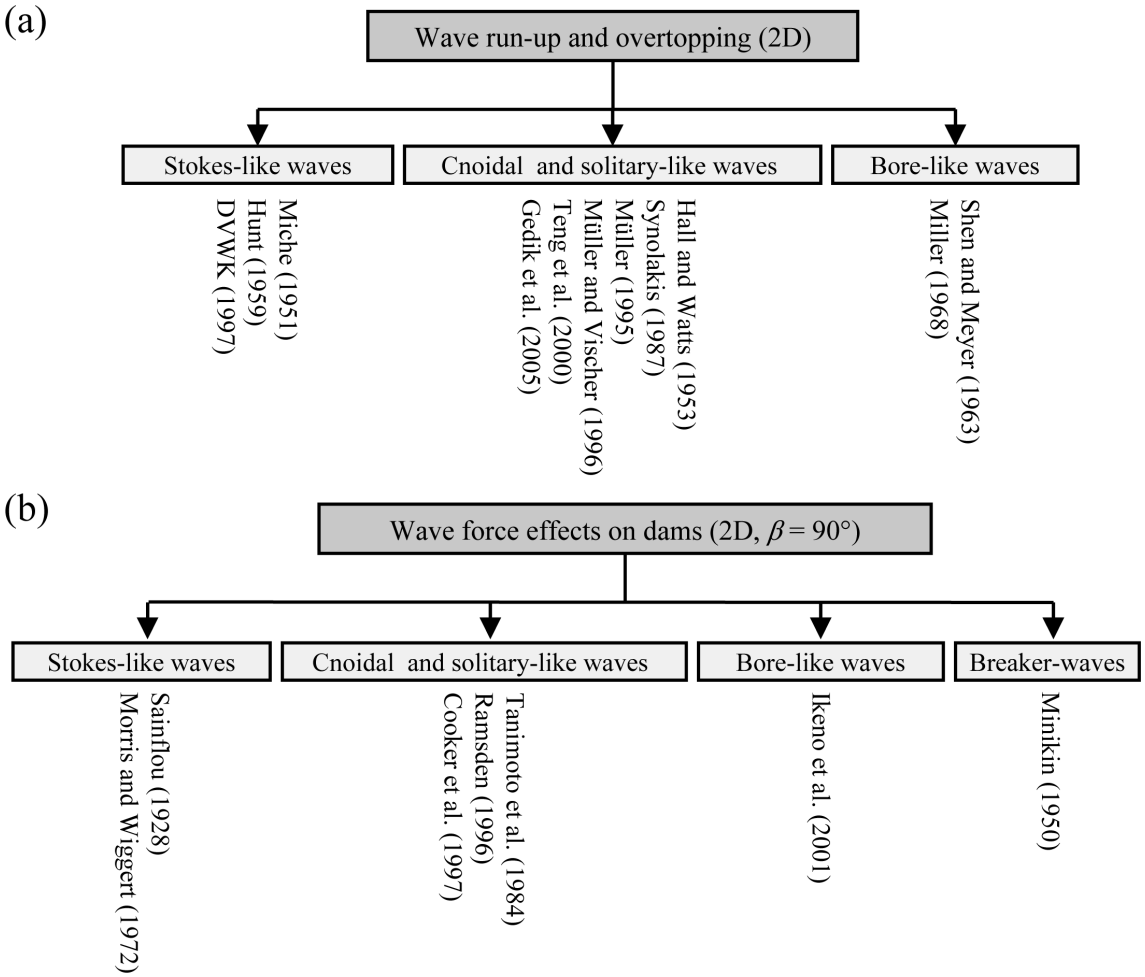

Figure B-2 Schematic classification of the generally applicable studies presented in Appendix B for (a) wave run-up and overtopping and (b) force effect.

Figure B-2 shows the schematic classification of the generally applicable studies on impulse wave effects on dams, as presented in Appendix B. In Figure B-2(a) the classification for wave run-up and overtopping is presented, as covered by Appendix B.3. The studies are further classified in the subsections on Stokes-like, cnoidal and solitary-like, as well as bore-like waves (Section 2.2; Appendix A.3.2.1). All equations are based on tests in wave channels (2D); 3D effects such as the reservoir geometry were indeed investigated, for example by Müller (1995), but could only be considered qualitatively and were not integrated in the generally applicable equations.

Figure B-2(b) shows the classification of studies of waves force effect on dams, as presented in Appendix B.4. Such studies have mostly been conducted to investigate the force effect on breakwaters to protect the coast, the results of which are here transformed to dams. Also, these studies consider only 2D effects; as general knowledge on 3D effects is not yet available. In addition, all these studies consider wave effect on a vertical dam face ($\beta = 90°$). The transformation of the resultant force into horizontal

and vertical components is shown for $\beta < 90°$ in Subsection 3.4.2. In addition to the three categories: Stokes-like, cnoidal and solitary-like as well as bore-like waves, as shown in Figure B-2(b), waves breaking as plunging breaker directly on a dam exists as a fourth category. If, for example, a solitary wave impacts as a plunging breaker (Figure B-10a) directly on the dam, a large local force of short duration is generated at the site of the enclosed air pocket. This phenomenon, which may cause localised damage, is discussed in Appendix B.4.4.

B.3 Wave run-up and overtopping

B.3.1 Stokes-like waves

Stokes-like waves were described in Section 2.2 and Appendix A.3.2.1. When they run-up the dam slope they most often do not break as the dam face slope β is too large and/or the wave height H is too small (Eq. B.28). For such non-breaking waves on a steep dam face which, moreover, move as deep-water waves, the run-up height R may be theoretically determined according to Miche (1951) from

$$\frac{R}{H} = \left(\frac{90°}{\beta} \right)^{1/2} . \qquad \text{(B.1)}$$

Should the wave nevertheless break, additional energy will be converted due to the air entrainment; as a result less energy is available for run-up. For breaking waves, the run-up height R determined with Eq. (B.1) will therefore be overestimated. The advantage and disadvantages of Eq. (B.1) are:

+ Only the wave height H and the run-up angle β need to be known.
− The equation is deduced from theory.
− It is only valid for non-breaking waves, but yields an upper limiting value for breaking waves.

DVWK (1997) proposed reduction factors k_D and k_R for *wind waves*, accounting for the permeability and roughness of the dam surface. Stokes waves are similar to wind waves, as they also exhibit oscillatory characteristics (Chapter 2). The corresponding reduction factors are given in Table B-1. As an example, the run-up height R for rip-rap is only about 55% of that for a smooth dam surface.

Other authors point out that on a flat shore the friction is more effective than on a steep shore. According to Hunt (1959), the run-up height R decreases for constant roughness, by 29% for a slope of 1:30, but by only 18% for a 1:10 slope, compared with a smooth bed.

Table B-1 Reduction factor ($k_D \cdot k_R$) accounting for the permeability and roughness of the dam surface (DVWK 1997).

Dam surface characteristics	$k_D \cdot k_R$
Smooth surface (concrete slabs with sealed joints, asphaltic concrete)	1
Concrete slabs with open joints	0.95
Pavement with sealed joints	0.90 - 0.95
Pavement with open joints	0.80 - 0.90
Grass, sand	0.75 - 0.85
Gravel	0.70 - 0.78
Rip-rap with rounded stone material, rough asphalt	0.60 - 0.65
Rip-rap with broken stone material	0.55 - 0.65

No literature on wave overtopping for Stokes-like waves was found. This is probably because such waves are of relatively small wave height H and represent therefore only a relatively small danger. The overtopping of Stokes-like waves may, however, be described with the studies of Müller (1995) and Müller and Vischer (1996), as referred to in Appendix B.3.2.

B.3.2 Cnoidal and solitary-like waves

Cnoidal and solitary-like waves were described in Section 2.2 and Appendix A.3.2.1. Hall and Watts (1953) conducted experiments on the run-up of solitary waves, for run-up angles in the range $5° \leq \beta \leq 45°$ and for impermeable beds. Irrespective of whether a wave breaks or not, they determined for the range $20° \leq \beta \leq 45°$ the empirical relationship

$$\frac{R}{h} = 3.05 \tan(\beta)^{0.13} \left(\frac{H}{h} \right)^{1.15 \tan(\beta)^{0.02}} . \qquad \text{(B.2)}$$

The advantages and disadvantages of this study are:

+ Equation (B.2) is often referred to in the technical literature.
+ Only the wave height H and the run-up angle β are required.
− The run-up angle lies only in the range $20° \leq \beta \leq 45°$.
− The experiments were conducted more than fifty years ago using old measurement techniques and wave generation system.

Synolakis (1987) conducted probably the most often cited work on the run-up of solitary waves. He deduced analytically a run-up equation for non-breaking solitary waves and subsequently confirmed it experimentally for a run-up angle $\beta = 2.9°$. This equation reads

$$\frac{R}{h} = 2.831(\cot\beta)^{1/2}\left(\frac{H}{h}\right)^{5/4} . \qquad \text{(B.3)}$$

Equation (B.3) is known in the technical literature as the "run-up law". Furthermore, Synolakis (1987) showed experimentally that for $\beta = 2.9°$ the run-up heights differ from one another for breaking and non-breaking waves. The former run less far up the dam slope, corresponding to their wave height H, than non-breaking waves. Figure B-6(a) shows the relative run-up height R/h as a function of the relative solitary wave height H/h, on a double logarithmic scale. Run-up heights from breaking and non-breaking waves do not follow the same trend. The advantages and disadvantage of the work of Synolakis (1987) are:

+ Equation (B.3) is analytical and was confirmed experimentally for $\beta = 2.9°$.
+ Equation (B.3) has established itself in the technical literature.
− The run-up angle β selected for the experiments is too small as compared with typical dam slopes.

Müller and Vischer (1996) investigated both the run-up height as well as the overtopping volume of impulse waves on dams with systematic model tests. They conducted 637 tests in the wave channel and 96 in the wave basin. The solitary waves were generated by dropping a solid body into the water at one end of the channel. Three dam slopes, namely vertical ($\beta = 90°$), 1:1 ($\beta = 45°$) and 1:3 ($\beta = 18.4°$) were tested. Most of the waves were non-breaking during run-up due to the relatively steep shore slope. The run-up height R was, with a deviation for most tests of less than ±10%, determined as

$$\frac{R}{h} = 1.25\left(\frac{H}{h}\right)^{5/4}\left(\frac{H}{L}\right)^{-3/20}\left(\frac{90°}{\beta}\right)^{1/5} . \qquad \text{(B.4)}$$

The original term $(\pi/2\beta)$ in Müller and Vischer (1996) was rewritten in Eq. (B.4) as $(90°/\beta)$, in order that β could be expressed in degrees. Maximum deviations of the measured values compared with Eq. (B.4) are +35% and −25%. The wave height H, the wave length L and the still water depth h relate as usual to the location in front of the dam. The parameter limitations to allow the application of Eq. (B.4) are relative wave height $0.011 < H/h < 0.521$, waves steepness $0.001 < H/L < 0.013$ and relative angle $1.0 < 90°/\beta < 4.9$ (Table 3-3). The overtopping volume V_0 per unit length dam crest for a freeboard $f = 0$ is given by

$$V_0/h^2 = 1.45\kappa\left(\frac{H}{h}\right)^{4/3}\left(\frac{T}{\sqrt{h/g}}\right)^{0.44} . \qquad \text{(B.5)}$$

Analogous to the equation of Poleni (e.g. Hager 1995), an overfall coefficient $\kappa = \kappa_q \kappa_b \kappa_w^{3/2}$ was used in Eq. (B.5), with κ_q as the overfall coefficient for steady flow, κ_b accounts for the influence of the crest width of the dam and κ_w takes account of the increased wave energy, as compared with steady flow and hence its higher flow velocity (Müller 1995). These three parameters are:

(a) $\kappa_q = 0.41$ ($\beta = 90°$), $\kappa_q = 0.47$ ($\beta = 45°$) and $\kappa_q = 0.51$ ($\beta = 18.4°$),

(b) κ_b can be determined from Figure 3-6(a) as a function of the relative maximum overtopping depth $a_{Max,T}/b_K$ and

(c) $\kappa_w = 1.3$ over the whole range $18.4° \leq \beta \leq 90°$.

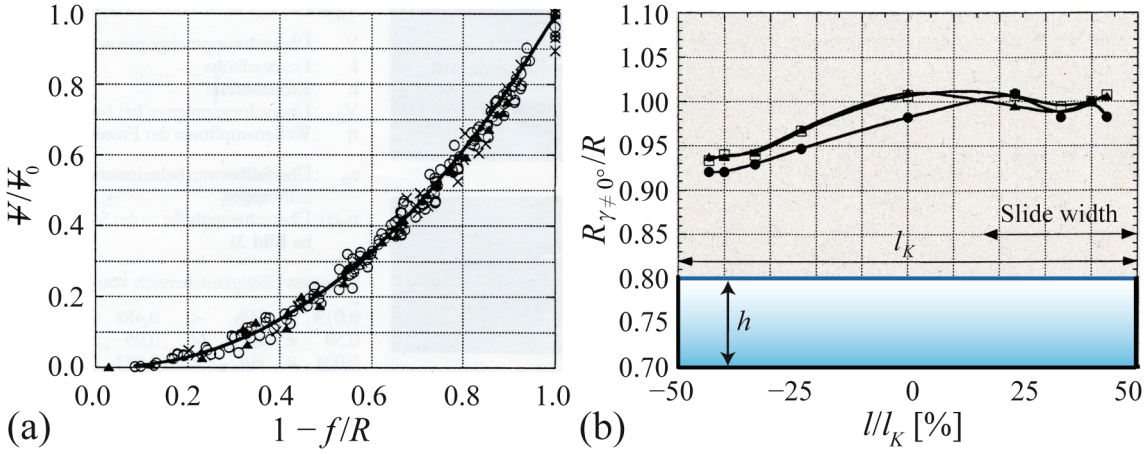

Figure B-3 (a) Influence of the relative freeboard f/R on overtopping volume $\forall/\forall_0$ and (b) influence of the incidence wave angle with the run-up height to the run-up height in the main impulse direction $R_{\gamma \neq 0°}/R$ as a function of the relative crest length l/l_K [%] (from Müller and Vischer 1996).

The maximum overtopping depth over a dam $a_{Max,T}$ is shown in Figure 3-6(b). This is somewhat bigger than the wave amplitude a in front of the dam and can therefore be approximated with the wave height H (Figure B-1). The crest width b_K is shown in Figure B-5. In the prototype the freeboard is normally $f > 0$, and the overtopping volume $\forall_0$ per unit length dam crest for $f = 0$ from Eq. (B.5) is correspondingly reduced, as shown in Figure B-3(a). This shows on the ordinate, for $f > 0$, the overtopping volume $\forall$, relative to $\forall_0$, and on the abscissa the parameter $(1 - f/R)$. The required run-up height R can be calculated from Eq. (B.4). The overtopping volume per unit length dam crest is given, according to Figure B-3(a), as

$$\forall/\forall_0 = \left(1 - \frac{f}{R}\right)^{11/5} . \qquad \text{(B.6)}$$

The parameter limitations applying to the use of the Eqs. (B.5) and (B.6) are: $0.019 < H/h < 0.488$, $0.59 < a/H < 0.95$, $0.001 < H/L < 0.023$, $9.0 < T(g/h)^{1/2} < 21.0$, $0.83 < c^2/(gh) < 1.40$ and $6.0 < L/h < 24.0$ (Table 3-4).

In addition to $\forall$, Müller (1995) provides an equation for the average discharge q_{0m} per unit length dam crest for $f = 0$ in the ranges $14 < T(g/h)^{1/2} < 22$ and $10.5 < t_0(g/h)^{1/2} < 13.5$. Müller (1995) also presented the relative overtopping duration $t_0(g/h)^{1/2}$ as a function of the relative wave period $T(g/h)^{1/2}$, as shown in Figure B-4(a). The maximum deviation is −12% and the data points in Figure B-4(a) were described by Müller (1995) with

$$t_0 (g/h)^{1/2} = 4\left(T\sqrt{g/h}\right)^{4/9} . \qquad \text{(B.7)}$$

The average discharge q_{0m} per unit length dam crest for $f = 0$ is obtained from the combination of Eqs. (B.5) and (B.7) as $q_{0m} = \forall_0/t_0$.

As well as the average discharge q_{0m}, the maximum discharge q_{0M} per unit length dam crest is important with regard to the erosion potential on embankment dams. Figure B-4(b) shows three typical normalised impulse wave profiles $\eta/a_{Max,T}$ as a function of the relative wave period t/T on the abscissa. The duration of overtopping t_0, as determined from Eq. (B.7), allows to determine a mean discharge; this is shown by the line (--) $\eta/a_{Max,T} = 0.5$ in Figure B-4(b), in which the grey areas lying above and below balance out for a chosen wave profile. The wave crest lies about 50% higher. The maximum discharge per unit length dam crest for $f = 0$ is, therefore, $q_{0M} \approx 2 \cdot q_{0m}$, but occurs for only a short period. Müller (1995) gives no discharge data for $f > 0$. As $\forall < \forall_0$, the values q_{0m} and q_{0M} for $f = 0$ are higher and hence overestimate the unknown values for $f > 0$.

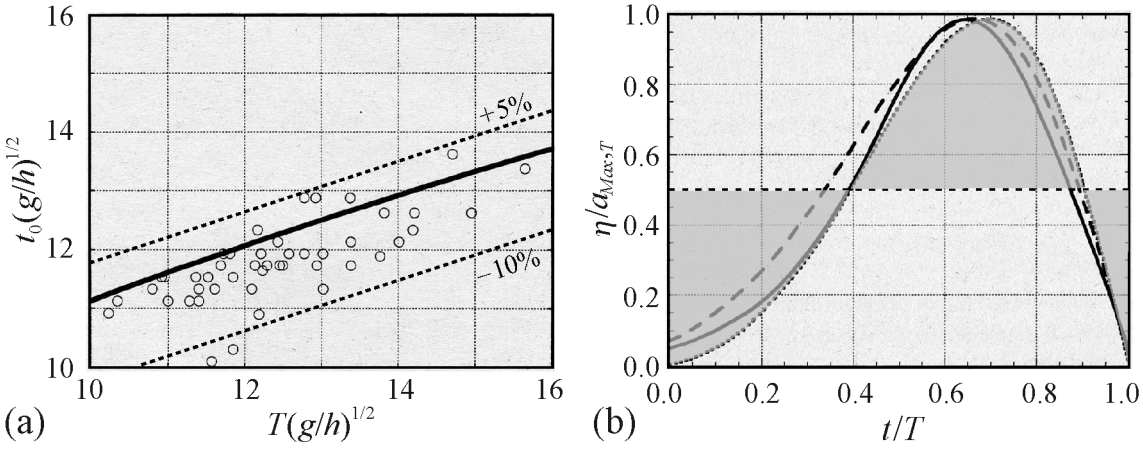

Figure B-4 (a) Relative overtopping duration $t_0(g/h)^{1/2}$ as a function of the relative wave period $T(g/h)^{1/2}$ with (—) Eq. (B.7) and (b) three normalised impulse wave profiles $\eta/a_{Max,T}$ as a function of the relative wave period t/T; the wave crest $\eta/a_{Max,T} = 1$ and hence the maximum discharge q_{0M} per unit length dam crest lie about 50% higher than the mean value (--) $\eta/a_{Max,T} = 0.5$ (after Müller 1995).

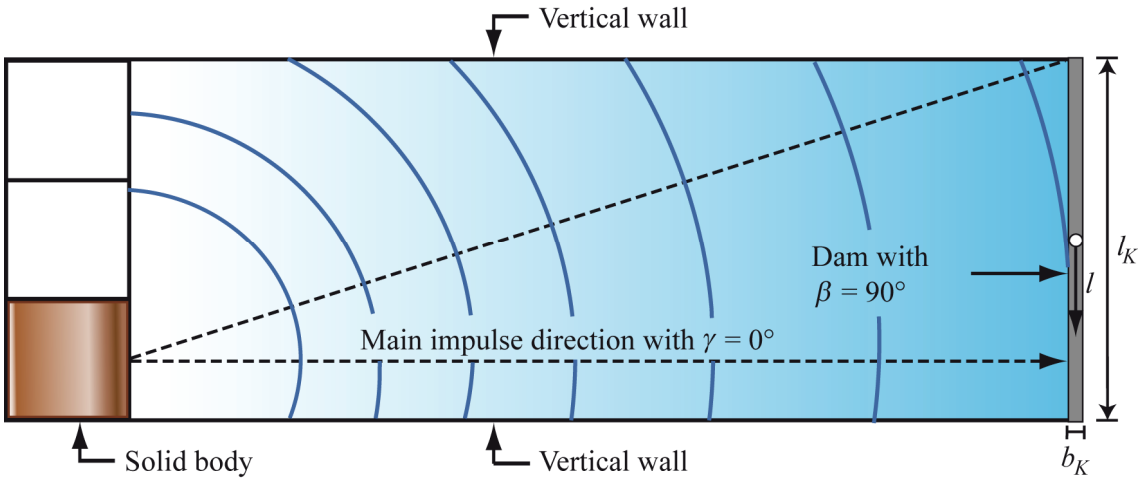

Figure B-5 Sketch of test layout to investigate the influence of the incidence wave angle, as shown in Figure B-3(b), on the run-up height R.

In addition, Müller (1995) investigated 3D effects with 96 tests, but his results mainly resulted in qualitative conclusions without generally applicable quantitative statements. The first 3D effect tested was the incidence wave angle. For this the wave was generated asymmetrically, as shown in Figure B-5. The solid body was dropped at a corner of the wave basin. Figure B-3(b) shows the run-up height $R_{\gamma \neq 0°}$ at the dam relative to the run-up height R in the main impulse direction, as a function of the relative crest length l/l_K. In this expression, l is the coordinate along the dam crest with the origin at the centre of the crest (Figure B-5). Generally, the run-up heights for oblique impulse waves at the reservoir shore are up to 13% less high than in the main impulse direction $\gamma = 0°$. These effects are mainly accounted for by the wave propagation angle γ in Eq. (3.13), for which the wave is largest in the main impulse direction.

As second 3D effect, the influence of the reservoir geometry was investigated, by using a V-section rather than a rectangular valley (Figure 4-4a). The impulse wave thereby propagates in the sloping shore area as a shallow-water wave and is thus shoaling (Section 4.2) due to the influence by the bed. Figure 4-4(b) shows for a lateral reservoir flank of 3:4, the relationship of the run-up height to the run-up height at the dam centre R/R_m, as a function of the relative flank width l/l_F. In the vicinity of the inclined shore the wave run-up heights are about 20% to 30% greater than in the dam centre. Green's law from Eq. (4.1) overestimates the run-up height at the dam flank. Müller (1995) gives two possible reasons: (i) the wave in the test does not move frontally to the lateral reservoir flank and (ii) the friction losses at the bed reduce the run-up height in the test compared with the theoretically deduced Green's law. The advantages and disadvantages of the investigations of Müller (1995) and of Müller and Vischer (1996) are:

+ Extensive investigation about run-up height R, overtopping volume ~~V~~ and estimates for the required freeboard f.

+ A large wave spectrum and range of dam face slopes from $18.4° \leq \beta \leq 90°$ is covered.
+ The data points in the diagrams show relatively little scatter and the diagrams themselves are available.
+ The overtopping duration of the overtopping volume is known for $f = 0$, and hence also the discharge.
+ They are based on many tests (733).
+ In addition to 2D experiments, 3D tests were also conducted.
− The results of the 3D tests could not be integrated into the generally applicable 2D equations.

Gedik et al. (2005) conducted experiments with solitary waves on a permeable sandy beach of constant slope 1:5 ($\beta = 11.3°$). For a few tests, the sand surface was covered with blocks. The sand had a grain density of $\rho_g = 2{,}630$ kg/m^3 and a grain size of $d_g = 0.00035$ m. The still water depth was $h = 0.33$ m, the solitary wave height was in the range $0.012 \text{ m} \leq H \leq 0.11$ m and the wave was non-breaking during run-up. Based on about 60 tests the relative run-up height was expressed with a coefficient of determination $R^2 = 0.95$ as

$$\frac{R}{h} = 4 \cdot 10^{-4} \left(\frac{H}{d_g} \frac{\rho_g}{\rho_w} \cot \beta \right)^{0.921} . \tag{B.8}$$

If the sand surface was covered with blocks of diameters d_b of 0.01 m to 0.0138 m the expression for the relative run-up height R/h, based on 20 tests, could be determined with a coefficient of determination $R^2 = 0.93$ as

$$\frac{R}{h} = 5 \cdot 10^{-3} \left(\frac{H}{d_b} \frac{\rho_g}{\rho_w} \cot \beta \right)^{0.954} . \tag{B.9}$$

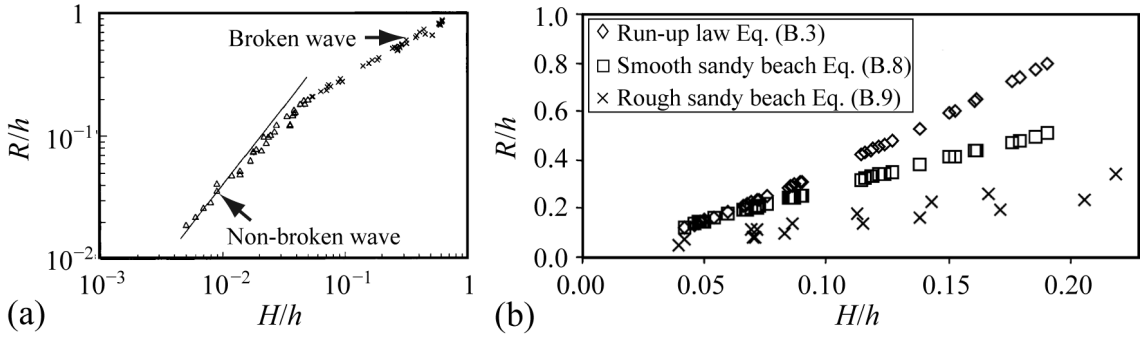

Figure B-6 Wave run-up with relative run-up height R/h to the relative solitary wave height H/h according to (a) Synolakis (1987) with broken and non-broken waves and (b) Gedik et al. (2005) with the run-up law of Eq. (B.3) and own tests on smooth and rough sandy beach.

Equations (B.8) and (B.9) are shown in Figure B-6(b) as a function of the relative run-up height R/h and the relative wave height H/h. Also indicated is the analytically deduced run-up law according to Eq. (B.3). This is well satisfied for $H/h = 0.07$ but deviates for $H/h = 0.19$ by about 30% from the test results on a smooth bed (Eq. B.8). The reason is that in Gedik et al. (2005) a permeable sandy beach was considered, whereby Eq. (B.3) was deduced on the assumption of an impermeable beach. Further, Eqs. (B.8) and (B.9) are compared with each other in Figure B-6(b). The blocks reduce the run-up height R by about 50%, and this agrees well with Table B-1. However, with $\beta = 11.3°$ only a relatively small run-up angle was investigated. The advantage and disadvantages of the investigation of Gedik et al. (2005) are:

+ The effect of the roughness and the permeability were investigated.
− A moderate number of tests was undertaken (60).
− Only a small run-up angle $\beta = 11.3°$ was tested.

Teng et al. (2000) found also that the bed friction reduced the run-up height. They conducted tests with solitary waves for run-up angles of $\beta = 10°$, 15° and 20°, with both one smooth and two rough (Manning-Strickler coefficients 0.018 $s/m^{1/3}$ and 0.024 $s/m^{1/3}$) surfaces. For $\beta = 20°$, the roughness had a negligible effect. For $\beta = 15°$ the run-up height for a rough bed was about 30%, for $\beta = 10°$ as much as 50% lower than for a smooth bed. Hence, the roughness effect for $\beta \geq 20°$ seems to be negligible. The advantage and disadvantage of the investigation of Teng et al. (2000) are:

+ The effect of both the roughness and the permeability were investigated.
− Only 35 tests were conducted with, for a dam, only small run-up angles in the range $10° \leq \beta \leq 20°$.

B.3.3 Bore-like waves

Bore-like waves were described in Section 2.2 and Appendix A.3.2.1. These are generated by large and rapidly impacting slide masses already in the slide impact zone (Appendix A.3.2.1), but also by breaking waves in the run-up zone. The description of bore run-up was mostly considered analytically but more rarely in hydraulic models (Müller 1995). The experimental study by Miller (1968), with run-up angles $2° \leq \beta \leq 15°$ overlapping only with the lowest range for dams, is an exception. Therefore, the technical literature (e.g. Shen and Meyer 1963; Miller 1968; Müller 1995) often recommends the theoretical equation

$$R = c^2 / 2g \,. \tag{B.10}$$

In this equation, c is the horizontal component of the bore celerity at the point of intersection of the still water level with the dam face (the coordinate origin in Figure B-1). For landslide generated impulse waves, the celerity c can be determined with the solitary wave celerity by using Eq. (3.3). The advantage and disadvantage of Eq. (B.10) are:

+ It is easy to apply.
− It has not been well proven by experiments.

B.4 Wave force on dams

B.4.1 Stokes-like waves

A standing wave (Clapotis) is formed if a wave is reflected and is superimposed on an approaching wave of identical size. As reflection without wave height loss is only possible at a vertical wall, the force effect for a standing wave is only valid for $\beta = 90°$. Standing waves have been described by Minikin (1950), Morris and Wiggert (1972), Wiegel (1964), Novak et al. (2001) and Dean and Dalrymple (1991). As the standing wave results from the superimposition of oscillatory waves, only Stokes-like waves may be approximated with this theory. For standing waves the wave nodes always remain in the same position but the areas between the nodes move up and down. Hence, a run-up movement occurs at the dam.

According to Sainflou (1928), the pressure distribution of a standing wave is not linear, but may be approximated as such. Figure 3-10(a) shows the definition sketch of the run-up of a standing wave. The most important assumptions of the theory of Sainflou (1928) are:

- The mean water level of a standing wave during run-up is at a height Δh above the still water level, whereby Δh can be calculated from Eq. (B.12).

- At a height of $H + \Delta h$ above the still water level, with H as the wave height, the water pressure is zero.

- The maximum pressure p_2 due solely to wave action occurs at the still water level (Figure 3-10b).

Figure 3-10(b) shows the pressure distribution from a standing wave running-up a vertical dam. That part of the distribution resulting solely from the wave is represented by the area “abcd”, and the total pressure distribution, including hydrostatic pressure from Eq. (3.21), corresponds to the triangle “agd”. Calculation of the force resulting only from the running-up wave is done in several stages:

a) Computation of the additional pressure p_1 on the dam foundation:

$$p_1 = \frac{\rho_w g H}{\cosh(2\pi h / L)}. \tag{B.11}$$

b) Computation of the average water level rise Δh:

$$\Delta h = \frac{\pi H^2}{L} \coth\left(\frac{2\pi h}{L}\right). \tag{B.12}$$

c) Computation of the pressure p_2 at the still water level:

$$p_2 = \frac{(\rho_w g h + p_1)(\Delta h + H)}{H + \Delta h + h}. \tag{B.13}$$

d) Computation of the additional horizontal force component ΔK_h per unit length dam crest resulting from impulse wave:

$$\Delta K_h = \frac{p_2(\Delta h + H)}{2} + \frac{(p_1 + p_2)h}{2}. \tag{B.14}$$

e) Computation of the additional horizontal force component ΔK_h per unit length dam crest resulting from impulse wave, with Eqs. (B.11) and (B.13) directly applied (gives the same result as Eq. B.14):

$$\Delta K_h = \frac{\rho_w g}{2}\left\{(h + \Delta h + H)\left[h + \frac{H}{\cosh(2\pi h / L)}\right] - h^2\right\}. \tag{B.15}$$

For Eq. (B.15) the hyperbolic cosine function $\cosh(y) = (e^{y} + e^{-y})/2$ and the hyperbolic cotangent function $\coth(y) = (e^{y} + e^{-y})/(e^{y} - e^{-y})$ are applied, with y as any given rational number. These functions are plotted in Figure 3-11. In addition to the horizontal force component ΔK_h from Eq. (B.15), the hydrostatic pressure has to be taken into account from Eq. (3.21). The elevation $z_{\Delta K,h}$ of the resultant of ΔK_h is given by Eq. (3.28). The advantage and disadvantages of Sainflou's (1928) standing wave model are:

+ It has established itself in the technical literature.
− It can only be used for vertical dams.
− It contains the relatively complicated terms cosh and coth, which are shown graphically in Figure 3-11.

B.4.2 Cnoidal and solitary-like waves

Tanimoto et al. (1984) investigated the pressure distribution at a vertical wall resulting from a sine wave (Figure 2-1). They assumed a tsunami (caused by a tectonic plate movement) which corresponds to a shallow-water wave and mobilises the entire water column down to the sea bed (Section 2.1). Although the profile of a Stokes-like wave is similar to that of the sine wave, a Stokes-like wave generated by a slide does not behave in the same way as a shallow-water wave. For this reason, the study of Tanimoto et al. (1984) is better suited to this section on cnoidal and solitary-like waves than to the section on Stokes-like waves. The linear pressure distribution resulting only from the wave is given by

$$\frac{p(z)}{\rho_w g a} = 2.2[1-(1/3)z/a] \qquad \text{for } 0 \le z/a \le 3 \text{ and} \qquad \text{(B.16)}$$

$$\frac{p(z)}{\rho_w g a} = 2.2 \qquad \text{for } z/a \le 0. \qquad \text{(B.17)}$$

The pressure distribution as determined from Eqs. (B.16) and (B.17) is shown in Figure B-9(a), from which the additional horizontal force component ΔK_h per unit length dam crest resulting from impulse wave can be determined as

$$\Delta K_h = 2.2\rho_w g a[(3/2)a + h]. \qquad \text{(B.18)}$$

The work of Tanimoto et al. (1984) has the following advantage and disadvantages:

+ The calculation is simple.
− The calculation is based on only a few tests.
− The Eqs. (B.16) and (B.17) have been taken from Fuminori et al. (2003), as the original paper is not available and was probably written in Japanese. As a consequence, the limitations and boundary conditions of these tests are unknown.

Ramsden (1996) generated solitary waves with a horizontal movable wall and investigated their effects on a vertical wall in a horizontal, 0.396 m wide, 36.6 m long wave channel with a water depth of about 0.175 m. A 0.0604 m wide strip of the wall, in the channel axis, was mounted on four force measurement sensors. With this strip, Ramsden (1996) determined both the force component and the bending moment resulting from the solitary wave. In Figure B-7 the corresponding maximum measured values are shown as a function of the relative wave amplitude a/h; in Figure B-7(a) the maximum total horizontal force component $K_{tot,h}$ per unit length dam crest resulting from an im-

pulse wave and hydrostatic pressure, and in Figure B-7(b) the maximum bending moment $BM_{tot,h}$ per unit length dam crest about the foundation resulting from the horizontal force of an impulse wave and hydrostatic pressure. For the remaining procedures in Appendix B.4 only the effects resulting from the impulse wave alone are considered. The different procedures in Appendix B.4.5 can then be compared with each other, the values of $K_{tot,h}$ are reduced below by the hydrostatic pressure effect, as determined from Eq. (3.21). Figure B-7 shows only a section of the original figure of Ramsden (1996). The rest of the data describe principally dam break waves or bores, which approach the wall over a dry bed or insufficient still water depth h. These data are not included in Figure B-7 and hence are not relevant for this manual. The measured total horizontal force component $K_{tot,h}$ in Figure B-7(a) is normalised with the horizontal component of hydrostatic force $K_{hs,h}$ per unit length dam crest resulting from a still water level displaced upwards by $2a$, given as

$$K_{hs,h} = (1/2)\rho_w g(2a+h)^2 . \tag{B.19}$$

Ramsden (1996) used the bending moment per unit length dam crest $BM_{hs,h}$ about the foundation resulting from the horizontal force of the hydrostatic pressure and a still water level displaced upwards by $2a$ from Eq. (B.19) to normalise the bending moment $BM_{tot,h}$ per unit length dam crest about the foundation resulting from the horizontal force of an impulse wave and hydrostatic pressure, as shown in Figure B-7(b). The equation for $BM_{hs,h}$ considers the lever arm $(2a + h)/3$ and is

$$BM_{hs,h} = (1/6)\rho_w g(2a+h)^3 . \tag{B.20}$$

The ratio $K_{tot,h}/K_{hs,h}$ and $BM_{tot,h}/BM_{hs,h}$ in Figure B-7 are almost always less than unity, and hence the measured values of the horizontal force component $K_{tot,h}$ and the bending moment $BM_{tot,h}$ are practically always less than the corresponding hydrostatic value given by Eqs. (B.19) and (B.20). The measured points are empirically approximated in this manual as

$$\frac{K_{tot,h}}{K_{hs,h}} = \left[1-1.5(a/h)\right]^{1/6} \qquad \text{for } 0 \le a/h \le 0.6 \text{ and} \tag{B.21}$$

$$\frac{BM_{tot,h}}{BM_{hs,h}} = \left[1-1.5(a/h)\right]^{1/6} \qquad \text{for } 0 \le a/h \le 0.6. \tag{B.22}$$

The same function was used for both the force component according to Eq. (B.21) and for the bending moment given by Eq. (B.22). The values $K_{tot,h}$ and $BM_{tot,h}$ therefore differ only by the lever arm, which is equal to $(2a + h)/3$. This lever arm is characteristic for a triangular pressure distribution. The pressure distribution of a solitary wave may,

therefore, be approximated by a triangular shape as shown in Figure 3-13(a). In order to conserve only the effect resulting from the solitary wave, the values from Eq. (B.21) are reduced by the effect of the hydrostatic pressure, as given in Subsection 3.4.2. The additional horizontal force component ΔK_h per unit length dam crest is thus

$$\Delta K_h = K_{tot,h} - (1/2)\rho_w g h^2 . \tag{B.23}$$

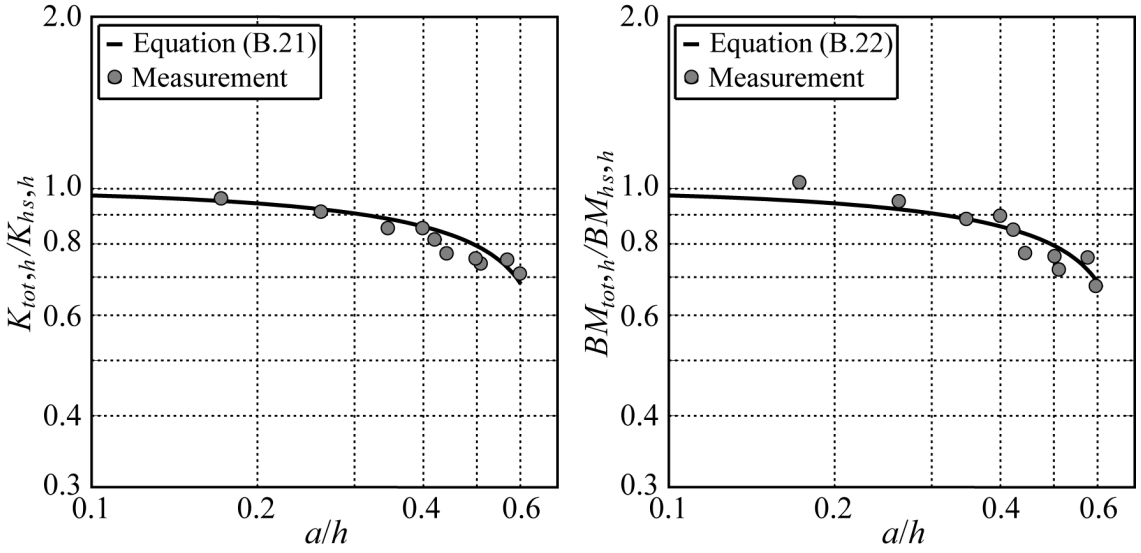

Figure B-7 Effects of solitary waves on a vertical dam as a function of the relative wave amplitude a/h: (a) relative horizontal force component $K_{tot,h}/K_{hs,h}$ per unit length dam crest inclusive hydrostatic pressure and (b) relative bending moment $BM_{tot,h}/BM_{hs,h}$ per unit length dam crest about the foundation resulting from the horizontal force of an impulse wave and hydrostatic pressure.

The advantage and disadvantages of the work of Ramsden (1996) are:

+ The pressure distribution may be reconstructed based on the measured bending moments.
− Only about 10 tests were conducted.
− Experiments were only carried out for vertical dams.

Cooker et al. (1997) investigated mathematically the run-up of a solitary wave on a vertical wall. They concentrated on the run-up height R and the force on the wall. The maximum force and the run-up height agreed well with an earlier numerical study by Fenton and Rienecker (1982). A few intermediate results of the computation of Cooker et al. (1997) were confirmed with the experiments conducted by Maxworthy (1976).

Figure B-8(a) shows the normalised maximum additional horizontal force component $\Delta K_h/(\rho_w g h^2)$ per unit length dam crest resulting from an impulse wave as a function of the relative wave amplitude a/h. The ordinate values in Figure B-8 have, compared with those presented by Cooker et al. (1997), been reduced by the hydrostatic

pressure, corresponding to a value of $\Delta K_h/(\rho_w g h^2) = 0.5$ on the ordinate, so as to give the horizontal force component ΔK_h resulting only from the impulse wave. Both the numerically computed values of Fenton and Rienecker (1982) (·) and the analytically deduced values of Cooker et al. (1997) (•) are shown. From Figure B-8(a) the maximum additional horizontal force component ΔK_h per unit length dam crest resulting *only* from the approaching solitary wave may be approximated linearly as

$$\Delta K_h = \rho_w g h^2 [2.1(a/h)] \qquad \text{for } 0 \le a/h \le 0.7. \qquad \text{(B.24)}$$

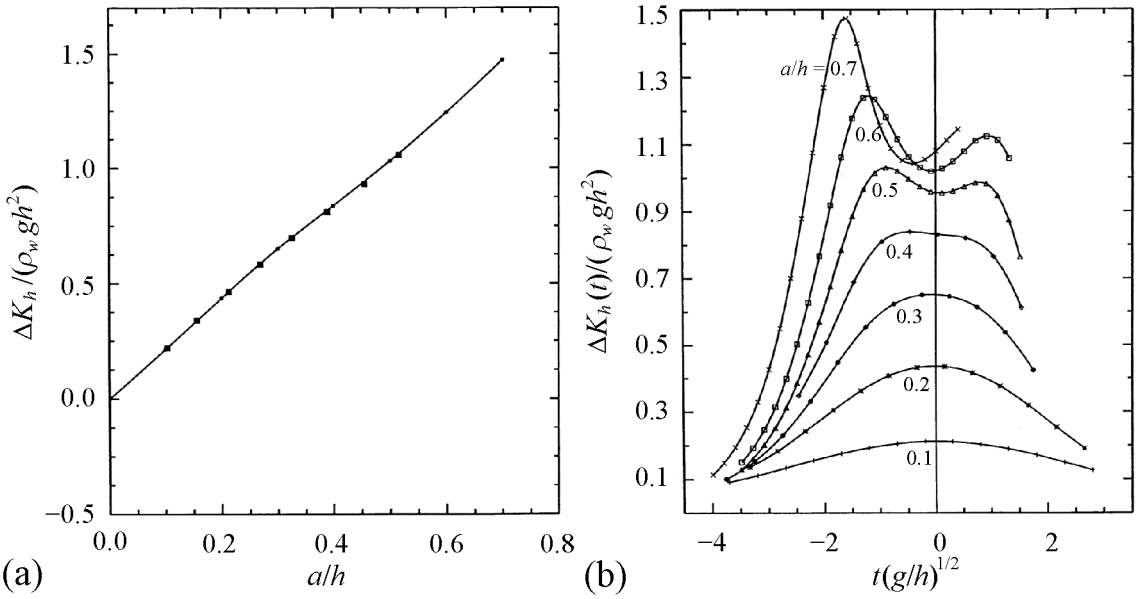

Figure B-8 Additional horizontal force component ΔK_h per unit length dam crest for a solitary wave against a vertical wall (a) as a function of the relative wave amplitude a/h and (b) as a function of relative time $t(g/h)^{1/2}$ for various values of the relative wave amplitude a/h (after Cooker et al. 1997).

Figure B-8(b) shows the horizontal force component $\Delta K_h(t)/(\rho_w g h^2)$ as a function of relative time $t(g/h)^{1/2}$ for various values of the relative wave amplitude a/h. The abscissa value $t(g/h)^{1/2} = 0$ corresponds to the point in time of the maximum run-up height R. The ordinate value is again reduced by $\Delta K_h(t)/(\rho_w g h^2) = 0.5$, corresponding to the hydrostatic pressure. Whilst for $0.1 \le a/h < 0.3$ the horizontal force component continually increases and then decreases, the horizontal force components for relative wave amplitudes $0.4 \le a/h \le 0.7$ have two peaks which occur before and after the time of maximum run-up. It may be seen from Figure B-8(b) that the maximum horizontal force component on the dam is of short duration. For the largest relative wave amplitude $a/h \approx 0.7$ (highest curve) and a typical prototype still water depth $h = 100$ m, the horizontal force component of the first peak, for example, is only $t \approx 4$ s above the ordinate value $\Delta K_h(t)/(\rho_w g h^2) = 1.1$. Cooker et al. (1997) give no information about the pressure distribution. The advantages and disadvantage of the work of Cooker et al. (1997) are:

+ A simple equation determines the additional horizontal force component ΔK_h resulting from a solitary wave.
+ Equation (B.24) is deduced on the basis of analytically computed values and was confirmed with numerically determined results; several intermediate results, not discussed here, agreed well when compared with those of experiments.
− Equation (B.24) is based on only 7 calculated values.

B.4.3 Bore-like waves

Ikeno et al. (2001) investigated experimentally the run-up of a bore against a vertical wall standing in water. The bore represented thereby a broken tsunami (caused by a tectonic plate movement). Taking as basis Eqs. (B.16) and (B.17) of Tanimoto et al. (1984), Ikeno et al. (2001) formulated the pressure distribution with the additional parameter φ as

$$\frac{p(z)}{\rho_w g a} = 2.2[1-(1/3)z/a]\varphi \qquad \text{for } 0 \le z/a \le 3 \text{ and} \qquad \text{(B.25)}$$

$$\frac{p(z)}{\rho_w g a} = 2.2\varphi \qquad \text{for } \; z/a \le 0. \qquad \text{(B.26)}$$

The parameter is $\varphi = 1.36$ for $0 \le z/a \le 3$, $\varphi = 1.36(1 + 0.52z/a)$ for $-0.5 \le z/a \le 0$ and $\varphi = 1.0$ for $z/a < -0.5$. Figure B-9(b) shows the pressure distribution on a vertical wall based on Eqs. (B.25) and (B.26). As distinct from the approach of Tanimoto et al. (1984) the bore causes a pressure peak at still water level which is higher than that of the sine wave in Figure B-9(a). With the aid of Eqs. (B.25) and (B.26) or the pressure distribution in Figure B-9(b), the additional horizontal force component ΔK_h per unit length dam crest resulting from impulse wave can be determined as

$$\Delta K_h = \rho_w g a\left[2.2h + 2.2 \cdot 1.36 \cdot (3/2)a + 0.792 \cdot (1/4)a\right]. \qquad \text{(B.27)}$$

The advantage and disadvantages of the study of Ikeno et al. (2001) are:

+ The computation is relatively simple.
− The computation is based on only a few tests.
− The Eqs. (B.16) and (B.17) have been taken from Fuminori et al. (2003), as the original paper is not available and was probably written in Japanese. As a consequence, the limitations and boundary conditions of these tests are unknown.

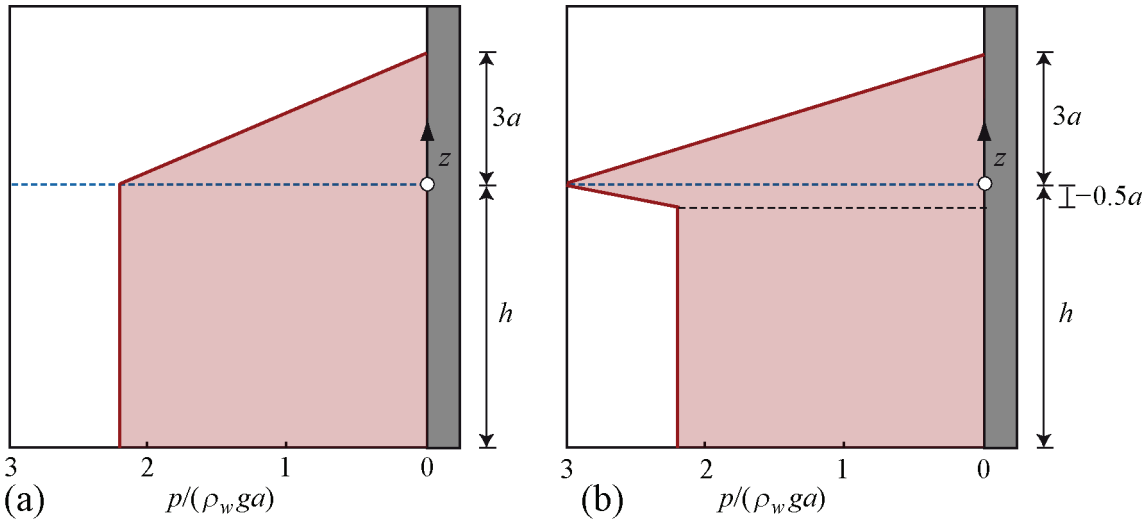

Figure B-9 Pressure distribution of tsunamis (caused by a tectonic plate movement) on a vertical wall: (a) for a shallow-water sine wave according to Eqs. (B.16) and (B.17) after Tanimoto et al. (1984) and (b) for a bore given by Eqs. (B.25) and (B.26) after Ikeno et al. (2001), based on the approach of Tanimoto et al. (1984).

B.4.4 Breaking waves

Sometimes an impulse wave breaks as a plunging breaker directly on the dam. If in such a case, as shown in Sequence (I) - (IV) in Figure B-10(a), an air pocket is trapped between the wave and the dam, a local but large force effect of short duration may develop and result in localised damage. This occurs, as shown in Figure B-10(a) in Sequence (IV), at the level of the air pocket. This force can, even if waves are breaking on the dam, only sometimes be measured in a physical model test. It is difficult to determine in an experiment under which conditions this large pressure occurs (Walkden and Bruce 2000) and research is still in progress (Peregrine 2003). For the design of dams or other structures for coastal protection this force is governing, although the occurrence of such waves is rare. A wave breaks as a plunging breaker if the so-called Iribarren number I < 2.5. This number is defined, according to Thomas and Hall (1992), as

$$\mathrm{I} = \tan\beta / (H / L)^{1/2} . \qquad \text{(B.28)}$$

For a dam with $\beta = 45°$, a wave height of $H = 5$ m and a wave length of $L = 20$ m, a value of, for example, I = 2 is obtained. If the wave breaks as a plunging breaker such a large localised force appears possible.

In practice the force component so produced on the vertical dam will be computed using the method of Minikin (1950). The pressure distribution resulting from the breaking wave is shown in Figure B-10(b), and consists of a dynamic pressure peak at the still water level and a static pressure resulting from the run-up height R. The maximum value of the dynamic pressure is

$$p_d = 2\pi\rho_w ghH / L\,. \tag{B.29}$$

On the assumption of a run-up height $R = H/2$, the additional static pressure is

$$p_s = (1/2)\rho_w gH\,. \tag{B.30}$$

The dynamic pressure p_d is typically several times larger than the static pressure p_s. The additional horizontal force component ΔK_h per unit length dam crest resulting from the plunging breaker is determined by the integration of the areas of dynamic and static pressure, as shown in Figure B-10(b), as

$$\Delta K_h = \frac{1}{3}Hp_d + \frac{1}{2}\rho_w gH[h + (1/4)H] = \rho_w gH\left[\frac{2}{3}\pi hH / L + (1/2)h + (1/8)H\right]. \tag{B.31}$$

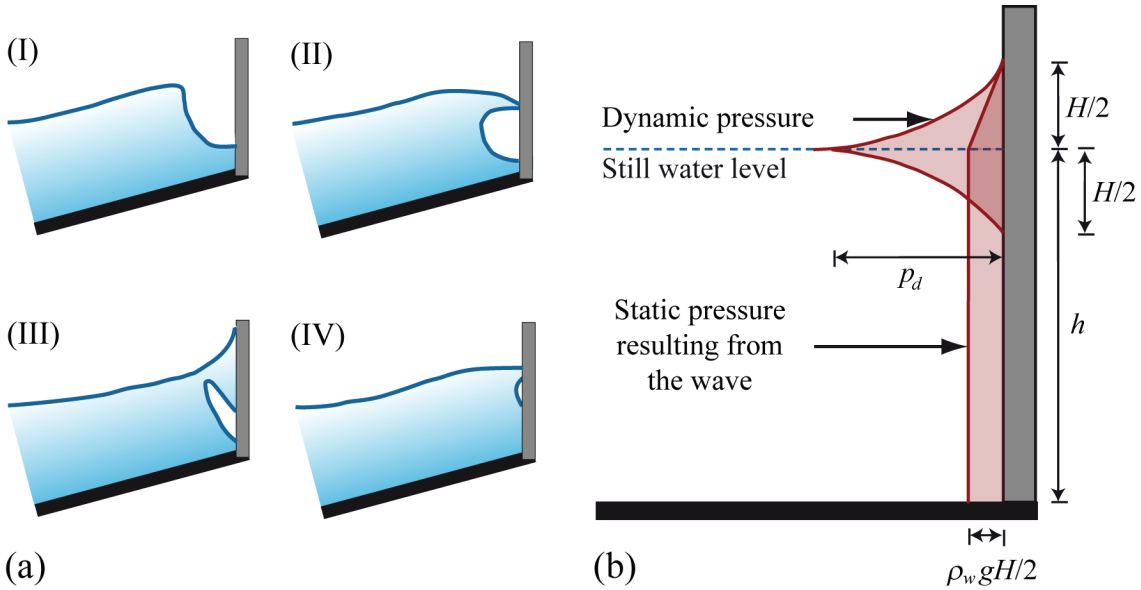

Figure B-10 Plunging breaker against a vertical wall (a) principle sketch with four stages of impact and (b) pressure distribution with the dynamic and static pressure components (after Minikin 1950).

If the dam is inclined at an angle β to the horizontal (Figure B-1), the proportion corresponding to the dynamic pressure p_d in Eq. (B.31) will be replaced with the term $p_d \sin^2\beta$, in order to determine the horizontal force component. The model presented by Minikin (1950) has the following advantages:

+ The computation is relatively simple.
+ The model has proven itself in coastal protection, for instance it is recommended by the Shore Protection Manual (USCE 1977).
+ The horizontal dynamic force component can be converted with the term $\sin^2\beta$ for any given dam face slope β.

B.4.5 Computation examples

In Appendix B.4 six different procedures for the computation of the additional horizontal force components ΔK_h per unit length dam crest resulting from impulse waves were described. Each of these can be used for specific wave types considered. To demonstrate the relations of the forces for the individual procedures, they are applied on two examples (i) and (ii). In doing so, the features of these example waves will be applied on all presented procedures, independent of which wave type they are developed for.

Example (i): wave height $H = 5$ m, wave length $L = 50$ m, wave amplitude $a = 2.5$ m, dam face slope $\beta = 90°$, still water depth $h = 100$ m and freeboard greater than the run-up height $f > R$.

Example (ii): wave height $H = 50$ m, wave length $L = 200$ m, wave amplitude $a = 35$ m, dam face slope $\beta = 90°$, still water depth $h = 75$ m and freeboard greater than run-up height $f > R$.

Table B-2 Additional horizontal force component ΔK_h per unit length dam crest for the computation examples (i) and (ii) and for the six studies presented in Appendix B.4; abbreviations: Slw = Stokes-like waves, cslw = cnoidal and solitary-like waves and blw = bore-like waves.

Study	Sainflou (1928)	Tanimoto et al. (1984)	Ramsden (1996)
Wave type	Standing wave	Sine wave (in shallow water)	Solitary wave
Impulse wave type	Slw	cslw	cslw
Equation	Eq. (B.15)	Eq. (B.18)	Eq. (B.23)
Example (i)	Hydrostatic pressure (basis): $K_{RW,h} = 49.0 \cdot 10^6$ N/m (Eq. 3.21)		
ΔK_h [N/m]	$3.2 \cdot 10^6$ (7%)	$5.6 \cdot 10^6$ (11%)	$4.7 \cdot 10^6$ (10%)
Example (ii)	Hydrostatic pressure (basis): $K_{RW,h} = 27.6 \cdot 10^6$ N/m (Eq. 3.21)		
ΔK_h [N/m]	$40.4 \cdot 10^6$ (146%)	$96.3 \cdot 10^6$ (349%)	$56.8 \cdot 10^6$ (206%)
Study	Cooker et al. (1997)	Ikeno et al. (2001)	Minikin (1950)
Wave type	Solitary wave	Bore wave	Plunging breaker
Impulse wave type	cslw	blw	Plunging breaker
Equation	Eq. (B.24)	Eq. (B.27)	Eq. (B.31)
Example (i)	Hydrostatic pressure (basis): $K_{RW,h} = 49.0 \cdot 10^6$ N/m (Eq. 3.21)		
ΔK_h [N/m]	$5.1 \cdot 10^6$ (11%)	$5.7 \cdot 10^6$ (12%)	$3.5 \cdot 10^6$ (7%)
Example (ii)	Hydrostatic pressure (basis): $K_{RW,h} = 27.6 \cdot 10^6$ N/m (Eq. 3.21)		
ΔK_h [N/m]	$54.1 \cdot 10^6$ (196%)	$112.9 \cdot 10^6$ (409%)	$40.7 \cdot 10^6$ (148%)

How large will be the additional horizontal force component ΔK_h per unit length dam crest resulting *only* from the wave? In Table B-2 the six studies are presented with the results of the two computation examples (i) and (ii). Against the wave type investigated in the respective study, the impulse wave type according to Appendix A.3.2.1 is specified, to which the corresponding equation should approximate namely Stokes-like, cnoidal and solitary-like as well as bore-like waves. The fourth and thirteenth lines describe the equation reference in Appendix B. In the light coloured area of Table B-2 the values for the additional horizontal force component ΔK_h resulting *only* from im-

pulse wave are included. For comparative purposes the values $K_{RW,h}$, resulting from the static pressure according to Eq. (3.21), are also presented. The percentages in brackets refer to these values.

Example (i): In the first example the forces ΔK_h are relatively close for all six methods, in the range $3.2 \cdot 10^6$ N/m $\leq \Delta K_h \leq 5.7 \cdot 10^6$ N/m (Table B-2). The additional horizontal force component resulting from the impulse wave is thus equal to 7% to 12% of that of the hydrostatic pressure $K_{RW,h}$.

Example (ii): In the second example an impulse wave ten times larger than in example (i) runs-up the dam. For the six studies, the values of ΔK_h have a greater variation and, relative to the hydrostatic pressure, are in the range 146% and 409% (Table B-2).

The two examples serve essentially for a comparison of the forces occurring in each of the models. It should be noted that the models for different wave types, and hence for different wave parameters, are deduced from different ranges of limitations, some of which are not satisfied in the examples. Therefore, the large differences between the models in example (ii) are not a cause of surprise. A further assumption was that the wave does not overtop. If this happens the force component is correspondingly smaller (Subsection 3.4.4).

B.5 Summary and literature used in the calculation procedure

For the run-up height R of unbroken waves, the empirical study of Müller and Vischer (1996) covers small Stokes-like waves and also cnoidal and solitary-like waves. As this study also allows the overtopping volume V and the freeboard f to be estimated, these computation equations are used for the run-up and overtopping in the computation procedure shown in Figure 3-1 and in Section 3.3. Müller and Vischer (1996) discussed only briefly bore-like waves, yet these are rare, extreme events whose occurrence is very unlikely. If, nevertheless, a bore is generated in the slide impact zone, it will after a relatively short relative streamwise distance X change into a solitary or cnoidal-like wave, as the bore entrains ever less air and the air already entrained will escape quickly (Figure A-15b).

The roughness and the permeability of a dam reduce the run-up height R of Stokes-like waves, as shown in Table B-1. The permeability may, however, be neglected. For larger impulse waves such as solitary waves the roughness reduces the run-up height, although, according to Teng et al. (2000), only for small run-up angles $\beta < 20°$. For bores, empirical data are lacking, but the reduction of the run-up height resulting from the roughness is considered small. As the roughness only partly reduces the wave run-up height, its influence on the computation procedure shown in Figure 3-1 is not considered.

3D effects such as the incidence wave angle on the dam or the reservoir basin geometry were studied by Müller (1995), but their influences could not be generally for-

mulated. The 3D effects can thus not be considered and must, as explained in Section 4.2, be estimated from case to case.

According to Synolakis (1991) only about 25% of all tsunamis break when they reach the coast. As in addition the run-up angle β is large for a dam, the waves are unlikely to break according to Eq. (B.28). Hence, the case described in Appendix B.4.4 is not considered in the computation procedure according to Figure 3-1. Furthermore, the additional horizontal force component ΔK_h in the computation example, for a wave breaking directly on the dam, is rather low, compared with the values obtained by other methods (Table B-2). If, for a breaking wave, the force effect is determined with the methods of Sainflou (1928) or Ramsden (1996), the results are on the safe side compared with those according to Minikin (1950). In other words, ignoring the method of Minikin (1950) does not involve any high risk.

With the exception of Eq. (B.21), the forces considered in Appendix B relate only to the additional force resulting from the waves. The horizontal force component per unit length dam crest resulting only from hydrostatic pressure $K_{RW,h}$, according to Eq. (3.21), has to be considered in addition.

More exact information is lacking on the experimental boundary conditions and limitations for the work of Tanimoto et al. (1984), on shallow-water sinus waves, and of Ikeno et al. (2001) on bores. Much better founded are, however, the methods of Sainflou (1928) for Stokes-like waves and of Ramsden (1996) as well as Cooker et al. (1997) for solitary-like waves. The last two methods result practically in the same horizontal force component ΔK_h. From the results of Ramsden (1996) it is deduced that the pressure distribution may be approximated as linear. In practical applications, Stokes-like waves are mostly expected. With regard to the force components, therefore, in the computation procedure in Figure 3-1, the Stokes-like waves will be described with the method of Sainflou (1928) and the remaining wave types with the method of Ramsden (1996). This differentiation between Stokes-like waves and the remaining wave types is possible with Eq. (3.23).

Neither the method of Sainflou (1928) nor that of Ramsden (1996) give any information on the separation of the force into static and dynamic components. The horizontal component of a static force is, according to Figure 3-8, independent of the dam face slope β. In addition, there is a vertical component. Because at the time of maximum run-up practically all kinetic wave energy is transformed into potential energy, the total force will be considered as static and the vertical component will be calculated using Eq. (3.22). Figure 3-1 summarises the selected methods for the computation procedure covered in Chapter 3.